

DELFT UNIVERSITY OF TECHNOLOGY

MASTER THESIS
AESM2606

Model research into the influence of battered piles on the lateral response of onshore wind turbine foundations under horizontal loading conditions through analytical and numerical 3D analysis

Author:

Daan van Nie (4482867)

Thesis supervisors:

Prof.dr.ir. K. G. Gavin

Dr.ir. F. Pisanò

Dr.ir. R.B.J. Brinkgreve

Ir. O.Mooijman [Royal HaskoningDHV]

A thesis presented for the degree of Master Section:
Subsurface engineering

August 9, 2022



Acknowledgement

The last year was a year with steep learning curves and good discussions which were not possible without my graduation committee; Prof. dr. ir. K.A. Gavin, Dr.ir. F. Pisanò, Dr.ir. R.B.J. Brinkgreve and my daily supervisor of the company Royal HaskoningDHV Ir. O.Mooijman. Without their supervision and knowledge the results of this thesis would not have been achieved. Besides my official committee, I would like to thank ir. J. van Es for helping me with his experience of Plaxis. Last but not least, I would like to thank Mabel, my family and my roommates for their support during these 7.5 months.

D. van Nie
Delft, July 2022

Abstract

In the low-lying parts of The Netherlands challenging ground conditions are often encountered. Thick layers of soft material such as peat and clay are present and pile foundations into deeper sand layers are required when objects are constructed that have to transfer significant loads to the subsurface without inducing settlement (differences). This also counts for pile foundations of wind turbines which, apart from compression and tension loads also are subjected to horizontal loading.

The horizontal translational stiffness is an important and depending on the wind turbine manufacturer governing aspect in the required dimensions of the pile foundation (number and type of piles). In order to improve this horizontal translational stiffness, the foundation designer usually opts for the use of battered (raked) piles. The basic principle is that the axial stiffness of the pile will, in this way, contribute to the horizontal stiffness of the foundation as a whole. The verification of wind turbine requirements usually involve the use of generally accepted analytical 2D methods, simplifying the more complex 3D effect, to model the interaction between soil-pile and the group effect for closely spaced piles. Although the analytical model generally provides good results, investments can reduce significantly when only a small amount of piles can be saved upon. Also the effort in the field is reduced when using vertical piles.

The analysis is performed in Plaxis 3D, a FEM program which can model pile groups and soil-structure interaction. A schematic subsurface profile is used which is representative for many parts of the western part of The Netherlands. Conservative-realistic Hardening Soil small strain parameters were derived from Royal HaskoningDHV (RHDHV) projects and were further optimized within the context of this study to reflect realistic soil parameters. The Hardening Soil small strain constitutive model is used as the most advanced model for describing ground behavior at small strains. A step-wise analysis is performed to check the influence of batter angles in each stage, namely single pile, simplified group and round wind turbine foundation. Each stage is validated with literature present in the study or with the analytical program D-sheetpiling. The analysis focuses on pile-soil interaction. Other load transfer mechanisms such as passive resistance and base shear are not considered

The wind turbine foundation was modelled with three different pile configurations of battered and vertical piles that are commonly applied in Dutch engineering practice. The basic pile group configuration and loads on the foundation are taken from representative projects from RHDHV. The analysis shows that in-line pile group efficiency is higher than predicted with proven analytical methods, possible optimization options can be created.

Model and project scope limitations prevented a one-on-one comparison of single piles and pile groups. Such a comparison is deemed meaningful as follow-up for the present study.

Soil movement within the complex pile groups showed different results for low displacements zones when using the three different pile configurations, lowering the influence of the group effect when using battered piles.

The 3D finite-element analysis clearly shows the positive effect of batter angle on translational stiffness. The rotation shows that the use of alternating batter angles result in cancellation of the clockwise rotation of vertical piles and counter-clockwise rotation of battered piles. The benefits of the batter angle with respect to a vertical pile foundation and rotation are quantified in the results part of this report.

Simplified relations between single pile and pile group efficiency are created. The relations showed different results for the positive effects of batter angles, which creates the need to investigate uncertain factors in later studies.

Contents

1	Introduction	1
1.1	Problem description	1
1.2	Scope and limitations	3
1.3	Research question	4
1.3.1	Primary research question	4
1.3.2	Secondary research questions	4
1.4	Methodology	6
1.4.1	Simplification of wind turbine	6
1.4.2	Single pile response	6
1.4.3	Group effect	7
1.4.4	Difference in p-multiplier	7
1.4.5	Alternating batter angle	8
1.5	Wind turbine manufacturers requirements	8
2	Literature review	10
2.1	Simplified single pile response under axial and lateral loading	10
2.2	Axially loaded piles for t-z curves	10
2.2.1	Simplified and elastic model	11
2.3	Lateral loaded piles for p-y curves	13
2.3.1	Non-linear spring model sand and clay	14
2.3.2	Limitations of API guidelines	15
2.3.3	Gapping of soil	16
2.4	Geometry of pile placement	16
2.4.1	Experimental pile spacing effect on lateral behaviour in clay	17
2.4.2	Load distribution in large pile groups under static and dynamic loading	18
2.4.3	Employment of P-multiplier in pile group analysis using depth dependency	18
2.5	Batter angle under static loading	19
2.5.1	Sand single pile lateral loading	19
2.5.2	Vertical combination loading for sand	20
2.5.3	Clay lateral loading	21
2.5.4	Vertical combination loading for clay	22
2.5.5	Consideration of batter angle in pseudo-static analyses of pile foundations	22
2.6	Influence of batter angle in a group	23
2.6.1	Group effect under change in batter angle	25
2.7	Finite element soil-structure interaction models	26
2.7.1	Modelling of stress-strain curves	26
2.7.2	Linear elastic modelling	26
2.7.3	Linear elastic perfectly plastic	27
2.7.4	Elasto-plastic strain hardening or softening	27
2.7.5	Failure criteria	28
2.7.6	Hardening soil small strain	28
2.7.7	Calculation of HS small parameters	29

2.8	Choice of pile use	30
2.8.1	Embedded beam	30
2.8.2	Interaction of pile-soil	32
2.8.3	Multi-linear soil modelling	32
2.8.4	Input parameters for embedded beams	33
2.8.5	Volume piles	33
2.9	Conclusion of literature study	34
3	Research layout	36
3.1	Engineering properties	37
3.1.1	Wind turbine specifications	37
3.1.2	Subsurface layering	38
4	Model setup	41
4.1	Influence of model plate	41
4.1.1	Loading scenario and constraints	42
4.2	Input parameters	43
4.2.1	Pile parameters for embedded piles	43
4.2.2	Pile parameters for volume pile	44
5	Static single pile response	45
5.1	Model size	46
5.1.1	Volume piles under horizontal loading conditions in x-y plane	47
5.1.2	Embedded beams under horizontal loading conditions in x-y plane	50
5.2	Mesh Coarseness	56
5.2.1	Model setup	56
5.2.2	Vertical piles	57
5.2.3	1:8 battered piles under positive loading	58
5.2.4	1:8 battered piles under negative loading	59
5.3	D-sheetpiling: single pile response evaluation	60
5.3.1	Model setup	60
5.3.2	Response of piles in D-sheetpiling for 35 kN horizontal loading conditions	61
5.3.3	The use of shell-factors in analytical modelling	61
5.4	Influence of batter angle on lateral stiffness for single piles	63
5.4.1	Influence of batter angle of lateral stiffness for mirrored two pile group	64
5.5	Conclusion of single pile static response	66
5.5.1	Model size	66
5.5.2	Mesh coarseness	66
5.5.3	D-sheetpiling reference	67
5.5.4	Influence of batter angle on lateral stiffness for single piles	67
6	Group efficiency of simplified group	68
6.1	General introduction	68
6.1.1	(Dynamic)P-multiplier	69
6.2	Group effect	70
6.3	Validation of group effect in Plaxis 3D	72
6.3.1	Parallel loading	72
6.3.2	Perpendicular loading	73

6.3.3	Skew loading	74
6.3.4	Conclusion of group validation	75
6.4	Parallel loading	76
6.4.1	Shadowing effect	76
6.5	Perpendicular loading	80
6.5.1	Edge effect	80
6.6	Conclusion: parallel and perpendicular loading	84
6.7	Skew loading	85
6.8	Conclusion of group efficiency of simplified fixed group	89
7	Vertical complex round foundation	92
7.1	Complex foundations	92
7.2	General validation of model for vertical piles	93
7.2.1	Influence of pile placement	94
7.2.2	Axial force distribution	95
7.2.3	Shear forces and stress distribution	98
7.2.4	Efficiencies	103
7.2.5	Displacement of the piles in x direction	105
7.2.6	Displacement of the piles in y direction	107
7.3	Conclusions of vertical complex round foundation	109
8	Influence of batter angle on complex round foundations	111
8.1	Definition of local axis	111
8.2	Axial force distribution	112
8.2.1	Vertical loading conditions	113
8.2.2	Combined loading conditions	113
8.3	Shear forces and stress distribution	117
8.3.1	Displacement of piles in x direction	121
8.3.2	Displacement of piles in y direction	121
8.4	Single pile response under batter angles	122
8.4.1	Efficiencies of battered pile groups	125
9	Comparison of vertical pile groups with alternating and 1:8 battered pile groups	127
9.1	Axial forces and displacements	127
9.2	Q12 shear forces and x displacements	129
9.3	Q13 shear forces and y displacements	130
9.4	Conclusion of three different pile group configurations	133
10	Pile group validation	135
10.0.1	Group efficiency for D-sheetpiling	135
10.1	Structural response	137
10.1.1	Vertical complex pile group	138
10.1.2	1:8 Battered piles	139
10.1.3	Alternating battered piles	139
10.1.4	Single vertical pile moment versus D-sheetpiling	140
10.2	Conclusion of pile group validation	141
11	Conclusion	144

12 Recommendations for further research	147
References	i

List of abbreviations

API	American Petroleum Institute
CTC	Centre to centre
FEM	Finite Element Method
HSsmall	Hardening Soil small strain
RHDHV	Royal HaskoningDHV

List of symbols

<u>Symbol</u>	<u>Property</u>	<u>Unit</u>
A	Area of pile (foot)	(m ²)
c	Cohesion	(kN/m ²)
c'_{ref}	Effective cohesion at reference stress level	(kN/m ²)
c_u	undrained shear strength	(kN/m ²)
d	Thickness	(m)
D	Diameter	(m)
Dr	Relative density	(-)
e	Void ratio	(-)
E	Young's modulus	(kN/m ²)
E_{50}^{ref}	Secant stiffness modulus in standard drained triaxial test at reference stress level	(kN/m ²)
EA	Axial stiffness	(kN)
EI	Bending stiffness	(kNm ²)
E_{oed}^{ref}	Tangent stiffness modulus for primary oedometer loading at reference stress level	(kN/m ²)
E_p	Young's modulus pile	(kN/m ²)
E_{ur}^{ref}	Unloading/reloading stiffness at reference stress level	(kN/m ²)
F	Force	(kN)
$F_{s;l;group}$	Single pile response in group	(kN)
$F_{s;l;single}$	Single pile response	(kN)
G	Shear modulus	(kN/m ²)
g	Gravity constant	(m/s ²)
G_0	Initial shear modulus	(kN/m ²)
G_s	Secant shear modulus	(kN/m ²)
G_t	Tangent shear modulus	(kN/m ²)
G_{ur}	Unloading/reloading shear modulus	(kN/m ²)
H_{ult}	Ultimate lateral displacement	(m)
I	Moment of inertia	(m ⁴)
K	Power plasticity dependent OCR relation	(-)
K_p	Passive earth pressure coefficient	(-)
K_0^{nc}	K_0 value normally consolidated	(-)
L	Pile length	(m)
m	Power stress level dependency of stiffness	(-)
M_p	Moment of plastic hinge	(kNm)
n	Soil resistance	(kN/m ³)
Nc	Bearing capacity factor	(-)
Ng	Group bearing capacity factor	(-)
n_{ki}	Subgrade modulus	(-)
N_{max}	Maximum axial force	(kN)
Nq	End bearing factor	(-)
O_{pile}	Circumference of pile	(m)

OCR	Over consolidation ratio	(-)
pf	Soil pressure at failure	(kN/m ²)
PIC	Percentage improvement lateral capacity	(%)
Ps	Shear capacity	(-)
P_{uh}	Ultimate lateral resistance	(kN)
qc	Tip resistance	(MPa)
R	Radius	(m)
r_m	Influence radius	(m)
s	Shape factor from cross section of pile footing	(-)
s	Pile spacing	(m)
σ_{vo}	Initial vertical stress	(kN/m ²)
SL	Deviatoric stress level in the soil	(kN/m ²)
s_u	Undrained shear strength	(kN/m ²)
$T_{bottom\ max}$	Maximum skin friction at pile foot	(kN/m)
$T_{top\ max}$	Maximum skin friction at pile head	(kN/m)
u	Deflection	(m)
V	Vertical loading	(kN)
w	Axial (compressional) displacement	(m)
y_c	Characteristic distance for mobilization	(m)
z	Depth	(m)

<u>Symbol</u>	<u>Property</u>	<u>Unit</u>
α	Undrained shear strength factor	(-)
α	Rheological coefficient depending on wear level	(-)
α_s	Pile class factor	(-)
β	Batter angle	(°)
β_s	Pile foot shape factor	(-)
$\Delta\sigma_{v0}$	Vertical stress increment	(kN/m ²)
ϵ	Strain level	(%)
γ	Volumetric weight	(kN/m ³)
γ	Shear strain	(-)
$\gamma_{0.7}$	Shear strain level at which G_0 is reduced to 72.2%	(-)
γ_{dry}	Dry volumetric weight	(kN/m ³)
γ_{sat}	Wet volumetric weight	(kN/m ³)
ϕ	Friction angle	(°)
ψ	Dilatancy angle	(°)
ρ	Density	(kN/m ³)
σ_{vo}	Vertical stress	(kN/m ²)
η	Pile group efficiency	(-)
ν	Poisson's ratio	(-)
χ	Compactibility	(-)
ξ	Spatial variability	(-)

Symbols Finite element modelling

Symbol	Property
T_{max}	Maximum shear stress
t^{skin}	Skin resistance of embedded beam
t_0^{skin}	Initial skin resistance of embedded beam
δt^{skin}	Force increment at integration points of embedded beam
T^{skin}	Material stiffness matrix of the interface element of an embedded beam
Δu	Relative displacement between soil and embedded beam
t_s	Shear stress in axial direction
t_n	Normal stress in horizontal direction
t_t	Normal stress in horizontal direction
K_s	Elastic shear stiffness
K_n	Elastic normal stiffness in horizontal direction
K_t	Elastic normal stiffness in horizontal direction
u_p	Beam displacement
u_s	Soil displacement
f^{skin}	Skin friction beam
f_0^{foot}	Initial force in beam foot spring
Δf_{foot}	Force increment in beam foot spring
F_{foot}	Material stiffness matrix of spring element at pile foot
G_{soil}	Shear modulus of the soil
$\gamma_{xy}, \gamma_{yz}, \gamma_{zx}$	Shear strain in xy, yx and zx direction
$\epsilon_x, \epsilon_y, \epsilon_z$	Strain in x, y and z direction
ϵ_v	Volumetric strain
$\sigma_x \sigma_y \sigma_z$	Stress in x, y and z direction
$\tau_{xy}, \tau_{xy}, \tau_{xy}$	Shear stress in xy, yz and zx direction

List of Figures

1	Definition of load direction and batter angle for horizontally loaded piles. . .	1
2	Pile movement under combined loading direction	6
3	Group of influence for the group effect.	8
4	Non-Linear approximation and softening behaviour of clay and bi-linear response of piles in sand under axial loading conditions	11
5	Failure modes for lateral capacity calculations. Murugan et al. [2017] . . .	13
6	Simplified p-y curve for nc clay and sand following API RP2GEO	15
7	Group effect of piles: shadowing effect, edge effect and gapping Rollins et al. [1998]	16
8	Influence of column(i) and row(j) size, load in direction of i Swallow and Sheil [2021]	17
9	The left figure represents the best fit curve and data from the first row with back-figured multipliers. The second figure contains the best fit and back-figured multipliers for second and third row Rollins et al. [2006] . . .	18
10	Influence of lateral capacity in regards to batter angle and density state Hazzar et al. [2017]	20
11	Influence of lateral capacity in regards to batter angle, density and vertical loading for sand Hazzar et al. [2017]	21
12	Influence of lateral capacity in regards to batter angle, density and vertical loading for clay Hazzar et al. [2017]	22
13	Overview of influence of vertical dead load on sandy soil symmetric battered pile groups Zhang et al. [2002]	24
14	Influence of batter angle on different configurations in battered and vertical piles Singh and Arora [2017]	25
15	Different type of modelling options Brinkgreve [2021a]	26
16	Shear modulus reduction and damping dependence on cyclic shear strain for NC and slightly OC clay Vuetic and Dobry [1991]	29
17	Stiffness of embedded interface along the pile	31
18	Embodiment of pile in soil elements Smulders et al. [2019]	32
19	General layout of experimental study in Plaxis 3D	36
20	Cross-section of representative wind turbine foundation foot	37
21	Top-view of representative wind turbine foundation layout	38
22	Schematic subsurface layering	39
23	Tip resistance corresponding to soil description	44
24	Influence of vertical dead load and lateral loading on radial and axial force distribution	46
25	Influence of loading on mesh size in x-y-direction for volume piles initially 16m deep with a mesh of 24m deep	47
26	Influence of loading direction on mesh size in z-direction for volume piles initially 24 m deep	48
27	Influence of positive loading direction on mesh size in x direction for volume piles	49
28	Influence of negative loading direction on mesh size in x direction for volume piles. The stress field is turned 180 degrees to compare the active and passive side	50

29	Influence of loading on mesh size in x-y-direction for new and old embedded beams initially 16 m deep with a mesh of 24 m deep	51
30	Influence of loading on mesh size in x-y-direction for new and old embedded beams initially 16 m deep with a mesh of 24 m deep	52
31	Influence of loading on mesh size in x-y-direction for new and old embedded beams initially 16 m in length with a mesh of 24 m deep under positive loading conditions	53
32	Influence of loading on mesh size in x-y-direction for new and old embedded beams initially 16 m in length with a mesh of 24 m deep under negative loading conditions. The stress field is turned 180 degrees to compare the active and passive side.	54
33	Influence of local refinement of 0.2 to element sizes surrounding the piles. .	57
34	Horizontal displacement for single pile under 35 kN horizontal loading conditions with different global and local coarseness for vertical piles	58
35	Horizontal displacement for single pile under 35 kN horizontal loading conditions with different global and local coarseness for 1:8 battered positive loaded piles	58
36	Horizontal displacement for single pile under 35 kN horizontal loading conditions with different global and local coarseness for 1:8 battered negative loaded piles	59
37	Model setup for D-sheetpiling	60
38	Output of d-sheetpiling for pile without head restrictions and 35 kN loading	61
39	Influence of lateral response in a group versus single pile lateral response .	63
40	Application of negative and positive batter angles in mirrored configuration	64
41	Influence of batter angle on simple mirrored two pile group	64
42	Schematic 2D representation of a wind turbine foundation. Loading is present from lower bottom to top of the figure.	68
43	Group effect of piles: shadowing effect, edge effect and gapping Rollins et al. [1998]	69
44	Influence of lateral response in a group versus single pile lateral response .	69
45	Influence of lateral response in a group versus single pile lateral response .	71
46	Testing scenario of parallel loading on ctc dependence	72
47	Testing scenario of parallel loading on pile placement	73
48	Testing scenario of perpendicular loading on ctc dependence	73
49	Testing scenario of perpendicular loading on pile placement	74
50	Testing scenario of skew loading for ctc dependence	74
51	Testing scenario on skew loading for pile placement	75
52	Parallel loading condition	76
53	Influence of pile efficiency in regards to pile location for parallel loading .	78
54	Influence of pile efficiency on pile number in skew direction	78
55	Influence of pile efficiency per pile group on pile number for parallel loading	79
56	Perpendicular loading condition	80
57	Influence of pile efficiency in regards to pile location for perpendicular loading	82
58	Influence of pile efficiency on pile number in perpendicular direction	83
59	Influence of pile efficiency per pile group on pile number for perpendicular loading	83
60	Skew loading condition	85

61	Influence of pile efficiency in regards to pile location for skew loading	86
62	Influence of pile efficiency on pile number in skew loading direction	87
63	Influence of pile efficiency per pile group on pile number for skew loading	87
64	Depth influence of ϵ_{xx} with increase in ctc spacing	90
65	Overlap of soil wedges before and after turning	91
66	Initial conditions of complex wind turbine foundation layout.	93
67	Initial loading conditions of complex wind turbine foundation.	94
68	Behavior of piles on different locations.	95
69	Uz displacements under combined lateral and vertical loading	96
70	Maximum axial forces per pile for different loading conditions	98
71	Ux displacements under combined lateral and vertical loading	99
72	σ_{xx} displacements under combined lateral and vertical loading	100
73	Q12 forces and Ux displacements under combined lateral and vertical load- ing	101
74	Q13 forces and Uy displacements under combined lateral and vertical load- ing	102
75	Q12 efficiency along analysed piles in complex vertical pile group	103
76	Q13 efficiency along analysed piles in complex vertical pile group	104
77	Q12 efficiency along analysed piles in complex vertical pile group	104
78	Effect of pile location on displacement and bending moment. Maximum and minimum displacement $1.55 * 10^{-3}$ m and $0.02 * 10^{-3}$ m for complex group. Maximum and minimum bending moment at 51.9 kNm and -16.5 kNm	105
79	Effect of group size and ctc distance on pile moment	107
80	U_y movement scaled 5000 times	108
81	Local axis configuration	112
82	Layout of alternating batter angles	112
83	Uz displacements under combined lateral and vertical loading conditions for 1:8 batter angle and alternating vertical -1:8 batter angle	115
84	Maximum axial forces per pile for different loading conditions under 1:8 and alternating batter angles	116
85	Ux displacements under combined lateral and vertical loading	117
86	σ_{xx} displacements under combined lateral and vertical loading	118
87	Maximum shear forces per pile for different loading conditions under 1:8 and alternating batter angles	119
88	Maximum shear forces per pile for different loading conditions under 1:8 and alternating batter angles	120
89	Effect of pile location on displacement for 1:8 and alternating battered pile groups. Maximum displacement of $1.45 * 10^{-3}$ and $1.44 * 10^{-3}$ m.	121
90	Effect of pile location on displacement for 1:8 and alternating battered pile groups. Maximum displacement of $1.5 * 10^{-4}$ and $2.2 * 10^{-4}$ m	122
91	Reference single pile response with true loading direction	122
92	Reference single pile response with true loading direction	123
93	Single pile response of 1:8 battered piles with approximated rotation fixed pile head conditions. Pile 15 represents the negative batter angle	124
94	Q12 efficiency for 1:8 and battered pile groups	125
95	Comparison of three different pile configurations for axial forces and uz displacement	127

96	Comparison of three different pile configurations for Q12 shear forces and ux displacement	128
97	Comparison of three different pile configurations for Q12 shear forces and ux displacement	129
98	Comparison of three different pile configurations for Q13 shear forces and uy displacement	130
99	Comparison of three different pile configurations for Q13 shear forces and uy displacement	131
100	Output of D-sheetpiling for pile with head restrictions and horizontal loading of 20 kN	135
101	Reading the bending moments in the local coordinate system	137
102	Comparison of vertical pile bending moment over depth for 3 bending moment directions	138
103	Comparison of 1:8 pile bending moment over depth for 3 bending moment directions	139
104	Comparison of alternating pile bending moment over depth for 3 bending moment directions	140
105	Comparison of Plaxis 3D and d-sheetpiling	141

List of Tables

2	Table of ground parameters per layer using Hardening Soil small strain stiffness constitutive model	40
3	Model setup parameter for additional structural support elements	42
4	Weak interface material to lower influence of plate shear forces	42
5	Skin resistance per layer for multi-linear axial resistance calculations	43
6	Empirical relation of Menard subgrade modulus and the tip resistance of the soil	61
7	Influence of ctc distance and batter angle on lateral displacement of 2 pile mirrored pile group	65
8	Maximum shear forces per pile under combined horizontal and vertical loading conditions of 20 kN and 500 kN per pile respectively for parallel loading.	76
9	Maximum shear forces per pile under pure horizontal loading conditions of 20 kN for parallel loading	77
10	Maximum shear forces per pile under combined horizontal and vertical loading conditions of 20 kN and 500 kN per pile respectively for perpendicular loading	80
11	Maximum shear forces per pile under pure horizontal a loading conditions of 20 kN for perpendicular loading.	81
12	Maximum shear forces per pile under combined horizontal and vertical loading conditions of 20 kN and 500 kN per pile respectively for skew loading.	85
13	Maximum shear forces per pile under pure horizontal a loading conditions of 20 kN for skew loading	85
14	Comparison of axial forces for scenario with 560 kN horizontal loading and without horizontal loading	96
15	Pile numbers equivalent to maximum U_x displacement and Q12 shear forces under combined loading conditions	101
16	Pile numbers equivalent to maximum U_y displacement and Q13 shear forces under combined loading conditions	102
17	Overview of (alternating) battered complex group axial response	113
18	Q12 shear forces and x displacement for 1:8 and alternating pile groups	120
19	Q13 shear forces and y displacement for 1:8 and alternating pile groups	121
20	Overview of displacement and axial force distribution for three different pile group configurations	134
21	Overview of efficiency factors for displacements	136
22	Summarizing table for the use of battered piles in complex wind turbine foundations	146

1 Introduction

During the last decades, the depletion of hydrocarbons and the insecurity of supplies resulted in the search for alternative energy resources. One of the sustainable alternative resources is the wind turbine. Technological advances over the last decades have made possible a steady increase in the size of the wind turbines, lowering the levelized cost of energy. In order to counter the increasing static (gravity, structural weight) and dynamic wind forces, the radius of the substructure needs to be adapted. To be able to design a more efficient and better suited wind turbine, a better understanding of the influencing parameters is needed.

1.1 Problem description

The use of piled foundations results in large amounts of variables that can influence the horizontal stiffness of a substructure, the primary factor of influence being the soil. Pile properties are secondary and geometry third. Design criteria for the geometry such as the batter angle are assumed and sometimes checked with 3D analytical software. These methods combine various proven analytical models for the behavior of horizontally loaded piles. All these models include some conservatism. The underlying interaction mechanisms are not well understood, and the use of batter angle as a generalised method to increase horizontal stiffness needs further verification. To understand the definition of the batter angle, the following figure is used to explain two scenarios of using a batter angle which depend on the loading direction. This representation shows only the application of horizontal load with the decomposition of forces in axial and radial direction.

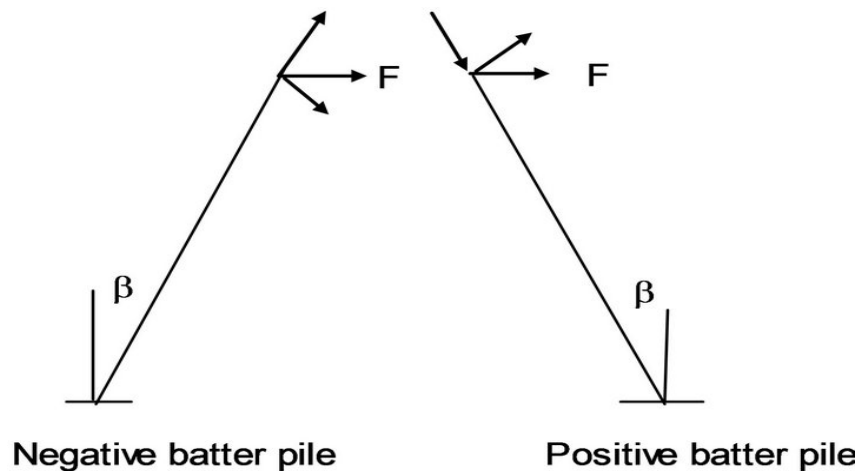


Figure 1: Definition of load direction and batter angle for horizontally loaded piles.

Most of the current methodology exists from papers from around 2000 such as *Veerstijfheid Paalfunderingen* by Everts [1998] or single pile 1D/2D programs, simplifying dynamic and lateral responses. Normally the dynamic response of the soil is assumed to be stiffer, while the use of battered piles is also assumed to create a stiffer translational response. As the pile groups become more complex by enlarging groups or applying batter angles, the combination of all these assumptions may lead to an inefficient design. This makes it worthwhile to investigate the integral foundation-soil interaction in one single model.

In order to understand how single piles are behaving in regards to pile groups used in wind turbine designs, a single pile will be evaluated in regards to the horizontal and vertical response for simplified (in-line) and complex (wind turbine) pile groups. The efficiency of the pile group with respect to the response of a single pile is determined as follows:

$$Efficiency\ pile\ group = \frac{F_{\bar{s};l;group}}{F_{\bar{s};l;single}} < 1 \quad (1)$$

This research will focus on better understanding round pile foundation interaction in regards to effect of batter angle on the response to horizontal loading conditions in a round foundation. This researched will be performed with Plaxis 3D software.

1.2 Scope and limitations

The problem as stated has been studied for decades from as early as Novak [1974] to more recent studies such as Zhang et al. [2021], especially in square or rectangular pile groups under horizontal and combined horizontal and vertical loading conditions. As the foundation of wind turbines are generally created in a circular way with piles on the outer edges, this research will concentrate on the group behaviour of battered piles in circular groups. The foundation of the wind turbine is generally made up of a stiff concrete base, the piles are attached to this base. As this problem comprises several sections, a simplified approach is adopted as stated by the title. Expansion of the topic in regards to the other sections can be done in later research. As the problem results in large amounts of calculations and influencing parameters, simplifications need to be applied to ensure the thesis can be completed in the limited amount of time. The following simplifications will be made:

- Geometry
 - An available foundation model with 28 piles is used. This model is previously, in a Royal HaskoningDHV (RHDHV) project, validated to withstand the loading conditions specified by the wind turbine manufacturer.
 - It is assumed that all the forces are carried by the piles alone, influence of the foundation in regards to base shear stresses and passive resistance are minimized.
- Structural integrity
 - The model will only consider relatively small strain deformation. Limit states will not be reached.
 - The connection between the piles and the foundation base is infinitely stiff.
 - Material properties of structural elements are homogeneous.
- Soil parameters
 - A typical Dutch subsurface layering with validated soil parameters is used. In-depth assessment of the soil parameters is not part of this study.
 - The output of the numerical model will be evaluated by a single pile analytical model generally used to assess the movement of pile groups.
 - Drained soil parameters are applied.
- Loading conditions
 - A (static) horizontal load is applied, representing the maximum operational loads (which are determined by the wind turbine manufacturer).
 - Axial displacements of the piles are not analysed specifically. Axial load displacements will be verified by comparison with values from engineering practice for the specific piles used.
 - Combined horizontal and vertical loading conditions will be evaluated.
 - The self weight of the tower and the foundation are always present and will be applied in each scenario.

1.3 Research question

1.3.1 Primary research question

The primary research question is as follows:

" What is the effect of battered piles on the lateral response of wind turbine foundations under horizontal loading conditions using numerical software "

This research question will be analysed in Plaxis 3D which can model pile groups in Finite Element Method (FEM). The results will be verified in a step-by-step approach. Results of the 3D FEM analysis will also be compared with the results of 2D analytical calculations to determine if and where optimizations can be found.

1.3.2 Secondary research questions

In order to answer the research question, secondary research questions are formulated to help answer the primary question. The first section is formulated to answer the influence of current use of non-linear soil modeling and setup of the used models. The second set of questions tests the hypotheses, explained in the methodology, and comprises the parameters of influence for group response. The last section tests the inter-relational effects of the parameters of influence in regards to the analytical and numerical program.

1. Description of physical effects of horizontal loading conditions on concrete piles in Plaxis 3D
 - (a) What is the difference in behaviour for the different types of pile FEM modelling (volume pile, embedded beam) options when applying horizontal loading conditions on the piles?
 - (b) Which physical parameters (soil type) are resulting in different lateral behaviour in regards to physical modelling?
 - (c) How does the batter angle change the response or translational stiffness for a single pile under horizontal or combined horizontal and vertical (dead) loading?
 - (d) Is there a difference in single pile lateral response between the analytical model and numerical model?
 - (e) Where does the difference between the two models come from?
2. Foundation response in 3D. Used for simplified group and complex group response
 - (a) What is the influence of the batter angle of a pile group under horizontal and combined horizontal and vertical loading on the translational stiffness?
 - (b) Are there model limitations that can have a significant effect on calculation results?
 - (c) Is the response in line with expectations in regards to single pile response?
3. The suitability of the used 3D modelling program for groups
 - (a) Is the pile group efficiency in the 3D FEM model comparable to the pile group efficiency as described with analytical models?

4. Inter relational effect of parameters

- (a) Can a simplified relation be developed between the use of batter angles in complex round foundations and the horizontal translational stiffness?
- (b) Can this relation be adopted to use in the current 2D analytical models, to approach a more realistic 3D FEM pile group?

1.4 Methodology

The approach and research that is used can be divided into two sections, namely: how do the results of 3D FEM analysis compare with the results of 2D analytical calculations (with Menard horizontal subgrade parameters and Reese and Impe [2002] pile group efficiency). The second section is the influence of lateral stiffness in group modelling using Plaxis 3D in regards to the use of batter angles. The following subsections will explain which steps need to be taken, to answer the secondary research questions.

1.4.1 Simplification of wind turbine

In order to assess the influence of lateral and vertical loading conditions, the influence of wind turbine tower will be neglected. The model will analyse a lateral load roughly at ground-surface level as visible in figure 2, while the vertical load will be applied precisely in the centre of the circular foundation.

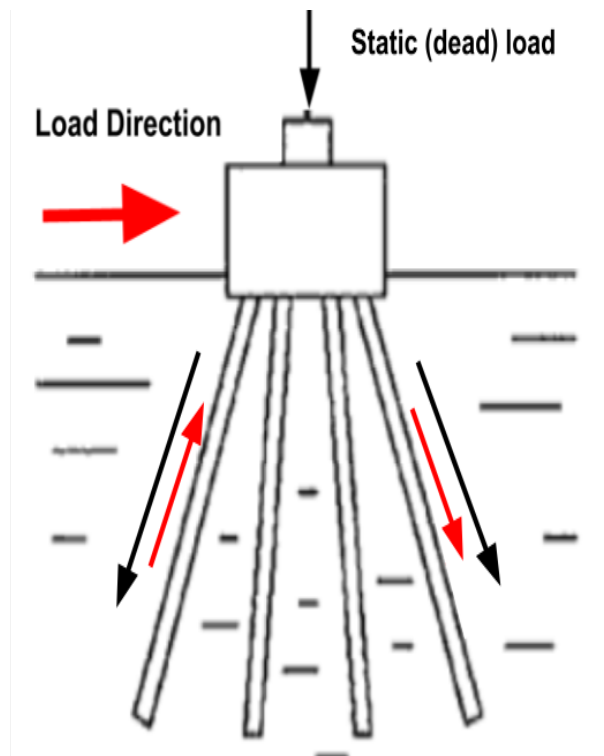


Figure 2: Pile movement under combined loading direction

The visualization is not on scale and it is noted that in operational conditions the changes in axial forces in the piles caused by horizontal loads are relatively small compared to axial loading from the self weight. In operational conditions, all piles remain under a (net) compression load.

1.4.2 Single pile response

In order to understand the behaviour of pile groups with battered piles and combined horizontal and vertical loading, the following steps will be taken to analyse single simplified response. The piles with their properties are taken from an existing project, proven to have sufficient lateral and vertical capacity. The single pile will be analysed for translational stiffness.

- Setup of vertical pile under lateral, vertical and combined lateral and vertical loading conditions in 3D Plaxis software.
- Setup of pile under a batter angle with lateral, vertical or combined lateral and vertical loading conditions in 3D Plaxis software.
- Check outcome with widely used 2D analytical software

These testing scenario's are also present when considering group response, but this will give an insight in simplified approach as well as create a baseline response for the schematic Dutch subsurface. The response of piles in groups in later sections can be compared with this simplified approach, to validate the influence of group effect or batter angle.

1.4.3 Group effect

Pile group efficiency can be described in 3 different effects, namely: shadowing effect, edge effect and wall effect. In a pile ring group, wall effect and shadowing effect are dominant. Edge effects play a minor role. In a pile ring group, wall effect and shadowing effect vary for each pile position. As a result, the load that is transferred to the subsurface differs for each pile. These differences are determined by looking at the shear forces that develop (in the horizontal plane) at pile head level. The shear force that develops (per pile) as compared to the shear force that develops in a single pile is called the p-multiplier. In this study, the main focus is on the relative efficiency of the piles within the group. The absolute efficiency (reduction of the lateral reaction force that the piles receive from the surrounding ground mass due to group effects) is not quantified in detail.

The factors of influence for the p-multipliers can be analysed in the three sections stated earlier. For the simplified group, both horizontal as well as combined loading conditions are used. For the real case scenario, only the combined loading conditions are used. This setup ensures that for every step taken, only one parameter is changed. The load is applied on a stiff plate connected to the pile heads, which results in a zero initial applied moment.

- Setup of vertical pile group under lateral, vertical and combined lateral and vertical loading conditions in Plaxis 3D software.
- Setup of pile group under different batter angles under lateral, vertical and combined lateral and vertical loading conditions in Plaxis 3D software.

The group effect can be compared to proven literature in order to asses the behaviour of pile groups. The behaviour of pile groups is generally tested under a set lateral displacements, giving the change in soil resistance in terms of maximum loading capacity and avoiding the influence of bending resistance of the pile. The testing scenario with an applied load cannot be compared directly to literature, but shows a good approximation of the group behaviour.

1.4.4 Difference in p-multiplier

As explained earlier, the influence on placement of piles in regards to loading direction can result in three different pile group interaction situations (wall, shadowing and edge). For the wall-formation and edge-effect piles, the p-multiplier will be higher. This is found due to the fact of:

- Wall effect: The increase in surface area as the formation of the wall effect results in larger load carrying capacity.
- Edge effect: piles on the edge of the groups have an even larger undisturbed soil mass surrounding the pile.

For the shadowing effect, the load carrying capacity will be lower. These piles are in a zone where pile-soil-pile interaction is the strongest, effectively reducing the horizontal subgrade reaction of the soil. Each of these effects are visible in the green zone, the wall formation, and the red zone, the edge effect and shadowing schematically illustrated in figure 3. Both groups are present two times, as the groups are also on their mirrored location. As the edge effect should be lower in a circular foundation in regards to square or rectangular foundations, this effect may be minimal. Generally speaking, the perpendicular zone (green zone) takes up more of the shear forces than the trailing zone (red zone).

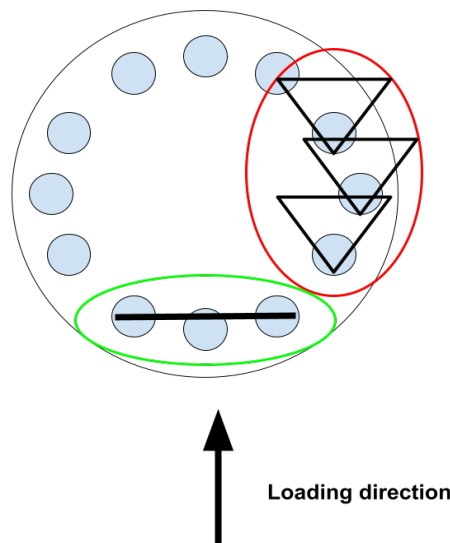


Figure 3: Group of influence for the group effect.

1.4.5 Alternating batter angle

The use of combined vertical and battered piles, alternating piles, can result in an increase or decrease in the described effects. The alternation for the red group in regards to section 3 can result in a larger wall formation and less influence of the shadowing effect. In contrast, this can also lead to a less desirable effect in comparison with only using battered piles. The influence of the group will be assessed on single pile level and compared to the simplified groups

1.5 Wind turbine manufacturers requirements

The demands for wind turbine foundations of the manufacturers are very different, resulting in different 'focus points'. During the thesis several conversations with a single manufacturer, Enercon, are made to understand the requirements for the foundation. The conversations lead to the following results:

- Dynamic application of loading may not be necessary, simplification to static horizontal loading conditions should result in the same response for the foundation.

- Limiting requirements are primarily lateral stiffness. The rotation of the foundation due to horizontal loading is less important due to the small scale.
- Rotation and lateral stiffness are analysed separately.

The requirements are only valid for Enercon and may be different for other suppliers. It is also stated that the lateral stiffness on its own again contributes to a moment being created, which shows that separate assessment oversimplifies the pile group response. This is not taken into account.

2 Literature review

The problem description comprises in general of three sections, namely:

- Which modelling parameters describe the physical behaviour of piles under horizontal loading in regards to lateral stiffness?
- How does the batter angle change this behaviour?
- How does grouping of the piles result in different lateral stiffness?

An initial scan of sources did not provide literature that describes in further detail the behaviour of a pile ring wind turbine foundation under lateral loading (analytical or finite-element). The aim of the literature survey was therefore changed to the following:

- Provide theoretical background on the modelling of laterally loaded piles.
- Support the choice of a model to analyse the behaviour of a pile ring wind turbine foundation.

2.1 Simplified single pile response under axial and lateral loading

In the current approach, the company uses a basic, solitary pile 2D model based on Menard ground parameters for piles. Group efficiency is accounted for with a Reese and Impe [2002] analysis. P-y curves are sometimes used if a more advanced 3D analytical model is developed. This is usually only done in challenging project conditions, challenging ground conditions in combination with strict wind turbine specifications.

The response of a load on a vertical pile results in two different equations, namely the lateral response (p-y curves) and the axial response (t-z) curves. The capacity due to combined loading cannot be directly interpreted, thus the combined conditions need to be investigated separately. Officially the American Petroleum Institute (API) RP2A is constructed for offshore platforms, but most of the basic design solutions and considerations can be applied to onshore foundations. The models mostly use a non continuum (Winkler) approach, which is the result of the use of different soil layers.

2.2 Axially loaded piles for t-z curves

First approximations when using analytical models is to implement two different simple solutions using a distributed (non-continuous) spring model: a theoretical load-transfer curve describing the unit skin friction transferred to the soil and the second method the simplified analytical method describing the soil shaft friction with a logarithmic relation in regards to radial displacements [Zhang and Zhang, 2012]. The first model thus uses a linear friction-displacement response, while more recent models use a non-linear radius depended response.

An example of the linear model is visible below from the API for axial response of a pile. As stated above, this model does not have radial dependence.

$$\tau_{sf} = \alpha s_u(\text{clay}) \quad (2)$$

$$\tau_{sf} = \beta \sigma'_{v0} < \tau_{s,lim}(\text{sand}) \quad (3)$$

The second linear part is visible as the skin friction (τ) reaches a maximum value $\tau_{s,lim}$. Where the α factor represents the undrained shear strength factor, dependent on the effective overburden pressure. The β factor, shaft friction factor, is normalized to the soil density and soil type. The behaviour of the single pile response is visible in figure 4. This figure also clearly shows that small displacements (small strains) already fully mobilizes the skin friction. After the maximum is reached, a range of possible residual shear strength factors is formulated.

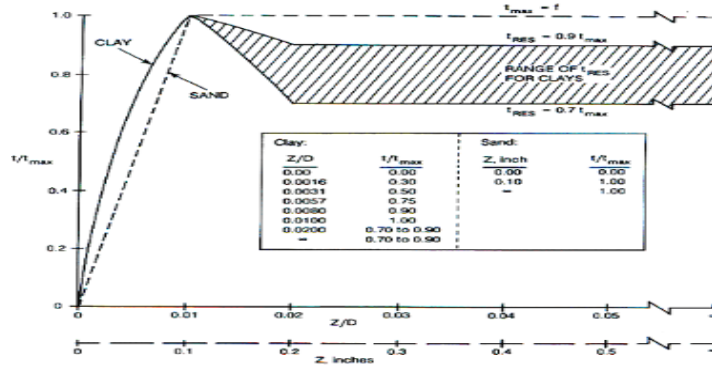


Figure 4: Non-Linear approximation and softening behaviour of clay and bi-linear response of piles in sand under axial loading conditions

As it is stated by several curves from the API, the pile tip load displacement curve (Q - z) is only mobilized fully after a displacement of $0.1 \cdot \text{Pile diameter}(D)$. This thus seems to have less influence on the total response of the pile and may be discarded in this simplified model.

2.2.1 Simplified and elastic model

Models such as Menard, but also Reese and Impe [2002] use a simplified approach in order to check the stress-strain behaviour. Validation of the models and description of the working principles can be found online.

A simplified model can be made to create a general understanding of the response,

The downward load (F) and upward forces (shear stress) are balanced by:

$$\frac{dF}{dz} = -\pi D \tau_s \quad (4)$$

With F the load, z the displacement in z direction, D the diameter of the pile and τ_s the skin friction. The compatibility of the pile can be described by

$$\frac{dw}{dz} = -\varepsilon_z \quad (5)$$

With w the compaction of the pile in z direction, ε_z the strain in z direction. This results in the compressional effects inside the pile. The elastic behaviour can then be modelled as

$$F = (EA)_p \varepsilon_z \quad (6)$$

With $(EA)_p$ the axial stiffness of the pile. The governing equation becomes

$$\frac{d^2w}{dz^2} = \frac{\pi D}{(EA)_p} \tau_s \quad (7)$$

A fully elastic solution for flexible piles is given below. The compatibility is given by the equation, where the shear modulus is inserted Pisanò [2020a]:

$$w = \int_R^\infty \gamma dr \approx \int_R^{r_m} \frac{\tau}{G} dr = \int_R^{r_m} \frac{R}{r} \frac{\tau_s}{G} dr \quad (8)$$

With γ the volumetric weight of the soil, G the shear modulus, R the radius of the pile and r the radius of influence. The implementation of the t-z curve at a radial distance:

$$w = \frac{\tau_s R}{G} \ln \left(\frac{r_m}{R} \right) \quad (9)$$

The governing equation becoming:

$$\frac{d^2 w}{dz^2} = \frac{2\pi G}{\ln \left(\frac{r_m}{R} \right) (EA)_p} w \quad (10)$$

This model also has several boundary conditions, which are needed to solve the integrals. $-(EA)_p \frac{dw}{dz} \Big|_{z=0} = V_{\text{head}}$, as the applied force must equal the vertical force at zero displacement. The second condition is given by $(EA)_p \frac{dw}{dz} \Big|_{z=L} = \frac{4R_{\text{base}} G_{\text{base}}}{1-\nu} w \Big|_{z=L}$ This represents the punching on the elastic halfspace, the zone to which elastic deformation takes place.

2.3 Lateral loaded piles for p-y curves

The lateral response of a single pile is given by so called p-y curves. In comparison with the axial response, the lateral response takes into account three different fixed-head failure modes in order to asses the input for the p-y curves. The head is fixed, as it is assumed that in a later stadium the piles are connected to a rigid pile cap in order to transfer the load to the piles. The failure modes are given below, which also show plastic hinges at the head. This may be the case when the fixed head condition cannot be applied, as the stiffness of the connection is too low.

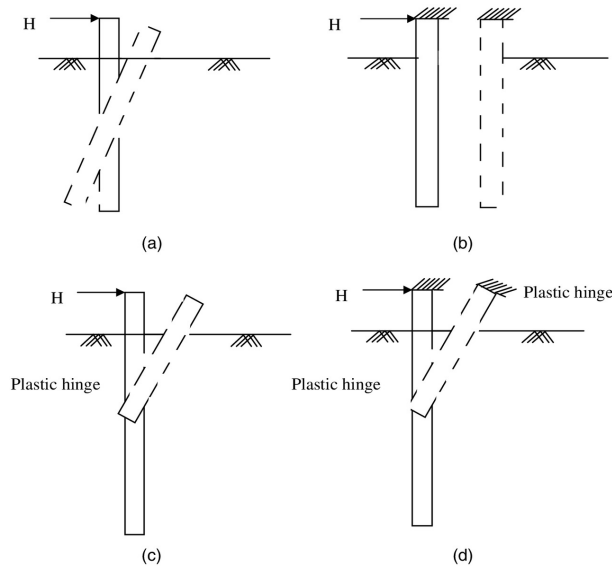


Figure 5: Failure modes for lateral capacity calculations. Murugan et al. [2017]

For each of the failure modes in clay, two different zones can be visible. The shallow failure mechanism results in gapping and sliding. This zone is described as roughly $3 \cdot D$ (diameter) deep, while the deep zone results in fan zoning surrounding the piles. These effects result in a depth dependency, till a maximum of $9Ds_u$ is reached with s_u the undrained shear strength.

For sand this effect is not visible, several methods are used and stated. The simplified method from Barton, Broms is given below:

$$P_f = DK_p^2 \sigma'_v = DK_p^2 \gamma' z \quad (11)$$

With the earth pressure coefficient (passive) given as

$$K_p = \frac{1 + \sin(\phi)}{1 - \sin(\phi)} \quad (12)$$

With D the diameter of the pile, σ'_v the effective vertical stress, γ' the dry volumetric weight of the soil and z the depth of calculation. It is stated that some of the problems can be analytically solved by using the simplified linear relation $P_f = nDz$ where n is given by $\gamma \cdot K_p^2$ with γ the volumetric weight, D the diameter and z the depth of calculation for homogeneous sand and $Nc \cdot k_{su}$ for a clay type material with Nc the bearing capacity factor. The failure modes stated in figure 5 then apply to different design charts resulting in the ultimate horizontal capacity. The examples for lateral translation and two hinged fixed head is given below.

$$H_{ult} = \bar{P}_f L = \frac{1}{2} n L D L \Rightarrow \frac{H_{ult}}{n D^3} = \frac{1}{2} \left(\frac{L}{D} \right)^2 \quad (13)$$

and

$$\frac{H_{ult}}{n D^3} = \frac{6^{2/3}}{2} \left(\frac{M_p}{n D^4} \right)^{2/3} = 1.65^{2/3} \left(\frac{M_p}{n D^4} \right)^{2/3} \quad (14)$$

Where H_{ult} the ultimate horizontal resistance, D the diameter of the used pile, n the soil resistance per unit depth, L the length of the pile and M_p the plastic pile head moment.

A more complex method is using the lateral springs for each section. In order to create this simplified model, the following equations are given by Pisanò [2020b]:

Moment equilibrium is given by

$$\frac{d^2 M}{dz^2} = -P \quad (15)$$

With M the bending moment and P the lateral load.

Compatibility

$$\chi = \frac{d^2 y}{dz^2} \quad (16)$$

Elastic behaviour of a pile

$$M = (EI)_p \chi \quad (17)$$

With $(EI)_p$ the bending stiffness of the pile.

Governing equation

$$\frac{d^4 y}{dz^4} = \frac{-P}{(EI)_p} \quad (18)$$

In order to solve this equation, we need the dependence of the p-y curve. To create this p-y curve, the following steps need to be followed. For a simplified approach, a linear spring stiffness model with depth can be used that uses the relation with the shear modulus ($k_{p-y} = 4G$). As it is stated that the soil depends on a shallow depth failure mode and a deep depth, a linear model should not be sufficient to model this behaviour.

2.3.1 Non-linear spring model sand and clay

As commonly known, a pile-soil interaction has a maximum resistance that can be mobilized. Two sections can be found, namely the linear regime and plastic deformation regime. A simplified approach for the p-y curve for drained sands in regards to API RP2GEO is given as

$$p = A p_f \tanh\left(\frac{n_{ki} X y}{A p_f D}\right) \quad (19)$$

Where the coefficient A is formulated as a function of depth and diameter for monotonic loading as $A = (3.0 - 0.8 \frac{z}{D})$, p_f the soil resistance per unit length and unit width, y the lateral displacement and n_{ki} the stiffness depth gradient. This function takes into account the transition from shallow failure to deep failure. n_{ki} The subgrade modulus can be read from design charts normalized to relative density and friction angle for sands above and below the water table. Where the ultimate lateral capacity is found to be formulated in two section, mentioned as the shallow depth and deep stated before.

$$P_{us} = (C_1 z + C_2 D) \gamma' X \quad (\text{shallow depth}) \quad (20)$$

and

$$P_{ud} = C_3 D \gamma' X \quad (\text{deep depth}) \quad (21)$$

Where the coefficients C_1, C_2, C_3 are given by design charts formulated in API RP2GEO and z the depth of calculation. When considering these parameters, it is visible that the curve indeed creates a smooth version of the simplified bi-linear relation visible below for sand. A linear approach of the clay function is also given below.

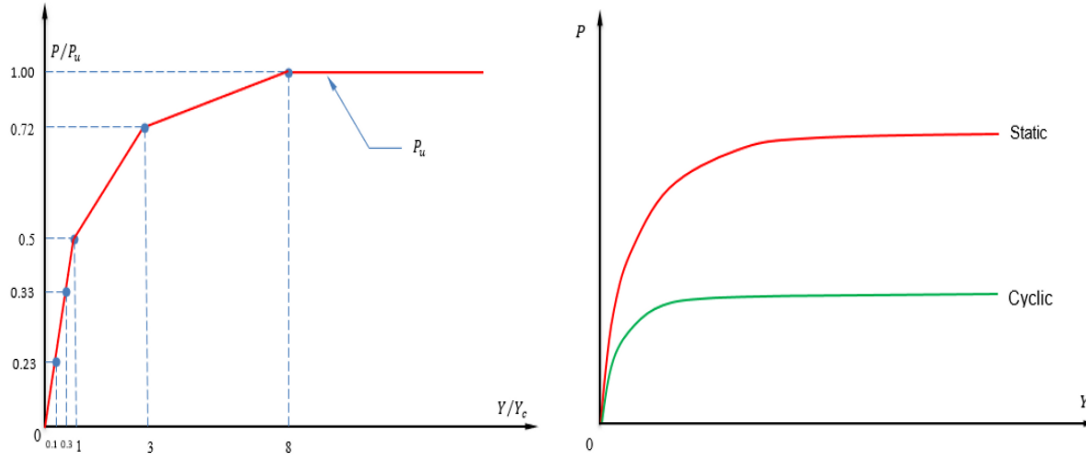


Figure 6: Simplified p-y curve for nc clay and sand following API RP2GEO

The linear approach of the clay section is made up of two formulas, stated from API RP2GEO:

$$\frac{p}{p_f} = 0.5 \left(\frac{y}{y_c} \right)^{1/3} \leq 1 \quad (22)$$

$$P_f = c_u D \left(3 + \frac{\gamma'}{c_u} X + J \frac{X}{D} \right) \quad \text{for } X \geq X_r \quad (23)$$

$$P_f = 9c_u D \quad \text{for } X \geq X_R \quad (24)$$

Where y_c is the characteristic distance for mobilization given by $2.5 * \epsilon_{50} D$, c_u is the undrained shear strength, σ_n the vertical effective stress, D the diameter, X the depth below surface and J an empirical value of 0.25 for medium clay and 0.5 for soft clay. The maximum value of $9s_u = 9c_u * D$ or '9' is given as the limit where the flow of particles is only considering lateral fan zoning, higher values result also in vertical zoning.

2.3.2 Limitations of API guidelines

The API guidelines give a rough estimation of the p-y analysis, eventually resulting in a moment equilibrium. Unfortunately the pile properties are less important, as stated that pile roughness and material properties are not taken into account. As mentioned before, the wind turbine is designed to have a simplified lateral loading condition but with the presence of possible soil gapping. As these responses are created for single piles, the radial dependence is non existing for lateral loading. In the more complex model, this should be taken into account.

2.3.3 Gapping of soil

El-Naggar and Novak [1995] stated the influence of non-linear dynamic soil modelling on the response of a structure, also investigated for a nuclear installation Datta et al. [2017] and several generic investigations such as Nogami et al. [1991]. They all stated that one of the primary reasons to use a non-linear soil model modelling are the discontinuities such as the effect of sliding and gapping. In order to model this discontinuity, several writers such as Novak and Nogami [1977] and more elaborate models such as Nogami et al. [1991] and Datta et al. [2017] stated that the creation of two zones with an inner zone with lower shear modulus can account for the non-linear response.

The modelling of these parts of this total behaviour is partly embedded in the use of the p-y and t-z curves as explained before.

2.4 Geometry of pile placement

As the single piles are placed in the standard wind turbine configuration, a single row of piles on the outside of a circular foundation, the interaction of piles on each other needs to be taken into account. The so called pile-soil-pile interactions is visible below under static lateral loading conditions. The overlapping zones behind each other results in shadowing, besides each other create edge effects and each horizontal movement result in soil gapping.

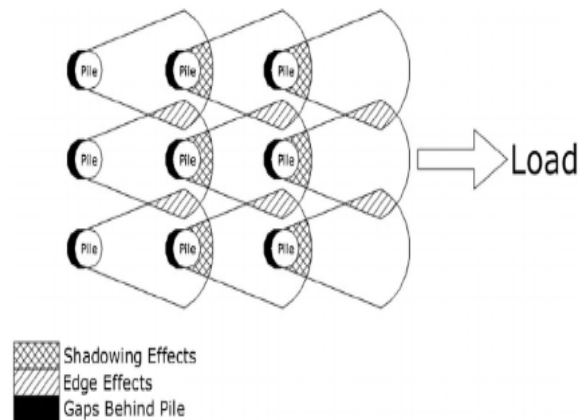


Figure 7: Group effect of piles: shadowing effect, edge effect and gapping Rollins et al. [1998]

In order to describe the group behaviour, so called p-multipliers are developed. These multipliers state the load that each pile carries in regards to normalized loads. Swallow and Sheil [2021] investigated the influence of the group shape on lateral response of the foundation. Plaxis 2D is used to model all the parameters. When considering several group configurations, the group capacity factor was found to be influenced by the shadowing effect or shear zone overlapping. When considering the group with the largest amount of piles perpendicular to the loading direction, even higher capacity factors can be seen for low spacing, this is contributed by the blocking of particles with $s/D < 1.2$ with s the pile spacing and D the diameter of the pile [Georgiadis et al., 2013] and forming a 'wall' with $D + 3s$ width [Swallow and Sheil, 2021]. The influence of roughness is taken into account, which directly shows that a rougher surface results in a single pile response

at greater distance than a smooth pile. As the number of columns and rows is increasing, the load distribution results in a more gradual division. The load capacity is highly non linear as visible below. As stated by the author, two mechanisms counter each other: the creation of more shadowing as the rows increase and the increase in equivalent wall size. The figure also shows that a small increase in amount of piles perpendicular to the loading direction results in extra lateral capacity.

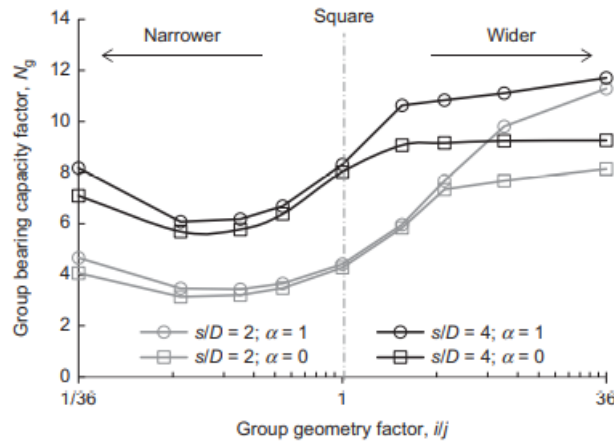


Figure 8: Influence of column(i) and row(j) size, load in direction of i Swallow and Sheil [2021]

When considering larger amounts of piles perpendicular to the loading direction, several trends are visible:

- Decrease in s/D results in larger p -multipliers for piles on the edges.
- Increase in piles perpendicular to the loading direction results in more gradual edge effect and shadowing effect.
- Roughness plays an role in smaller group sizes when considering load in the column direction, after $s/D > 3$, and is the most important factor when considering amount of rows.
- Bearing capacity is almost completely influenced by number of rows in in the group.
- AASHTO and FEMA guidelines gives lower bound p -multipliers.

2.4.1 Experimental pile spacing effect on lateral behaviour in clay

The investigation of Rollins et al. [2006] presents full-scale results of group influence on lateral loads using steel pipes. It was stated by the authors that the p -multipliers that are found are considerably lower than the GROUP [Reese and Impe, 2002] multipliers. As stated, the single pile response is within the normally accepted 10% margin error and has an excellent agreement [Rollins et al., 2006]. They also found that the reloaded piles did not have a good agreement, which is the result of gapping. For the first rows, the full scale tests with back-calculated p -multipliers are higher than assumed using the normally used multipliers from AASHTO. The trailing rows behave roughly in the middle of the existing models from Group and AASHTO. It was found, and also confirmed by the findings of Swallow and Sheil [2021] that the first row multipliers are much higher than the

second, the second much higher than the third and after the third almost no decrease in multipliers is found. The increase in pile spacing was found to be of less influence after $5D$, which is visible below. The first row has almost no group effect after $s/D > 6.5$, the trailing rows after roughly 7.5 diameters. When taking the findings into account it was clearly visible that the group effect in the GROUP model is diminished after roughly 3 ctc spacing's for the first row and 5 for the trailing rows, which is not the case when considering the back-calculated p-multipliers of the test. Unfortunately the p-multipliers in different columns were not interpreted.

When considering the moment of the piles using the found p-multipliers, shallow depth moments were adequately found. The moments at deeper depths after the peak value were underestimated, as the decrease in moment was less in regards to depth than expected by the programs.

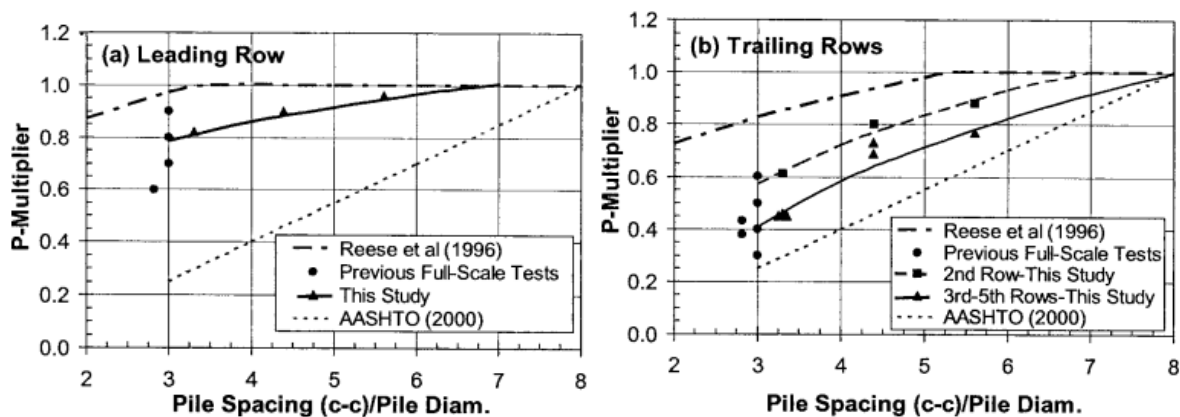


Figure 9: The left figure represents the best fit curve and data from the first row with back-figured multipliers. The second figure contains the best fit and back-figured multipliers for second and third row Rollins et al. [2006]

2.4.2 Load distribution in large pile groups under static and dynamic loading

In contrast to Rollins et al. [2006], the test of Lemnitzer et al. [2008] tested the influence on one single pile group of 3×3 size with concrete piles. The test used the prediction of a single pile and extrapolated this to assess the group response of the 3×3 group using calibrated model of Lemnitzer et al. [2007] and the group efficiency factor in comparison with the p-y multipliers. They found that at small displacements (< 0.626 inch), the response of the piles is not dependent on the stiffness of the used piles. The used model as stated before had a good correspondence with the single pile response, while a response with a lower reinforcement percentage corresponded well to the group response. The group response was considered with a efficiency factor, which was the lowest at low displacements (< 0.35 inch) and tends to 1 at failure.

2.4.3 Employment of P-multiplier in pile group analysis using depth dependency

Ashour and Ardalan [2011] evaluated the influence of soil parameters on the p-multipliers for a 3×2 and 2×3 pile group. The common practise now is to apply the multiplier as a constant factor of depth, but this may not be the case as stated by Ashour and Ardalan

[2011]. The strain wedge method introduces a 3D triangular overlapping system (visible below) that takes into account the loading conditions, deflections and depth [Ashour et al., 2004]. It is stated that the passive soil wedge is based on the triaxial test, where the major principle stress-strain relation is determined ($E = SL\Delta\sigma_{hf}/\epsilon$) as calculated below with ϕ =effective friction angle, ϕ_m mobilised friction angle, $\Delta\sigma_{hf}$ horizontal stress change at failure.

$$\begin{aligned}
 SL &= \frac{\Delta\sigma_h}{\Delta\sigma_{hf}} = \frac{\tan^2(45 + \varphi_m/2) - 1}{\tan^2(45 + \varphi/2) - 1} \\
 \Delta\sigma_{hf} &= \bar{\sigma}_{vo} \left[\tan^2\left(45 + \frac{\varphi}{2}\right) - 1 \right] \\
 \Delta\sigma_{hf} &= 2s_u \quad (\text{clay})
 \end{aligned} \tag{25}$$

Where SL is the deviatoric stress level in the soil, ϕ_m the mobilized friction angle, ϕ the friction angle, $\Delta\sigma$ the stress increment and s_u the undrained shear strength. This clearly shows the effect of this mechanism: with increasing stress, the mobilized friction angle increases resulting in lower Young's modulus. The overlapping of the soil then results in more deflection, leading to a deeper wedge. The model also correctly assumes different P_m values for each deflection, as a higher deflection results in a lower p multiplier. The influence on pile-row side spacing is found to be of higher influence with density or stiffness increases of sand and clay respectively.

2.5 Batter angle under static loading

Several papers have investigated the response of single battered piles (Zhang et al. [1999], Singh and Arora [2017] etc) under only later and combined lateral and vertical loading conditions. Hazzar et al. [2017] investigated a finite difference model, which is checked with data from several papers for both sandy and clayey soils. After validation of the model to several experiments, the response of the different soil densities is given in figure 10 for lateral loading. For vertical loading, see figure 11. While it seems that battered piles are responding with less displacement, it is found that the shaft friction decreases with the increase of batter angle [Hanna and A.Y.Afram, 1987]. This may be the fact of the reduction of the average mobilised angle of friction and the fact that the vertical earth coefficient needs to be taken into account following the result of Hanna and A.Y.Afram [1987]. This conclusion thus says that a simple vector decomposition of the forces is not possible, as the loading conditions increase and decrease the mobilized forces as a function of vertical loading conditions.

2.5.1 Sand single pile lateral loading

It is clearly visible that an increase in negative pile batter results in higher later capacity, while increase in positive batter angle results in a steady state or even decline of the capacity. Both Zhang et al. [1999] and Hazzar et al. [2017] described the effect of the increase in later capacity as the fact that the decrease in the angle results in an increase in σ_3 resulting in a stress increment $\Delta\sigma_{v0}$, eventually resulting in an increase in shear strength. The positive change results in a decrease in σ_3 and thus a decrease in shear strength.

When considering confining pressures of the piles at -12.5° and 12.5° , an increase is visible for the negative batter angle which is commonly known to behave as a stronger material.

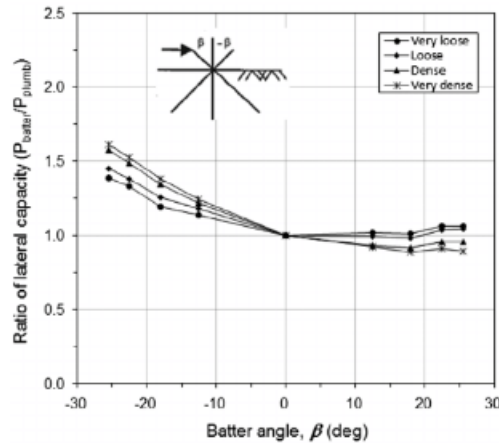


Figure 10: Influence of lateral capacity in regards to batter angle and density state Hazzar et al. [2017]

2.5.2 Vertical combination loading for sand

When the lateral loading is combined with vertical loading, the positive effect of the negative batter angles diminishes. As is visible for all the soil densities at different batter angles, the lateral load capacity decreased for negative batter angles while an increase is found for positive batter angles. This was also described by Karthigeyan et al. [2006], which found the same dependence namely the increase in density of the material in regards to increase in lateral loading. This effect is explained by Zhang et al. [2002] as the fact that the the bending moment by the vertical load causes extra lateral resistance, resulting in lower P_{uh} . The positive batter angle results in a bending moment that diminishes the lateral load component, thus increasing the P_{uh} .

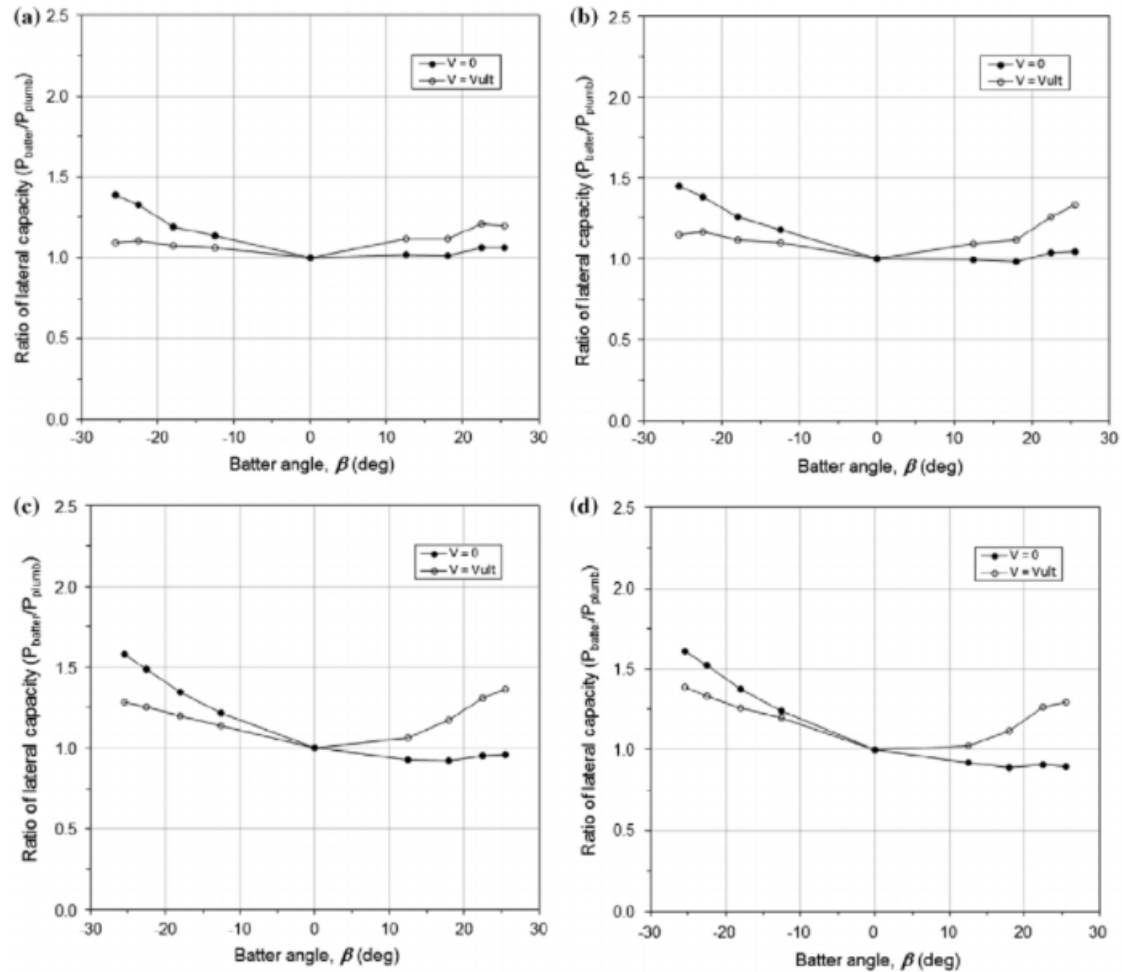


Figure 11: Influence of lateral capacity in regards to batter angle, density and vertical loading for sand Hazzar et al. [2017]

Figure 11 shows clearly that the influence of combined loading results in a negative effect for the negative batter angles, while the positive batter angles are found to have higher capacities under combined loading. It was stated by Hazzar et al. [2017] that the vertical loading is thus as important as the batter angle of the piles. Again it is made visible that the vertical loading inclusion results in a decrease in σ_3 when considering the Mohr-Coulomb model for the negative batter angle and an increase for the positive batter angle.

2.5.3 Clay lateral loading

The same trends can be concluded for clay, as the negative batter angle results in higher lateral capacities. For positive angles, the 12.5° does have approximately the same solution as the 0° batter angle, whereas the 25.5° results in a slight increase in lateral capacity. It was concluded that the ratio of lateral capacity is not dependent on the undrained shear strength. The batter angle increase results in increase in lateral resistance and will develop power resistance Hazzar et al. [2017].

2.5.4 Vertical combination loading for clay

Again it was found that combination with vertical loading results in lower lateral capacities, but for both negative as positive batter angles. The differences are minimal and roughly visible before 50 mm lateral deflection.

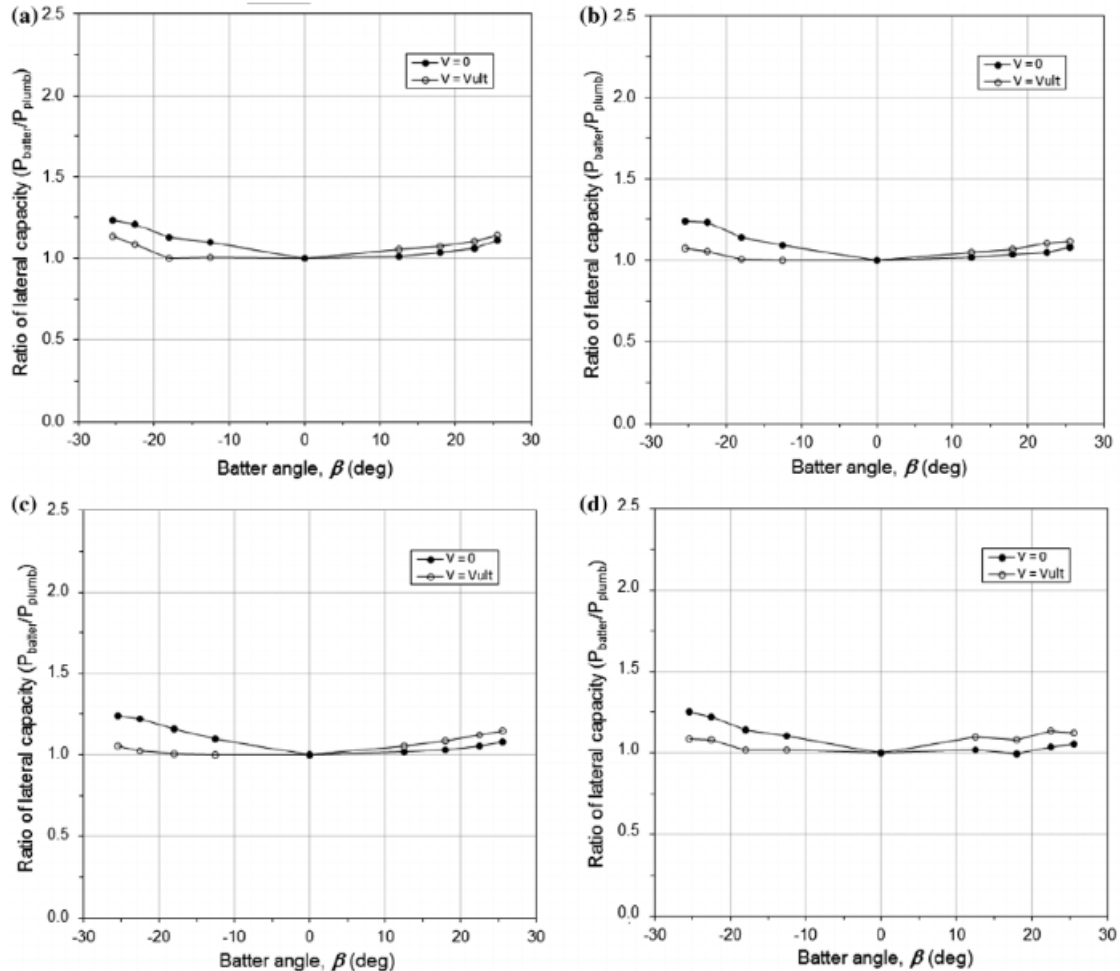


Figure 12: Influence of lateral capacity in regards to batter angle, density and vertical loading for clay Hazzar et al. [2017]

When considering figure 12, again the influence of shear strength was found to be of no influence. When considering both the vertical as horizontal loading as $PIC = \frac{V_{v=v} - V_{v=0}}{V_{v=0}}$, the total influence of shear strength seems to be present in contrast to earlier conclusions.

2.5.5 Consideration of batter angle in pseudo-static analyses of pile foundations

Wang and Orense [2022] experimented with pseudo-static vertical and horizontal loading conditions on single piles in FEM programs. The use of a single sand layer which can be interchanged for 3 different types of sand, ensures that the influence of soil properties can be taken into account. To model the subsurface correctly, they implemented a depth of $L * \cos(\alpha) + 6 * D$ where L is the length of the pile, α the batter angle and D the pile diameter that is used. A proposed relation between the batter angle and pull-out or bearing capacity is formulated as

$$P_{axial} = \cos(0.55\alpha)[\cos(0.55\alpha) + 0.1\alpha] - 1 \quad (26)$$

The shear capacities, which are given in negative shear and positive shear direction or positive and negative batter angle, show a decrease of shear forces under positive batter angle and increase in batter angle. The negative shear direction results in an increase in shear forces under negative shear and an increase in batter angle. It was found that the relative stiffness of the pile is really important, which results in the following equation for shear resistance which is in line with what is found from Zhang et al. [1999]

$$P_s = f(Dr)f\left(\frac{E_p I_p}{E_s D^4}\right)f(\alpha) \quad (27)$$

Negative shear

$$P_{s-} = (7.16Dr + 1.04) \left[\ln\left(\frac{E_p I_p}{E_s D^4}\right) - 13.6 \right] \sin \alpha \quad (28)$$

Positive shear

$$P_{s+} = -(51.13Dr + 16.14) \sin \alpha \quad (29)$$

Using the equations with real testing scenario's resulted in an acceptable match with the experimental data.

Here P_s represents the negative and positive shear capacities P_{s-} or P_{s+} , Dr is the relative density of sand, α is batter angle in radians, and $E_p I_p / E_s D^4$ is the stiffness ratio between the pile and soil.

2.6 Influence of batter angle in a group

Zhang et al. [2002] tested the group response of 3x3 and 4x4 piles with a 1:2 and 2:1 forward and reversed batter angle (angle of 1:4 till 1:16) for the 3x3 group, while the 4x4 group had a 1:1 forward and reversed batter angle. The dead loads are stated as a percentage of the ultimate vertical loading. A general trend was found, where the dead load did not seem to influence the results for the 3x3 group for more than 10% for the 3F6R arrangement (slightly larger). The figure below gives a summary of the found lateral resistance under vertical loading.

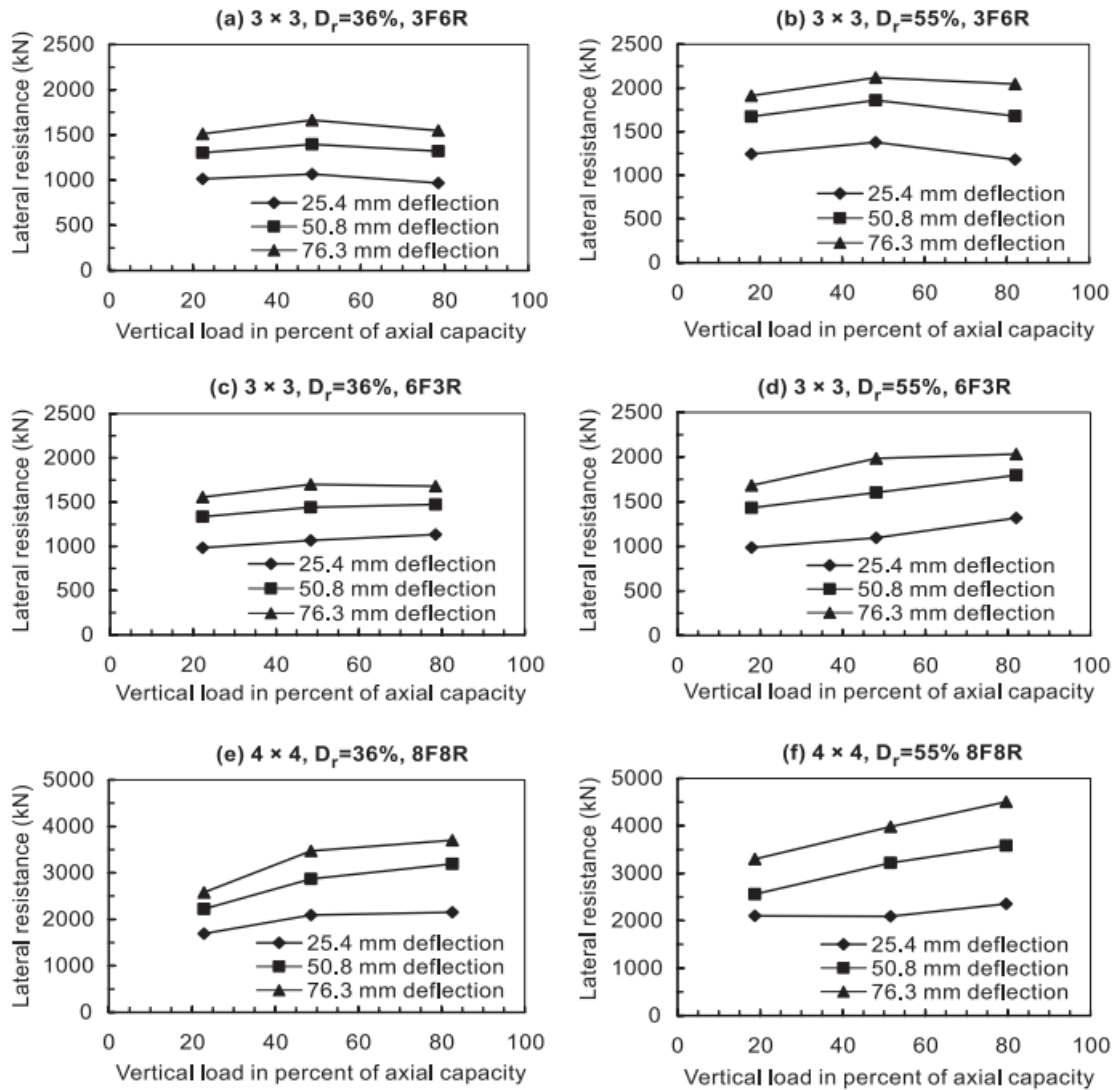


Figure 13: Overview of influence of vertical dead load on sandy soil symmetric battered pile groups Zhang et al. [2002]

The following trends are clearly visible:

- Higher density sand result in higher lateral capacity
- Increase in vertical loading results in increase in lateral capacity, but only for the first two loading cases (except 4x4 group)
- Forward (positive) batter angles result in lower lateral capacity than reversed batter angles.

It was stated by Zhang et al. [2002] that under extreme events, the standard load test with roughly $0.2 \cdot P_{uv}$ is sufficient as worst case scenario. It was also stated by the author that 3 failure mechanisms may be present. The first is the compressional and tensional forces. As the uplift resistance is mobilized at smaller displacements than compression, the tensional stresses may be limiting [Zhang et al., 2002]. Higher vertical loading results in diminishing of tensional forces in the piles. When the vertical load is too large, compressional forces are mobilized first and lower lateral capacity (see figure 13a) is found. During the tests and

the conclusions of Meyerhof and Arisoy [1994], very loose and loose sands have almost no influence on the lateral capacity for reverse and forward batter respectively. The influence for dense and very dense was much larger. No test was performed to assess the exact influence of the batter angle itself on the several soil types. Zhang et al. [2002] concluded that the vertical response also results in lateral displacements in the piles creating shear forces. The negative batter angle results in negative subgrade reaction with moving downward. The p-y curve then results in a larger lateral resistance for pile A.

2.6.1 Group effect under change in batter angle

Singh and Arora [2017] studied the effects of batter angles in groups, with several combinations of forward and reversed angles till group sizes of 16 piles. It is generally found that the maximum lateral resistance is found with batter angles between 20 and 25°, lowering after 25°, visible in the figure below. This figure also confirms the positive influence of negative batter angles: increases in lateral resistance with larger group sizes and less impact when placed incorrectly in regards to loading condition (positive batter angle) than the gains when placed correctly. This was also confirmed by tests with Bajaj et al. [2017] that concluded that the influence of negative batter angles result in 16% increase, while the positive batter angle has a 11% decrease. It was stated that the positive batter angle followed the response of the plumb pile, while the negative batter formed a more linear relation after 6 mm displacement.

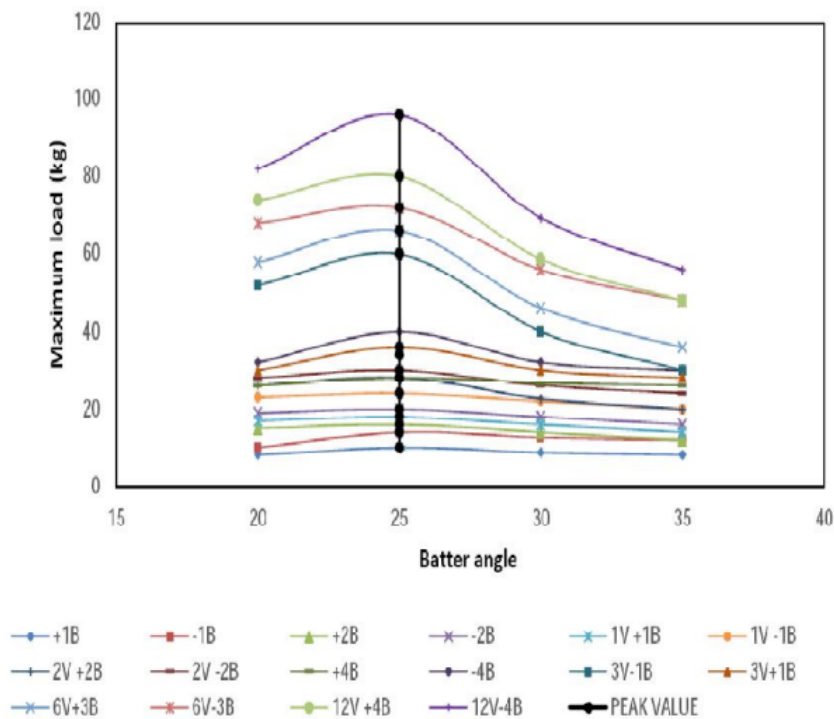


Figure 14: Influence of batter angle on different configurations in battered and vertical piles Singh and Arora [2017]

2.7 Finite element soil-structure interaction models

The various literature sources that were discussed previously in this chapter focuses on specific pile configurations (and pile types). Round pile ring configurations such as applied for onshore wind turbines are not specifically addressed. Consequently, there are no benchmark cases that describe a validated approach that can act as starting point.

In view of this gap in literature sources, a generally applicable soil-structure approach must also be considered. The model of choice is the Hardening Soil small strain model, such as implemented in finite-element Plaxis 3D software.

As stated in section 2.1 non linear behaviour of soils needs to be taken into account for Plaxis 3D software. The behaviour of large structures is primarily influenced by the small strain response of the soil, as the structures cannot move more than a couple of centimeters which is a requirement of the turbine manufactures. This small strain behaviour is roughly visible at 0.001% strain.

2.7.1 Modelling of stress-strain curves

The modelling with the help of so called p-y curves and t-z curves in analytical software is an approximation of the models used by numerical modelling programs such as Plaxis. In order to create the match with the stress-strain behaviour of different soil types, several models were created. As stated by Brinkgreve [2021b], Novak and Sheta [1982], Novak and Aboul-ella [1978], Novak [1974], the shear modulus or modulus reduction curve is an important factor of influence of small-strain modelling besides the strain dependent stiffness. In order to explain the different upgrades in the models made over the years, a few (simplified) models will be explained.

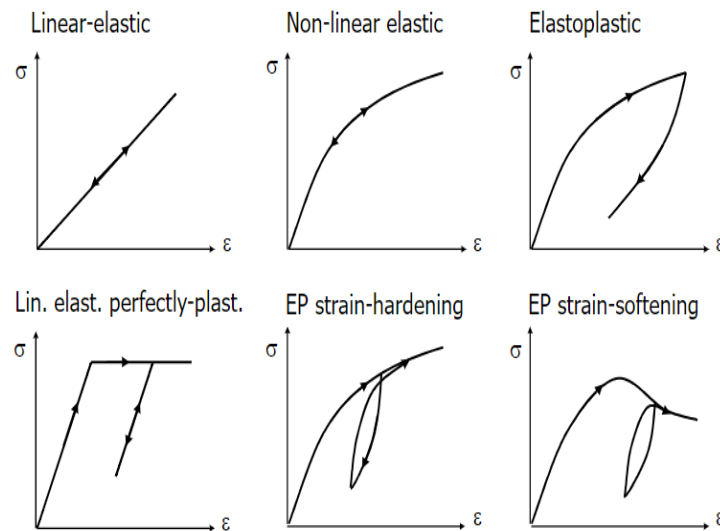


Figure 15: Different type of modelling options Brinkgreve [2021a]

2.7.2 Linear elastic modelling

A first basis of the model is the linear elastic model, using the simplified Hooke's law $\sigma = E * \epsilon$. This model uses the input of Young's modulus E , which is described by Poisson's ratio ν . The shear modulus G can be described by both parameters as $E = 2 * G(1 + \nu)$.

It is stated that this model cannot be used for the subsurface modelling. The complete isotropic linear elastic deformation behaviour is stated as:

$$\underline{\underline{\sigma}} = \frac{E}{1 + \nu} \left[\underline{\underline{\varepsilon}} + \frac{\nu}{1 - 2\nu} \varepsilon_v \underline{\underline{I}} \right] \quad (30)$$

$$\begin{bmatrix} \sigma_{xx} \\ \sigma_{yy} \\ \sigma_{zz} \\ \tau_{xy} \\ \tau_{yz} \\ \tau_{zx} \end{bmatrix} = \frac{E}{(1 + \nu)(1 - 2\nu)} \begin{bmatrix} 1 - \nu & \nu & \nu & 0 & 0 & 0 \\ \nu & 1 - \nu & \nu & 0 & 0 & 0 \\ \nu & \nu & 1 - \nu & 0 & 0 & 0 \\ 0 & 0 & 0 & \frac{1}{2} - \nu & 0 & 0 \\ 0 & 0 & 0 & 0 & \frac{1}{2} - \nu & 0 \\ 0 & 0 & 0 & 0 & 0 & \frac{1}{2} - \nu \end{bmatrix} \begin{bmatrix} \varepsilon_{xx} \\ \varepsilon_{yy} \\ \varepsilon_{zz} \\ \gamma_{xy} \\ \gamma_{yz} \\ \gamma_{zx} \end{bmatrix} \quad (31)$$

2.7.3 Linear elastic perfectly plastic

In comparison with the linear elastic model, the linear elastic perfectly plastic model creates a bi-linear relation in regards to the stress strain relation, visible in figure 15. The second section, the addition to the linear elastic model, is created by using the Mohr-Coulomb failure contour. This is described by the addition of parameters cohesion c , friction angle ϕ and dilatancy angle ψ . This is the first introduction of a yield surface. As this model creates a perfect horizontal response in the stress-strain curve, the response for the plastic behaviour is thus fixed and not strain dependent. This means that the contour is fixed, and does not expand in any way. This model does not represent soil behaviour correctly with our small strain response.

2.7.4 Elasto-plastic strain hardening or softening

Hardening soil is originally based on a hyperbolic stress-strain function for drained sands from Kondner and Zelasko [1963]. The hyperbolic model, which is more generally known as the Duncan and Chang model, is described as the start of the hardening soil model and is used as basis. The hardening soil model is using:

- Double hardening principle
 - Shear hardening
 - Cap hardening
- Soil dilatancy

The last two figures represent elasto-plastic strain hardening or softening model. This considers two sections, namely the linear part that is described by Hooke's law again, the plastic part by hardening or softening behaviour. The hardening behaviour is described by the development of the yield function and can develop two versions, namely the kinematic and strain hardening behaviour. The kinematic hardening model uses the translation of the yield surface, thus needing a description of the stress increment. This type of hardening is primarily used for plastic strain accumulation, found under cyclic loading conditions. This type of hardening is not available in Plaxis. The strain hardening, as pictured in figure 15, is available in two different types of hardening. The compression hardening, or

cap hardening, and the shear hardening, or friction hardening. The compression hardening results in displacement of the cap, resulting in irreversible plastic strains. The shear hardening is defined by the increase in deviatoric loading, the increase in loading in a particular direction. As the shear hardening is approaching the failure line, this can lead to (local) failure in regards to compression hardening. In comparison with an isotropic loading condition, both strain hardening types result in increase in elastic surface.

Softening behaviour is found when the yield contour is shrinking due to plastic straining, found as cohesion softening or friction softening. The friction softening results in smaller angle between the higher and lower contour, while the cohesion softening results in inward translation. This portion is not used in the Hardening Soil model as the name already explains.

2.7.5 Failure criteria

As shortly mentioned before, the failure criterion determines the surface or elastic region of the model. In general the Mohr-Coulomb criterion or yield function is accurate enough to model the soil response. Improved models such as models Lade and Matsuoka behave in a more gradual way in the σ_1, σ_2 and σ_3 space and improved the shear strength criterion for soils and sand respectively. As those models are not implemented in Plaxis, the Mohr-Coulomb model is being used.

2.7.6 Hardening soil small strain

It is clearly visible in figure 15 that the initial stress-strain curve is modelled as linear elastic perfectly plastic behaviour. In more advanced models, this linear elastic perfectly plastic behaviour is only visible in very small strain ranges. This concept is further explained by the Hardening soil small strain model.

The strain-dependency of stiffness is taken into account as an add-on on the elastic formulation, thus creating an overlay which can serve several models. The stiffness at very small strains tend to very stiff response, while increase in strain levels result in decrease in stiffness. This is visualized in a modulus reduction curve, showing the secant shear modulus as a function of shear strain on log scale. The stress-strain relation of many types of different soils can be described by this function. Both of the curves can be expressed in relative terms to G_0 and γ_0 which are the small strain initial shear modulus and the shear strain that corresponds to a G_0 reduction to 72.2%. After full strain reversal, the response again starts from G_0 , which can be used for cyclic behaviour. The following relation can be displayed:

$$G_s = \frac{G_0}{1 + 0.385\gamma/\gamma_{0.7}} \quad (32)$$

$$G_t = \frac{G_0}{(1 + 0.385\gamma/\gamma_{0.7})^2} \quad (33)$$

With G_t the tangent shear modulus and G_s the secant shear modulus. It is visible that the stiffness is therefore both strain as well as stress dependent. For the constitutive model, the differential stiffness is required. It is formulated by $G_t = d\tau/d\gamma$, which is approximated by multiplying with $1/(1+0.385*\gamma/\gamma_{0.7})$. For real case scenario's, the shear stiffness does not drop to very small values as shown by a simplified modulus reduction curve. The lower

value is approximated by the cut-off or G_{ur} , the unloading/reloading shear modulus, or stated as:

$$G_{ur} = \frac{E_{ur}}{2(1 + \nu_{ur})} \quad (34)$$

These equations are a simplified response, which was first mentioned by Hardin [1972], by using depth dependent parameters and the plasticity index as formulated by

$$G_0 = 625 \frac{OCR^k}{0.3 + 0.7e^2} \sqrt{P_a \sigma_0} \quad (35)$$

With OCR the overconsolidation ratio, e the void ratio and σ_0 the mean effective principle stress. The more simplified method, visible in formula's 32 and 33 for both small as well as large strains, is created by DOS SANTOS and CORREIA [2001]. By using the relation for smaller ranges as $\gamma_r = \gamma_{0.7}$.

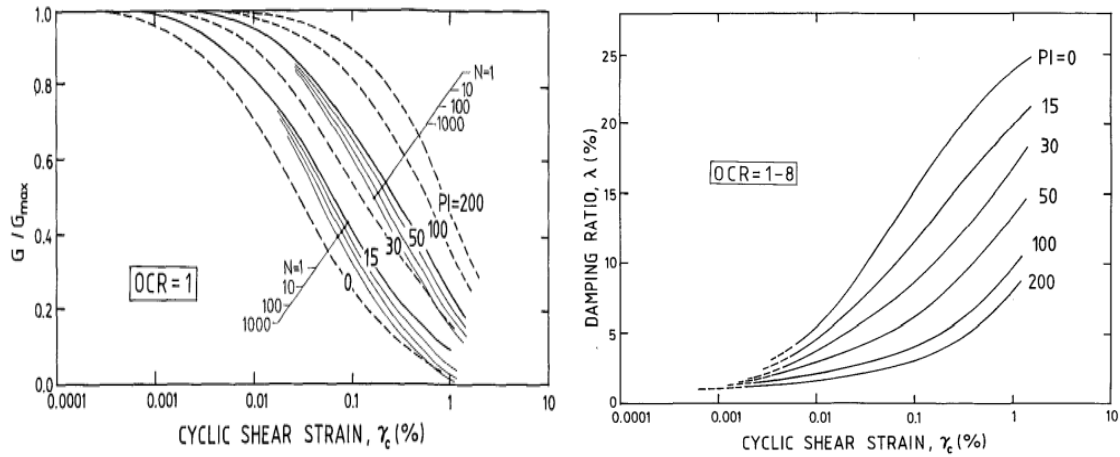


Figure 16: Shear modulus reduction and damping dependence on cyclic shear strain for NC and slightly OC clay Vuetic and Dobry [1991]

The figures create a depth and plasticity dependency, as well as the cyclic unloading/reloading behaviour. The plasticity index is primarily used for small grain soils, where a more general model only shows one of the reduction curves.

2.7.7 Calculation of HS small parameters

The addition of G_0 and $\gamma_{0.7}$ parameters for small strain response normally requires laboratory tests. In the last couple of years, empirical relations are being developed for HS_{small} in general by Benz et al. [2009], for sands by Brinkgreve et al. [2010]. Fine grained material parameter by Taukoor et al. [2019] and Godlewski [2018] are describing the behaviour of different types of soils on the stiffness module. The relation to cyclic loading is also made for medium to fine grained soils by Santos and Correia [2000]. While some of the conversions by empirical relations are automatically made in Plaxis, fine tuning between possible parameters and their interrelational effects may need to done manually. A short description of some of the manual alterations are explained in section 3.1.

2.8 Choice of pile use

For the modelling of the substructure in a finite-element model, the choice needs to be made between physical modelling of the piles using volume piles or to use the embedded beam function. The model that best approaches reality is the volume pile. Unfortunately, this requires a very dense mesh, especially when small-strain behaviour needs to be investigated. Calculation time is affected accordingly. Alternatively embedded beam rows can be applied in Plaxis 3D. The embedded beam row is a mathematical approximation of the cross-section of a volume pile, that does not require the use of a very dense mesh. In order to explain this concept, the next paragraphs will explain the differences between volume pile modelling and embedded beam modelling.

2.8.1 Embedded beam

The embedded beam is modelled as a line element, a beam, without modelling the physical volume that normal piles have. The behaviour and material parameters are defined as a normal 3D beam element, thus behaving as a normal beam. The interaction with the surrounding soil is made by using embedded interface elements along and below the pile. This zone surrounding the pile is being modelled as a linear elastic zone, while a elastoplastic response can also be chosen. For our case, the modelling will be done far below the plastic limit which ensures that the maximum shear stress in axial direction is lower than the actual axial shear stress. This will then comply to $|t_s| < T_{\max}$.

The equation that needs to be solved in order to assess the bearing capacity of the whole pile, is made up of two different equations:

$$t^{skin} = t_0^{skin} + \Delta t^{skin} \quad (36)$$

With t_0^{skin} being the initial skin resistance and Δt^{skin} the force increment. The force increment is made up of

$$\Delta t^{skin} = T^{skin} \times \Delta u \quad (37)$$

Where T^{skin} is the material stiffness matrix and Δu the relative displacement of the pile versus the soil. In order to model this behaviour in 3D, the following local coordinate system is being used:

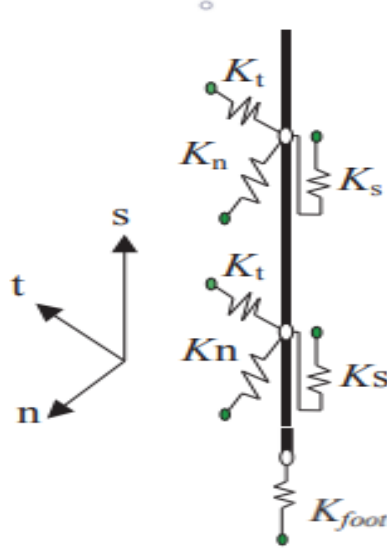


Figure 17: Stiffness of embedded interface along the pile

In order to explain how the embedded beam is modelled, the basic equation that can be solved is a combination of equation 37 defined for each local direction.

$$\begin{bmatrix} t_s \\ t_n \\ t_t \end{bmatrix} = \begin{bmatrix} K_s & 0 & 0 \\ 0 & K_n & 0 \\ 0 & 0 & K_t \end{bmatrix} \begin{bmatrix} u_s^p - u_s^s \\ u_n^p - u_n^s \\ u_t^p - u_t^s \end{bmatrix} \quad (38)$$

Where u^p , u^s , K_s , K_n and K_t are the displacement of the pile, displacement of the soil, the elastic shear stiffness of the embedded interface elements and the elastic normal stiffness of the embedded interface elements.

The same equations can be found for the single spring for the base resistance of the pile, the stiffness matrix K_{foot} . While the skin resistance is made up of a matrix of 3 directions, the vertical direction is modelled as having one spring constant for the footing

$$f^{skin} = f_0^{foot} + \Delta f^{foot} \quad (39)$$

With f_0^{foot} and Δf^{foot} are the initial force and the force increment in the footing. Where the incremental foot resistance is made up of

$$\Delta f^{foot} = F^{foot} \times \Delta u \quad (40)$$

With F^{foot} and Δu the material stiffness matrix of the spring element of the footing and the relative displacements respectively. Where the maximum capacity under elastic deformations is given by $F_{foot} < F_{max}$.

In order to correctly model the subsurface with the embedded beam, the values are chosen such that the stiffness of the embedded interface elements does not influence the total elastic stiffness of the pile-soil interaction. The following equations are used:

$$K_s \gg G_{soil} \quad (41)$$

$$K_n = K_t = \frac{2(1-\nu)}{1-2\nu} K_s \quad (42)$$

2.8.2 Interaction of pile-soil

After the initial setup of the subsurface, the embedded beams are introduced. During the meshing of the system, new nodes are generated along the beam element already existing nodes. These special interface elements are created to connect the existing soil nodes and the new pile nodes. As visible, the embedded pile nodes are not necessarily on the existing 10 noded soil elements. This results in interpolation from the existing element shape functions, which may cause stress discontinuities and mesh dependence of the model Smulders et al. [2019]. In the new embedded beam formulation, this behaviour is less visible as the new embedded beam is modelled more accurate and smoother with less mesh dependence Smulders et al. [2019].

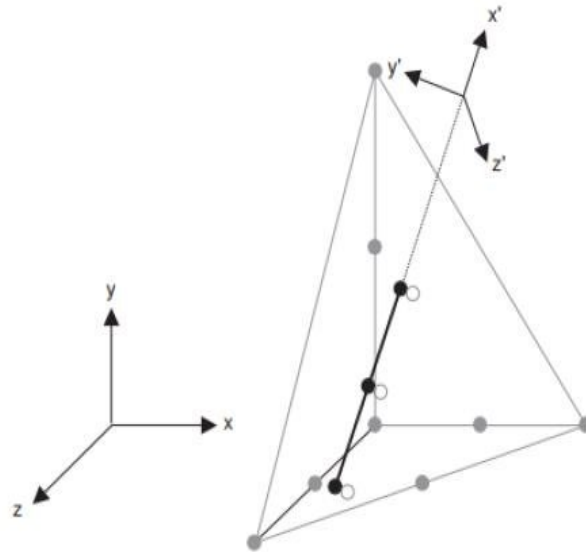


Figure 18: Embodiment of pile in soil elements Smulders et al. [2019]

The modelling of the embedded beam is then split up in two different elasto-plastic zones, the base resistance at the end of the pile and the skin resistance. The base resistance is in unit force, while the skin resistance is in force per circumference per meter. As the circumference of the pile is constant over depth, the skin resistance is simplified to force per meter. As already explained above, limitations are taken into account by introducing plastic zones after the max resistance is found.

As the pile does not model a physical volume, an elastic zone surrounding the beam is created. This bearing capacity zone is determined by the pile parameters, primarily the equivalent diameter by $R_{eq} = \sqrt{(A/\Pi)}, \sqrt{(2I_{avg}/A)}$ with $I_{avg} = (I_2 + I_3)/2$. With A the are of the pile and I the moment of inertia. This realistic pile bearing capacity zone lets the beam almost behave as a volume pile. Unfortunately the installation effects are not taken into account, besides that the interaction is not modelled on the edges of the elastic zone but at the centre of the beam.

2.8.3 Multi-linear soil modelling

The use of the maximum shear and base resistance can be taken into account in three different models, namely the linear, multi-linear and layer dependent modelling. For the linear approach, the T_{max} has a linear relation from T_0 till T_{max} . This is primarily

used for single layer models. The layer-dependent approach is a direct relation between the strength parameters of the layers, namely the cohesion and friction angle, and the maximum shear force. This is taken into account by using a reduction factor, which influences the strength parameters as:

$$\begin{aligned}\tan \varphi_i &= R_{inter} \tan \varphi_{soil} \\ c_i &= R_{inter} c_{soil}\end{aligned}\tag{43}$$

With ϕ the friction angle and c the cohesion. The multi-linear approach is used in this case, to take into account multiple soil layers while also knowing which layers does have a controlled contribution to the total skin resistance. Calculations are made by using 47 for each upper and lower layer boundary. No depth dependency is taken into account.

2.8.4 Input parameters for embedded beams

The properties for the embedded beam are input for an embedded pile material set. As explained above, the bearing capacity is calculated with the input parameters T_{max} and F_{max} , besides the standard strength parameters of concrete the Youngs-modulus E and volumetric weight γ .

2.8.5 Volume piles

Volume piles are modelled as soil elements. As the soil elements create a physical boundary in the soil, the meshing will result in more elements. These elements need to be modelled in such a way that the 10 node tetrahedral elements are placed inside (pile) and outside (soil) taking into account the physical barrier between the two types of material. The pile will mostly be modelled as linear elastic solid object, surrounded by interface elements to model pile-soil interaction. The soil itself using a non-linear elastoplastic soil constitutive model. While it is stated that this results in higher amounts of elements, the accuracy in the lateral direction is higher Smulders et al. [2019].

The accuracy in lateral direction can potentially reach a real case displacement, but needs to have a fine enough mesh to model the circular shape of the pile using the tetrahedral elements. When coarser meshes are being used, the corners that are created by the elements can result in hanging/ sacking on the non-smooth interface corner points. Especially in the case of using small strain, small displacements this principle can influence the comparison of volume piles with embedded beams. The refinement of the mesh does not have a general rule, which creates the need for a iterative process for the local refinements (Brinkgreve, personal contact).

2.9 Conclusion of literature study

The literature study is being held to assess the influence of several factors on the research questions, but primarily giving an insight in the following subjects. Most of the questions are formulated as main sub questions, some clear follow-up questions.

1. What is the difference in behaviour for the different types of pile modelling options when applying horizontal loading conditions on the piles in the Plaxis 3D?
2. Which type of constitutive soil model(s) are suitable for the analysis of pile-soil interaction at small strains?
3. What is the group effect and how does it affect pile efficiencies in the group?
4. How does the batter angle change the response or translational stiffness for a single pile under horizontal or combined horizontal and vertical loading?
5. How is the effect of a batter angle influencing the group efficiency for a foundation?

It is clearly visible that both the group effect as well as the batter angles influence the translational stiffness of the piles per soil type as well as loading conditions. Generally the bending stiffness is being discarded and not present in the read literature, which may result in discarding the complete moment stiffness as output of the thesis. The assessment of accuracy in regards to the single pile response should be easily analysable with the data given in the papers for vertical and battered piles. The comparison is already made between model data and experimental data for single piles, resulting in less time needed to prove this aspect. As the group response is generally created for square or rectangular foundations, evaluation of model data with experimental data will be complicated or impossible. The loading conditions for static loading are applied at ground-surface level, which is not realistic in regards to the loading for wind turbine foundations.

Different papers provide a simplified relationship for a good approximation in the setup of a FEM model. While the models are based on real (engineering) situations, as proven by comparisons, most of the models concentrate on a single soil layer. The results cannot be transposed directly to the multi-layered ground model that is used in this study.

Considering small strain constitutive models, the hardening soil small strain model is judged to be suitable for modelling the expected small strain behaviour. It is recognised that a Plaxis 3D analysis with the use of the HS small constitutive parameters requires more input, relative to the standard 2D analytical approach.

The type of pile modelling will result in differences in lateral precision, but also in the amount of elements used as volume piles result in volumetric modelling which increases the amount of elements. A choice between precision and efficiency needs to be made, especially for the size of the project with 28 piles. After the literature study, the topic is found to be still largely undocumented which underlines the needs to assess the behaviour of these types of foundations in more detail.

In short:

1. The behaviour of a wind turbine pile ring foundation under lateral loading is not described in detail in existing literature.

2. The HS small constitutive model is reckoned suitable for the analysis that is described in this thesis
3. The choice between volume pile or embedded beam model requires further substantiation (accuracy in relation to mesh size)

3 Research layout

In order to start the research, a general layout of the topics which are being researched is made. This general layout shows the steps that need to be taken in order to formulate the answer on the research question(s) in this experimental phase.

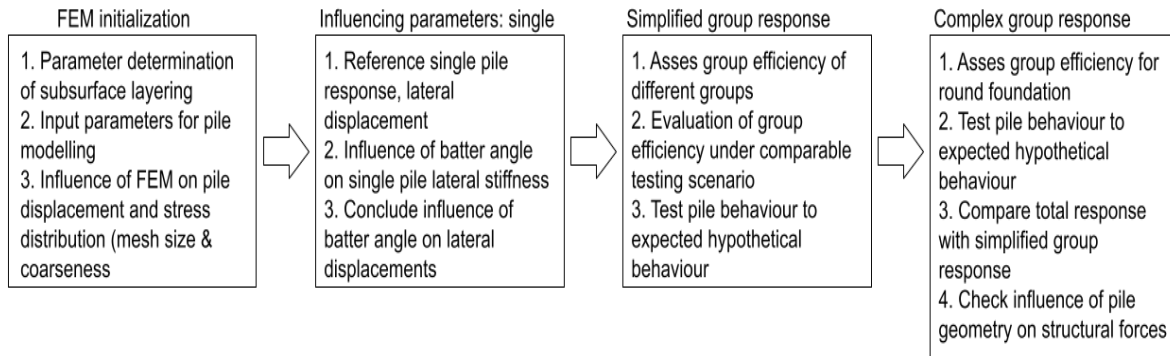


Figure 19: General layout of experimental study in Plaxis 3D

1. The first part will be the setup of the FEM in Plaxis 3D. Choices surrounding the extensive input parameters of the program need to be simplified and stated. The mesh influence will be checked to see which type of finite element mesh results in an optimal combination between efficiency and accuracy.
2. In this part, a single pile is modelled to make certain all input parameters and program settings are realistic. Outcomes are compared with results of analytical calculations. Batter angles are also applied to check the model response
3. The third part will asses group response in the FEM software for in-line configurations and compare or validate this with existing (experimental) results. Validation in regards to Reese and Impe [2002] will prove the group effect. This in-line group assessment can be performed as direct comparison with Reese and Impe [2002] due to the same pile head displacements. Verification between different groups result in relative comparison.
4. In the last part, the behaviour of the (complex) pile ring foundation under lateral loading is investigated. The foundation solution with vertical piles is taken as reference case. The behaviour with batter angles and alternating batter angles will be compared to the vertical pile group.

3.1 Engineering properties

The description of soil-pile interaction describes that the soil is the most important factor in the response of the substructure. The aim of this thesis is to describe the lateral response of pile ring wind turbine foundations in typical ground conditions that can be encountered in projects in the western part of The Netherlands. To this end a realistic/schematic soil profile was defined with a top layer and soft peat/clay overburden on Pleistocene sand.

The pile diameter was matched to that of the commonly used driven cast-in place pile type (Vibro 559 mm). The piles were modeled as wished-in place, the pile-driving effects were not taken into account.

3.1.1 Wind turbine specifications

For this project, a large wind turbine with a total weight of roughly 600 tonnes is used. This weight is an approximation by an Enercon structural engineer as being relevant for current as well as next generation wind turbines. These projects concluded that the average lateral loading conditions per pile are between 15-30 kN and that the static vertical pile load is comprised of roughly 150-200 kN for the wind turbine alone (without the weight of the concrete pedestal). In order to take into account any irregularities and group effect, both the lateral loading and the vertical loading are increased to 35 kN and 250 kN respectively.

For further analysis a real case scenario is being used, where the foundation pedestal is shown in figure 20.

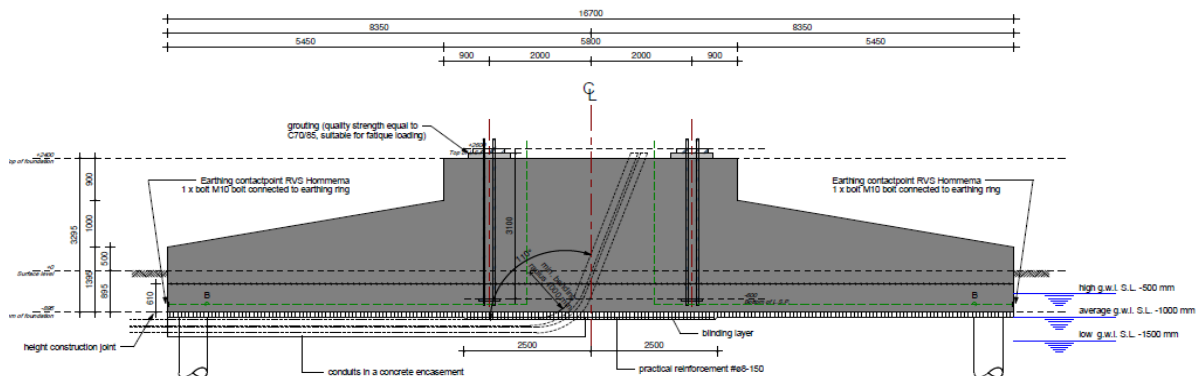


Figure 20: Cross-section of representative wind turbine foundation foot

As the load of the pedestal and piles is added to the self-weight wind turbine, the total vertical load applied to the piles is increased to 500-600 kN. The total horizontal loading condition of this specific turbine is approximated to be 560 kN, which means that with a example footing of 28 piles a horizontal load of roughly 20 kN is applied to each pile. This load is officially applied 3.3 m above the piles, 2.4 m above ground level, at the top of the footing. In the analysis of the single piles and the simplified pile group, this load is applied at pile head level.

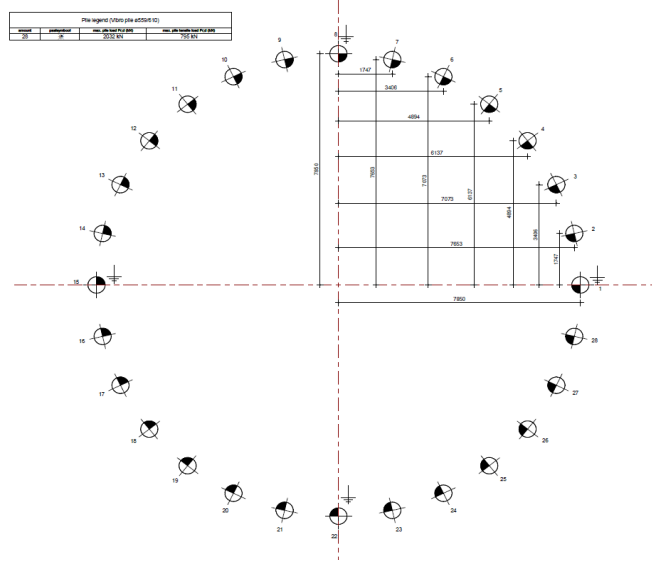


Figure 21: Top-view of representative wind turbine foundation layout

3.1.2 Subsurface layering

Large parts of the Dutch subsurface are described by a 'polder', especially in the area's that are selected as potential locations for wind turbine projects. These lands primarily consist of land reclamation, cultivated marshes and flood plains. The area's are defined by a large amount of peat and clay in the roughly upper 10 m of the layering, while the deeper layers primarily consist of several distinct sand layers. While clay is normally assumed to be less compressionable because of the low permeability, the peat is highly compressionable and is present in the higher parts of the layering. This assures that these peat layers contribute largely to subsidence in the lower parts of The Netherlands. While most of the layers are taken as a realistic-conservative approach with the chosen parameters, the fact that the subsidence and compression of the peat most likely results in higher strength parameters. It needs to be taken into account that a parametric survey for the subsurface parameters is not part of this thesis. The parameters below are gathered from several projects from RHDHV and optimized within the scope of this thesis.

The general strength parameters (ϕ , ψ , c_{ref} and q_c) are taken from NEN9997 2B with their corresponding volumetric weights. The drainage type is set to drained, validated soil parameters are used. The horizontal loads are of short duration which would mean that the soil will respond in an undrained or stiffer manner. Drained parameters, validated within projects, are however readily available and the slightly weaker response is not seen as a determining factor in the outcome of this study (Mooijman, personal contact). In order to assess the parameter set several checks are performed:

For weak layers:

$$E_{50}^{ref} < E_{ur}/2 \quad (44)$$

With E_{50}^{ref} the secant stiffness modulus in standard drained triaxial testing at reference stress level, E_{ur} the unloading/reloading stiffness at reference stress level. To use the input of the modulus reduction curve we need to have a $G_0 > G_{ur}$, where the lower limit is given by the unloading/reloading parameters as given already in section 2.7.6.

$$G_{ur} = \frac{E_{ur}}{2(1 + \nu)} \quad (45)$$

With G_{ur} the unloading/reloading shear modulus, where a section with small strains has a high ratio of G/G_{ur} . The parameters are taken from a survey from existing wind turbine foundation locations and checked with the formula's described. The iterative process applied by Plaxis ensures that the parameter set is approximating real soil conditions. In order to model the subsurface correctly, it is chosen to adapt a higher friction angle for peat than assumed by NEN9997 table 2B (Brinkgreve, personal contact). Several other parameters are then adapted to ratio as stated above.

The iterative process formulated as:

1. Check the relative differences between each soil type and parameter
 - Friction angle is conservative, spoken from experience and increased to normally used values (except the increase for peat).
 - G_0 showed same value for peat and clay, this should be less for peat due to the material properties.
 - E_{oed} too low for clay in comparison to peat and general knowledge shows a relative increase for clay.
 - $\gamma_{0.7}$ can sustain larger strain levels before 0.722 of G_0 is reached, therefore extending the range for peat.
2. Check with stated ratio's
 - Increase in E_{oed} results in an increase in E_{50}^{ref} with a factor of 2
 - Computational limitations of low E_{oed} for peat resulted in a needed decrease in K_0 value, which results in an increase in ϕ

These results are given in the following data set, where the values between brackets are the old values before the iterative process. A general layout of the subsurface is given in figure 22. The water table is formulated as typical polder model and set at -1 meter.



Figure 22: Schematic subsurface layering

Table 2: Table of ground parameters per layer using Hardening Soil small strain stiffness constitutive model

Parameter	Drainage type (-)	γ_{dry} (kN/m ³)	γ_{sat} (kN/m ³)	E_{50}^{ref} (kN/m ²)	E_{oed}^{ref} (kN/m ²)	E_{ur}^{ref} (kN/m ²)	power m (-)	c^{ref} (kN/m ²)	ϕ' (°)	ψ' (°)	$\gamma_{0.7}$ (-)	G_0^{ref} (kN/m ²)
Top layer (Clayey sand)	Drained	16.0	16.0	3800	2500	15000	0.8	5.0	28.0 (22.5)	0.0	$5.0 * 10^{-4}$	35000
Peat (Soft)	Drained	11.0	11.0	2000	1000	6000	1.0	2.0	20.0 (15.0)	0.0	$1.0 * 10^{-3}$ ($5.0 * 10^{-4}$)	20000
Clay (Soft)	Drained	15.0	15.0	5000 (3000)	2500 (1500)	12000	0.9	2.0	25.0	0.0	$5.0 * 10^{-4}$	25000
Sand (Loose)	Drained	17.0	19.0	25000	25000	100000	0.5	0.0	31.0 (31.0)	0.0	$2.0 * 10^{-4}$	150000
Sand (Medium)	Drained	18.0	20.0	35000	35000	140000	0.5	0.0	35.0 (32.5)	2.5	$2.0 * 10^{-4}$	200000

4 Model setup

The first aspect that will be investigated is the pile model type in relation to mesh size. The three types that will be considered are volume pile, embedded beam and "new" embedded beam (not yet implemented in the latest version of Plaxis 3D at the time of writing of this report). Secondly, the influence of model boundaries will be investigated.

The piles will be modelled in a subsurface as shown in figure 22 with the layer parameters from the layers as summarized in table 2. A driven cast-in pile type with a diameter of 559 mm will be used in the model. In The Netherlands this is the most commonly applied pile system for wind turbine foundations. The water table will be added at a depth of -1m and is left free to drain from the top boundary, visible in figure 22. The model is axisymmetric due to the vertical and horizontal loading conditions, but it is chosen to model the complete model with 28 piles. This is done due to the initial setup for dynamic calculations, where vibrations and damping may be different for the structural elements. The displacement of the model will be read from the nodes of the piles, while stresses and strains are read from stress-points.

The boundary conditions are set as standard meaning that the bottom surface is fixed by a rigid support, no displacement is allowed in any direction. For the sides of the mesh, the xz plane is fixed in y direction, the yz plane in x direction. This means that the boundaries are not completely fixed and supported by so called roller supports, resulting in displacements that cannot go 'through' the boundary plates. The embedded beams and volume piles are modelled with concrete material properties as stated in table 3.

4.1 Influence of model plate

The modelling of the pile group that is representative for a wind turbine foundation requires a connection between the piles and foundation slab or pedestal. As the model does not take into account any structures in the soil-structure interface, three different models are tested to ensure that only the piles will receive horizontal and vertical load. To provide a scenario where the piles are completely influencing the model behaviour, four different scenarios are tested to find the scenario where the pile receives the highest amount of lateral and vertical forces.

1. The plate is modelled as infinitely stiff. This ensures that the embedded beams can be modelled as having a rigid connection with the concrete base.
2. Change of interface
 - (a) Realistic interface of surrounding soil.
 - (b) Very stiff interface in comparison with surrounding soil (1000 times stiffer).
 - (c) Very weak interface with a factor 1/1000th stiffness and strength parameters $c=1$ and $\phi = 0$.

From the results it was clear that the differences between the axial forces and lateral forces acting in the piles were minimal. This shows that the top layer is a weak layer that cannot sustain any loading. When considering the best scenario in regards to direct transfer of forces, the model with a very weak interface transferred the highest amount of forces directly to the embedded beam.

Table 3: Model setup parameter for additional structural support elements

	Concrete (embedded beam/ foundation base)	Concrete (volume pile)	Stiff plate	Unit
E	30000	30000	30000	kN/m ²
gamma/ gamma_sat	5	25	0	kN/m ³
diameter/ thickness	0.559	0.559	1	m
ν	-	0.2	-	(-)
Material model	-	Linear elastic	Elastic	(-)
Drainage	-	Non-porous	-	(-)

Table 4: Weak interface material to lower influence of plate shear forces

	Value	Unit
Material model	HS small	(-)
Drainage type	Drained	(-)
γ/γ_{sat}	16	kN/m ³
E_{50}^{ref}	38.0	kN/m ²
E_{oed}^{ref}	25.0	kN/m ²
E_{ur}^{ref}	150.0	kN/m ²
Power (m)	0.8	(-)
c'_{ref}	1	kN/m ²
ϕ'	0.0	
ψ	0.0	
$\gamma_{0.7}$	$5 * 10^{-4}$	(-)
G_0^{ref}	350	kN/m ²

4.1.1 Loading scenario and constraints

For single piles the load will be applied directly on the pile head, where pile groups receive a surface load. None of the piles receive a fixity and are free to move. Pile heads with pile plates (groups) are modelled with either a hinged connecting for validation of the investigation of Reese and Impe [2002] or a real scenario with fixed pile head connection. This will be explained per section which type of connection is present.

4.2 Input parameters

4.2.1 Pile parameters for embedded piles

The structural characteristics for the analysis of horizontal forces acting on a pile are determined by its cross-section and the material properties of the pile. For concrete that remains under compressive loads, which is always the case in operational conditions, the approximate volumetric weight and Young's modulus are given by uncracked concrete, a widely accepted parameter set.

Plaxis 3D requires the axial skin friction and base resistance as input, which can be determined by the multi-layer approach. It is chosen to model this with a multi-linear approach to know the influence of each layer on the skin resistance.

$$\begin{aligned}
 N_{\text{pile}} &= F_{\text{max}} + \frac{1}{2}L_{\text{pile}} (T_{\text{skin,start, max}} + T_{\text{skin,end, max}}) \\
 N_{\text{pile}} &= F_{\text{max}} + \sum_{i=1}^{n-1} \frac{1}{2} (L_{i+1} - L_i) (T_i + T_{i+1})
 \end{aligned}
 \tag{46}$$

With F_{max} the maximum allowable base resistance, L the length of the pile and T the skin resistance at start or end. The equation is made up of an increasing skin friction with depth, added to a constant base resistance. This formula gives an indication of the axial skin resistance, while the real cases consider multi-linear approach as each layer has his own properties. The multi-linear approach is visible as summation. The skin friction is found to be a function of

$$\begin{aligned}
 T_{i/\text{max}} &= 2\Pi R_{\text{eq}}\tau_i \text{ with } \tau_i = \alpha_s q_c \\
 T_{\text{min}} &= 0
 \end{aligned}
 \tag{47}$$

With R_{eq} the equivalent pile radius or in this case the true radius of the pile, α the undrained shear strength factor and q_c the tip resistance of the layer. This formula is used for end bearing piles, which is true in our case. Most of the bearing capacity will be from the deeper sand layer, visible in the fact that the skin resistance per meter is much higher than previous layers. For the values stated in table 5, a factor of 0.85 (ξ) is used standard for parameter variations inside the layers. In order to model the behaviour correctly, it is chosen to not use this standard ξ , but rather having unfactored skin resistances.

Table 5: Skin resistance per layer for multi-linear axial resistance calculations

	Layer identification	Upper boundary (m)	Lower boundary (m)	q_c (MPa)	Max skin resistance (kN/m)	Max skin resistance Unfactored (kN/m)
1	Top layer	0	-1	2	41.7	49.2
2	Peat	-1	-3	0,1	2.08	2.46
3	Clay	-3	-8	0,2	6.25	7.38
4	Sand loose	-8	-10	5	104.2	122.9
5	Sand medium	-10	-20	13	270.9	319.6

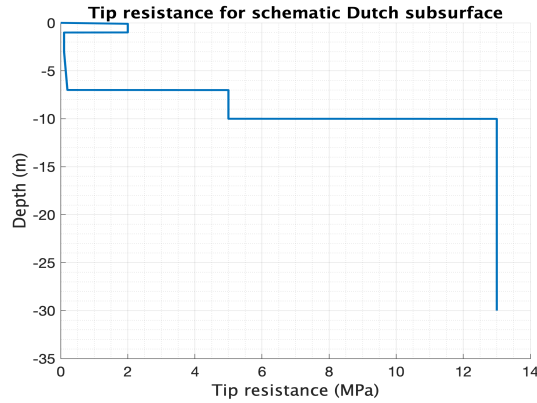


Figure 23: Tip resistance corresponding to soil description

In order to calculate the base resistance, the method of Koppejan can be used. This method is stated in NEN9997, formulated as:

$$q_{b,max} = \frac{1}{2} \times \alpha_p \times \beta \times s \times \left(\frac{q_{c;||;gem} + q_{c;||;gem}}{2} + q_{c;||;gem} \right) \quad (48)$$

$$F_{max} = q_{b,max} * A_{pile}$$

The parameters are taken from pile information in NEN9997. The explanation of the factors are given below

- α_p pile class factor (in this case: 0.7 [-])
- α_s pile class factor (in this case: 0.014 [-])
- β pile foot shape factor (in this case: 1.0 [-])
- s shape factor from cross section of pile footing (in this case: 1.0 [-])
- q_c Cone resistance of layer [MPa]

Using this approach and comparing this with the given data-sheets from RHDHV results in a unfaored base resistance of 2183 kN.

4.2.2 Pile parameters for volume pile

The bearing capacity of a volume pile can be determined directly in the Plaxis model from pile-soil interaction. This does however require a calibrated choice of the interface characteristics (R_{inter}) between pile and soil. This requires a separate, extensive analysis which is not within the scope of this thesis.

5 Static single pile response

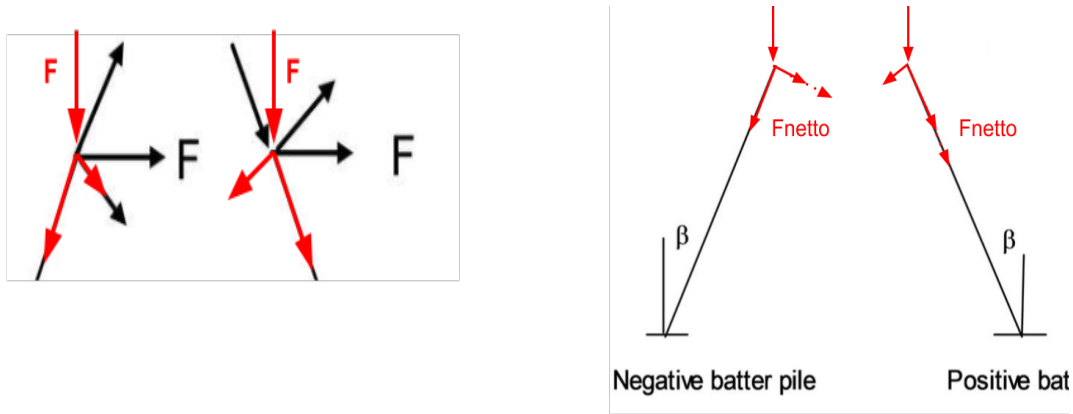
To check which parameters and pile modelling choices are determining the output or the displacement/stiffness requirements for the foundation, the single pile reference response is being assessed. This section will conclude which type of pile modelling approaches real world pile behaviour. In order to do so, several steps are being taken. First the static loading conditions will be applied. In order to check the influence of input parameters, the model-size and mesh-coarseness will be analyzed first. For the analysis the loading conditions are taken to be the average load that each pile needs to bear in order to not fail. In order to assess the worst case scenario, this pile is loaded as average load carrying pile in a group. This means that the single pile response is roughly 1.2 times higher than the single pile response to ensure that unfavorable effects can be taken into account and the pile does not reach a failure state. This is taken into account as group response of piles can result in efficiencies ranging between 0.8 and 1.0. The mesh size is set to medium with 0.2 local refinements, which was found to have the best computational time to precision ratio as will be explained in a later section.

The single pile response will be assessed on three different loading scenario's, which are defined by the angle the pile makes with the horizontal plane. An indication of the loading direction and the meaning of positive and negative batter angle is given below. This single pile reference point is needed to assess the efficiency of a single pile in the pile group. The batter angle is applied as reference point for complex battered pile groups.

Figure 1 shows the influence of batter angle of piles on pure horizontal loading conditions, while figure 24 the same reaction with horizontal and vertical loading conditions. When applying a horizontal load, the forces will be decomposed in pure axial and pure radial loading. A positive batter angle will ensure axial forces downwards, a negative batter angle results in axial forces upwards.

Combining this loading scenario with a vertical death load results in a more axially orientated loading scenario for the positive batter angle, while the negative batter angle receives a more radially orientated loading scenario. This is visible in figure 24b as the positive batter angle has an addition of lateral and vertical loading in the axial direction while the negative batter angle shows the addition in the radial direction. This same principle results in larger lateral forces for negative loading, result in an extra rotation of the pile head, with extra lateral displacement as result. While negative loading does result in less axial forces, the limiting factor is the lateral loading condition for these piles.

The assumptions for these movements are only considering initial free head conditions. As fixed pile head conditions are present when modelling pile groups, this may alter the explanation given before.



(a) Combined vertical and horizontal loading

(b) Net forces

Figure 24: Influence of vertical dead load and lateral loading on radial and axial force distribution

5.1 Model size

Mesh size is one input parameter in the Plaxis program. The initialisation of a new project requires the input of the minimum and maximum x,y and z directions in order to create the subsurface. The z-direction is primarily of influence for large static vertical loads when applied close to the maximum bearing capacity. As the piles are assumed to not approach failure, and the maximum load is far below the maximum vertical loading conditions, the area of influence underneath the piles is small. Wang and Orense [2022] found the influence zone in z direction for a single pile under static loading conditions results in the following equation:

$$L * \cos(\beta) + 6 * D \quad (49)$$

Where β is the batter angle and D the diameter of the used piles. As the length of the piles is taken on average to be 16 m with a diameter of 0.559 m, the z-minimum should lay around:

$$16 * \cos(90 - 82.9) + 6 * 0.559 = 19.23m \quad (50)$$

This response is also confirmed by checking the zone of influence in the z-direction as visible in figure 26.

Each of the piles is checked on two different points of interest, visible in the x-y plane and the x-z plane. In order to check if stress fields are cut off in area's of high stress, a lower boundary of 0.45 kN/m² is taken to ensure that enough of the displacements are captured with the applied force in the model without unnecessarily increasing the amount of elements. This lower boundary is roughly 1.5% of the total load applied horizontally, 0.1 % when considering the vertical dead load.

The second point is displacements. Again roughly 1% is taken as lower boundary for the horizontal and vertical displacements. Combining both points then result in a rough 3D zone of high influence, knowing this zone can ensure an optimized mesh in x,y and z direction.

To ensure that no extra vertical/ horizontal displacement is taken into account for the battered piles under both vertical and lateral loading, the battered piles will only be analysed using lateral loading only. This is done to minimize extra unrealistic free pile head movement.

5.1.1 Volume piles under horizontal loading conditions in x-y plane

Using the mentioned stress concentrations of <1% of the applied force horizontally and the found displacements at the edges at <1% of the total displacements, the two graphs below are created. It is clearly visible that the boundaries at -8 and 8 m for both the x and y direction are far enough away to ensure that no stress cut-offs are visible in the upper and lower boundaries. The zoomed in displacement, with a width of -1.65 to 0.65 m, shows that the majority of displacements are happening in the first 0.8 m from the pile.

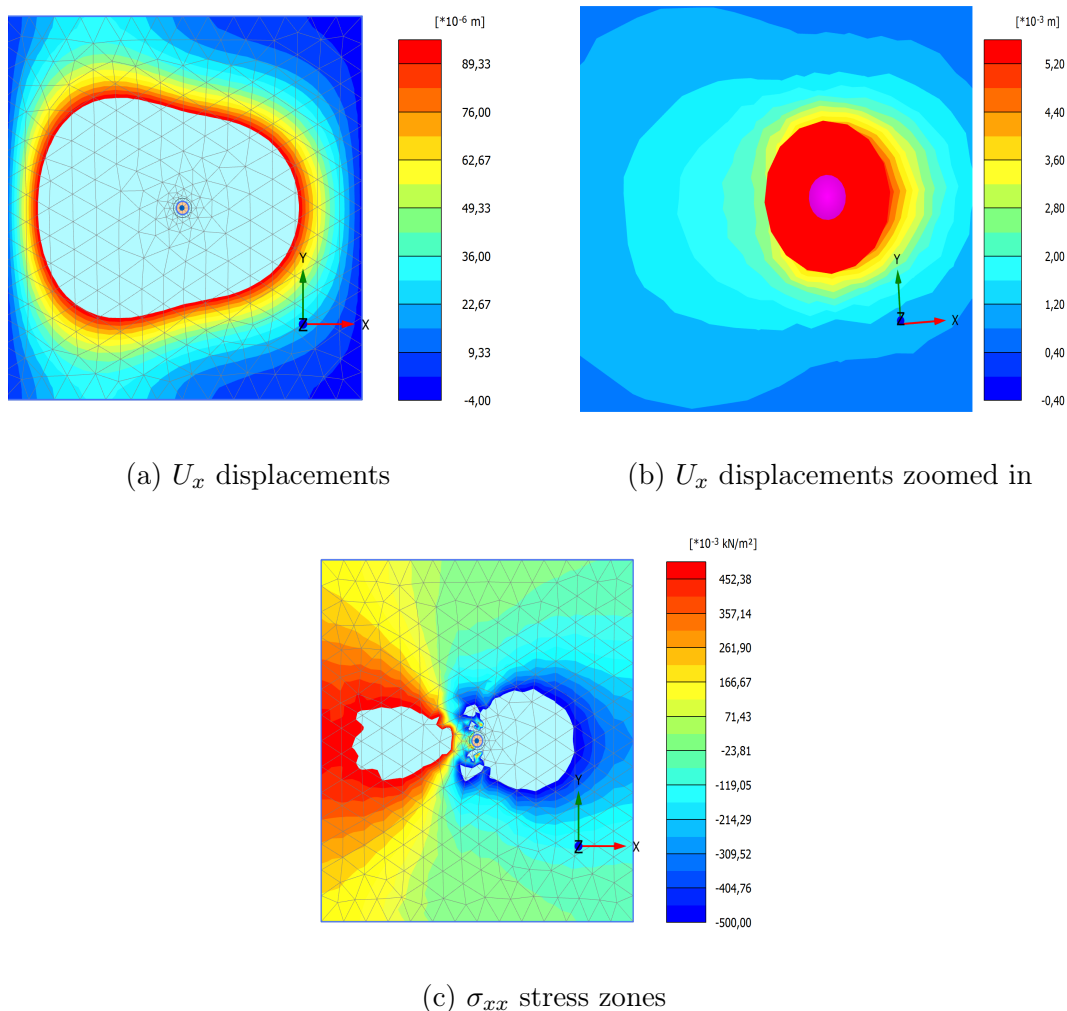
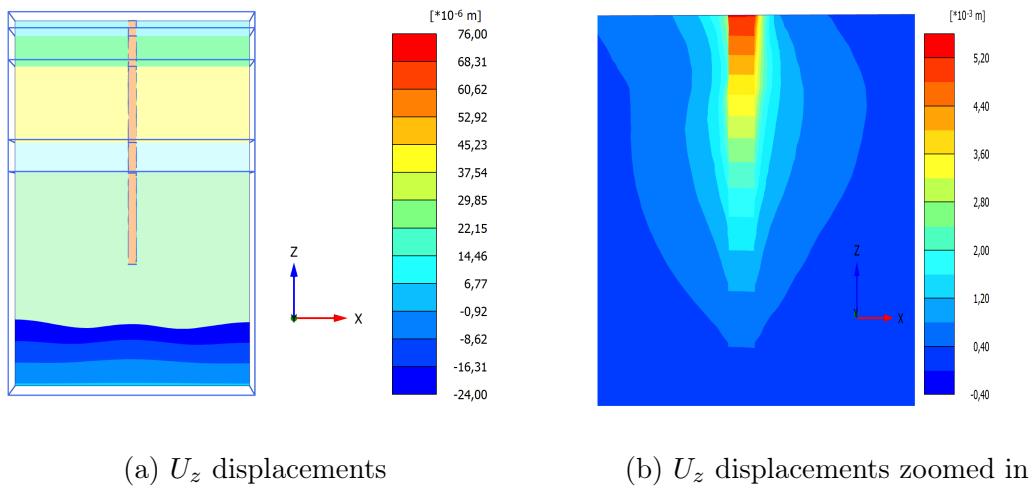


Figure 25: Influence of loading on mesh size in x-y-direction for volume piles initially 16m deep with a mesh of 24m deep

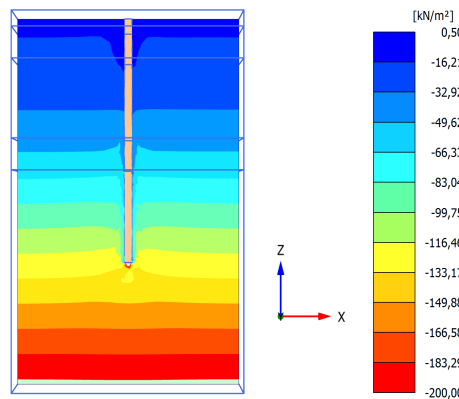
The z-direction will have a slightly different pattern. When considering the σ_{zz} also the soil-stress will be visible in layers, as depth increases the total stress in each lower point

will also increase. The zoomed in displacement in z direction has a depth of -5.5m, which shows that the majority of displacements are found in the first 5.5m.



(a) U_z displacements

(b) U_z displacements zoomed in



(c) σ_{zz} stress zones

Figure 26: Influence of loading direction on mesh size in z-direction for volume piles initially 24 m deep

It is chosen to alter the lower stress-levels according to the presence of soil-weight stresses. It is visible in both the stress-fields as well as the displacements fields that the lower disruptions are located around -17.5 m and -19.8 m respectively. Considering the found relation from Wang and Orense [2022] mentioned before, this relation can approach the lower level of the mesh-size as $16 * \cos(90 - 82.9) + 6 * 0.559 = 19.23m$.

The same check is made for 1:8 battered piles, only loaded horizontally. The first set of figures is contributed to positive loading, the second set to negative loading conditions. As the batter angle does not make a difference in the length of the pile and the batter angle, a general lower level is assumed.

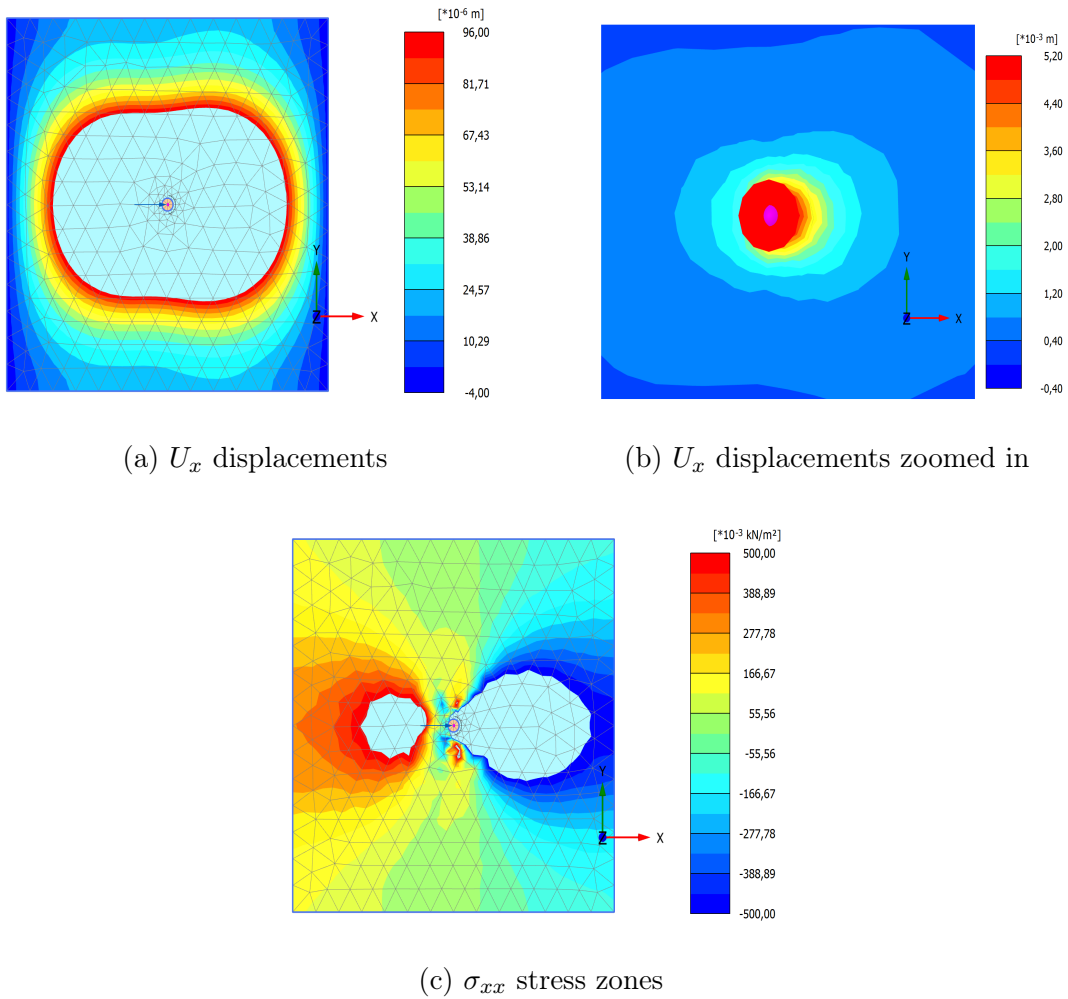


Figure 27: Influence of positive loading direction on mesh size in x direction for volume piles

The positive loading direction results in a slightly larger passive side stress-field in comparison with the vertical pile with combined loading conditions. The area of influence for the U_x displacements are slightly larger in the passive direction in comparison with the vertical piles. The zoomed in section from -1.9 till 1.9 m shows that the majority of the displacements are found in the first 0.8 m. This is in line with the expectations of the vertical pile.

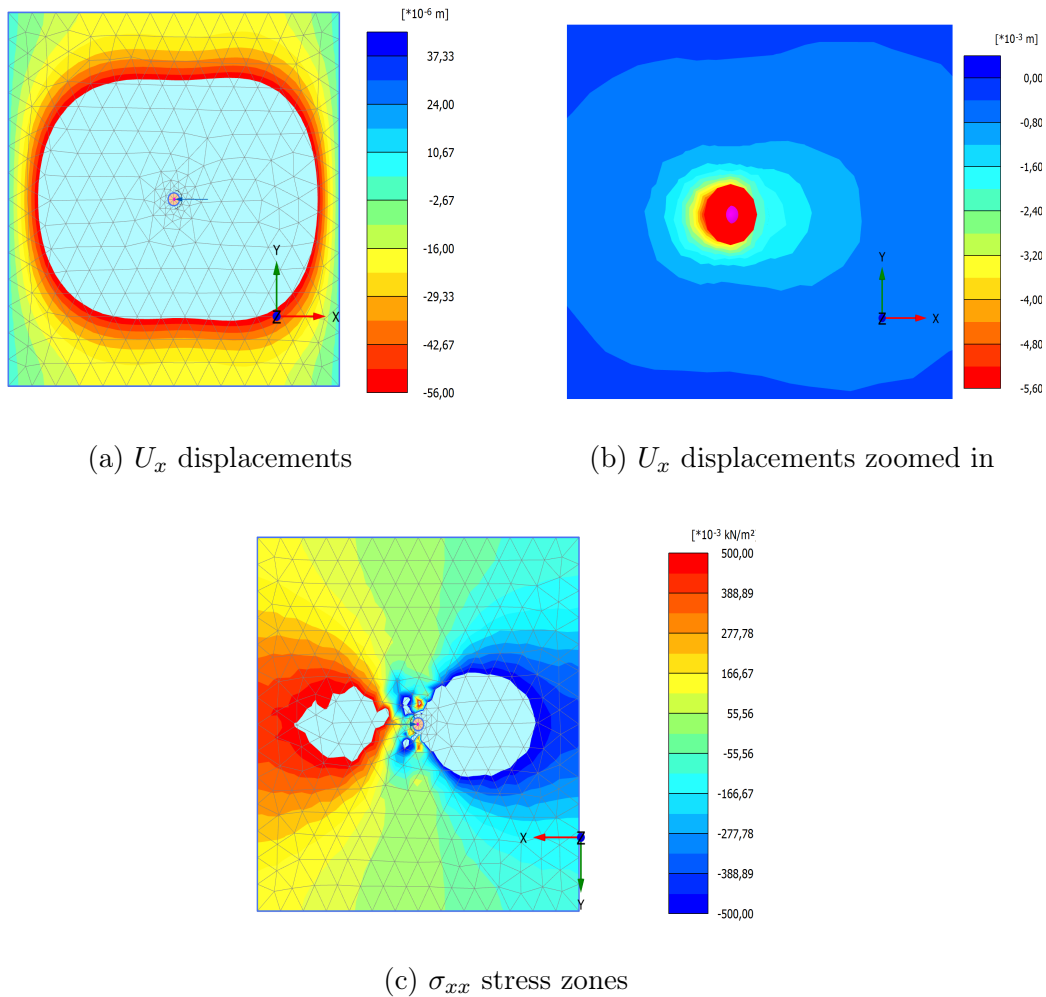
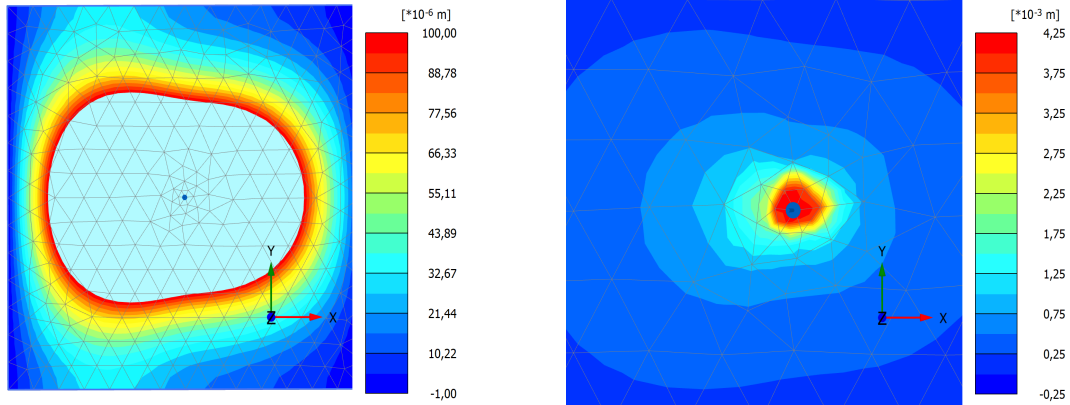


Figure 28: Influence of negative loading direction on mesh size in x direction for volume piles. The stress field is turned 180 degrees to compare the active and passive side

For the negative loading direction the zone of influence for the passive side for σ_{xx} approaches that of the vertical pile. The active side is slightly smaller. The displacement field has a larger field than both the positive as well as vertical loading conditions. While the displacements are still within the limits, a smaller mesh should not be considered. The zoomed in section from -1.8 till 1.9 m shows again that a large portion of the displacement is captured in this area, most of it in the first 0.8 m from the midpoint of the pile. When considering the vertical loading conditions for the vertical pile, the negative batter angle results in a stress-field that is more comparable with a pile under combined loading conditions.

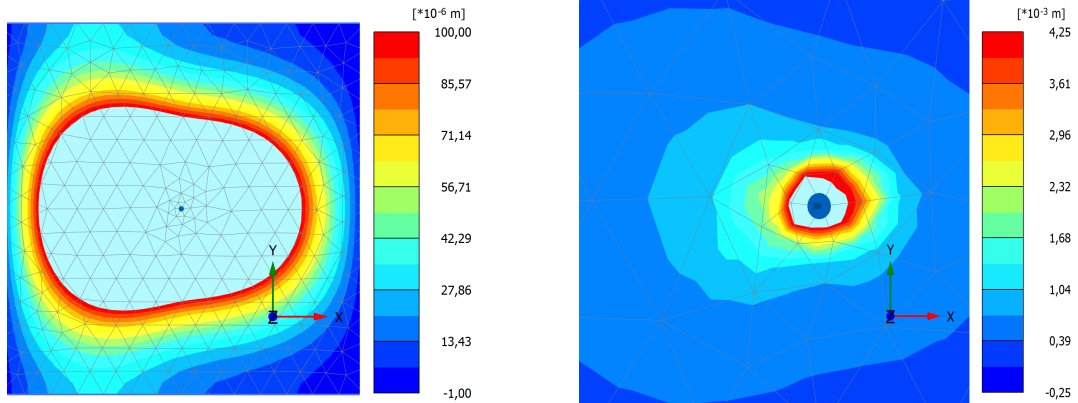
5.1.2 Embedded beams under horizontal loading conditions in x-y plane

The same procedure can be used to check the results for embedded beams. The skin friction and base resistance are input parameters, which can influence in σ_{xx} stresses. A first check between the volume piles and embedded beams can be made in regards to stress-fields and displacement-fields. As there are two different embedded beams, namely the old and new version, these two will be compared to the volume pile.



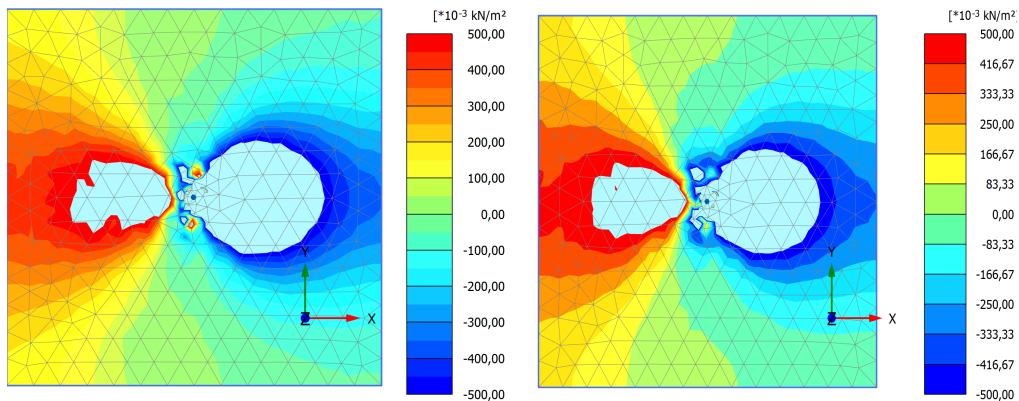
(a) U_x displacements New

(b) U_x displacements zoomed in (-3.5 - 2.7m) New



(c) U_x displacements Old

(d) U_x displacements zoomed in (-2.1 - 1.6m) Old



(e) σ_{xx} stress zones New

(f) σ_{xx} stress zones Old

Figure 29: Influence of loading on mesh size in x-y-direction for new and old embedded beams initially 16 m deep with a mesh of 24 m deep

The shapes of the displacement-fields and stress-field are in line with what is expected from embedded beams. The old embedded beam seems to mimic the volume pile in regards

to both fields the best. It is visible that with using the same scale, the old embedded beam results in a zone where nothing is colored thus in a higher maximum displacement. The zoomed in section shows that the largest portion of displacement happens inside x direction of -1.8 till 1.6 m.

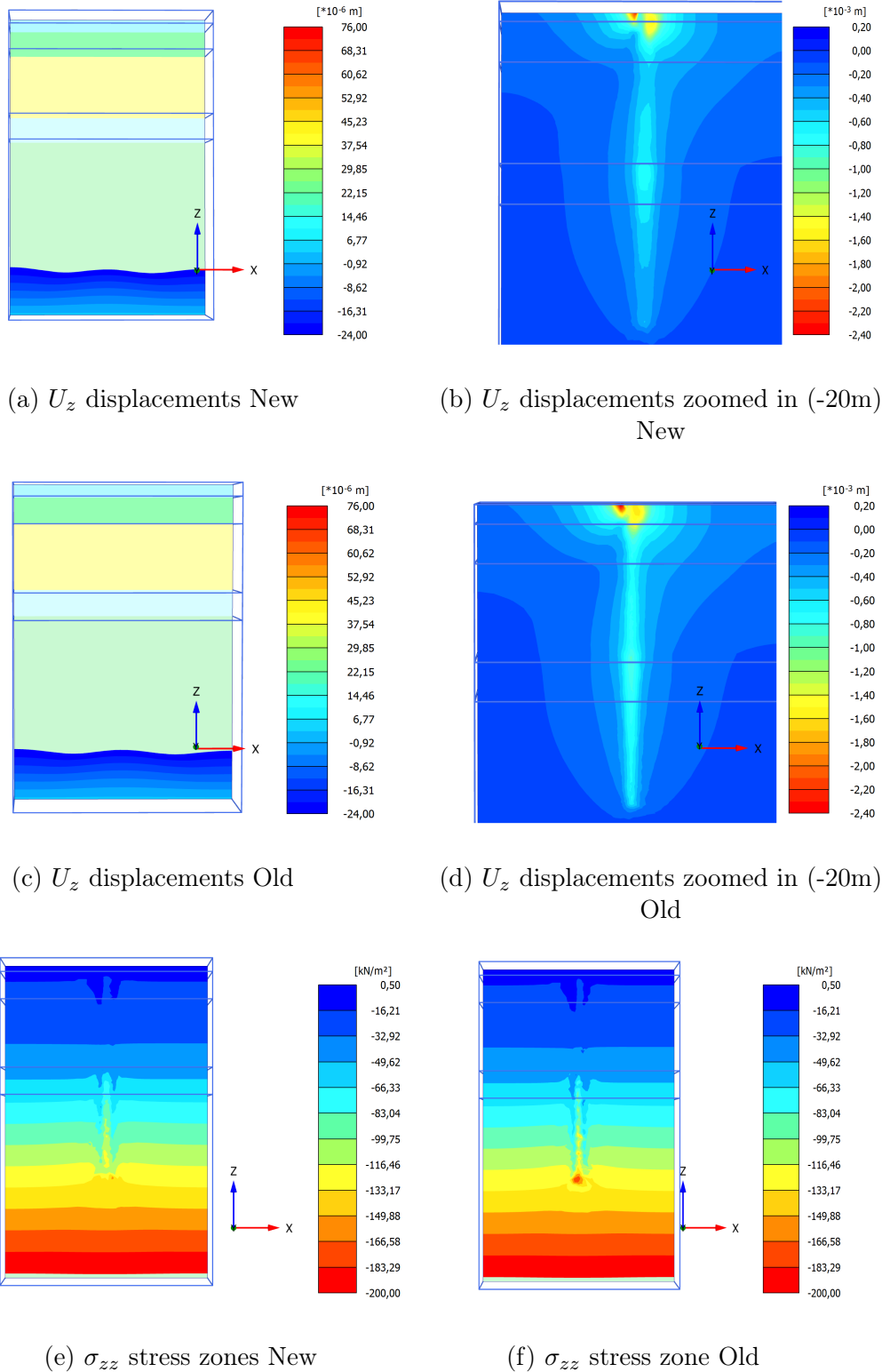
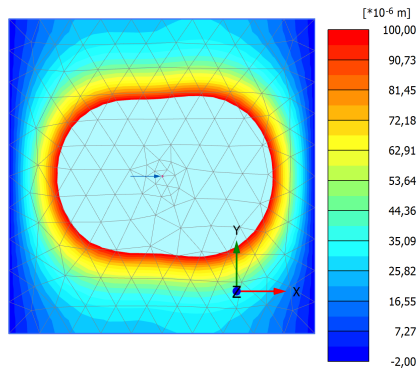
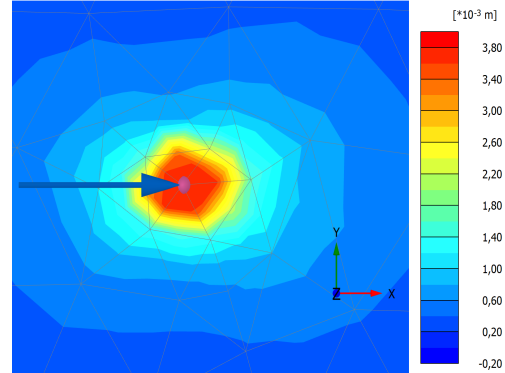


Figure 30: Influence of loading on mesh size in x-y-direction for new and old embedded beams initially 16 m deep with a mesh of 24 m deep

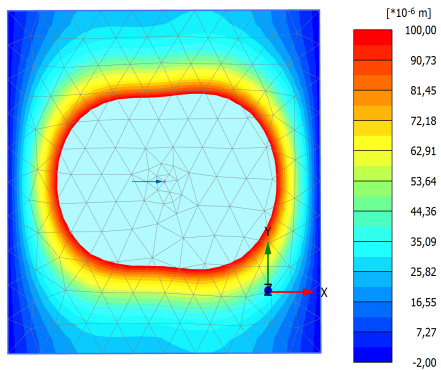
The difference in z direction is found to be minimal. Only a small high stress section directly below the pile footing marks the differences. While the old embedded beam zoomed in seems to have a rough continuum displacement along the complete pile, the new embedded beam zoomed in only seem to have a higher displacement in the middle of the pile. The upper and lower section seems to have less displacements.



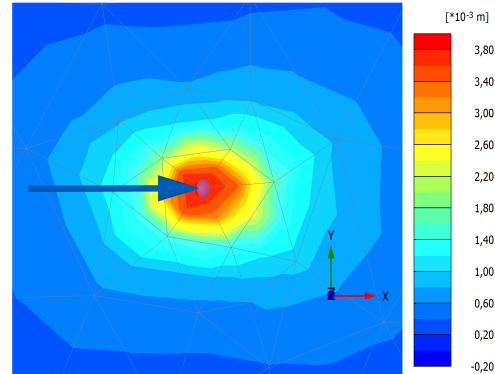
(a) U_x displacements New



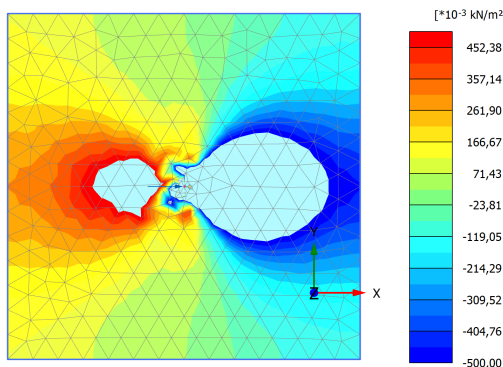
(b) U_x displacements zoomed in (-1.9 - 2.3m) New



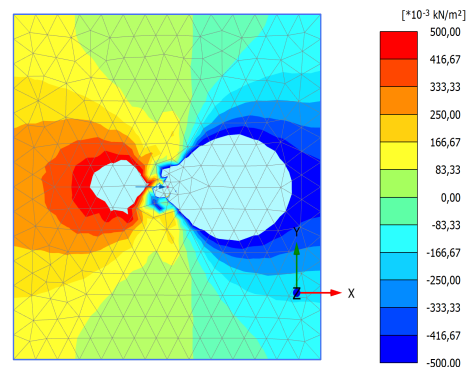
(c) U_x displacements Old



(d) U_x displacements zoomed in (-1.9 - 2.7m) Old



(e) σ_{xx} stress zones New



(f) σ_{xx} stress zones Old

Figure 31: Influence of loading on mesh size in x-y-direction for new and old embedded beams initially 16 m in length with a mesh of 24 m deep under positive loading conditions

The positive direction shows very little to no difference in regards to stress fields and displacement fields. Only when considering the zoomed in section form -1.8 till 1.9 m, a small deformation in the highest displacement field is found while the rest of the contours are roughly the same.

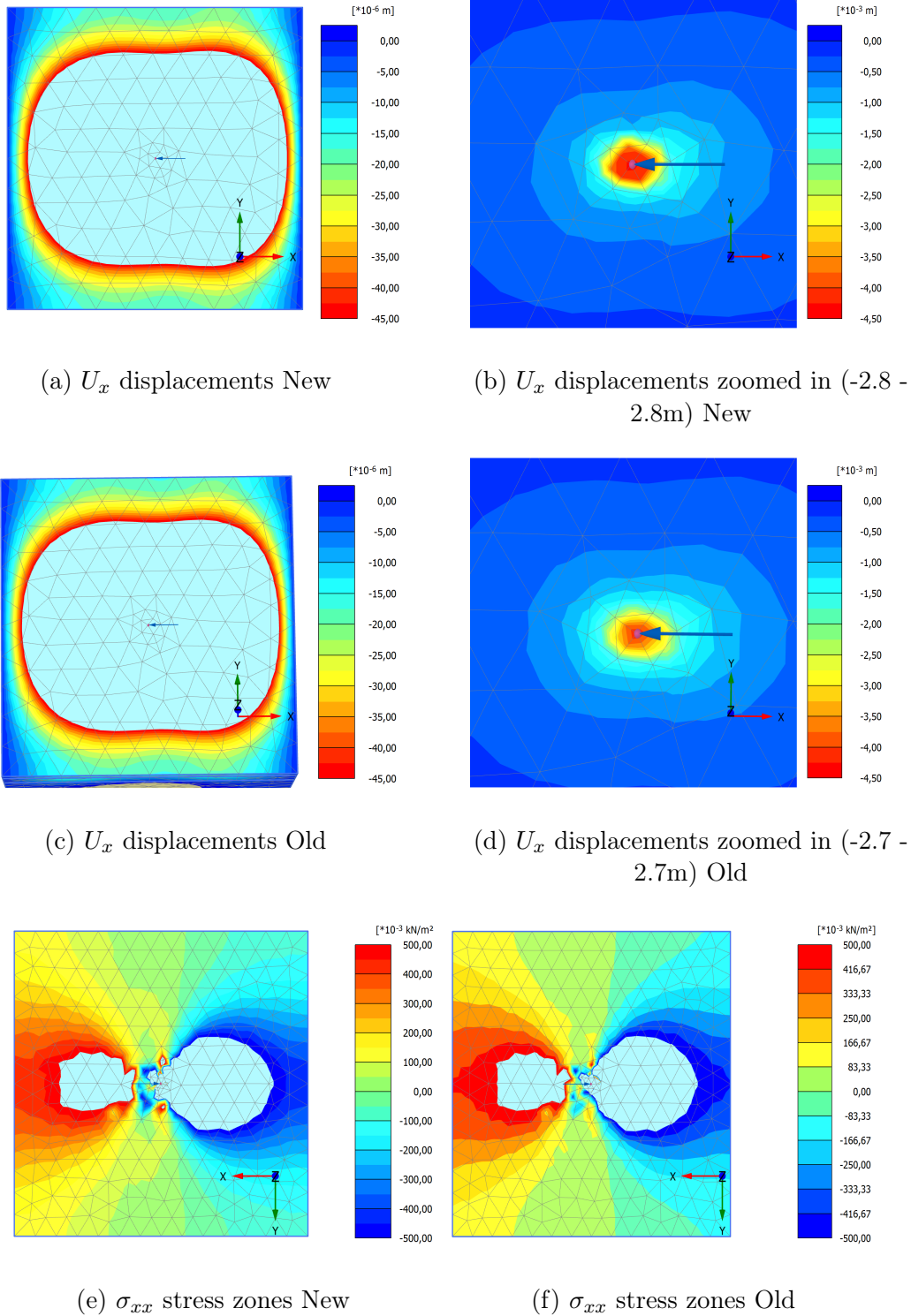


Figure 32: Influence of loading on mesh size in x-y-direction for new and old embedded beams initially 16 m in length with a mesh of 24 m deep under negative loading conditions. The stress field is turned 180 degrees to compare the active and passive side.

The same conclusions can be drawn for the positive loading scenario as with the negative loading scenario. The zoomed in section shows a slightly different high displacement field for the new embedded beam. The overall displacement field is comparable, with the high displacement fields in the same -1.8 till 1.9 m.

It is visible in the comparisons made between the volume pile, new embedded beam and old embedded beam that the mesh-size of 16x16 should not have a large influence on the total displacements important for our settlement and lateral stiffness calculations in later stages. The figures made clear that the boundaries are at enough distance to ensure that no stress concentrations are present. The z direction was taken to be -24 m. Considering the stress-fields and displacement-fields, this can be changed to -20 m as none of the volume piles and embedded beams under several loading conditions exceed this level with discontinuities in the z displacement fields.

The zoomed in sections in the x direction showed that the highest concentration of displacements happen directly besides the pile, with the highest concentration in a radius of 1.6 m surrounding the pile. The figures made clear that the zone of influence is slightly smaller in the y direction, showing that the x direction mesh-size is the limiting factor.

5.2 Mesh Coarseness

Section 2.8.5 described the hanging effect of the volume piles. In order to avoid this effect, the mesh-coarseness can be changed with two different settings. The global coarseness can be set on predefined coarseness settings, varying between very coarse to very fine in 5 steps. Introducing a very fine mesh can resolve the problems described, but may increase the calculation time as more elements are made.

In order to solve the problem that elements at larger distances from the displacements are also modelled smaller, a local refinement can be used. This refinement, especially for volume piles, can be used to increase the amount of elements that should have the highest influence on the total displacement. These elements are located nearby the pile. Elements further away will then be modelled following the global coarseness. By doing this, optimisation of the amount of elements can be made.

The influence is measured under a horizontal loading condition of 35 kN for both volume piles as well as the embedded beams. The top displacement is always found at the top point of the beam. This displacement is plotted for both the defined local coarseness and the global coarseness.

5.2.1 Model setup

The local refinement of 0,2 is chosen to be plotted over all global coarseness lines to ensure that the volume piles are modelled with enough elements to avoid hanging/sacking. This local coarseness is then also adopted for the embedded beams. Using all the data from the local coarseness, this upper limit also ensures that a rough horizontal asymptote is visible in all three piles.

The model is created by using the -8 till 8m and -8 till 8m x and y direction model size, explained in section 5. The model is setup as explained by section 4 with the embedded beam or volume pile centre at 0,0,0 (x,y,z), with three different phases:

1. Initialization: only soil layers and water table are present
2. Phase 1: Activation of embedded beam with length of 16 meters in vertical or battered orientation.
3. Phase 2: Addition of point load on top of embedded beam of 35 kN.

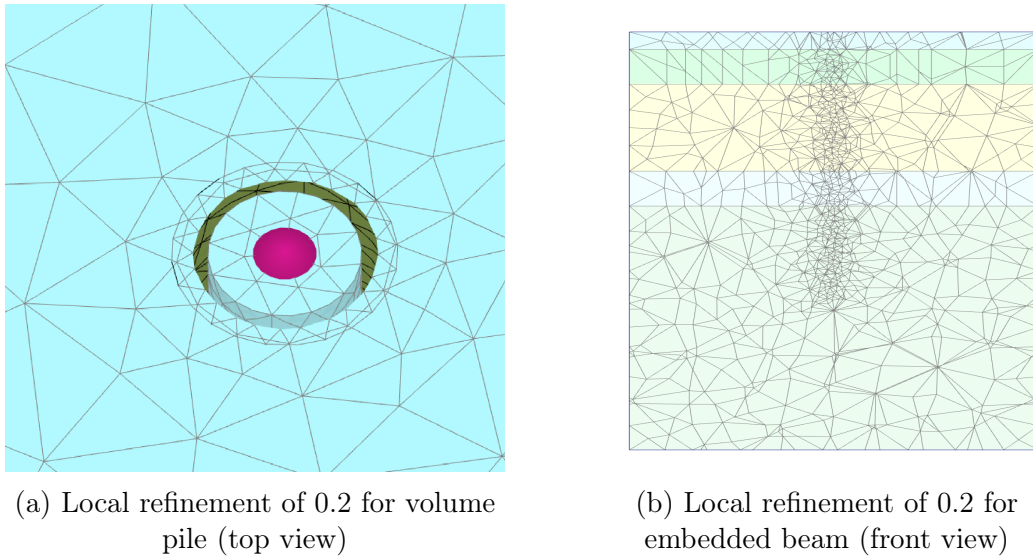
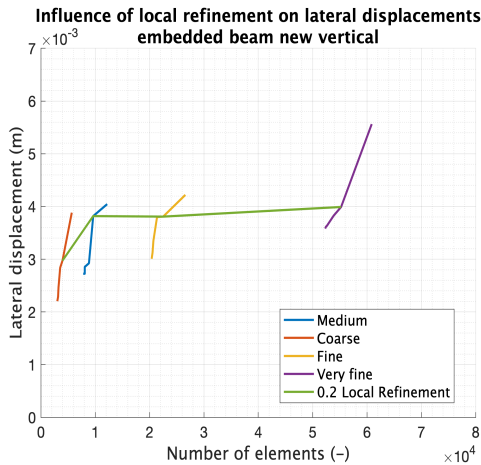


Figure 33: Influence of local refinement of 0.2 to element sizes surrounding the piles.

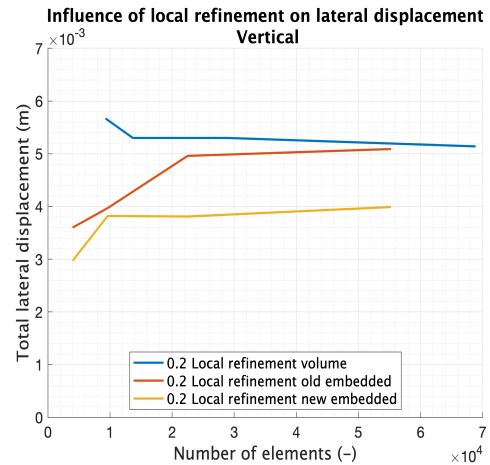
5.2.2 Vertical piles

The first loading scenario is the vertical loading on vertical piles. An example of the graphs with local as well as global refinement is shown. It is shown that the fine global mesh generally introduces a horizontal asymptote, while the section between medium and fine with 0.2 local coarseness also ensures this asymptote.

The lateral behaviour of the volume pile should in theory be more in line with true soil behaviour as the local coarseness is fine enough to prevent sacking. As the local coarseness of 0.2 was visually checked to have at least 20 elements in the pile per unit depth, this should behave as a real pile. The embedded beams are therefore compared to the volume pile, to ensure an optimized realistic lateral response. The old embedded beam does approach the asymptote at roughly $5.0E-3$ m horizontal displacement the best, while the new embedded beam approaches the asymptotic behaviour faster.



(a) Horizontal displacement embedded beam new

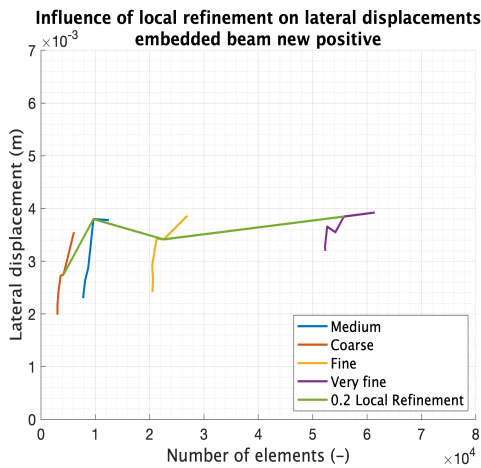


(b) Horizontal displacement with coarseness medium and 0.2 for global and local respectively

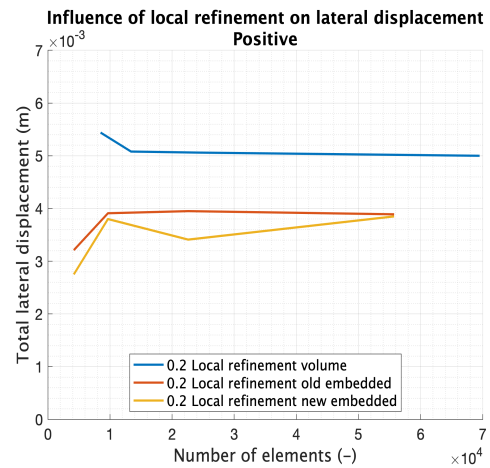
Figure 34: Horizontal displacement for single pile under 35 kN horizontal loading conditions with different global and local coarseness for vertical piles

5.2.3 1:8 battered piles under positive loading

The influence on positive loading direction also favours the behaviour of the old embedded beam in regards to displacements. The new embedded beam does not reach an asymptote in the global and local refinement ranges. The difference between the volume pile modelling and embedded beam modelling for horizontal displacement increases to at least 25%.



(a) Horizontal displacement embedded beam new

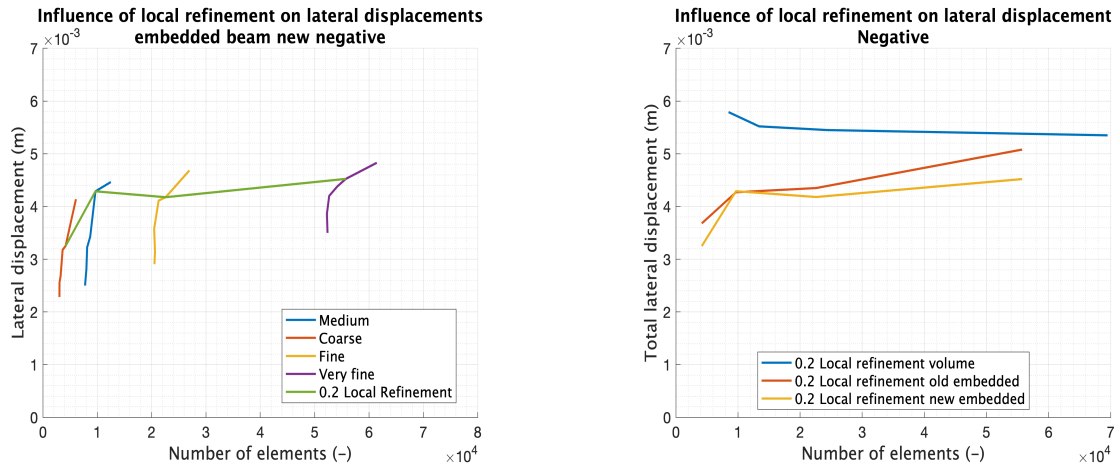


(b) Horizontal displacement with coarseness medium and 0.2 for global and local respectively

Figure 35: Horizontal displacement for single pile under 35 kN horizontal loading conditions with different global and local coarseness for 1:8 battered positive loaded piles

5.2.4 1:8 battered piles under negative loading

The same factors are visible as under positive loading conditions. The horizontal asymptote is not visible under the old embedded beam, this asymptote is present with the new embedded beam. The displacements of the old embedded beam do approach the displacements of the volume piles, because of the absence of the asymptotic behaviour.



(a) Horizontal displacement embedded beam new

(b) Horizontal displacement with coarseness medium and 0.2 for global and local respectively

Figure 36: Horizontal displacement for single pile under 35 kN horizontal loading conditions with different global and local coarseness for 1:8 battered negative loaded piles

When considering the three different load tests, two factors of influence are important to compare. The first factor is the presence of an asymptote in the data set. This asymptote ensures that extra refinement is not necessary as the behaviour is already captured in the lower global refinements. The global refinements steps that are necessary increase the computational time, it is clearly visible that the new embedded beams does approach the asymptotic behaviour better and faster than the old embedded beam.

In contrast to the last finding, the old embedded beam lowers the displacement error in contrast to the new embedded beam, especially in the global section from fine to very fine. The second section from coarse to medium is modelled the same or with higher displacement by the new embedded beam, making it a better choice in approaching the real response.

The differences in regards to displacements between the volume pile and embedded beam can also be explained by the different types of skin and base resistance input or automatic calculations made by the program (volume pile). As stated earlier, this effect can be minimized by adopting different R_{inter} values for the volume pile or changing the maximum skin resistance input for the embedded beams. As a complete comparison is deemed beyond the scope of the thesis, the choice of pile modelling is based on these responses visible above.

5.3 D-sheetpiling: single pile response evaluation

RHDHV uses D-sheetpiling as reference for the displacements and stiffness as explained. This section will perform the same analysis to create the baseline response as expected by analytical subsurface modelling programs.

5.3.1 Model setup

D-sheetpiling is a 2D software, which models the pile as a single pile. The same input parameters are used for the soils as given in section 3.1 and 4. The input for D-sheetpiling is limited for the soil to: Unit weight (dry, saturated), cohesion and friction angle with the Brinch-Hansen method. A Menard modulus of subgrade reaction is applied automatically when the type of soil is selected. An example of a soil layer is given below with the input of the used concrete (vibro) piles.

(a) Soil layer input

	Import profile from library	Name	Material type	Section bottom level [m]	Elastic stiffness EI [kNm²]	Diameter [m]	Mr.charzel* [kNm]	Modification factor k_mod** [1]	Material factor gamma_m [1]	Reduction factor on maximum moment [1]	Mr.del [kNm]	Reduction factor on EI [1]	Note reduci fact
▶ 1	...	Vibro 559 mm E=30 uncrack	Concrete	-16.00	1.438000E+05	0.58	0.00	1.00	1.10	1.00	0.00	1.00	

(b) Concrete pile input

Figure 37: Model setup for D-sheetpiling

The last input parameter is the Menard (E_{mod}) and is not directly related to the the Youngs-modulus. An empirical relation is used that is described as:

$$\frac{1}{k_h} = \begin{cases} \frac{1}{3E_m} \left[1.3R_0 \left(2.65 \frac{R}{r_0} \right)^\alpha + \alpha R \right] & \text{if } R \geq R_0 \\ \frac{2R}{E_m} \times \frac{4(2.65)^\alpha + 3\alpha}{18} & \text{if } R < R_0 \end{cases} \quad (51)$$

With k_h the modulus for horizontal subgrade reaction, E_m the pressiometric modulus, R_0 a constant equal to 0.3m and R the radius of the pile in m and α the rheological coefficient. Normal correlation between E_m and q_c can be found as follows:

Table 6: Empirical relation of Menard subgrade modulus and the tip resistance of the soil

	E_m	q_c (MPa)	E_m (kN/m ²)
Peat	$(3-4)*q_c$	0.1	0.3-0.4
Clay	$(2-3)*q_c$	0.2	0.4-0.6
Loam	$(1-2)*q_c$	2	2.0-4.0
Sand	$(0.7-1)*q_c$	5/13	3.5-5/9.1-13

It is chosen to use the upper limits, as the small strain response that is expected by the limited movement must use a high Menard modulus to approximate both Plaxis and the realistic physical model.

In order to assess the response with a fixed pile head as used by the Plaxis 3D model, the pile head of the model is fixed in a (concrete) slab to prevent rotation as reference for the pile group. A single pile response without fixation is used to assess the displacement of the single pile response in Plaxis 3D.

5.3.2 Response of piles in D-sheetpiling for 35 kN horizontal loading conditions

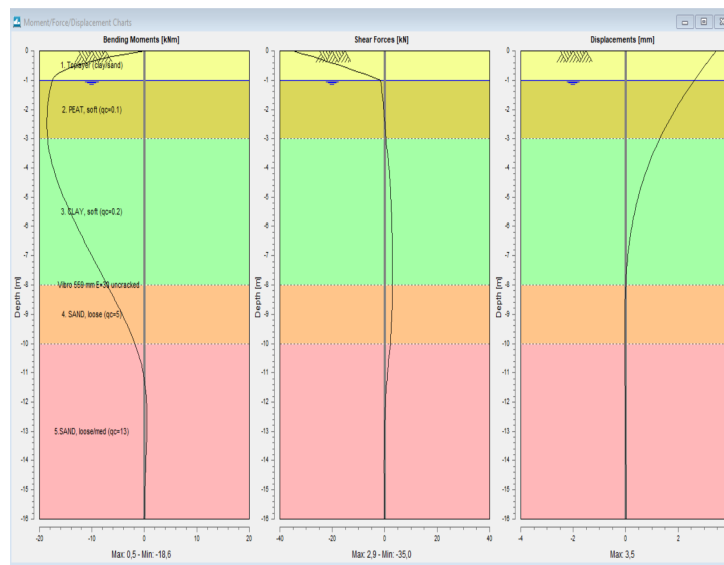


Figure 38: Output of d-sheetpiling for pile without head restrictions and 35 kN loading

The lateral displacement of the used concrete pile is 3.5 mm without head restrictions. The displacements of the single pile reference for this subsurface is described by a displacement of 3.8 mm in Plaxis 3D without head restrictions. Plaxis 3D also showed that the displacements are very small at a depth of 6 meters for both loading scenario's, where D-sheetpiling showed the displacements till a depth of 9 meters. This response could be underestimation of stiffness of the clay layer.

5.3.3 The use of shell-factors in analytical modelling

D-sheet single pile is a 2D method. The method does use a pile and not a wall, but the problem stays 2D. It is stated by Arend [2010] that the primary influence of program are

the horizontal subgrade reaction modulus and the ground pressure coefficients. The use of the Menard method does not take into account a shell factor explicitly. The use of the Brinch-Hansen method, which is combined with the Menard method, does take into account the differences between a (sheetpile) wall and single pile. When using the single pile model, this is already taken into account. Quantification of these shell factors are not described, therefore limiting a direct comparison between D-sheetpiling and Plaxis 3D.

Due to the differences in modelling, an exact comparison between the programs is difficult to make. The response shows that a difference is present between the two types of pile modelling, which may be contributed to too high Emod parameters or even shell-factors. This validation is only made to show that the responses are roughly comparable.

5.4 Influence of batter angle on lateral stiffness for single piles

The pile efficiency in regards to batter angles is tested under five different batter angles, under two different loading conditions. The piles are tested for vertical placement, 1:8 till 1:11 negative loading scenario and 1:8 till 1:11 positive loading scenario.

The single piles were loaded with a 35 kN lateral load with 250 kN horizontal load. This loading scenario will be changed to 35 kN lateral load with a 500 kN vertical load in order to assess the single pile response of the piles for a real ultimate limit state loading case. For the pile setup, a local coarseness of 0.2 with a global medium coarseness is taken. This is in-line with the optimized mesh. The pile heads are not fixed for both loading cases.

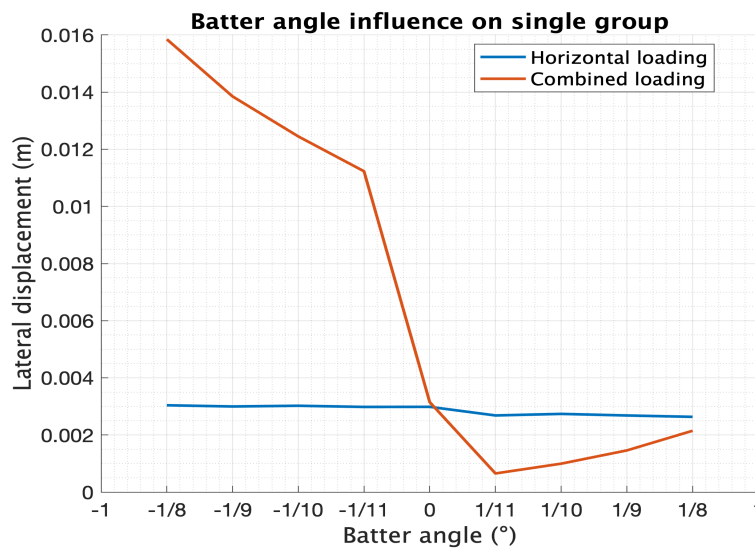


Figure 39: Influence of lateral response in a group versus single pile lateral response

When reviewing the data from figure 39 several trends are visible:

1. Combined loading conditions result in higher displacement under negative loading and lower displacements under positive loading conditions.
2. The horizontal loading group have slightly lower displacements under positive loading conditions than under negative loading conditions.
3. The negative influence of the negative batter angle is much larger than the positive influence of the batter angle in regards to lateral displacements under combined loading conditions.

The trends visible under combined loading conditions for battered piles are having an extra bending moment in regards to vertical loading cases. This effect should be less on the u_x displacements with vertical piles, as addition of the vertical loading for vertical piles should only influence u_z displacements. This effect should also be more present under negative loading than under positive loading, as the loading direction of positive loading assures the forces to be axially loaded. This 'axial' positive loading case has much more capacity than the negative loading case, as the surface in z direction is larger than

x direction ensuring a larger capacity.

In later stages, the piles will be modelled with a fixed pile head, which will result in different results in regards to the influence of batter angles.

5.4.1 Influence of batter angle of lateral stiffness for mirrored two pile group

The setup of this section is to form a pile group of two mirrored piles, to ensure no extra displacements are taken into account for comparison to vertical piles. The pile group will be modelled with 4 positive, 4 negative batter angles and with vertical piles.

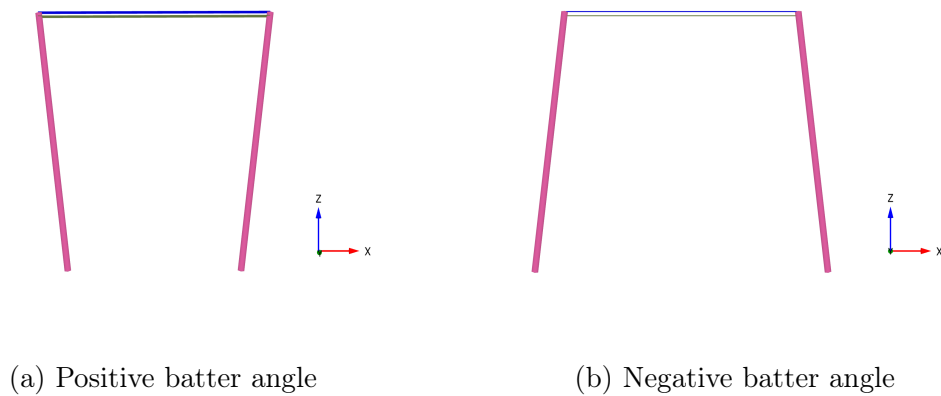


Figure 40: Application of negative and positive batter angles in mirrored configuration

In line with the finding from Reese and Impe [2002], the piles will be modelled with a ctc distance of at least 7.0D to ensure no trailing effects are visible. As the positive batter angle results in a decrease in ctc distance, an extra ctc distance of 7.2D is taken into account. The first test will be run on a ctc distance of 16.5D. A test scenario will be run at the real ctc distance of 15.7 m or 28.5D.

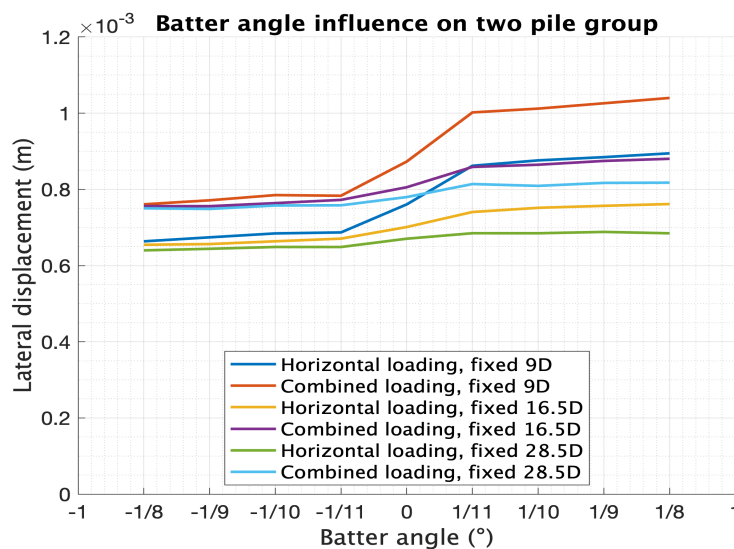


Figure 41: Influence of batter angle on simple mirrored two pile group

Comparing simplified two group response from figure 41 with figure 39 we see that combined loading configurations give higher lateral displacements. This is in line with the expected as explained before, the battered piles will have an extra lateral displacement due to extra pile head deformations of the vertical load. Where the positive loading scenario for a single pile results in higher axial forces, thus less displacement, this principle is not visible with simplified groups.

Comparing the different ctc distances, we can see that the influence of negative batter angles are roughly the same over the ctc distances with the same loading condition. The increase in positive batter angle does create larger differences for both horizontal and combined loading and decrease in ctc distances. An overview of the increase or decrease in lateral movement efficiency is given below in table 7, as supplement to figure 41.

Table 7: Influence of ctc distance and batter angle on lateral displacement of 2 pile mirrored pile group

Loading condition	CTC (D)	Batter angle								
		-1/8 (-)	-1/9 (-)	-1/10 (-)	-1/11 (-)	0 (-)	1/11 (-)	1/10 (-)	1/9 (-)	1/8 (-)
Horizontal loading	9	1.15	1.13	1.11	1.11	1.00	0.88	0.87	0.86	0.85
	16.5	1.07	1.07	1.06	1.05	1.00	0.95	0.93	0.93	0.92
	28.5	1.05	1.04	1.03	1.03	1.00	0.98	0.98	0.97	0.98
Combined loading	9	1.15	1.13	1.11	1.11	1.00	0.87	0.86	0.85	0.84
	16.5	1.07	1.07	1.05	1.04	1.00	0.94	0.93	0.92	0.92
	28.5	1.04	1.04	1.03	1.03	1.00	0.96	0.96	0.95	0.95

The table makes clear that there are no efficiency differences between the two loading conditions. The influence of the ctc distance is clear, as closely spaced piles result in higher efficiencies than at distances where the piles cannot influence each other. The lowest efficiencies are found with the use of the real ctc distance of 28.5D.

The use of a mirrored two pile groups gives difficulties in determining the contribution of each pile on the axial and lateral loading capacities. This setup therefor approximates the behaviour of the use of battered piles in a simplified mirrored two pile group.

5.5 Conclusion of single pile static response

The three different piles are evaluated on their response to increase in model size, but also to the increase or decrease of local and global mesh coarseness. These sections are made to ensure that

- Influence of mesh size is being diminished to ensure only change in parameters such as loading conditions are taken into account.
- An optimal combination of precision and accuracy is taken into account by using a combination of global and local coarseness.
- A reference point is created that can be used to assess the displacements in x, y and z direction with besides references for shear forces and axial forces.
- A check on lateral displacement is performed in D-sheet piling, to ensure that the modelling parameters are in line with an analytical model. This check is also performed to make differences between the normally used analytical program and Plaxis 3D visible.
- A general idea of the influence of batter angles is made, to check if the later groups react the same in regards to efficiency and displacements with an increase/decrease in batter angle.

5.5.1 Model size

The influence of using the three different piles are minimal when considering stress and displacement fields. While some differences are present, the absolute differences between the piles are in the range of 10^{-3} m for displacements under the representative loading scenario. The stress fields showed minor changes, while having the same range of stress concentrations. These small differences may also be contributed to rounding errors in the program, rounding errors in the input or even numerical inaccuracy at that level. All the piles showed that for a single pile response the area of -8 till 8 meters results in enough space to minimize boundary effects. Larger model sizes are required when increasing the group size, using the same methodology as described for single pile analysis.

5.5.2 Mesh coarseness

Considering figures 34a, 35a and 36a an optimization can be made by combining several local and global refinements. Increasing the local refinement does seem to have the most effect. This is primarily visible between a medium and fine global mesh with local refinement of 0.2. As this local refinement is already high, the global should not make any difference. This is visible in the fact that an asymptote is visible, while the combination with lower global refinement ensures less elements are needed.

Using a global medium refinement with a local 0.2 refinement gives approximately the same horizontal displacement results for new embedded beams and old embedded beams. Considering a faster generation of the horizontal asymptote for the new embedded beam, the new embedded beam should suffice in approximating the lateral behaviour of concrete (volume) piles the best.

5.5.3 D-sheetpiling reference

Comparison with D-sheetpiling results in different displacements, 3.5 mm in D-sheetpiling versus 3.8 mm in Plaxis creating a deviation of 0.3 mm. Both programs use a very stiff response, to ensure that small strain behaviour is captured correctly. D-sheetpiling shows that the displacements and bending moments are present till lower depths than Plaxis 3D, potentially underestimating the response for the deeper clay layer. A direct comparison between the programs is difficult to make due to differences in analytical versus numerical approximations and the use of shell factors.

5.5.4 Influence of batter angle on lateral stiffness for single piles

The use of batter angles was considered for single pile, resulting in an extra pile moment and displacement, and the use of the mirrored two pile group to avoid this effect. Both sections showed opposite results, where section 5.4.1 showed a response which is more in line with the expectations from the literature review. The negative batter angle should create less displacements as found by several of authors. Correlations between batter angles and axial capacity are given by Wang and Orense [2022], but only displacements are taken into account due to the limitations of lateral stiffness and not the axial capacities.

The report of Wang and Orense [2022] does show a general increase with a batter angle of 1:8 for both axial as well as shear forces in the range of several percent. Taking into account the difference in piles and subsurface profile, the range of efficiencies for the tested batter angles are in line with the literature values when comparing with displacements. The difference in loading capacity cannot be directly related to differences in displacements, but give an rough estimate of the efficiency increase.

Considering the true distance between the mirrored piles, the efficiencies for both loading conditions result in small differences between 1:10 and 1:8 batter angles. The setup of the model makes it difficult to know which pile is the limiting pile in regards to displacements and therefor shear force mobilization.

6 Group efficiency of simplified group

6.1 General introduction

In order to understand the group behaviour of the complex 3D wind turbine foundation, three different simplified groups are being analysed. These groups represent three different sections that may be present when analysing the 3D behaviour, stated being two groups under parallel and perpendicular loading directions. The third group is having an oblique loading direction. In order to make clear which group can be found where, figure 42 shows each location. Each of these groups will be analysed on shadowing effect, edge effect and presence of these effects under different piles spacings. These spacings are expressed in diameters, generally being between 2.5 a 3.0 diameters from each other (Mooijman, personal contact).

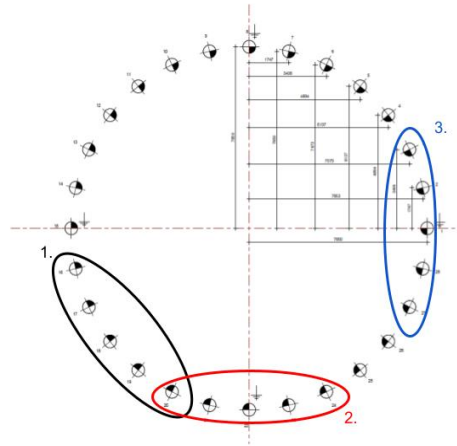


Figure 42: Schematic 2D representation of a wind turbine foundation. Loading is present from lower bottom to top of the figure.

To create a more elaborate figure that represents the stated zones of influence, the following figure is used to explain the edge and shadowing effect. Overlapping of several zones can result in a different maximum load each of the piles can withstand due to disturbed soil surrounding the piles. Normally this effect is visualized in the group efficiency. An efficiency lower than 1 thus implies that the combined group of n piles has a lower total lateral or vertical capacity than n times a single pile. This can be formulated as:

$$Efficiency\ pile\ group = \frac{F_{\bar{s};l;group}}{F_{\bar{s};l;single}} < 1 \quad (52)$$

With $F_{\bar{s};l;group}$ being the average group load capacity at an x loading condition, $F_{\bar{s};l;single}$ the single pile load capacity under an $\frac{1}{n}$ loading condition.

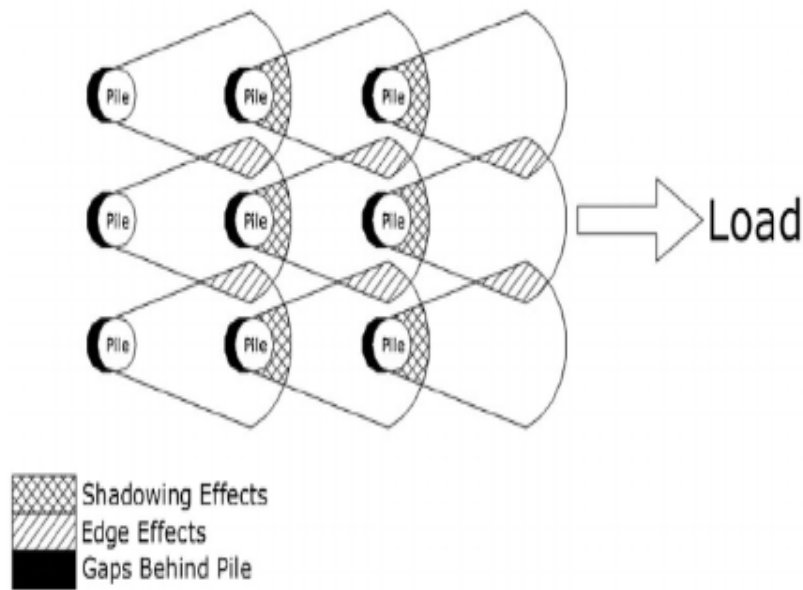


Figure 43: Group effect of piles: shadowing effect, edge effect and gapping Rollins et al. [1998]

6.1.1 (Dynamic)P-multiplier

The efficiency of a pile group is expressed in a p-multiplier. This p-multiplier is essentially the same as the efficiency factor explained in section 6.1. The name is changed as normal usage of single pile performance is linked to p-y curves. As mentioned already, this curve described the displacement of the pile at a particular applied force. Considering the group behaviour, this would lead to a lower force needed for the same displacement or in our case the displacement increases with the same applied force. As the p-y curves are a output of the spring characteristics, this particular response is only valid for a particular depth with a single spring.

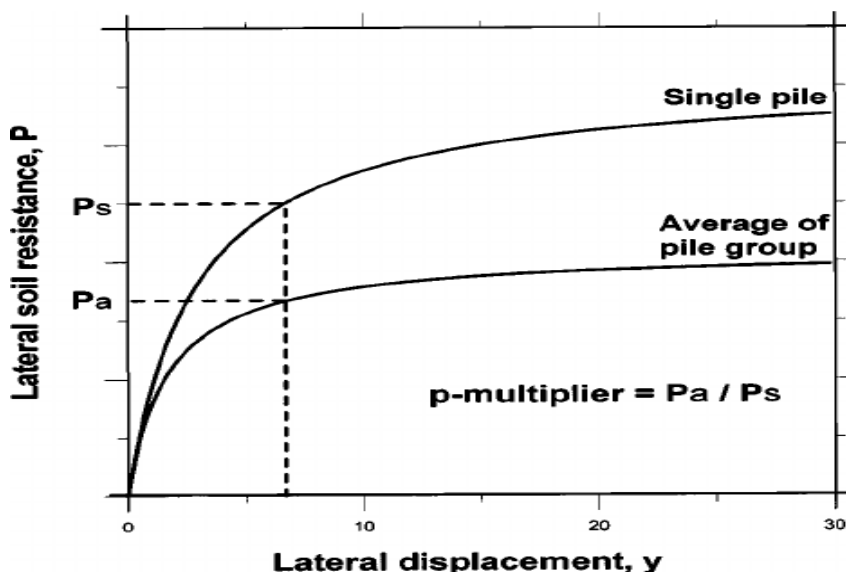


Figure 44: Influence of lateral response in a group versus single pile lateral response

6.2 Group effect

Group effects are a complex interplay between pile diameter, pile roughness, horizontal and vertical ctc distances and normally interpreted by RHDHV by using relations developed by Reese and Impe [2002]. This approach is a composition of experimental testing and using programs to mimic the group behaviour. In order to check that the behaviour in Plaxis is in line with what is expected from theoretical and practical test cases, the data from the this research will be compared to the found data for parallel, perpendicular and skew loading conditions.

The following formula are used by RHDHV to approach the p-multipliers Reese and Impe [2002]:

For perpendicular loading:

$$e = 0.64 \left(\frac{s}{b}\right)^{0.34} \text{ for } 1 \leq \frac{s}{b} \leq 3.75, e = 1.0, \frac{s}{b} \geq 3.75 \quad (53)$$

For parallel loading leading row:

$$e = 0.7 \left(\frac{s}{b}\right)^{0.26} \text{ for } 1 \leq \frac{s}{b} \leq 4.0, e = 1.0, \frac{s}{b} \geq 4.0 \quad (54)$$

For parallel loading trailing rows:

$$e = 0.48 \left(\frac{s}{b}\right)^{0.38} \text{ for } 1 \leq \frac{s}{b} \leq 7.0, e = 1.0, \frac{s}{b} \geq 7.0 \quad (55)$$

For piles under skew loading directions:

$$e^2 = (e_i^2 \cos^2 \phi + e_s^2 \sin^2 \phi) \quad (56)$$

With s the ctc distance, b the pile diameter and ϕ the angle between the pile group and the loading direction. It is visible that the curves behave as a single pile after a particular ctc distance of pile diameters is reached. The data is corrected for a deflection of 1/50th of the pile diameter. The formula's are plotted to see the ctc dependence over the practical limits of field placement of piles.

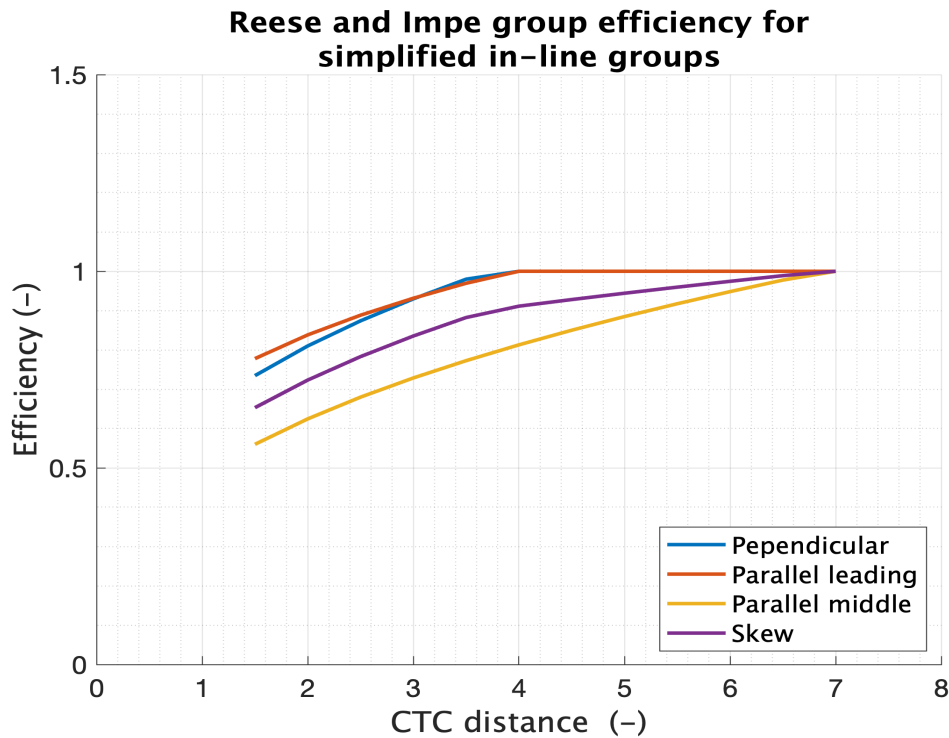


Figure 45: Influence of lateral response in a group versus single pile lateral response

The data from which these approximate relations are created are from Cox 1984, Franke 1988, Prakash 1962, Schmidt 1981 & 1985, Shibata 1989 and Wang 1986. The tests were performed with different soil conditions, different pile types such as concrete and aluminum, different diameters and different load conditions. While figure 45 does not show this data, the lines are an approximation of the reality and it should be remarked that the different experimental circumstances cannot prove the exact relations. This remark is also made by the authors Reese and Impe [2002].

The used data from Reese and Impe [2002] is primarily focused on using one single soil layer, while our model uses a combination of several layers as explained. The second difference is the loading condition, as the data primarily uses data from near failure pile displacement and shear forces.

6.3 Validation of group effect in Plaxis 3D

In order to test the group effect in Plaxis 3D using stated soil conditions and no influence of the plate, a hinged setup is used with a prescribed displacement of $1/50D$ and the use of the weak interface layer. The three different sections as mentioned in section 6.2 are evaluated separately.

6.3.1 Parallel loading

In parallel loading we should expect a higher efficiency factor for the leading pile which should not change after a ctc distance of $4.0D$, the trailing piles should approximate a single pile response at $7.0D$.

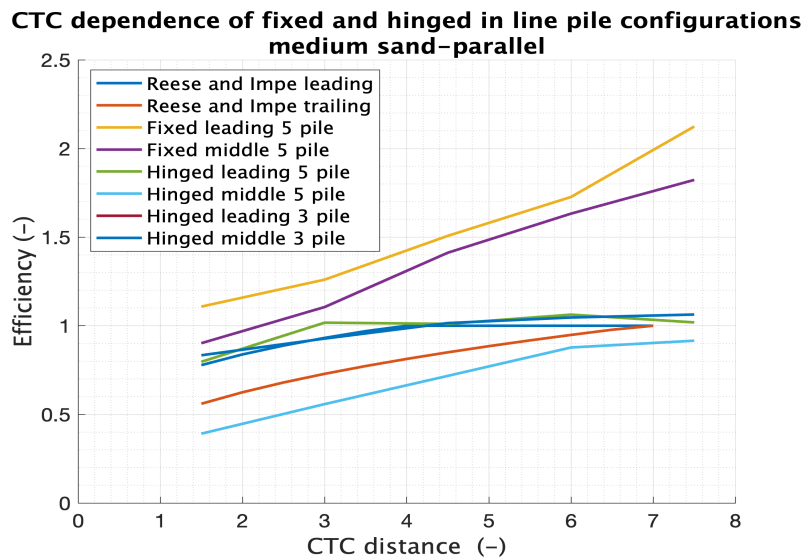


Figure 46: Testing scenario of parallel loading on ctc dependence

The pile placement should ensure that at higher ctc distances, the response should be roughly flat as the efficiency should be roughly 1. Larger pile groups should have larger differences between middle piles and leading piles due to amplification of the already present differences.

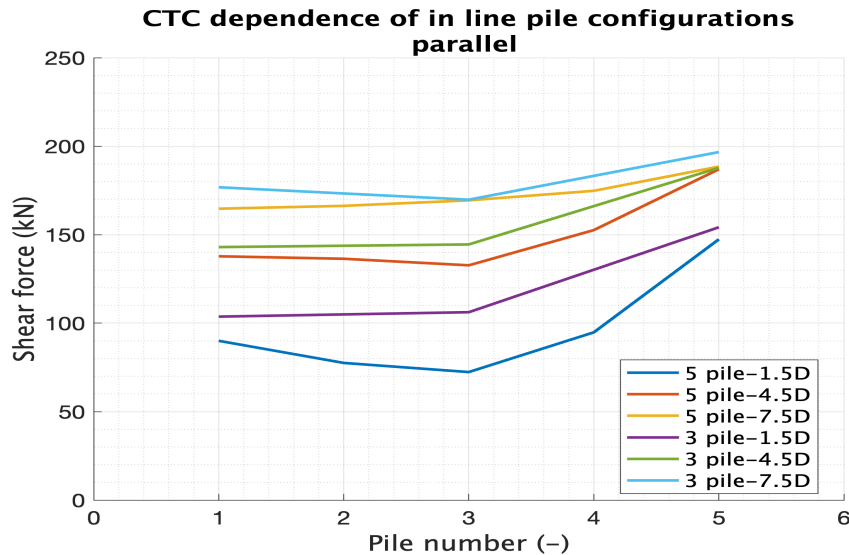


Figure 47: Testing scenario of parallel loading on pile placement

Both the trends are clearly visible in figure 46 and 47. The behaviour of shadowing is correctly implemented in Plaxis 3D. The influence of fixed and hinged pile head modelling on the efficiencies are also clearly visible in figure 46

6.3.2 Perpendicular loading

For perpendicular loading we expect the edge effect, the outer piles will have higher shear forces due to undisturbed grounds at the sides facing outside from the pile group. The middle piles should behave less efficient due to the lower amount of undisturbed grounds.

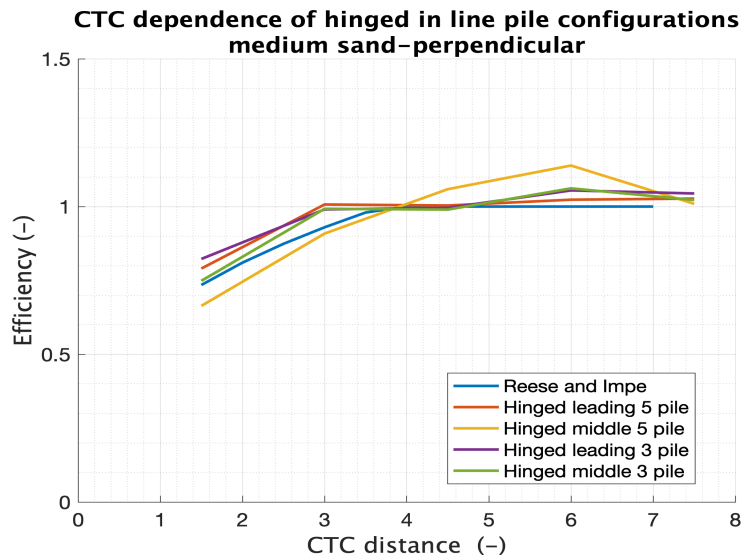


Figure 48: Testing scenario of perpendicular loading on ctc dependence

The pile placement should ensure that at higher ctc distances than 3.0, the response should be roughly flat as the efficiency should be roughly 1.

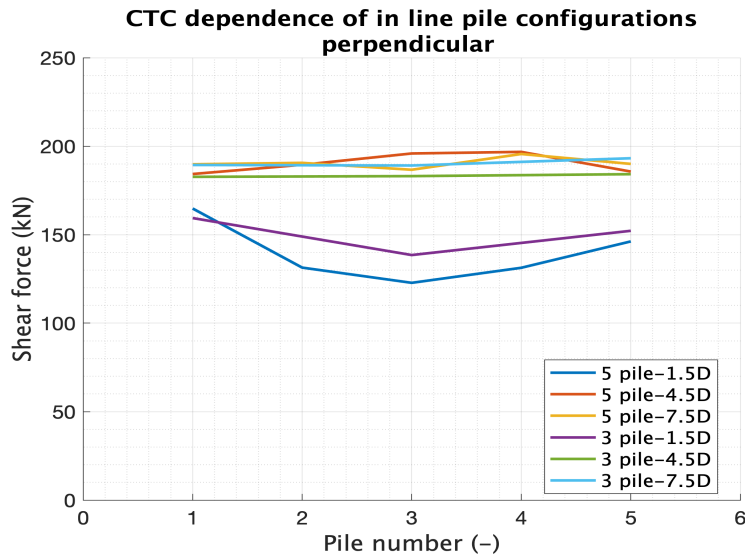


Figure 49: Testing scenario of perpendicular loading on pile placement

Both the trends are clearly visible in figure 48 and 49 as flat response after 3.0D. Before a ctc distance of 3.0D it shows that the edge piles react roughly the same. The edge effect is correctly implemented in Plaxis 3D.

6.3.3 Skew loading

Skew loading should give a combination of effects. Pile number 5 and 3 or 1 should behave as a higher efficiency edge pile than the middle piles. A slight increase in efficiency from pile 5 to 3 or 1 should be visible, as this is the leading edge pile.

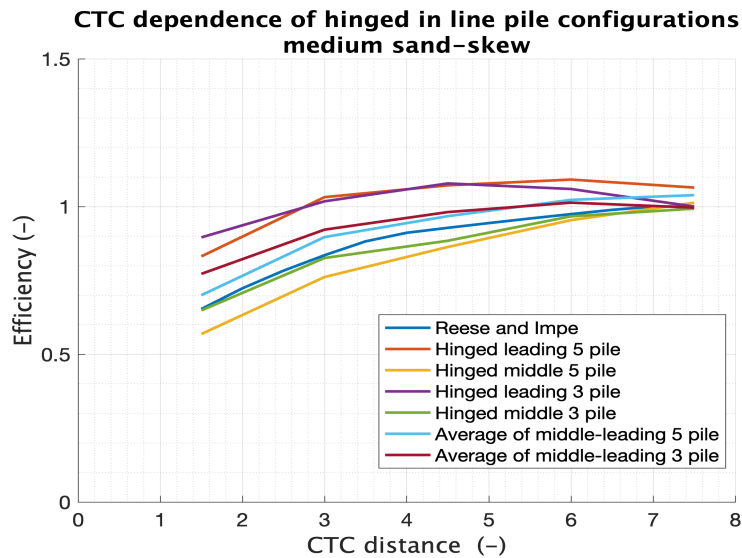


Figure 50: Testing scenario of skew loading for ctc dependence

After ctc distance 7, a flat response should be visible over all the piles.

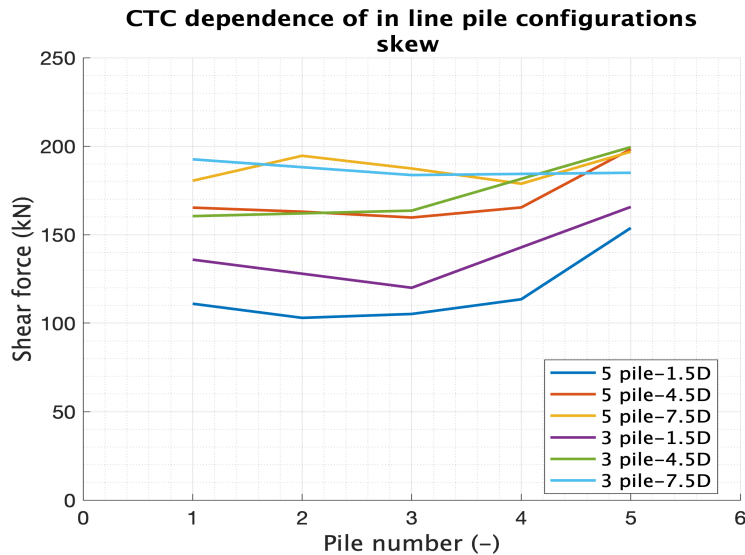


Figure 51: Testing scenario on skew loading for pile placement

The average efficiency factors follow the skew Reese and Impe [2002] line. Pile 5 reacts as higher efficiency pile as expected by the trailing pile effect. The smaller group of 3 piles shows an increase in the last trailing pile, less visible for the 5 pile group. An approximate flat response is found after a ctc distance of 7.0 as expected.

6.3.4 Conclusion of group validation

When considering the separate conclusions and matches with the Reese and Impe [2002] empirical relation, the group effect is taken into account when modelling pile groups and behaves as expected. The skew loading group also behaves as expected, but as the parallel group deviates slightly from the pattern the skew response also deviates slightly from a perfect response. The smaller pile groups of 1.5D do however show a higher efficiency response with last trailing rows that is difficult to explain.

This comparison shows that the response of the pile group can be compared, even when applying a preset load and not a displacement as used by Reese and Impe [2002].

6.4 Parallel loading

As visible in group 3 in figure 42 and 43 parallel loading conditions can result in the shadowing effect. The effect that the distortion of the surrounding ground results in less load carrying capacity in both vertical as horizontal capacity. In order to test this theory, the efficiency of small groups is checked ranging between 3 and 5 piles. By checking several group sizes in regards to parallel loading, the increasing influence of the shadowing effect can be demonstrated from the leading piles to the trailing piles.

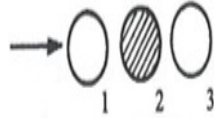


Figure 52: Parallel loading condition

6.4.1 Shadowing effect

In order to assess the influence of the pile group sizes and pile position will be compared for the parallel loading. The tables below will give an overview of the maximum shear forces found at the head of the piles.

Table 8: Maximum shear forces per pile under combined horizontal and vertical loading conditions of 20 kN and 500 kN per pile respectively for parallel loading.

Pile group	etc distance (-)	Pile number (kN)					Pile analysis			
		<u>1</u>	<u>2</u>	<u>3</u>	<u>4</u>	<u>5</u>	Average (kN)	Offset (%)	Middle pile offset (-)	Front pile offset (-)
1x1	-	20.29	-	-	-	-	20.29	-	-	-
1x3	2.0D	22.87	16.3	20.49			20.09	1.00	0.83	1.00
	2.5D	22.64	17.37	20.6			20.20	0.43	0.86	1.02
	3.0D	22.12	17.47	20.43			20.01	1.34	0.86	1.01
	3.5D	22.18	17.61	20.61			20.13	0.77	0.87	1.02
1x4	2.0D	24.55	17.52	16.69	21.66		20.10	0.92	0.83	1.07
	2.5D	23.6	16.3	17.11	22.4		20.00	1.42	0.84	1.10
	3.0D	23.5	17.33	17.57	22.38		20.20	0.47	0.87	1.10
	3.5D	23.05	17.31	17.63	21.84		20.16	0.64	0.87	1.08
1x5	1.5D	28.86	18.33	16.54	16.79	26.18	21.34	-5.18	0.82	1.29
	2.0	26.13	17.68	16.67	17.52	22.46	20.09	0.98	0.82	1.11
	2.5D	24.64	17.81	17.12	17.73	23.03	20.07	1.10	0.84	1.14
	3.0D	24.08	17.87	17.3	17.98	23.63	20.172	0.58	0.86	1.16
	3.5D	24.19	17.82	17.14	17.75	23.56	20.09	0.98	0.84	1.16

Table 9: Maximum shear forces per pile under pure horizontal loading conditions of 20 kN for parallel loading

Pile group	ctc distance (-)	Pile number (kN)					Pile analysis			
		<u>1</u>	<u>2</u>	<u>3</u>	<u>4</u>	<u>5</u>	Average (kN)	Offset (%)	Middle pile offset (-)	Front pile offset (-)
1x1	-	20.44	-	-	-	-	20.44	-	-	-
1x3	2.0D	20.87	16.8	22.66			20.11	1.61	0.82	1.11
	2.5D	21.08	17.07	22.63			20.26	0.88	0.835	1.11
	3.0D	20.82	17.17	22.16			20.05	1.91	0.84	1.08
	3.5D	20.89	17.57	22.17			20.21	1.12	0.86	1.08
1x4	2.0D	22.08	17.08	17.1	24.27		20.13	0.98	0.84	1.19
	2.5D	21.78	16.91	17.13	24.47		20.07	0.98	0.84	1.20
	3.0D	21.92	17.19	17.71	24.03		20.2	0.99	0.87	1.18
	3.5D	21.82	17.18	17.76	23.57		20.08	0.98	0.87	1.15
1x5	1.5D	23.31	17.39	16.82	17.91	25.45	20.178	0.99	0.82	1.24
	2.0D	23.3	17.21	16.61	17.75	25.63	20.1	0.99	0.81	1.25
	2.5D	22.88	17.57	16.78	18	25.39	20.12	0.98	0.82	1.24
	3.0D	22.69	17.49	17.07	18.15	25.55	20.19	0.99	0.84	1.25
	3.5D	22.65	18.6	18.11	19.00	25.38	20.15	0.99	0.84	1.24

A first impression shows that the average of the piles under the three different configurations show no large deviations in respect to the single pile analysis. When considering the middle pile of the groups, larger deviations are found. These middle pile offsets are in line with what is expected from group behaviour stated by the data from Reese and Impe [2002]. The front pile offset results in an efficiency factor higher than 1, which can have the following reason: The piles are not loaded to their full potential. This means that the group effect may result in redistribution of forces to which pile has the most undisturbed ground in the direct neighbourhood. As the piles have a larger potential, these piles will take up most of the loading.

Plotting the data in the figure with group efficiency, we can see several trends.

1. As the piles are not loaded to their full potential, the ctc distance is not influencing the pile efficiency by a large amount.
2. The trailing piles behave in a small upward slope, while the leading piles tending towards lower efficiency factors.
3. Larger group sizes have much more variation in group efficiency factors than smaller group sizes.
4. Average group efficiency for all the piles in the pile groups is within 98% of the capacity a single pile has in regards to lateral loading conditions.

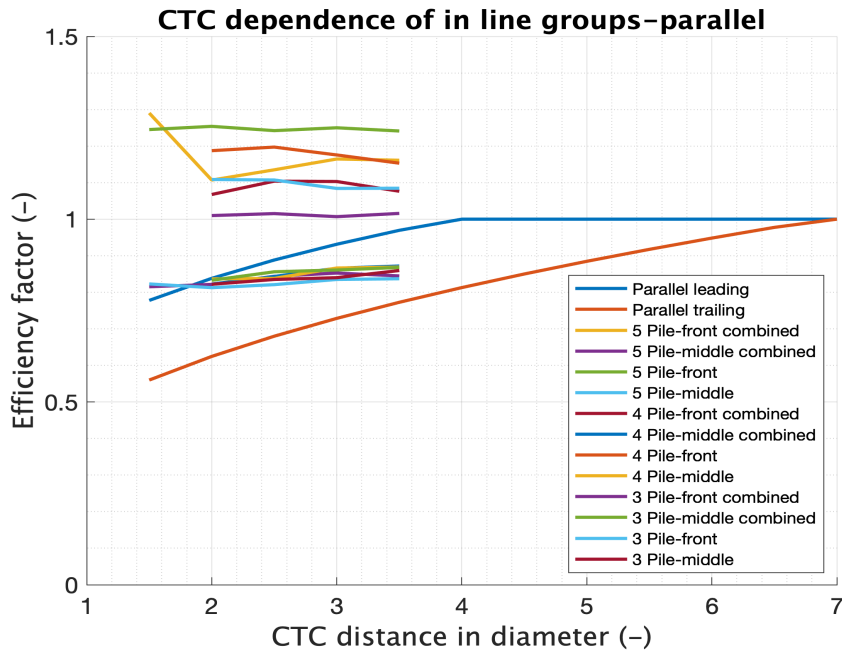


Figure 53: Influence of pile efficiency in regards to pile location for parallel loading

Figure 53 shows that the average leading pile and middle pile have the same efficiency difference as expected from the trend lines. The efficiency factors are higher than expected, having a translocation of roughly 0.2. What cannot be clearly shown in figure 53, is the behaviour of the separate piles in regards to each other for the three used groups. The data is plotted to the maximum shear force, using the 2.5D ctc distance as middle group.

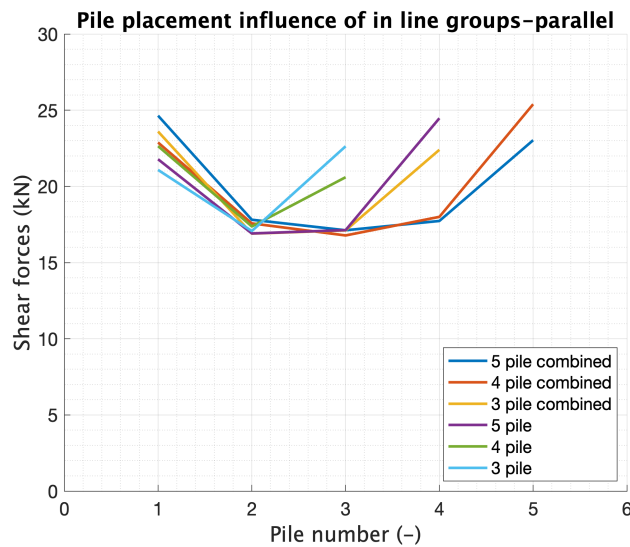


Figure 54: Influence of pile efficiency on pile number in skew direction

The behaviour of combined loading and only lateral loading is clearly visible. The combined loading conditions result in less difference in the maximum shear forces for piles in a group. Furthermore, several trends are visible:

1. Enlarging the number of piles in pile groups increases the leading pile group maximum shear forces and efficiency factor.

2. The last trailing pile has an increased maximum shear force when compared to the previous trailing piles. A slight increase in shear forces is visible when under combined loading conditions as well as enlarging the group size in comparison with only lateral loading and smaller groups.
3. Middle trailing pile maximum shear forces are roughly the same in all configurations.

In order to understand the influence of enlarging etc distances for each pile group, the 2D and 3.5D etc distances for each pile configuration are plotted below. As the differences are minimal between combined and only lateral loading, it is chosen to plot the data for combined loading conditions.

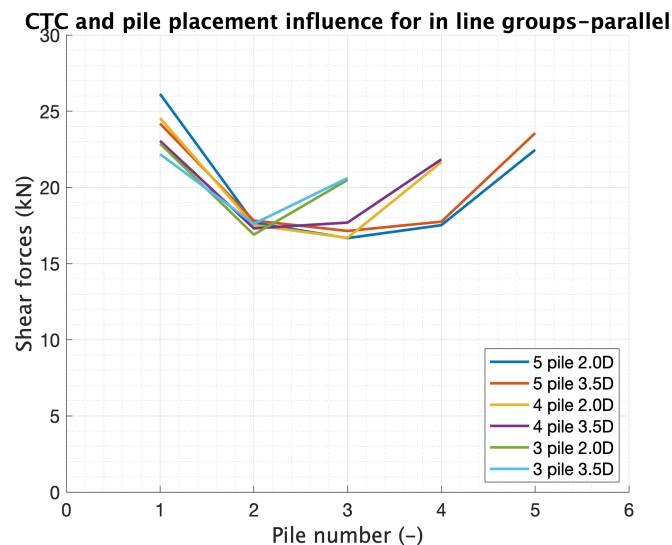


Figure 55: Influence of pile efficiency per pile group on pile number for parallel loading

The same primary aspects are visible in figure 54 and 55. Increasing the etc distance results in slightly larger maximum shear forces for every pile, but increases the difference in efficiency factors intra group. The last trailing pile has an increased maximum shear force and even surpasses the shear forces of the leading piles when increasing the group size and decreasing the etc distance.

Both figures 54 and 55 show that the shadowing effect is visible for the trailing piles. The larger groups also show that the decrease in efficiency after the second middle pile, or third pile, is minimal and should stay constant. This principle is visible as increasing etc distance or group size does not influence the middle pile response. Several experiments confirm this principle Rollins et al. [1998] and Rollins et al. [2006].

6.5 Perpendicular loading

As described already in section 6.1, the second group present in a wind turbine foundation is the perpendicular loaded section, section 2. Primary effects that can be visible when loading a group perpendicular is the edge effect, the effect where the edge piles have the most virgin soil and thus the highest load carrying capacity, and the wall formation effect. This effect is primarily present with small ctc distances of $s/D < 1.2$ with D the diameter and s the ctc distance. The total wall will then have a width of $D+3s$ Swallow and Sheil [2021].

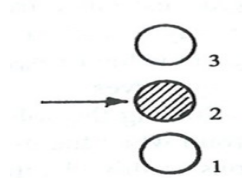


Figure 56: Perpendicular loading condition

6.5.1 Edge effect

To understand the pile loading conditions under perpendicular loading, the two cases of combined horizontal and vertical and only horizontal loading is given below.

Table 10: Maximum shear forces per pile under combined horizontal and vertical loading conditions of 20 kN and 500 kN per pile respectively for perpendicular loading

Pile group	ctc distance (-)	Pile number (kN)					Pile analysis			
		<u>1</u>	<u>2</u>	<u>3</u>	<u>4</u>	<u>5</u>	Average (kN)	Offset (%)	Middle pile offset (-)	Edge pile offset (-)
1x1	-	20.29	-	-	-	-	20.29	-	-	-
3x1	2.0D	21.27	17.97	21.51			20.25	0.2	0.89	1.06
	2.5D	21.06	18.87	21.16			20.36	-0.36	0.93	1.04
	3.0D	20.88	19.0	20.67			20.18	0.53	0.94	1.02
	3.5D	20.87	19.34	20.73			20.31	-0.11	0.95	1.02
4x1	2.0D	22.26	18.83	18.54	21.88		20.37	-0.43	0.91	1.08
	2.5D	21.75	18.47	18.3	22.17		20.17	0.58	0.90	1.09
	3.0D	21.73	18.66	18.19	21.96		20.135	0.77	0.89	1.08
	3.5D	21.38	19.09	19.09	21.08		20.16	0.64	0.94	1.04
5x1	1.5D	24.7	17.17	18.01	17.57	24.58	20.41	-0.57	0.89	1.21
	2.0	23.19	18.4	18.08	18.39	23.2	20.25	0.19	0.89	1.14
	2.5D	22.48	19.41	18.02	18.71	22.59	20.24	.023	0.89	1.11
	3.0D	22.14	19.23	18.41	18.93	22.15	20.17	0.58	0.91	1.09
	3.5D	21.6	19.66	18.99	18.76	22.05	20.21	0.37	0.94	1.09

Table 11: Maximum shear forces per pile under pure horizontal a loading conditions of 20 kN for perpendicular loading.

Pile group	etc distance (-)	Pile number (kN)					Pile analysis			
		<u>1</u>	<u>2</u>	<u>3</u>	<u>4</u>	<u>5</u>	Average (kN)	Offset (%)	Middle pile offset (-)	Edge pile offset (-)
1x1	-	20.44	-	-	-	-	20.44	-	-	-
3x1	2.0D	21.66	16.98	21.95			20.20	1.19	0.83	1.07
	2.5D	21.31	18.03	21.38			20.24	0.98	0.88	1.05
	3.0D	21.11	18.26	20.83			20.07	1.82	0.89	1.02
	3.5D	21.10	18.76	20.87			20.24	0.96	0.92	1.02
4x1	2.0D	23.05	17.95	17.55	22.63		20.30	0.7	0.86	1.11
	2.5D	22.16	17.9	17.66	22.71		20.10	1.63	0.86	1.11
	3.0D	22.23	18.07	18.43	22.35		20.27	0.83	0.90	1.09
	3.5D	21.72	18.52	18.56	21.31		20.03	2.0	0.91	1.04
5x1	1.5D	25.2	16.92	16.65	17.38	26.19	20.27	0.84	0.81	1.23
	2.0	24.01	17.77	17.27	17.85	23.99	20.18	1.28	0.84	1.17
	2.5D	23.12	18.89	17.38	18.22	23.15	20.15	1.41	0.85	1.13
	3.0D	22.68	18.71	17.93	18.59	22.53	20.09	1.7	0.877	1.10
	3.5D	22.16	19.11	18.38	18.48	22.55	20.14	1.49	0.90	1.10

Both the tables show that the offset of the average pile shear force is roughly at single pile level. The combined loading condition ensures a higher efficiency factor compared to only lateral loading conditions for the middle piles. The range of efficiency factors are also centered around 0.90 for the middle pile, while the edge pile has a larger efficiency factor in comparison to the middle pile. The combined loading conditions do result in lower intra group differences between middle piles and edge piles.

The edge effect is as expected from the found data, as the outer piles should roughly behave the same in regards to maximum shear forces because of the same amount of undisturbed surrounding ground. This is clearly visible for both combined as lateral only loading conditions, having an average of 2% offset between the outer piles. This offset increases for lower etc distances and for larger group sizes.

The data can be plotted again in comparison with Reese and Impe [2002], with the same remark that the loading conditions are far under critical loading conditions. This can lead to load distributions that give efficiency factors higher than one.

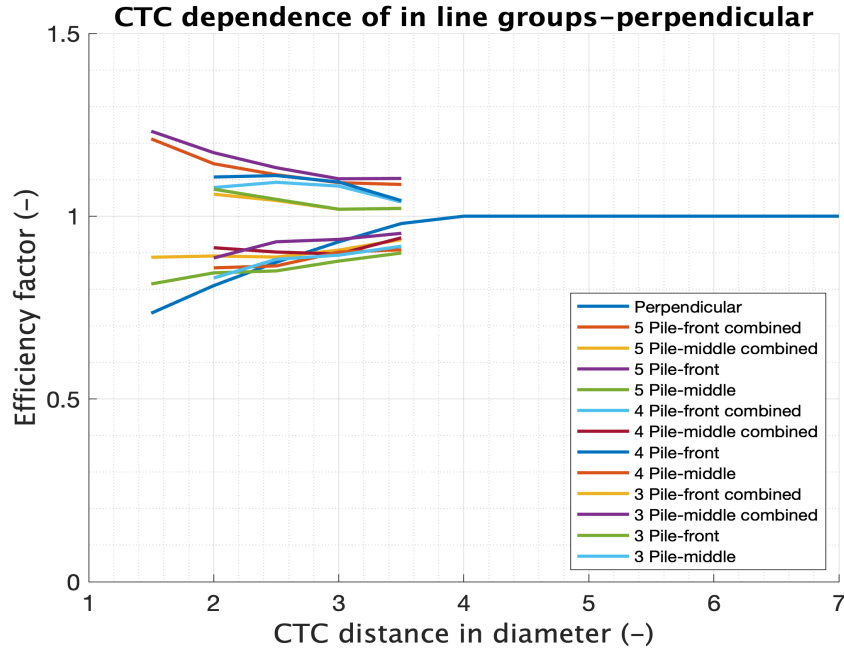


Figure 57: Influence of pile efficiency in regards to pile location for perpendicular loading

Again the edge or leading piles have a higher efficiency factor, but as the perpendicular group only has a single comparison with the data from Reese and Impe [2002] it is expected to centre more around the best fit line created by the authors. This is the case, as extreme values are present and the curves tend faster to the trend line. For the middle piles this means an upward trend with increasing ctc distances, while the edge piles have a negative trend with increasing ctc distances. These effects can be explained by:

- Increase in ctc distance results in less overlap of the shear zones, meaning that the edge effect becomes less important for a single pile response in the group. This means that increasing ctc distances result in higher middle pile efficiency factors, while the edge piles have relative decreasing factors.

To understand the behaviour inside a pile group with respect to the shear forces, the piles are again plotted using the maximum shear forces for the 2.5D ctc distance. This shows the effect of enlarging or reducing pile groups.

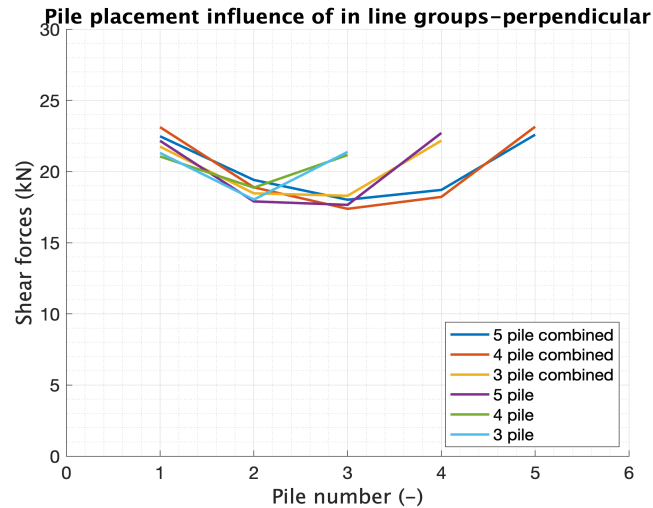


Figure 58: Influence of pile efficiency on pile number in perpendicular direction

Figure 58 shows the increase in shear forces at the edges of the group, number 1 and 5. The difference in loading conditions does not result in large differences in maximum shear forces. However, the decrease in maximum shear forces for the edge piles results in higher middle pile shear forces. A slight increase in maximum shear forces is visible for the edge piles when enlarging the groups.

The last part is the comparison of the groups with lower ctc distances to groups with higher ctc distances. Each pile group will be compared on 2.0 ctc and 3.5 ctc distances for combined loading scenarios.

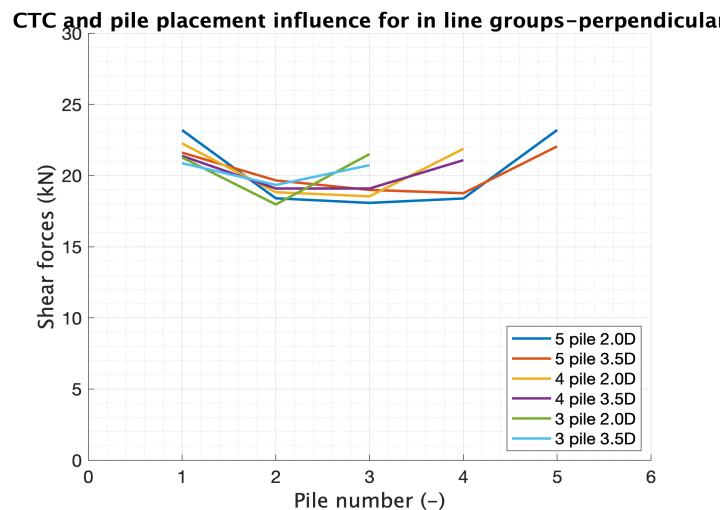


Figure 59: Influence of pile efficiency per pile group on pile number for perpendicular loading

Close pile spacings are having slightly larger maximal shear forces per pile. Smaller groups seem to be having less difference in intra maximum shear forces. Figure 59 confirms trends that are proven by both tables 10 and 11. Due to close spaced piles the edge piles will take up more of the shear forces, while lowering the efficiency of the middle piles. This effect becomes less when increasing the ctc distance as stated before.

6.6 Conclusion: parallel and perpendicular loading

The first two groups are mostly analysed in literature studies when considering group effects. The small lateral load may result in less accurate results, this is also visible in the fact that the groups do not behave exactly like the trend lines predicted. The average group efficiency is roughly 1, The behaviour of the parallel loading conditions can be described with the following points:

1. Combined loading conditions result in higher middle pile efficiency factors. It also lowers the leading pile offset, meaning a better distribution of forces in the group.
2. Increasing group sizes result in increasing differences in middle pile-leading pile efficiency factors.
3. The response of the pile groups for the middle piles is roughly the same over the different group sizes.
4. Increasing the ctc distance for the limited range of wind turbine foundation ctc distances leads to a marginal increase in the efficiency of the leading and last trailing piles.
5. Initial decrease in efficiency for the first trailing piles is in line with what is expected from the shadowing effect.
6. The last trailing pile behaves as a leading pile, sometimes even surpassing the efficiency factor of the leading pile. This effect was also visible for closely spaced hinged pile groups validated by the response of the validated pile group.

For the perpendicular loading conditions the following points are found:

1. The edge effect is clearly visible in all the pile groups. Pile 1 and 5 are having roughly the same response, which is higher than the middle piles.
2. The absence of trailing piles result in a response that is closer to the trend line created by Reese and Impe [2002]
3. Increase in ctc distance decreases the efficiency of the edge piles, while it increases the efficiency of the middle piles.
4. The combined loading conditions results in larger differences between edge and middle piles.

When comparing both the groups, the effects of perpendicular loading and parallel loading are minimal in regards to the shear force capacities. The combined loading scenario result for parallel loading in a more gradual efficiency distribution, while the perpendicular loading conditions increases the differences. The increase in ctc distances are increasing the efficiency for the parallel load conditions, decreasing the efficiency for perpendicular loading conditions.

As mentioned, the data is compared to Reese and Impe [2002]. The results are back-calculated to $1/50$ of the pile diameter, meaning in this case a pile head displacement of 1.1 cm. For our highest shear force cases, the 5 pile 1.5D ctc distance for both parallel and perpendicular loading result in 4.5 mm and 2.7 mm. This means a much smaller displacement over diameter ratio, which may influence the differences visible between the found trend lines and produced data from Plaxis.

6.7 Skew loading

The last loading group is the skew loading group. The group is a complex interplay between the parallel and perpendicular loading groups, also visible in the way Reese and Impe [2002] interpreted the trend line 56. The combination of the lines can result in the combination of described effects for both groups.

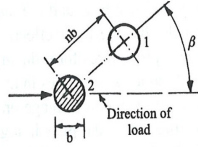


Figure 60: Skew loading condition

Table 12: Maximum shear forces per pile under combined horizontal and vertical loading conditions of 20 kN and 500 kN per pile respectively for skew loading.

Pile group	etc distance (-)	Pile number (kN)					Pile analysis			
		<u>1</u>	<u>2</u>	<u>3</u>	<u>4</u>	<u>5</u>	Average (kN)	Offset (%)	Middle pile offset (-)	Front pile offset (-)
1x1	-	20.29	-	-	-	-	20.29	-	-	-
3x1	2.0D	12.97	9.83	13.6			12.13	0.60	0.48	0.67
	2.5D	13.21	10.66	13.35			12.4	0.61	0.53	0.66
	3.0D	13.19	10.84	12.93			12.32	0.61	0.52	0.64
	3.5D	12.72	10.59	12.84			12.05	0.59	0.52	0.63
4x1	2.0D	14.07	10.58	10.67	14.28		12.4	0.61	0.53	0.70
	2.5D	13.91	10.38	10.55	13.99		12.21	0.60	0.52	0.69
	3.0D	13.12	10.35	10.31	13.58		11.84	0.58	0.51	0.67
	3.5D	12.58	10.05	9.99	12.50		11.28	0.56	0.50	0.62
5x1	1.5D	15.14	10.61	10.00	10.51	15.75	11.56	0.56	0.49	0.78
	2.0	14.14	10.61	10.06	10.5	14.77	11.32	0.55	0.50	0.73
	2.5D	13.47	10.22	9.62	10.25	14.00	10.89	0.54	0.47	0.69
	3.0D	12.39	9.81	9.27	9.84	12.45	10.33	0.51	0.46	0.61
	3.5D	11.65	9.08	8.91	9.28	11.87	9.73	0.48	0.44	0.59

Table 13: Maximum shear forces per pile under pure horizontal a loading conditions of 20 kN for skew loading

Pile group	etc distance (-)	Pile number (kN)					Pile analysis			
		<u>1</u>	<u>2</u>	<u>3</u>	<u>4</u>	<u>5</u>	Average (kN)	Offset (%)	Middle pile offset (-)	Front pile offset (-)
1x1	-	20.44	-	-	-	-	20.44	-	-	-
3x1	2.0D	12.98	9.654	13.68			12.10	0.59	0.47	0.67
	2.5D	13.16	10.35	13.65			12.39	0.61	0.51	0.67
	3.0D	13.1	10.58	13.34			12.34	0.60	0.52	0.65
	3.5D	12.64	10.43	13.11			12.06	0.59	0.51	0.6
4x1	2.0D	14.16	10.35	10.39	14.67		12.39	0.61	0.50	0.72
	2.5D	13.85	10.19	10.37	14.36		12.19	0.60	0.50	0.70
	3.0D	13.05	10.16	10.13	13.83		11.79	0.58	0.50	0.68
	3.5D	12.47	9.894	9.934	12.78		11.27	0.55	0.48	0.63
5x1	1.5D	15.26	10.46	9.75	10.30	16.16	12.39	0.61	0.48	0.79
	2.0	14.3	10.33	9.83	10.35	15.27	11.81	0.58	0.48	0.75
	2.5D	13.44	10.09	9.46	10.11	14.33	11.30	0.55	0.46	0.70
	3.0D	12.37	9.67	9.14	9.70	12.9	10.58	0.52	0.45	0.63
	3.5D	11.62	8.96	8.83	9.17	12.19	10.06	0.49	0.43	0.60

Differences between combined loading and only horizontal loading are very small for both the front piles as well as the middle piles. The behaviour of the pile group under the loading scenarios are therefore the same. Small deviations start to occur when larger group sizes are considered. The efficiency of both the middle pile and front piles are lower than found with perpendicular or parallel loading.

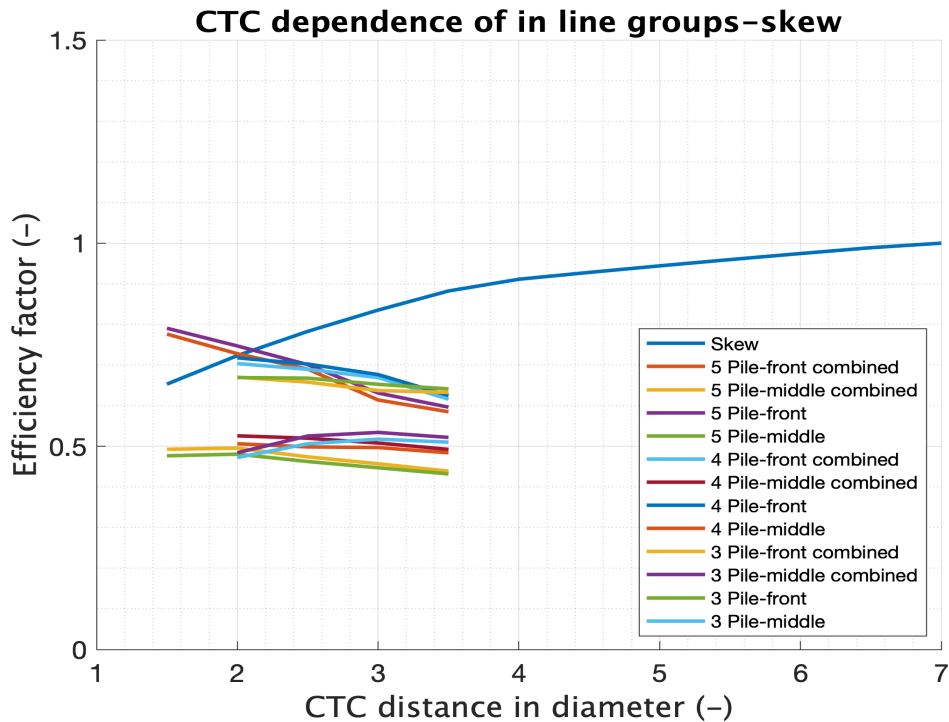


Figure 61: Influence of pile efficiency in regards to pile location for skew loading

The efficiency is lower than expected, even declining fast for the leading or edge piles. The higher ctc distances seem to create an asymptotic behaviour. Both the pile locations tend to a negative trend, in contrast to the positive trend with ctc distance of the trend line.

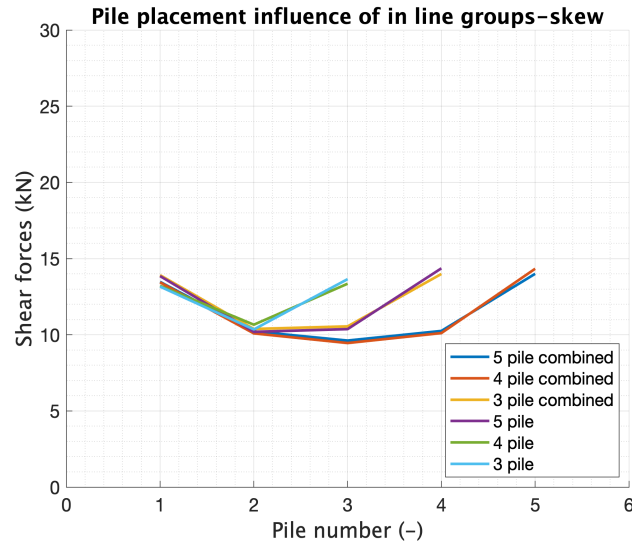


Figure 62: Influence of pile efficiency on pile number in skew loading direction

It is again made visible that there is no influence of type of loading on the response of the pile group.

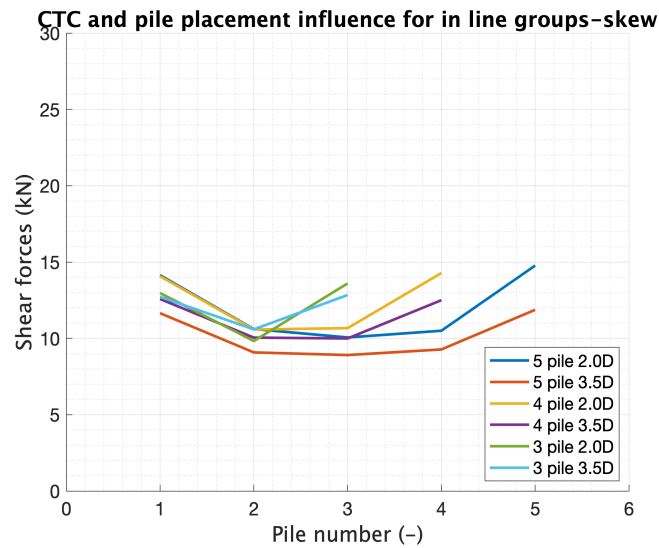


Figure 63: Influence of pile efficiency per pile group on pile number for skew loading

Differences in ctc distance results in fairly large differences in both the leading or edge piles, where the middle piles are again constant in all the groups. The 5 pile group with ctc distance of 3.5 is translated roughly with 2 kN downwards, which cannot be explained as the rest of the groups behave the same.

When considering the response of the skew loaded group, the response is in line with a combination of properties of the parallel and perpendicular loading groups. Comparing figure 58 with 61 the maximum shear force distribution is roughly the same, but at lower average shear forces. Figure 63 matches with the maximum shear force distribution of figure 59 again with a lower maximum shear force. The response of figure 61 is difficult to compare, but the trends are again more visible with figure 57 than with figure 53 which

shows only horizontal asymptotes. Considering the rough comparisons made, the skew pile group seems to behave more like a perpendicular loading group than a parallel loading group. Still it needs to be taken into account as third distinctive group, as increase in group sizes may result in larger differences

6.8 Conclusion of group efficiency of simplified fixed group

Three different groups are used to assess the response of a single pile in a fixed group to a single pile. As the pile groups are loaded with the same lateral loading conditions per pile as the single pile, the behaviour should approximate the behaviour of Reese and Impe [2002] fitted curves. The testing conditions for the fitted curves are under different circumstances, namely:

1. Load applied to the group is equal to a deformation in lateral direction of $1/50D$, which is roughly 6 times more than the applied load.
2. Subsurface is not a single layer with a single soil type.
3. Piles are modelled as hinged with a plate or as single piles with an applied force for each pile separately.

Due to this difference in modelling, several trends are visible that should not be present with the described circumstances mentioned above.

1. Parallel loading conditions
 - (a) The ctc influence is less present under fixed pile groups. As the applied load for the fixed model is smaller than the load needed for the $1/50D$ deformation, not all the soil is mobilized between the piles. This immobilization assures that a larger range of ctc distances do not meet this mobilization criteria, thus having no to little ctc distance influence. This is proven by the 0.98 efficiency factor for the total group, which means almost no group effect is visible. This incomplete mobilization also ensures that the piles are behaving far above and far below their expected efficiency, creating a more extreme load division.
 - (b) The increase of the last trailing pile in regards to the shear forces is primarily visible for lower ctc distances. Increasing the ctc distances results in a decrease in depth of the strain influence of the last trailing pile. Larger sections with increased strain concentrations at lower ctc distances are visible. With higher ctc distances, the wedges between the piles showed an increase in strain levels and concentration. This shows that lower ctc distances result in an increase in size of active soil wedges both in depth and in width, which can increase the total shear forces for the last trailing pile. This combined effect with the increase in strain levels and size of the wedge for earlier trailing piles results in smaller differences between the trailing piles for larger ctc distances.

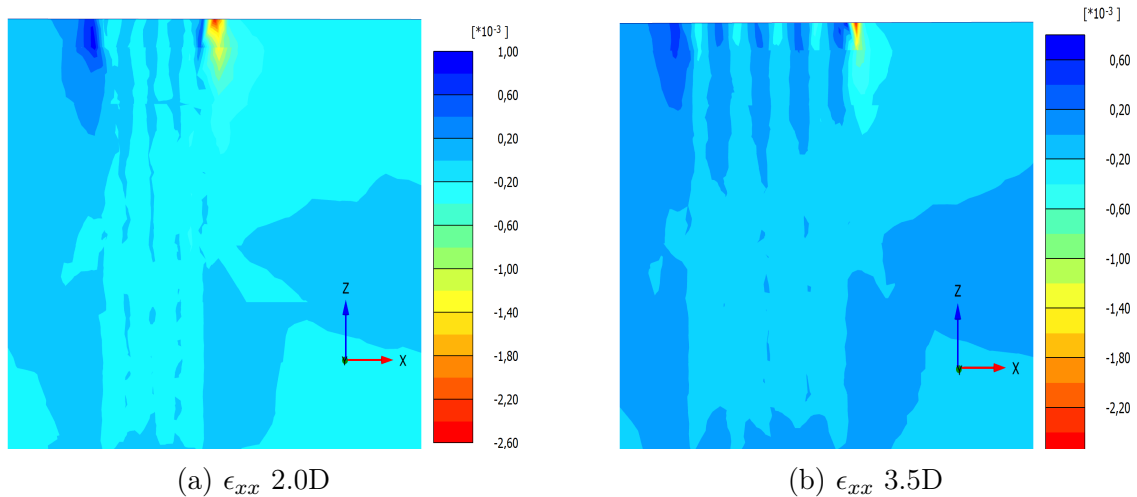


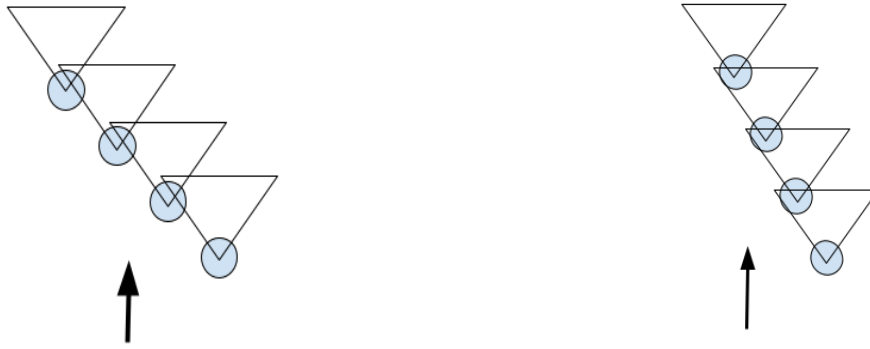
Figure 64: Depth influence of ϵ_{xx} with increase in ctc spacing

2. Perpendicular loading conditions

- (a) The ctc distance has a negative slope, tending to an efficiency of 1. An increase in ctc distance thus results in normalization of the middle piles and edge piles, meaning that the deviation becomes lower. This is in line with expectations surrounding ctc distances and means that overlap of mobilized soil zones is more present under perpendicular loading than parallel loading. This is the case as displacements under perpendicular loading are higher than under parallel loading, ensuring a better fit with the Reese and Impe [2002] response and increasing the size of the mobilized soil wedges.

3. Skew loading conditions

- (a) The ctc distance has a substantial negative slope, resulting in efficiencies at roughly 0.6. This is much lower than the trend lines are considering as efficiency factor. As the orientation of the structure results in readings of Q12 shear forces, the pile configuration ensures a turning moment around the axis of the pile group. The smaller pile groups are having Q13 shear forces roughly equal to Q12 forces, while larger groups have less rotation capacity with lower Q13 forces. The absence of the Q13 forces will therefore translate the 'real' efficiency to lower values, while addition of the Q12 and Q13 shear forces result in efficiencies equal to the perpendicular loading group.
- (b) The geometry of the skew group ensures combined overlapping wedges, as the wedges are placed diagonally over each other. As mentioned in the parallel loading condition, the piles should not have an influence of the used ctc distances for that effect but it does have an edge effect mentioned in perpendicular loading. As the shear forces in the loading direction are lower, the displacements are higher visible from the perpendicular loading which results in larger wedges. As the wedges increase, both the perpendicular loading ctc distance effect increases as well as the parallel loading. As the structure moves, the wedges also turn slightly, bringing them closer together and reinforcing the effect.



(a) Initial skew loading

(b) Resultant skew loading after slight clockwise turning due to lateral forces

Figure 65: Overlap of soil wedges before and after turning

7 Vertical complex round foundation

The determination of the group effect is primarily focused on square or rectangular buildings considering small pile groups turbines. Matlock et al. [1980] considered steel piles in a circular configuration without infill of the inner section. This configuration matches with that of a wind turbine foundations as shown in section 3.1.1. The setup was tested under horizontal static loading conditions and compared with the output of a single load. The tests are done on the outer edges of our range of ctc distances, between 1.8 and 3.5D. Conclusions from this single research are:

1. A two times smaller pile group with 5 piles with a 2.2 times larger ctc distance of 4.0 results in almost half of the deflections at the same average lateral load.
2. Highest efficiencies for the leading piles in 10 pile group, for the 5 pile group the highest efficiencies for the last trailing piles.
3. Closely spaced pile groups with 10 piles result in efficiencies of roughly 0.4.

The outcome of this research can be used to test the validity of the complex foundation.

7.1 Complex foundations

Considering single pile response and simplified group response, the complex group geometry of a circular foundation is introduced. As mentioned before, the complex geometry introduces several important influencing factors when changing the geometry, mentioned below.

1. Ctc spacing and number of piles are interrelated
 - (a) Cap radius is limiting factor, increase or decrease influences the used amount of concrete.
 - (b) Increase or decrease in lateral stiffness: more piles result in total higher shear forces. This will be countered or limited by the minimum ctc distance, besides the lowering of the shear forces due to overlap of soil wedges.
2. Batter angle
 - (a) Use of batter angle influences the lateral displacement positively for negative batter angles.
 - (b) Alternating vertical and batter piles can result in the parallel sections in increase of surface area, thus higher shear forces in those area's.

To asses the influence of each section, the three sections mentioned above are tested for influence of batter angle, influence of increase or decrease of ctc distance and last the influence of alternating batter angles.

7.2 General validation of model for vertical piles

In order to avoid any stress concentrations and displacements surrounding the boundary edges, the boundary is set at 44 meters from the starting point at (0,0,0). Doing this results in a local displacement which is below 1% of the total displacements. The boundary conditions of the model are modelled as standard, meaning a normally fixed X and Y interface with a fully fixed z_{min} and free z_{max} . In comparison with the simplified group response, the horizontal loading conditions are taken to be 20 kN per pile, with proven setup of 28 piles results in 560 kN lateral loading. The vertical loading conditions are calculated as self weight of the foundation base, 10500 kN, and the wind turbine, 5320 kN, meaning a total load of 15820 kN resulting in 565 kN vertical load per pile. In order to model the behavior correctly, the horizontal and extra vertical turbine load are added as extra load 3.29 meters from the bottom of the foundation, 2.4 meters above ground level as surface load. This means that the foundation is embedded in the subsurface at a depth of -0.895m. The base weight is correctly implemented as a concrete base having a vertical load per pile of 375.4 kN, which is roughly the same as the pre-calculated weight of 375 kN per pile including the weight of the pile. All the piles will be modelled as fixed, comparable with the existing wind turbine.

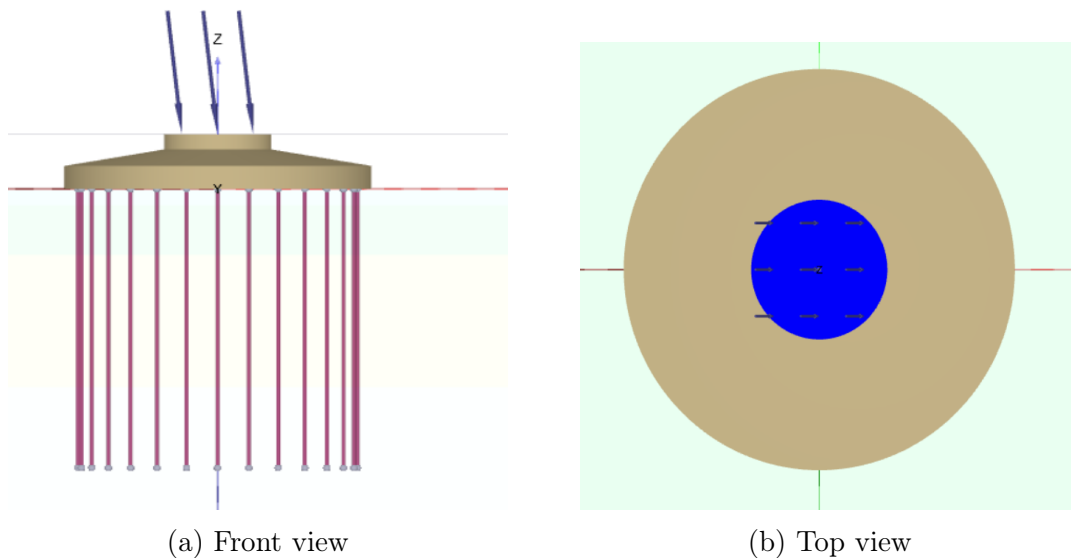


Figure 66: Initial conditions of complex wind turbine foundation layout.

The setup of the complex model in Plaxis 3D is done in four different steps: Initial, F1 Construction, F1 Construction.2 and F2 Loading. Each of the steps is described below. In order to see the influence of each loading step on the movement of the structure, for each of the loading steps the displacements are set to zero. This also ensures that the most important loading step, the loading of the complete structure, is taken into account without influence of activating embedded beams or construction the slope leading to heave.

- Initial: initialisation of the subsurface without any structures
- F1 Construction: A slope of 1/4.5 is made to make sure the sides of the embedded foundation head does not influence the pile stiffness.

- F1 construction.2: activating embedded beams, embedded beam base-plate and negative interface of this plate.
- F2 load: construction of base with total load 10500 kN and apply the vertical load of 5320 kN and horizontal loading of the wind turbine of 560 kN on an height of 2.4 meters above ground level. A fifth phase can be added to apply first vertical (dead)load and second the horizontal loading.

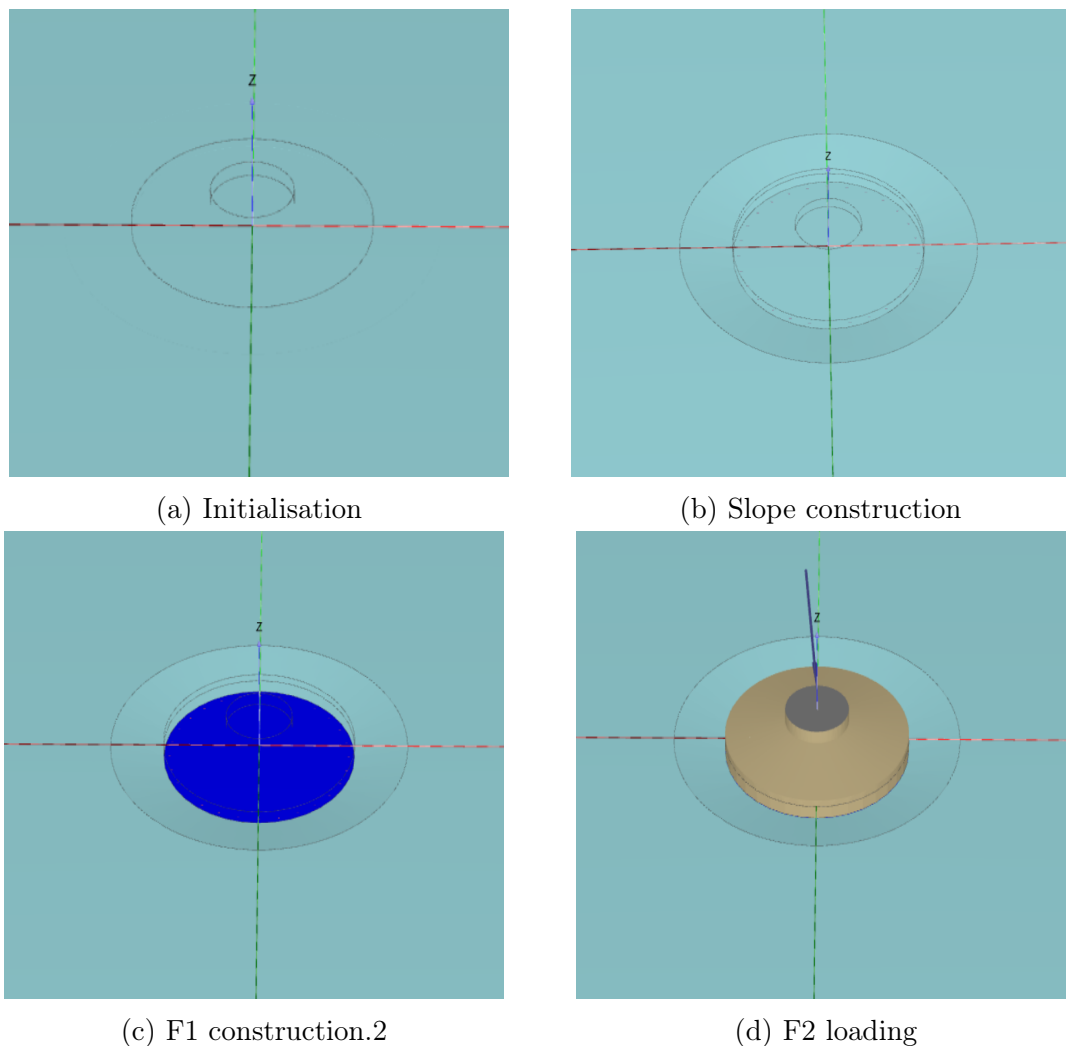


Figure 67: Initial loading conditions of complex wind turbine foundation.

The use of a slope surrounding the foundation base does result in different stress states for the soil directly below the slope. At maximum this results in a difference of the deleted layer, 0.895 m, taken into account the top layer weight of 16 kN/m³. This results in a stress state difference of almost 14.3 kN/m² and may influence the behaviour of the foundation.

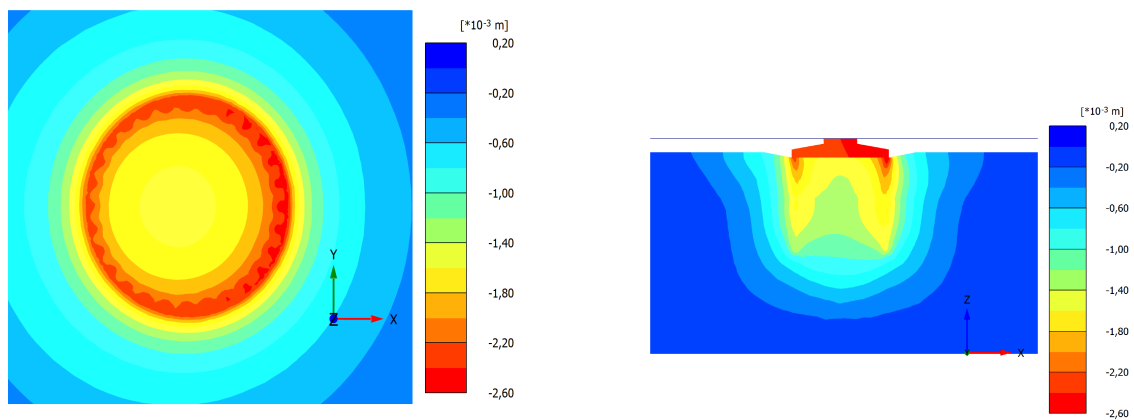
7.2.1 Influence of pile placement

In order to check the behaviour of the pile group under combined lateral and vertical load, the structure is being assessed in regards to group behaviour, section 6. Primary

Table 14: Comparison of axial forces for scenario with 560 kN horizontal loading and without horizontal loading

Pile Number	Maximum displacement (m)			Maximum axial forces (kN)			Offset to vertical displacement (-)		Offset to vertical forces (-)		Dynamische pile head spring (MN/m)	
	Combined	Vertical only	Vertical separate	Combined	Vertical only	Vertical separate	Combined	Vertical separate	Combined	Vertical separate	Combined	Vertical separate
1	$-2.47 * 10^{-3}$	$-2.36 * 10^{-3}$	$-9.02 * 10^{-5}$	-601.1	-578.2	-603.8	1.05	1.01	1.04	1.00	200.8	283.5
4	$-2.45 * 10^{-3}$	$-2.36 * 10^{-3}$	$-7.26 * 10^{-5}$	-592.6	-578.9	-601.9	1.04	1.01	1.02	0.98	159.7	316.9
8	$-2.35 * 10^{-3}$	$-2.36 * 10^{-3}$	$-9.33 * 10^{-6}$	-573.4	-574.3	-571.9	1.00	0.99	1.00	1.00	127.8	257.8
12	$-2.26 * 10^{-3}$	$-2.35 * 10^{-3}$	$2.25 * 10^{-5}$	-554.1	-582.1	-559.7	0.96	0.97	0.95	0.99	297.6	992.3
15	$-2.24 * 10^{-3}$	$-2.35 * 10^{-3}$	$3.04 * 10^{-5}$	-547.3	-576.0	-553.0	0.95	0.96	0.95	0.99	249.9	758.9
18	$-2.27 * 10^{-3}$	$-2.35 * 10^{-3}$	$2.29 * 10^{-5}$	-555.5	-579.7	-551.1	0.96	0.97	0.96	1.01	279.6	1249.4
22	$-2.36 * 10^{-3}$	$-2.36 * 10^{-3}$	$-9.06 * 10^{-6}$	-573.2	-572.9	-574.7	1.00	1.00	1.00	1.00	59.0	197.3
26	$-2.45 * 10^{-3}$	$-2.36 * 10^{-3}$	$-7.24 * 10^{-5}$	-597.9	-578.3	-595.8	1.04	1.01	1.03	1.00	211.8	241.3
AVG	$-2.36 * 10^{-3}$	$-2.36 * 10^{-3}$	$-7.26 * 10^{-5}$	-574.4	-577.5	-576.5	1.0	1.0	0.99	1.00	198.3	537.2

The data from table 14 shows that the foundation is dipping downward on the right, visible in increase and decrease of axial forces for piles number 1 and 15 which are on the outer edge of the foundation. For the displacement and axial force offset both sides of the pile setup are stated in table 14. It shows a mirrored response with the axis on the x axis. This mirrored response shows that the movement of the foundation is purely around a single axis, located around the y-axis. This forward dipping of the foundation is visualized in figure 69. When looking at table 14, a larger offset for u_z displacements is visible in comparison to the axial forces. The largest offset is found at pile 1 and 15 which are the outermost piles from the rotation axis. Comparing the offset for combined loading, the displacement offset gives 1.05 and 0.95 while the force offset gives 1.04 and 1.05. For the separate vertical and horizontal loading the differences are smaller, between 1.01 and 0.96 and 1.01 and 0.98 for vertical displacement offset and vertical force offset respectively. This is expected as the small strain behaviour is reset, ensuring only displacements due to horizontal forces are taken into account. To check the combination of displacement and axial forces, a pile head spring is calculated. It is mentioned by Mr. Mooijman (personal contact) that a rough estimate should lie around 200 MN/m. The dynamic pile head spring is as average value in line with expectations, resetting the displacements result in increases to 2.5 times the estimated spring stiffness for the vertical separate loading conditions. The vertical separate spring stiffness does not take into account the vertical displacements, but does take into account the vertical forces as only small strains are reset creating unreliable results.



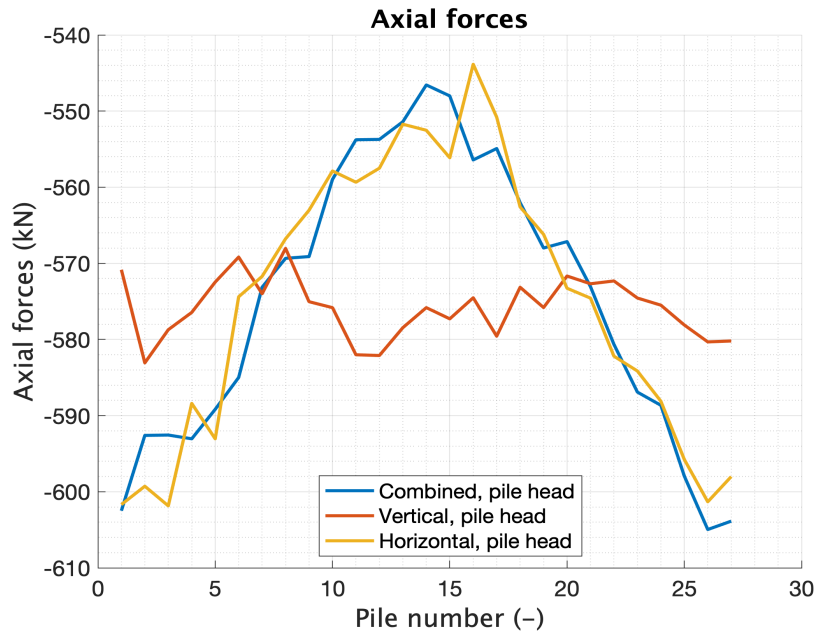
(a) Global view of U_z displacement

(b) Side view of U_z displacement

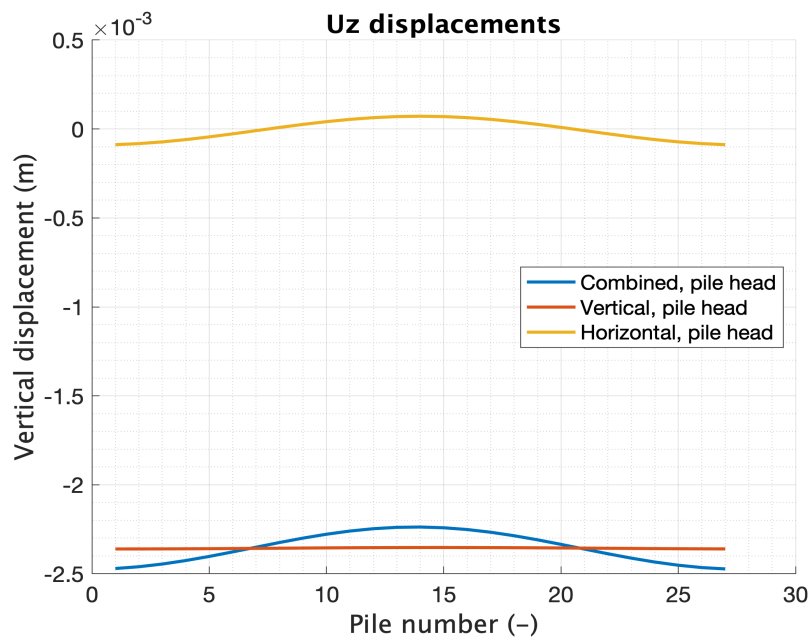
Figure 69: U_z displacements under combined lateral and vertical loading

The results of the table are shown in the figure 70, where the middle piles behave as a turning axis and thus only receive moderate displacements equal to only vertical loading conditions. The outer piles have higher displacements under the combination of horizontal and vertical loading conditions and show the dip towards the right. The positive displacements are filtered to show the movement of the piles and foundation base, as the positive values are found in the slope due to heave. The distribution of axial forces in the foundation are shown in figure 70.

Both the figures show the influence of horizontal loading on the axial distribution, but this will only result in a small offset as explained before due to the effect of horizontal loading. Figure 70a shows clearly that a small deviation in axial forces is present in the pile group, but create an average horizontal response of -575 kN as expected by the vertical dead loads. Applying the horizontal loading results in a redistribution with the largest forces at the dipping side, smallest forces at the rising side. This same behaviour is visible for the displacements in figure 70b, the reset horizontal displacements combined with the vertical loading displacements results in the combined displacements as expected by the reset.



(a) Axial loading displacement



(b) Axial loading displacement

Figure 70: Maximum axial forces per pile for different loading conditions

7.2.3 Shear forces and stress distribution

The shear forces and σ_{xx} distribution can show the influence of pile placement on the efficiency of the pile in regards to a single pile response for the complete structure. As the plate and piles are modelled as stiff, no difference in u_x is visible between piles. The cross sections shown here are taken at a depth of 1 meter, roughly 10 cm below the lowest section of the foundation head.

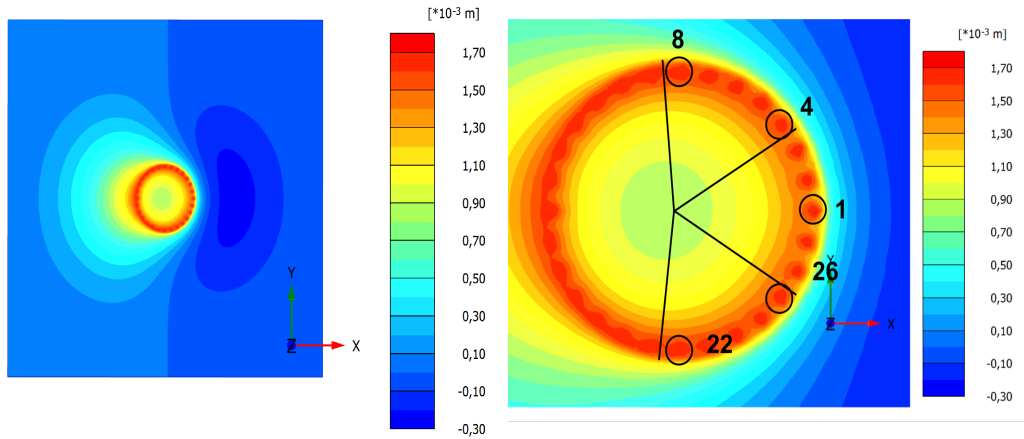
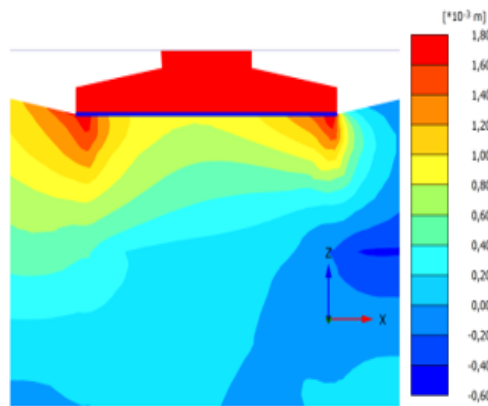
(a) Global view of U_x displacement(b) Zoomed in view of U_x displacement(c) Side view of U_x displacementFigure 71: U_x displacements under combined lateral and vertical loading

Figure 71a shows that every pile has an estimated 1.7 mm displacement as expected by the stiff pile-plate response. Figure 71b shows that the leading piles behave as separate piles in regards to higher displacement (visualized with red), which is expected using the ctc distance of $3.034D$. The area's directly behind the leading piles do result in overlap of shear zones as the mobilized soil wedges become wider. Figure 71c shows the overlap of higher displacements zones.

The second section, located at the upper and lower part of the foundation show increasing overlap of the high displacement zones surrounding the piles. Pile number 4, located at 1 hour, shows the first overlap and is visualized in figure 71b as black line. This shows that the parallel response of the foundation begins at this pile and mirrored at pile 26. Increasing overlap due to parallel loading conditions results in gradual increase to highest banded displacement fields from pile 8 onward. The lower displacement banding starts at pile 5, the lowest displacement banding is already present from pile number 1 on wards. While we expect a triangular wedge behind the foundation for high displacement, the 'flow' of soil surrounding the structure results in tail like displacement fields, extending till 9 meters behind the structure. The lower displacement do result in extension of the displacement field in a triangular pattern, visible by the blue and yellow extension till 28 meters behind the structure.

Considering the stress concentration surrounding the piles in x direction, σ_{xx} , higher stress concentrations mean that these piles take up more of the shear forces and therefore having higher efficiency than piles without high concentrations of stress. A general introduction of the efficiency expectations of leading, trailing, edge and middle piles is already given in section 6.

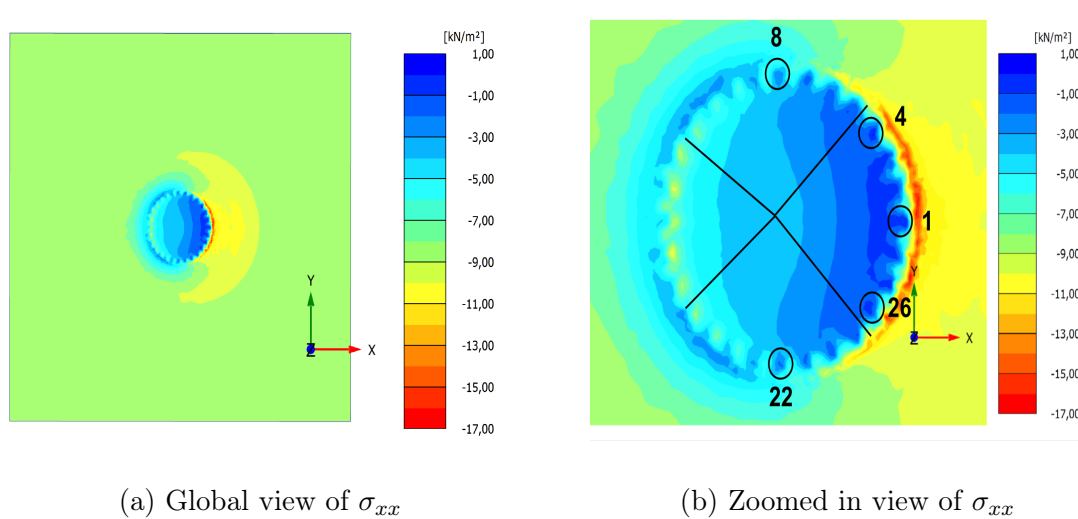


Figure 72: σ_{xx} displacements under combined lateral and vertical loading

Figure 72b shows that a large amount of stress is concentrated at the right side of the foundation. Pile number 1 has the largest high stress field, followed by 4 and 26 which gradually decreases till pile 8 and 22. The piles on the right hand side result in high stress concentrations on the outer side of the foundation, almost zero at the inside of the foundation. The difference in high stress or high displacements zones is due to the fact that the counteracting forces for movement from left to right result in high stress concentrations at the outside, hindering the movement, while the translation results in high displacement inside.

While earlier research in section 6.1 showed that piles after a ctc distance of 7D or at least 4D for parallel loading should not have any influence of the leading piles, even the piles at number 15 do not have very high stress concentrations. The color does result in a general increase on the inside of the foundation from -7 to -9 kN with small concentrations till -11 kN surrounding the outer trailing piles, but the behaviour suggests that the piles have a large influence of the trailing pile effect.

Both the displacement and stress fields show that the ground inside the foundation does not behave as a single block of soil, shown in figure 71c. This movement as block of soil is only visible for a smaller portion of the in-cased ground. The circular block does have differences in stress states as visible in figure 72b.

Considering the actual Q12 shear forces per pile, the visualization of figure 72 should match the response of the shear forces. For the combined conditions, the lower middle pile shear response due to trailing effect and the higher shear response of pile number 1 confirm this. The minimum Q12 response is roughly the same for all loading scenario's, with a minimum for vertical and combined loading at pile 15. The response of the maxima increases with combined loading scenario. This increase can be related to the combined

loading scenario's with lateral loading. As the lateral load creates a baseline for the Q12 response per pile, the vertical loading conditions ensures that the extra rotation of the pile head result in extra downward and rightward movement. This movement is partly translated into extra Q12 shear forces, creating a slightly higher Q12 response.

The displacements are as expected and do not vary over the piles, as the pile heads are fixed and show the largest displacements. It does show that the combined loading scenario results in a relative increase versus the separate dead load and horizontal applied load scenario. The pile head response are as expected, where the largest shear forces are found in the leading perpendicular pile group and primarily activated by the horizontal loading. The vertical translation in shear forces is roughly the applied 20 kN and shows the correct implementation of the horizontal loading.

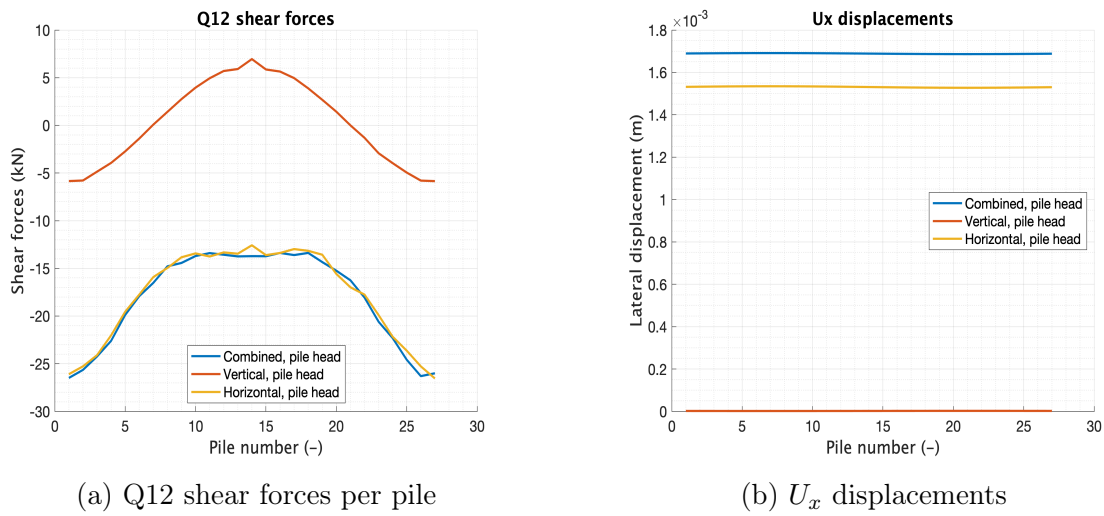


Figure 73: Q12 forces and U_x displacements under combined lateral and vertical loading

Table 15: Pile numbers equivalent to maximum U_x displacement and Q12 shear forces under combined loading conditions

Pile	U_x _max (m)		U_x _min (m)		Q12_max (kN)		Q12_min (kN)	
	Vertical combined	Vertical separate						
1	$1.69 * 10^{-3}$	$1.53 * 10^{-3}$	$-1.92 * 10^{-4}$	$1.68 * 10^{-5}$	17.3	21.3	-29.5	-28.6
4	$1.69 * 10^{-3}$	$1.53 * 10^{-3}$	$-1.28 * 10^{-4}$	$1.58 * 10^{-5}$	5.6	6.0	-24.2	-24.1
8	$1.69 * 10^{-3}$	$1.53 * 10^{-3}$	$8.65 * 10^{-6}$	$1.50 * 10^{-5}$	3.9	7.6	-16.5	-15.9
12	$1.69 * 10^{-3}$	$1.53 * 10^{-3}$	$-2.86 * 10^{-5}$	$1.78 * 10^{-5}$	7.0	7.6	-13.4	-13.8
15	$1.69 * 10^{-3}$	$1.53 * 10^{-3}$	$-4.68 * 10^{-5}$	$1.95 * 10^{-5}$	10.5	9.6	-13.7	-12.6
18	$1.69 * 10^{-3}$	$1.53 * 10^{-3}$	$-2.08 * 10^{-5}$	$1.79 * 10^{-5}$	6.9	11.6	-13.6	-13.0
22	$1.69 * 10^{-3}$	$1.53 * 10^{-3}$	$2.28 * 10^{-5}$	$1.49 * 10^{-5}$	5.2	5.8	-16.2	-17.0
26	$1.69 * 10^{-3}$	$1.53 * 10^{-3}$	$-1.23 * 10^{-4}$	$1.62 * 10^{-5}$	6.7	6.1	-24.6	-23.6
AVG	$1.69 * 10^{-3}$	$1.53 * 10^{-3}$	$-6.35 * 10^{-5}$	$1.67 * 10^{-5}$	7.89	9.44	-18.98	-18.57

While Q13 forces should be low and should not be changing over all the pile numbers as there is no load acting in the y direction of the foundation, the skew configuration showed that the forces can be present in these 'skew' loading sections. The round layout of the piles should ensure no turning of the foundation, due to the counteracting forces as the layout is mirrored. The U_y movement was therefore tracked for each of the piles to check if no movement was found. While the movement was very little, at maximum

$3.11 * 10^{-4}$ m which is roughly 5% of the total vertical movement or 20% of total lateral movement, the location of the maximum movement in y direction was not directly related to the maximum Q13 shear forces found in the pile group, shown in figures 74a and b. The values are stated in table 16.

The pile heads of the piles are modelled as infinitely stiff, a fixed connection. This ensures that no difference in displacement should be encountered over the piles in the pile group. The difference is limited in the x direction, given the same maximum displacement and a range between $-1.92 * 10^{-4}$ till $8.65 * 10^{-6}$ for the minimum displacement for combined loading. The movement in y direction gives a U_y maximum displacement range of $3.08 * 10^{-4}$ till $4 * 10^{-6}$ m and a minimum range of $-3.11 * 10^{-4}$ till $-6.6 * 10^{-6}$. The range shows that the displacement in y direction is probably over the complete pile length, while the displacement in x direction results in a fixed response over depth after a certain depth.

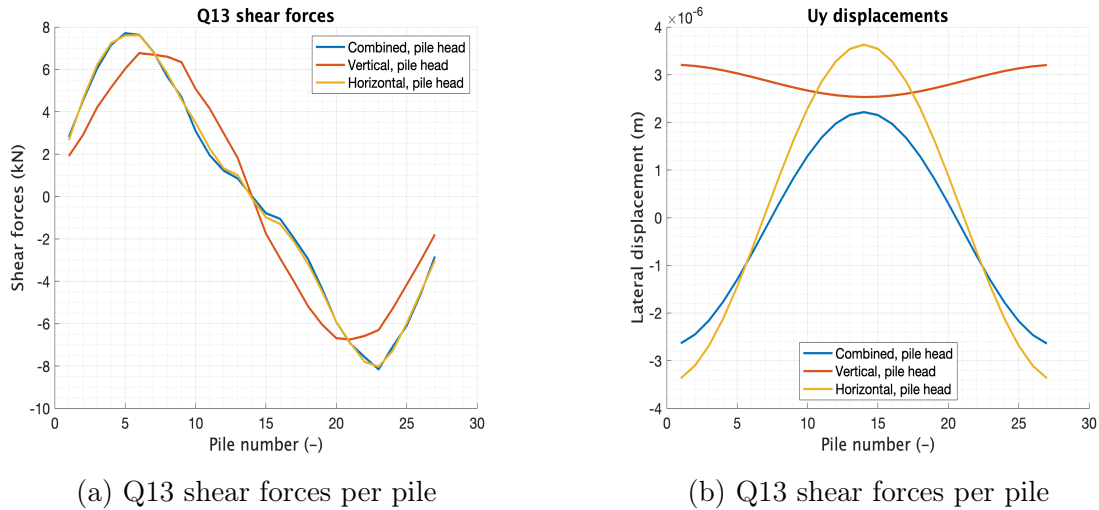


Figure 74: Q13 forces and U_y displacements under combined lateral and vertical loading

Table 16: Pile numbers equivalent to maximum U_y displacement and Q13 shear forces under combined loading conditions

Pile	U_y max (m)		U_y min (m)		Q13_max (kN)		Q13_min (kN)	
	Vertical combined	Vertical separate						
1	$5.03 * 10^{-6}$	$3.79 * 10^{-7}$	$-6.49 * 10^{-6}$	$-3.46 * 10^{-6}$	2.1	1.7	-1.0	-2.5
4	$4.55 * 10^{-5}$	$1.26 * 10^{-6}$	$-1.99 * 10^{-4}$	$-2.47 * 10^{-5}$	7.0	7.0	-4.7	-4.8
8	$5.08 * 10^{-5}$	$8.73 * 10^{-8}$	$-3.11 * 10^{-4}$	$-2.90 * 10^{-6}$	7.0	9.8	-11.5	-4.1
12	$3.44 * 10^{-5}$	$2.19 * 10^{-5}$	$-1.70 * 10^{-4}$	$-1.99 * 10^{-6}$	3.6	9.2	-4.6	-4.2
15	$4.54 * 10^{-6}$	$3.63 * 10^{-6}$	$-4.41 * 10^{-6}$	$-2.34 * 10^{-9}$	2.3	1.1	-2.4	-1.2
18	$1.76 * 10^{-4}$	$2.86 * 10^{-6}$	$-5.10 * 10^{-5}$	$-2.00 * 10^{-5}$	8.6	4.5	-8.6	-7.2
22	$3.08 * 10^{-4}$	$3.23 * 10^{-6}$	$-6.31 * 10^{-5}$	$8.73 * 10^{-8}$	6.7	8.5	-11.0	-11.8
26	$2.09 * 10^{-4}$	$2.39 * 10^{-5}$	$-4.88 * 10^{-5}$	$-2.69 * 10^{-6}$	6.4	8.1	-8.3	-9.5
AVG	$1.04 * 10^{-4}$	$7.16 * 10^{-6}$	$-1.07 * 10^{-4}$	$-6.95 * 10^{-6}$	5.45	6.25	-6.51	-5.66

The piles at the centre of the skew loading groups, namely piles 4,12,18 and 26 are having a larger maximum shear force than the expected, where the peak forces are expected at

piles 8 and 22. While the shear forces are expected when considering the simplified skew loading groups, the fixed complex pile group show maximum and minimum Q13 forces that are in the range of the Q12 shear forces for combined loading.

Figure 74b showing the displacements suggest that the pile heads have the highest displacements at piles that are not receiving the largest Q13 shear forces. As these displacements are very small, this may be the result of turning of the foundation where the y displacements are eventually turning in x displacements between piles 1-8, 8-15, 15-22, 22-1.

7.2.4 Efficiencies

To check the efficiencies of the piles in regards to the shear forces each pile receives, the efficiencies for Q12 and axial forces (N) are given. As the loading of a single pile result in almost no Q13 forces, this efficiency has factors which are much higher than the expected range between 0 and 1. This figure will only show the global distribution of forces along the piles for both horizontal as combined loading conditions.

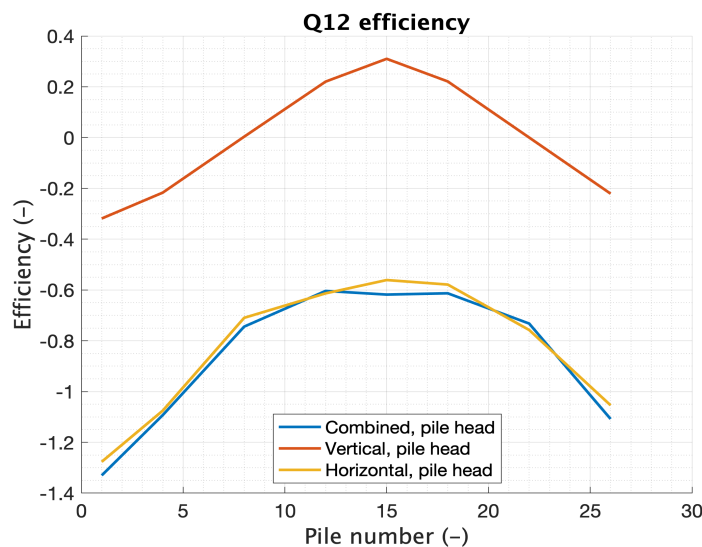


Figure 75: Q12 efficiency along analysed piles in complex vertical pile group

Figure 75 shows the expected response of Q12 efficiencies, already visible in figure 73a. The efficiencies are the highest for the leading perpendicular pile group and form a minimal efficiency at the trailing perpendicular pile group. The vertical pile group does show the same pile group dependence with a vertical translation of 1, resulting in an average efficiency of 0.

The average efficiency is roughly in line with the expected response of square completely filled pile group as normally used as reference by RHDHV using a combination of perpendicular and parallel loading groups of Reese and Impe [2002]. The efficiency found with this type of grouping results in an average of 0.8, while the circular pile group receives a efficiency of 0.86.

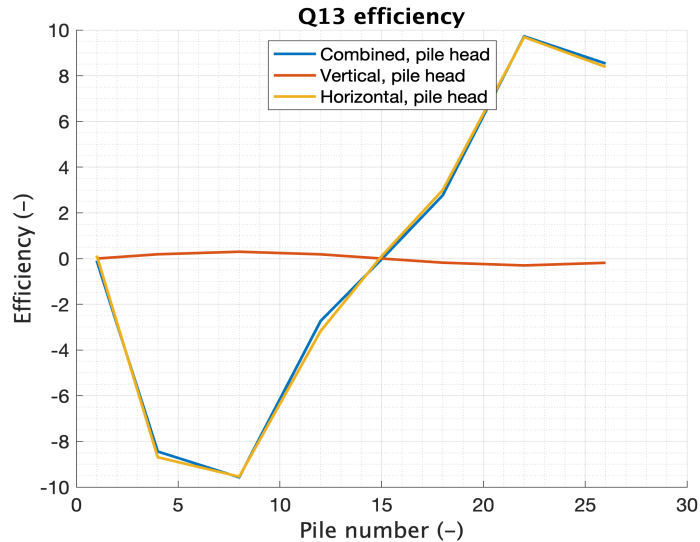


Figure 76: Q13 efficiency along analysed piles in complex vertical pile group

The Q13 loading conditions influence the efficiencies much more than the Q12 loading conditions. While the response or curve of the efficiency shows the pile placement dependence, the efficiencies are almost three times higher for the vertical only and combined loading conditions. This effect can be the result of the reference single pile, as the measured Q13 shear forces are roughly 1/400th of the combined Q13 forces and 1/200th of the vertical forces. Due to the very low response of the single pile, which is expected as a single pile should not create movement in a direction which it isn't loaded, this response results in unusable results. The efficiencies of all the loading scenario result in an average of 0.00

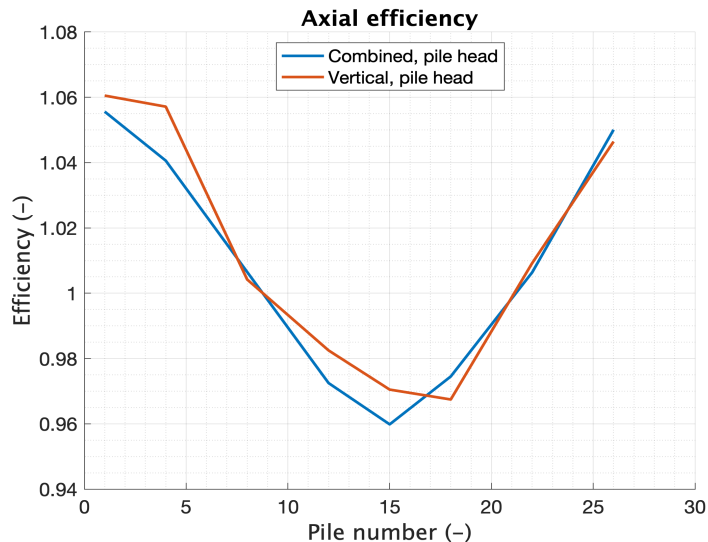


Figure 77: Q12 efficiency along analysed piles in complex vertical pile group

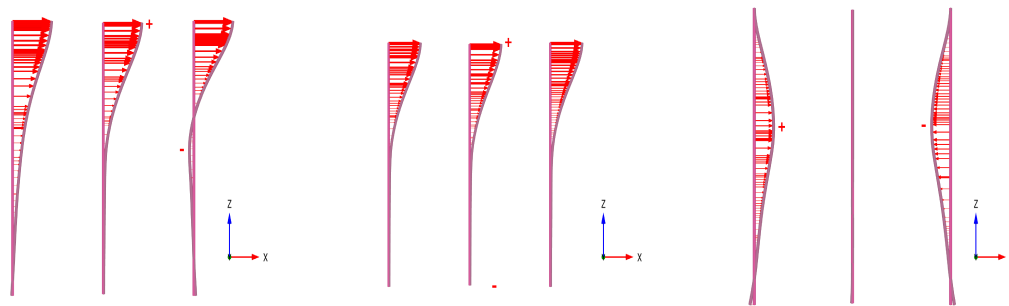
The last response is found in the axial efficiencies of the piles. As all the piles contribute to the vertical loading conditions, the response is flatter than the Q12 and Q13 shear forces. The dipping of the structure is visible as a decrease surrounding pile 15 for the maximum axial forces as suspected by the uplift on that side. An efficiency of roughly 1

was already expected using the results from table 14, which is needed for the efficiency to ensure a stable situation.

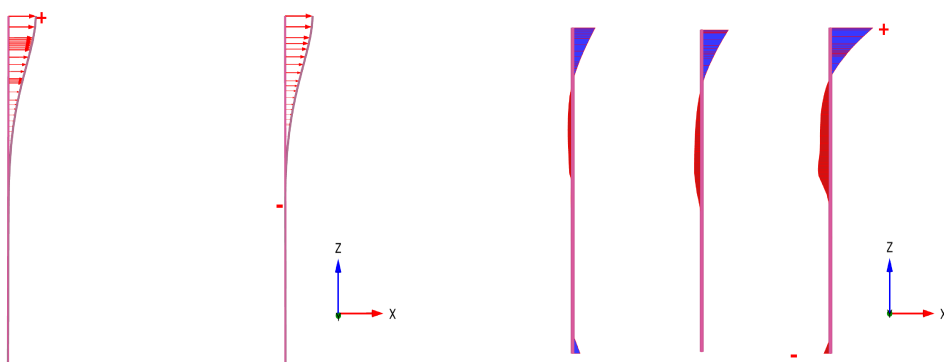
Considering table 14, we see the same effect and range of efficiencies as when comparing to the single pile response. Due to the steady state, all the piles have an average response equal to the single pile response. For vertical pile configurations a comparison with a single pile is therefore deemed senseless, a direct comparison can be made as shown in table 14.

7.2.5 Displacement of the piles in x direction

While all the piles have a fixed head condition, ensuring the same maximum displacement on pile head level, the differences in bending moment and displacements already visible in the simplified group response, are also present on different pile locations in the complex group. A clear indication of the differences is already given by the pile movement for the first leading pile number 1, trailing pile number 8 and last trailing pile number 15.



(a) Pile movement U_x (pile number 1 on the right) scaled 2000 for single phase combined loading
 (b) Pile movement U_x (pile number 1 on the right) scaled 2000 for pure horizontal loading
 (c) Pile movement U_x (pile number 1 on the right) scaled 2000 for pure vertical loading



(d) Pile movement of 2 pile group (pile number 1 on the right) scaled 2000
 (e) Pile moment (pile number 1 on the right) scaled 0.05

Figure 78: Effect of pile location on displacement and bending moment. Maximum and minimum displacement $1.55 \cdot 10^{-3}m$ and $0.02 \cdot 10^{-3}m$ for complex group. Maximum and minimum bending moment at 51.9 kNm and -16.5 kNm

Comparing the figures shows that the leading piles receive a larger moment than the trailing piles, concentrated at the upper locations. This is in line with the expectations of a moment, as integration of the moment in regards to dz results in the deflection of the pile:

Deflection

$$y = y(z) \quad (57)$$

Slope

$$S = \frac{dy}{dz} \quad (58)$$

Curvature

$$\phi = \frac{d^2y}{dz^2} \quad (59)$$

Moment

$$M = EI * \phi \quad (60)$$

As the shear forces are the largest at pile number 1, the lowest at pile number 15, the moment will decrease from pile 1 till 15. This leads to a decrease in the slope present in the deflections, clearly visible in the deflection of figure 78a.

Considering the effect of the pile movement under a 2 pile group, spaced at the same distances as pile 1 and 15 in the complex group, the movement was expected to behave in the same manner as stated earlier. The 2 pile group was tested under ctc distances of 1.5, 3.0 and 4.5 to see if the same displacements are found for closely spaced piles. The displacement found in all configuration matches that of figure 78b, which shows that the same response is not visible in the simplified pile groups.

Increasing the group size to larger groups with 5 piles, shows the influence of ctc distance on both the vertical strain as well strain in x direction. This does not show the same response as found with figure 78a in regards to the displacement.

Figure 78 shows that the extra displacements of the piles must be a combination of horizontal and vertical forces, as the horizontal only loading scenario does show the expected response.

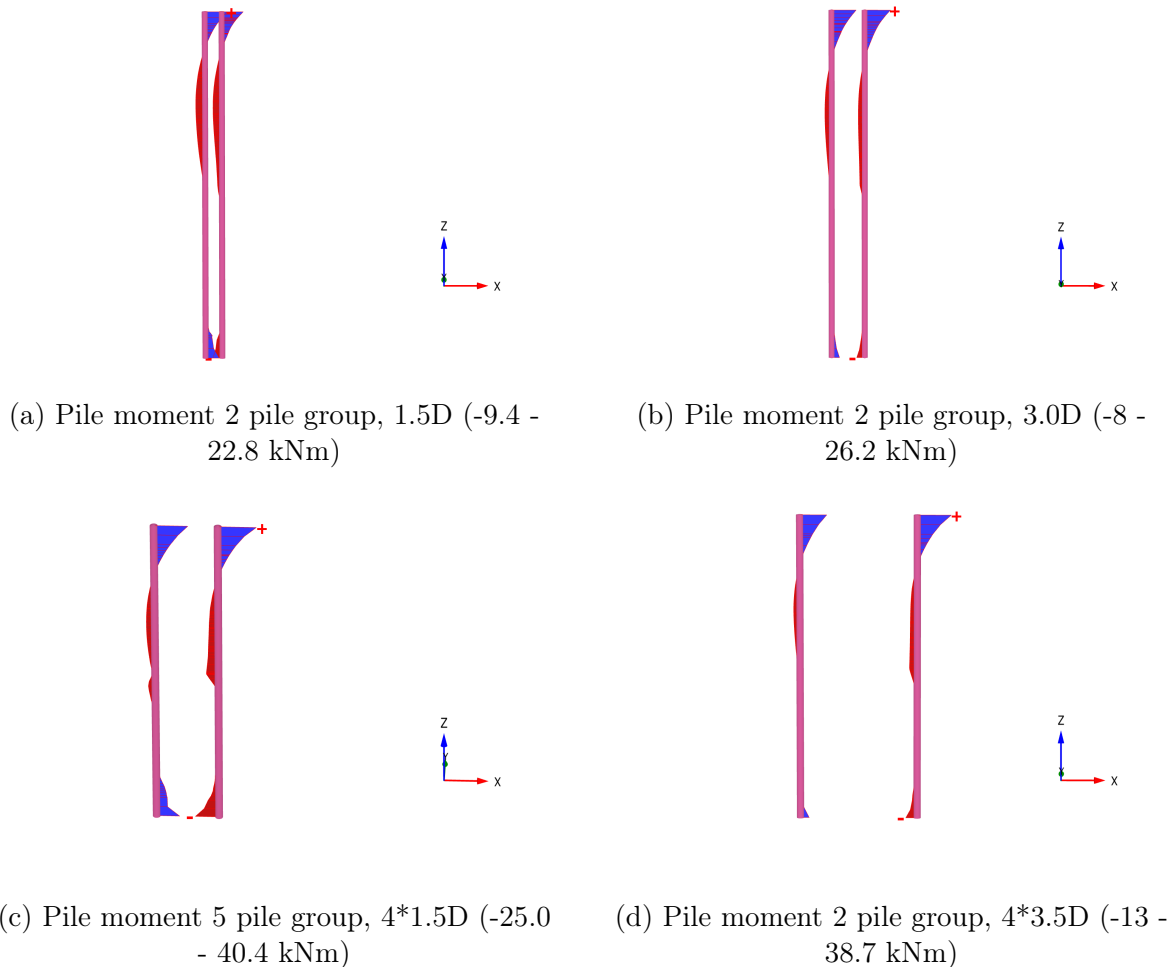


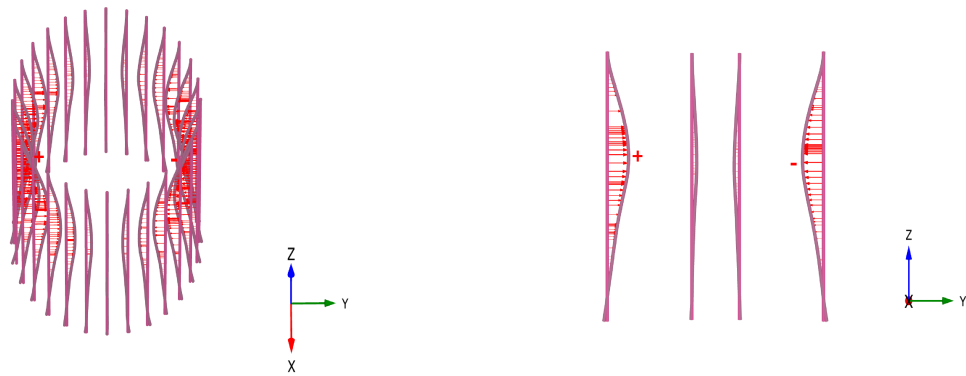
Figure 79: Effect of group size and ctc distance on pile moment

Figure 79a and b show that the difference in moment increases with larger ctc distances, 79c and d show that this decreases with an increase in ctc distance. No clear effect between the ctc distances and pile group increase is visible for the influence on pile displacement over depth.

All the scenario's in both figure 78 and 79 show different zero-moment locations along the pile. For the complex group from figure 79a, the first zero-moment results is found at -8.5 meters, the trailing piles at the end of the pile at -16 meters. The zero-moment of the leading piles is located in the middle of the loose sand layer.

7.2.6 Displacement of the piles in y direction

The movement in y direction showed a mirrored response considering figures 74a and b. The movement does confirm the creation of a slightly oval shape in the middle, where as the fixed head and fixed lower section result in a normal circular shape. The stiff plate ensures that non of the bending comes from the unequally distributed loading conditions.



(a) Movement of piles in y direction

(b) Movement of pile 22, 16, 14, 8 in y direction (from left to right)

Figure 80: U_y movement scaled 5000 times

The fixity of the piles in y direction is as mentioned only on top and at the bottom of the pile. The movement of both piles are comparable at $3.1 * 10^{-4}m$. It needs to be taken into account that the movement is roughly 1/5th of the total lateral movement, which is very small.

It seems that piles in the two perpendicular groups show less displacement, visible as piles in figure 80 in positive and negative x direction. This is due to the increase in x displacement under vertical loading scenario for these piles, while only y displacements are read from the piles. Considering the total response of both x and y displacements results in the same inward bending.

7.3 Conclusions of vertical complex round foundation

The complex foundation with vertical piles is modelled as designed by RHDHV. This section considered the influence of the pile placement in a circular way and compared this with the already present test scenario's of simplified pile groups. The location of the piles that are chosen to give an in-depth comparison and investigation are centered along the the perpendicular, parallel and skew pile groups.

The largest difference is the increase of group size, with a combination of the simplified pile groups in one general model. While most of the groups were not visible as separate loading group in the complex pile group, the following aspects are relevant for both simplified as well as complex group layout:

1. The largest shear forces are concentrated at the the first leading piles of 1-4-26 as proven by Matlock et al. [1980]. The second perpendicular pile group of piles 12-15-18 does behave more efficient than the trailing piles in front of these piles, but should behave as a separate perpendicular pile group after a ctc distance of 28.5 between the perpendicular pile groups.
2. The parallel loading conditions are primarily visible in sections between piles 5 and 12, clearly showing a decrease in efficiency from pile 5 till pile 12. The circular layout assures that the efficiency should again increase after the piles move out of line to a perpendicular loading situation, but this effect is not visible.
3. The simplified groups shows that skew loading conditions result in decrease in (apparent) efficiency due to a decrease in Q_{12} and increase of Q_{13} forces. This effect is also visible as increase of Q_{13} forces at the centre piles of the skew loading groups.
4. Soil movement within the pile ring group does show differences in displacements, a higher displacement field overlaps both the perpendicular pile groups showing a clear influence of apparent trailing effect after large ctc distances.
5. Large redistribution of shear forces results in location dependent bending (moments).

The distribution of the axial forces is as what is expected by a structure dipping on the right hand side. The shape and size increase of both the high and low displacement field do confirm the displacement of the structure in the horizontal plane. The individual response of high displacement and stress fields in the first perpendicular loading group, eventually leading to high displacement and stress banding, shows the combination of the perpendicular and parallel loading effect. Due to the round foundation, this trailing effect is also visible when comparing the leading and trailing perpendicular pile group as shown by figure 71.

The displacement of the leading pile and trailing piles results in an increase in depth dependency for later trailing piles in x direction. This effect is described by the increase of shear forces, leading to a moment increase. This effect is visible when using the separate horizontal and vertical loading scenario's, combination of those displacements result in an addition for pile 15 and a subtraction for pile 1 showing the combined response. The response of the simplified pile groups do not show this extra x displacement under

vertical only loading conditions, using the same vertical loading scenario. The mirrored movement in y direction results in a hourglass shape, with a movement of roughly 1/5th of the maximum movement in x direction.

8 Influence of batter angle on complex round foundations

This section will first use the existing 28 vertical pile structure, to assess the influence of batter angle on the round pile group. A limiting batter angle of 1:8 is taken, as placement of the the drilling equipment under larger angles is not possible. In order to assess the same angles as mentioned in section 5.4.1, the piles will be placed under -1:8,1:1 and 1:8 batter angles. Unfortunately, the ctc distance at positive batter angles can result in placement of pile tips closer together than the vertical placement predicts. At an angle of 1:8, the piles reach a minimum ctc distance of $20.9D$ or 11.7 meters for opposite piles. This ctc distance can decrease with depth to a value of $2.34D$ considering the side-to-side placements, which is the zone where the building process can negatively impact the concrete piles. Most of the wind turbines are build with negative batter angles. To ensure a realistic case without pile tip influence a first analysis with relevant batter angles is considered.

8.1 Definition of local axis

The orientation of the local axis is normally fixed in three directions, namely x,y and z. The z direction is defined by the batter angle used for the pile and is always orientated along the pile shaft. The x and y direction are fixed to local axis 2 and local axis 3, which are changing when applying a batter angle in a circular foundation. As vertical piles result in no change in axis directions due to absence of the batter angle, this effect is not visible with the vertical complex pile group.

In order to avoid the rotation of the axis and therefor the output of Q12 and Q13 forces, these forces are fixed in the x and y direction. The z direction is still orientated along the pile axis in order to correctly read the axial forces. While this results in approximately correct readings for the pile shear forces, the orientation for piles 8 and 22 result in the largest influence of the batter angle. Due to this effect, the maximum and minimum shear forces for piles 8 and 22 and their directly surrounding piles are lower than with true horizontally orientated local axis 2 and 3.

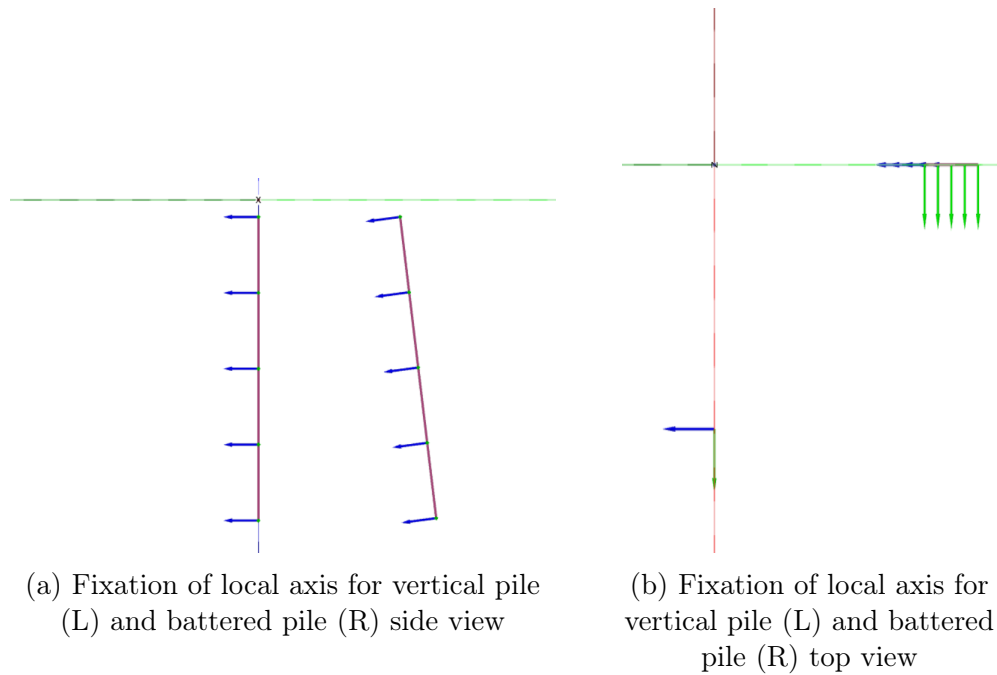


Figure 81: Local axis configuration

8.2 Axial force distribution

As mentioned already in 5.4 and in the introduction, the use of a batter angle can result in an axial orientation of the combined horizontal and vertical forces. The use of a mirrored design always results in the use of a negative and positive batter angle in regards to the loading direction, which can result in cancellation of the positive and negative working principles of the battered piles. The alternating batter angle with straight and battered piles result in the use of the following configuration for 28 piles:

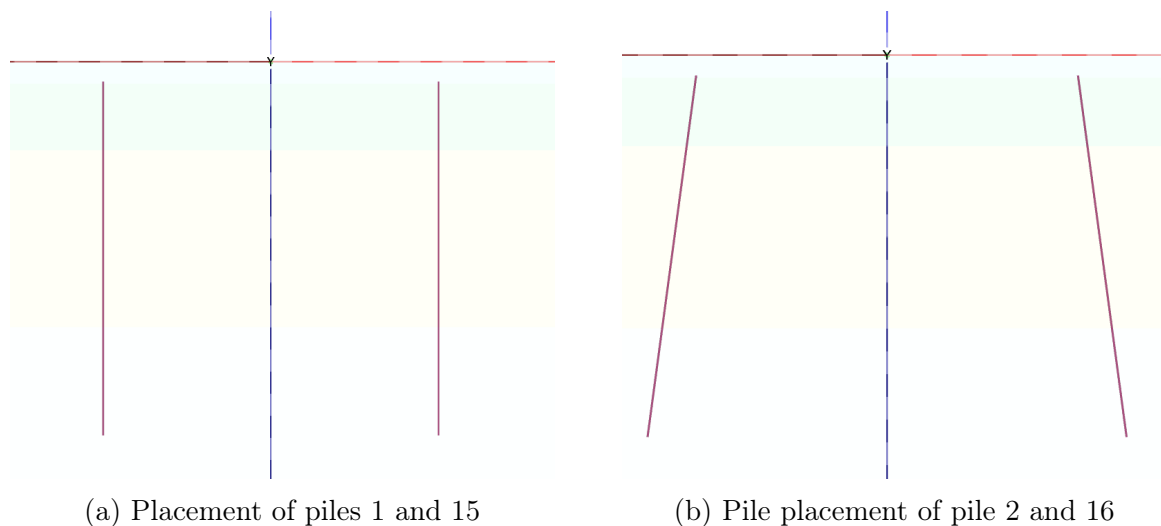


Figure 82: Layout of alternating batter angles

Configurations with different amount of piles can result in non-mirrored pile placements, visible for example with 26 pile configurations. The analysis will be performed with the

complete vertical loading and horizontal loading and with only vertical loading conditions to check the influence of the addition of lateral loading.

Table 17: Overview of (alternating) battered complex group axial response

Pile Number	Maximum displacement (m)				Minimum axial forces (kN)				Offset to vertical displacement (-)		Offset to vertical forces (-)		Dynamic pilehead spring (MN/m)	
	Combined (1:8)	Combined (alternating)	Vertical (1:8)	Vertical (alternating)	Combined (1:8)	Combined (alternating)	Vertical (1:8)	Vertical (alternating)	1:08	Alternating	1:08	Alternating	1:08	Alternating
1	-2.01 * 10 ⁻³	-2.12 * 10 ⁻³	-2.08 * 10 ⁻³	-2.11 * 10 ⁻³	-611.5	-529.0	-579.2	-554.3	0.96	1.01	1.06	0.95	421.9	1533.4
4	-2.02 * 10 ⁻³	-2.12 * 10 ⁻³	-2.08 * 10 ⁻³	-2.11 * 10 ⁻³	-603.8	-668.4	-584.8	-603.3	0.97	1.01	1.03	1.11	306.6	4178.5
8	-2.08 * 10 ⁻³	-2.12 * 10 ⁻³	-2.08 * 10 ⁻³	-2.11 * 10 ⁻³	-578.8	-607.6	-585.5	-606.6	1.00	1.00	0.99	1.00	2018.6	109.0
12	-2.14 * 10 ⁻³	-2.11 * 10 ⁻³	-2.08 * 10 ⁻³	-2.11 * 10 ⁻³	-564.4	-549.4	-583.8	-604.1	1.03	1.00	0.97	0.91	334.3	19886.4
15	-2.15 * 10 ⁻³	-2.11 * 10 ⁻³	-2.07 * 10 ⁻³	-2.11 * 10 ⁻³	-554.4	-576.1	-582.5	-550.7	1.04	1.00	0.95	1.05	364.3	247924.2
18	-2.14 * 10 ⁻³	-2.11 * 10 ⁻³	-2.07 * 10 ⁻³	-2.11 * 10 ⁻³	-561.2	-543.1	-576.5	-609.1	1.03	1.00	0.97	0.89	244.8	63097.9
22	-2.08 * 10 ⁻³	-2.11 * 10 ⁻³	-2.07 * 10 ⁻³	-2.11 * 10 ⁻³	-578.2	-609.6	-580.1	-611.3	1.00	1.00	1.00	1.00	500.0	247.8
26	-2.02 * 10 ⁻³	-2.12 * 10 ⁻³	-2.08 * 10 ⁻³	-2.11 * 10 ⁻³	-606.4	-668.5	-579.2	-599.6	0.97	1.01	1.05	1.11	473.8	4979.4
AVG	-2.08 * 10 ⁻³	-2.12 * 10 ⁻³	-2.08 * 10 ⁻³	-2.11 * 10 ⁻³	-582.3	-594.0	-581.5	-592.4	1.00	1.00	1.00	1.00	583.0	42744.6

Table 17 concludes the maximum displacements in z direction for axial loading with the corresponding maximum forces. The table shows the influence of the batter angle on axial force distribution as expected by the explanation in figures 24a and b. This force distribution results in:

1. Increase in axial forces for the dipping pile group, decrease for the uplifting group. The alternating pile group shows almost no difference in vertical movement
2. Axial force increase for the battered piles due to the use of the batter angle as shown by the average axial forces
3. Axial force redistribution with higher forces for the battered piles and lower forces for the vertical piles

8.2.1 Vertical loading conditions

Comparing the outcome of table 14 with table 17 we can see that the average loading conditions are roughly the same with a maximum difference of 4 kN, as expected by the same vertical loading conditions when considering the complete 28 pile group. Those forces are -581.4 kN for the 1:8 batter angle under vertical and combined loading, -579.2 kN for alternating batter angles under vertical and combined loading. All piles analysed except piles with number 1 and 15 are placed under a batter angle in the alternating group. This is visible as a large increase in axial loading conditions for those piles due to decomposition of forces, while the straight piles receive a much lower axial force. While table 14 shows a large difference in average vertical forces, this effect is due to absence of the same amount of vertical as battered piles in the analysed piles.

When considering the vertical displacement, the displacements of the pure vertical loading scenario increases with the alternating batter angles. As expected, the battered piles result in decomposition of the forces which will create a horizontal and vertical movement. While the difference is roughly $4.0 * 10^{-5}$ for the alternating and 1:8 batter angle, the increase results in a difference of 1.9%.

8.2.2 Combined loading conditions

Addition of the horizontal loading conditions shows that the piles on the right hand side (piles 1,4,26), the side where the foundation has uplift, results in increase in axial forces. The dipping side results in an decrease in axial forces, visible in pile 12,15 and 18. Piles

8 and 22 are behaving as average piles. This effect is visible for the 1:8 pile group, as all piles are under the same batter angle. The axial response for the alternating batter angle for piles 8 and 22 shows an increase. Pile 8 and 22 should behave as average axial pile load, due to the location of the turning axis.

Comparing the combined loading conditions for the alternating pile group shows that the horizontal load is increasing the axial forces in the 1:8 battered piles and decreases them for the vertical piles on the uplift side (right side). Piles 1, 4 and 26 also show large differences in axial forces for the alternating pile group when comparing to the 1:8 battered pile group. The difference between the maxima and minima axial forces present with only vertical loading conditions result in a difference of 60 kN at maximum. This difference increases with using combined loading conditions to almost 125 kN. The combination of different batter angles results in a large increase in axial force distribution along piles with the same batter angle under the same loading conditions and same displacement groups. The displacement groups being the perpendicular, skew and parallel locations.

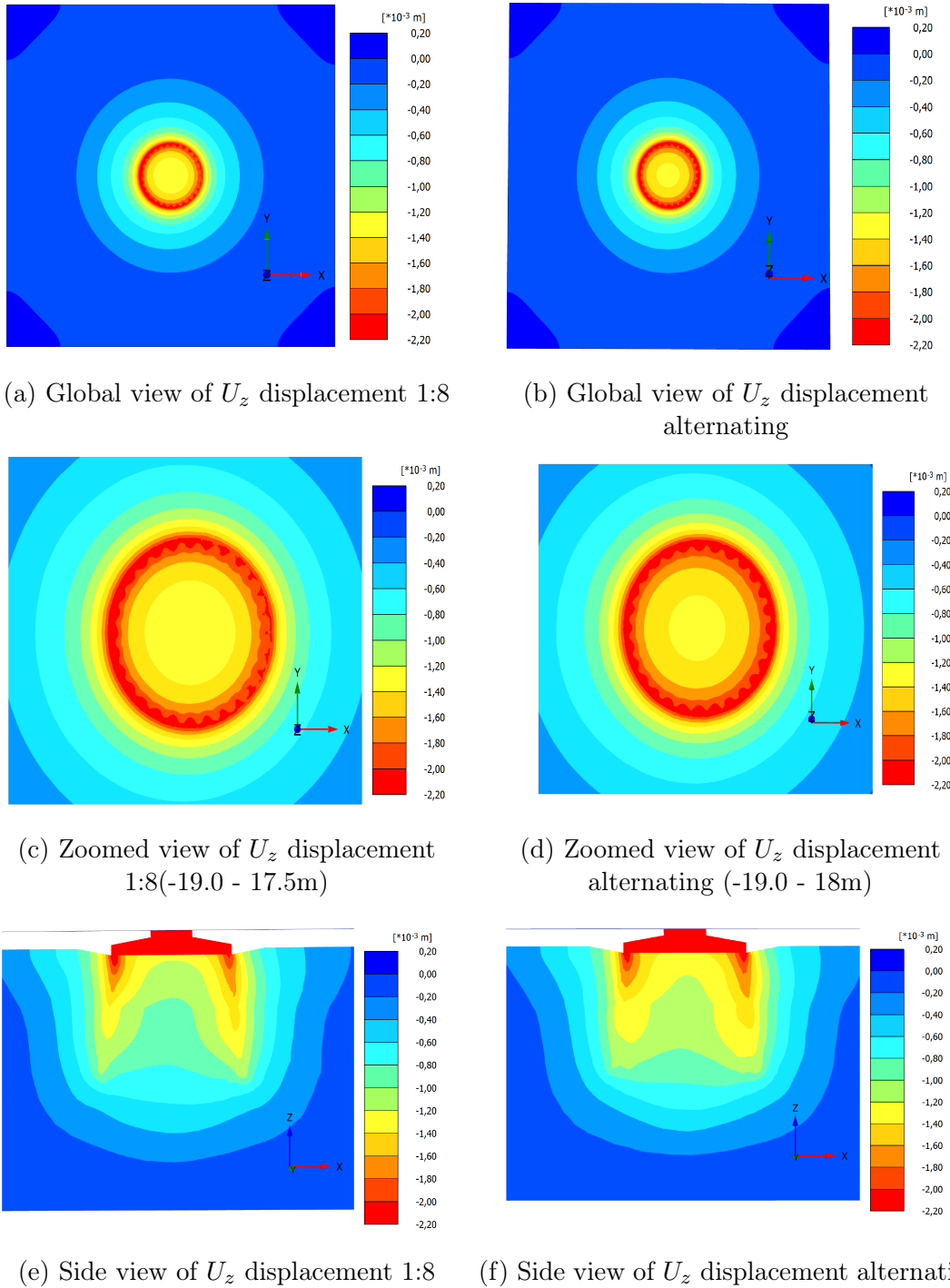


Figure 83: U_z displacements under combined lateral and vertical loading conditions for 1:8 batter angle and alternating vertical -1:8 batter angle

Figure 83a and b show the influence of alternating batter angles and complete 1:8 battered structure. The 1:8 battered pile group in figure 83a and b shows a displacement distribution which is equally distributed. Zoomed in figure c shows a more concentrated high displacement banding (orange) surrounding the piles with a large lower displacements fields (yellow) in the middle of the pile ring group than subfigure D. This larger middle section with lower displacements is expected, as the use of alternating batter angles result in a more gradual decrease in (high) displacement banding inwards due to load distribution over a larger area.

Figure 83e and f shows that the z displacement is along the whole pile length for both complex groups. The axial forces seem to be more evenly distributed, visible in a smaller high displacement field on the right hand side in comparison to the alternating batter angles an in-line with the expectations as stated above. While table 17 combined alternating response shows that pile 1 has a lower axial force than pile 15, the surrounding piles of pile 1 carry much larger loads for the combined loading conditions. This effect can increase the high displacement zone surrounding pile 1 and decreasing it with pile number 15. This creates the apparent increase in high displacements on the right hand side.

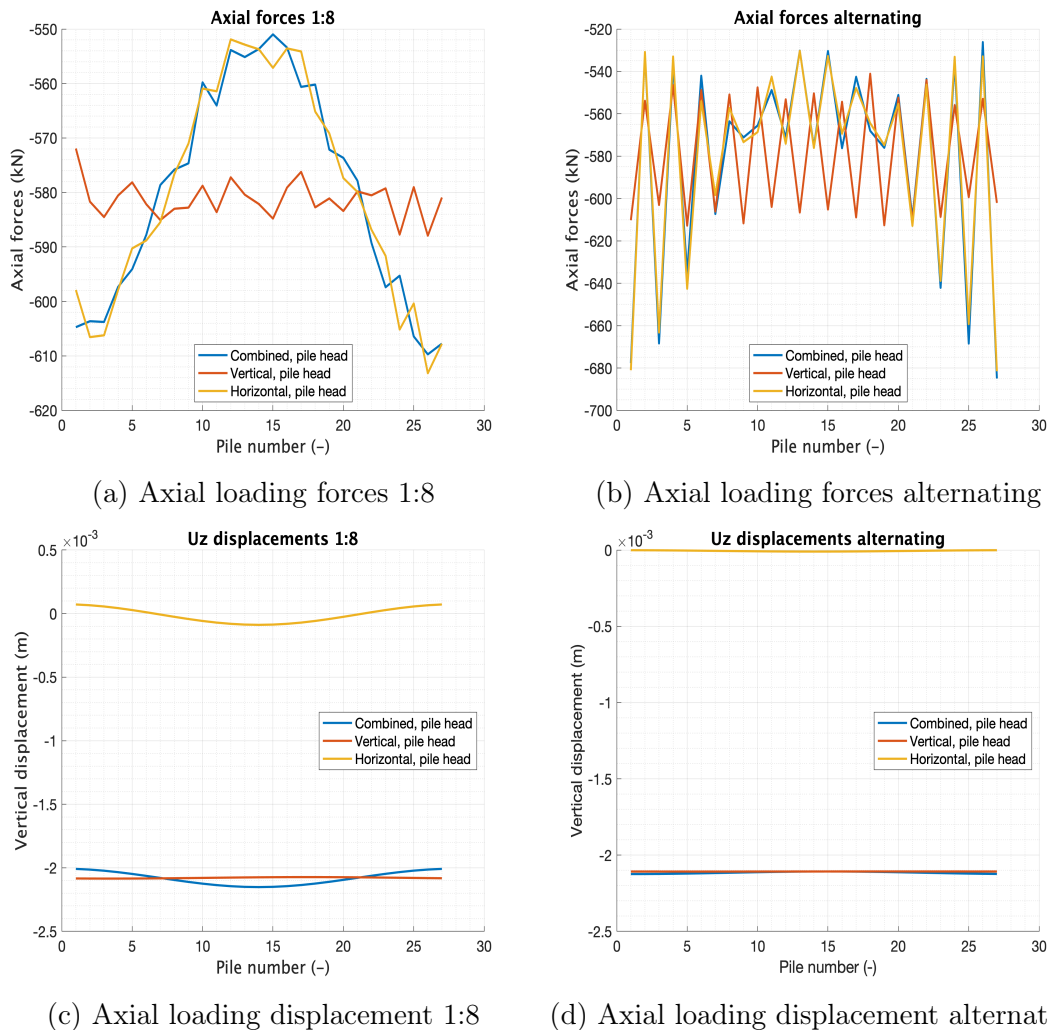


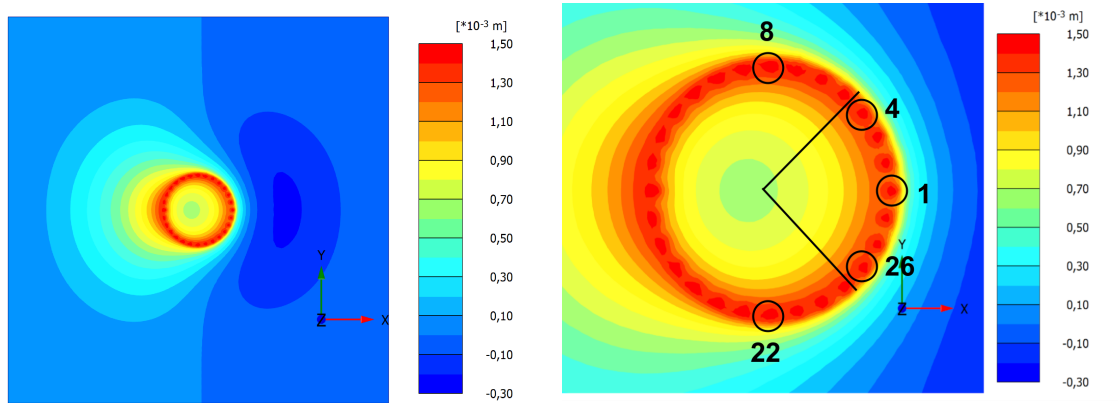
Figure 84: Maximum axial forces per pile for different loading conditions under 1:8 and alternating batter angles

The axial loading conditions of both the 1:8 and alternating pile group are shown in figure 84. Comparing the response with the vertical pile group, the 1:8 battered pile group shows a slight increase in minima and maxima axial forces. The alternating batter angle results in alternating 'saw' axial loading conditions. The axial loading differences for the alternating pile group decreases to pile 15 and increase again from pile 15 to 28. The average loading conditions of the alternating group seem to follow the axial force distribution of the 1:8 battered group. The displacement of figure 84c and d show that the z displacement over the complete structure is not pile dependent for alternating pile

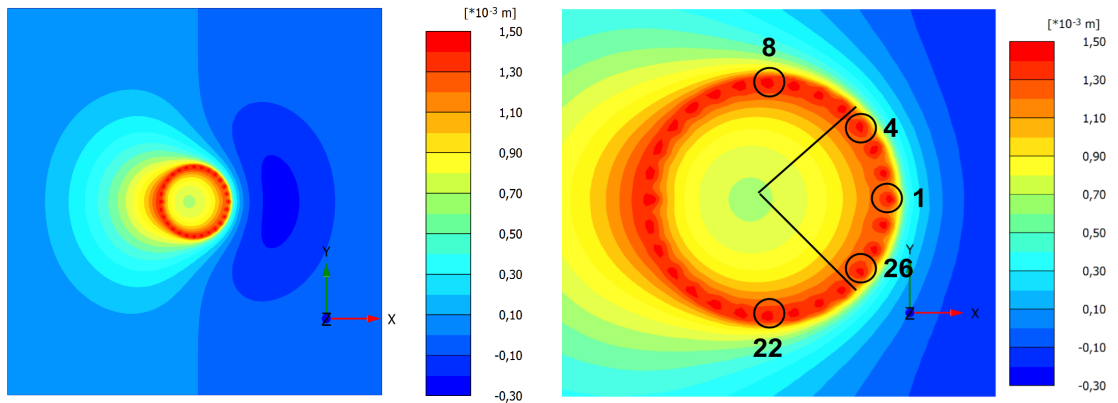
group, slightly for the 1:8 battered pile group.

8.3 Shear forces and stress distribution

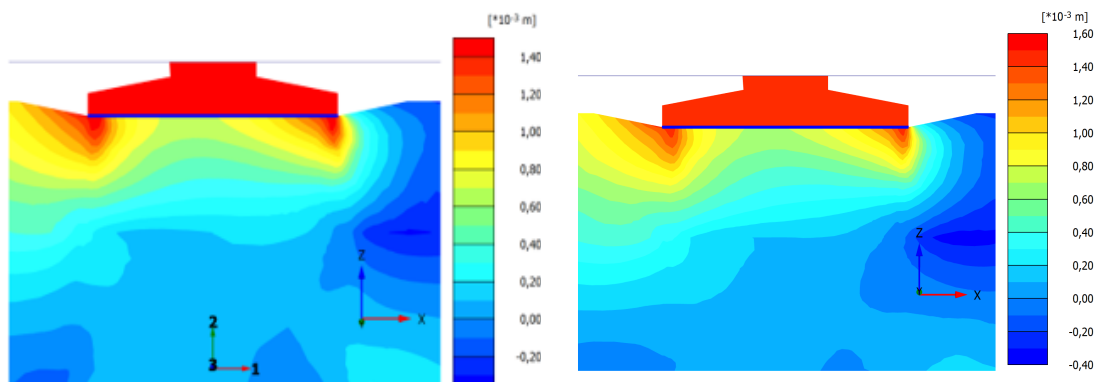
The shear force distribution can describe the efficiency of the pile in the pile group, primarily visible in shear force or stress concentration surrounding the piles. The analysis of the pile group will be performed in a similar matter as the vertical analysis, looking into the σ_{xx} and σ_{yy} stresses and shear forces in Q12 and Q13 direction.



(a) Global view of U_x displacement zoomed 1:8 (b) Zoomed in view of U_x displacement 1:8



(c) Global view of U_x displacement alternating (d) Zoomed in view of U_x displacement alternating



(e) Side view of U_x displacement 1:8 (f) Side view of U_x displacement alternating

Figure 85: U_x displacements under combined lateral and vertical loading

Figure 85 shows the individual response of the piles over the complete pile group. A small increase in the oval high displacement shape directly surrounding the pile in figure 85b and d as expected by the trailing effect, is visible after pile 7 and increases till pile 13, decreases after 13 again till pile 15. This response shows the increase of trailing effect and decrease as the trailing pile group goes into a perpendicular orientated pile group. Comparing the results with figure 71 shows that the alternating batter angles creates a larger low displacement field between the piles.

Comparing figures 85e and f, shows that increase in the use of amount of 1:8 battered piles result in a larger low displacement zone in the middle of the soil mass. Combining this with the results from figure 71 shows that the vertical piles result in the largest single high displacement field, which becomes less when using an increased amount of battered piles. This effect potentially shows that the trailing perpendicular pile group with 1:8 battered piles acts as an higher efficiency pile group.

To check the stress field surrounding the piles, the piles are checked for the σ_{xx} stress states for both the complete structure as a zoomed in version.

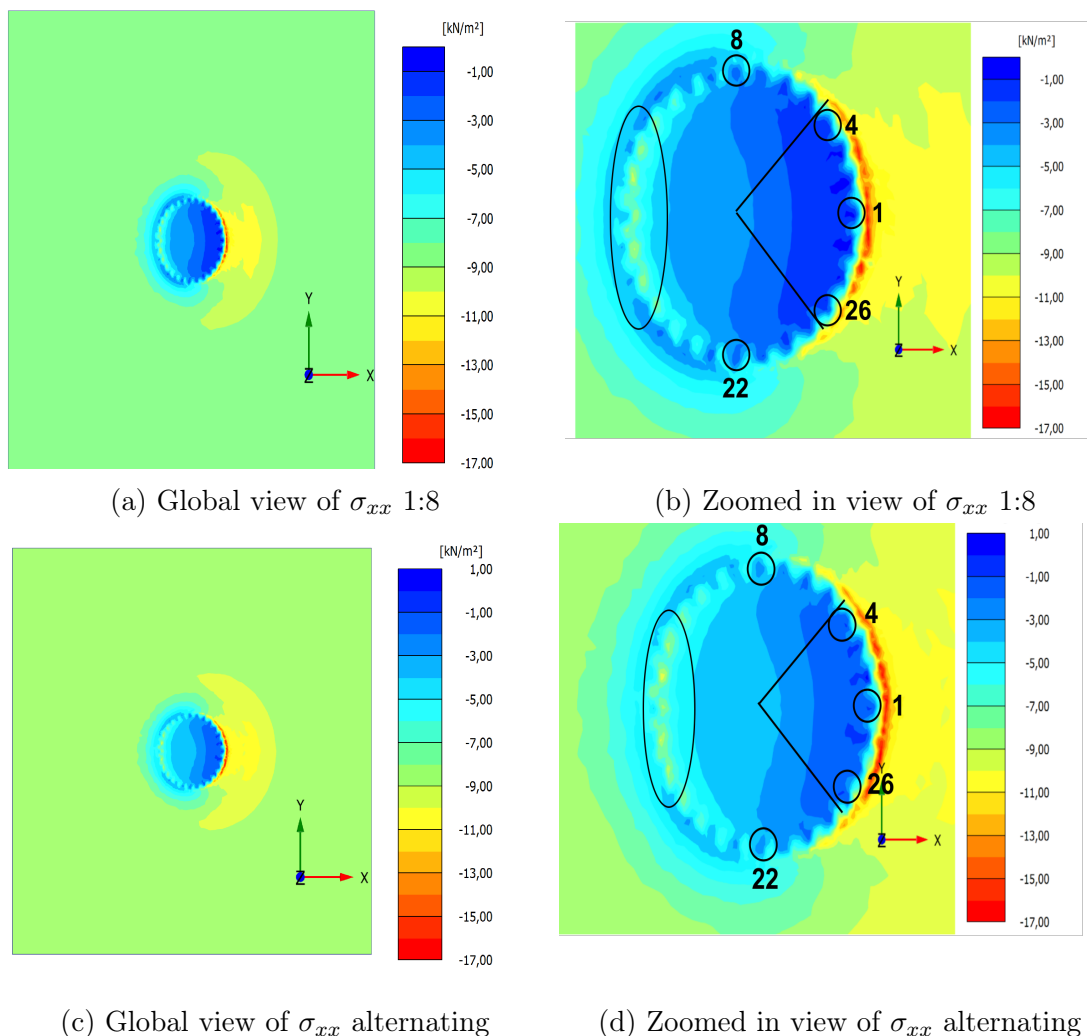


Figure 86: σ_{xx} displacements under combined lateral and vertical loading

Differences between the figures are minimal and show only minor changes at the left side of the foundation, creating a larger high stress zone surrounding the structure for the 1:8 battered group

The same conclusions from section 7.2 apply to the groups when using batter angles. A slight increase in efficiency is visible for the trailing perpendicular pile group as stated in figure 86b and d, while sub figure d shows a slight decrease in comparison to sub figure b. The extra displacement and shear stresses per pile are plotted below for both configurations.

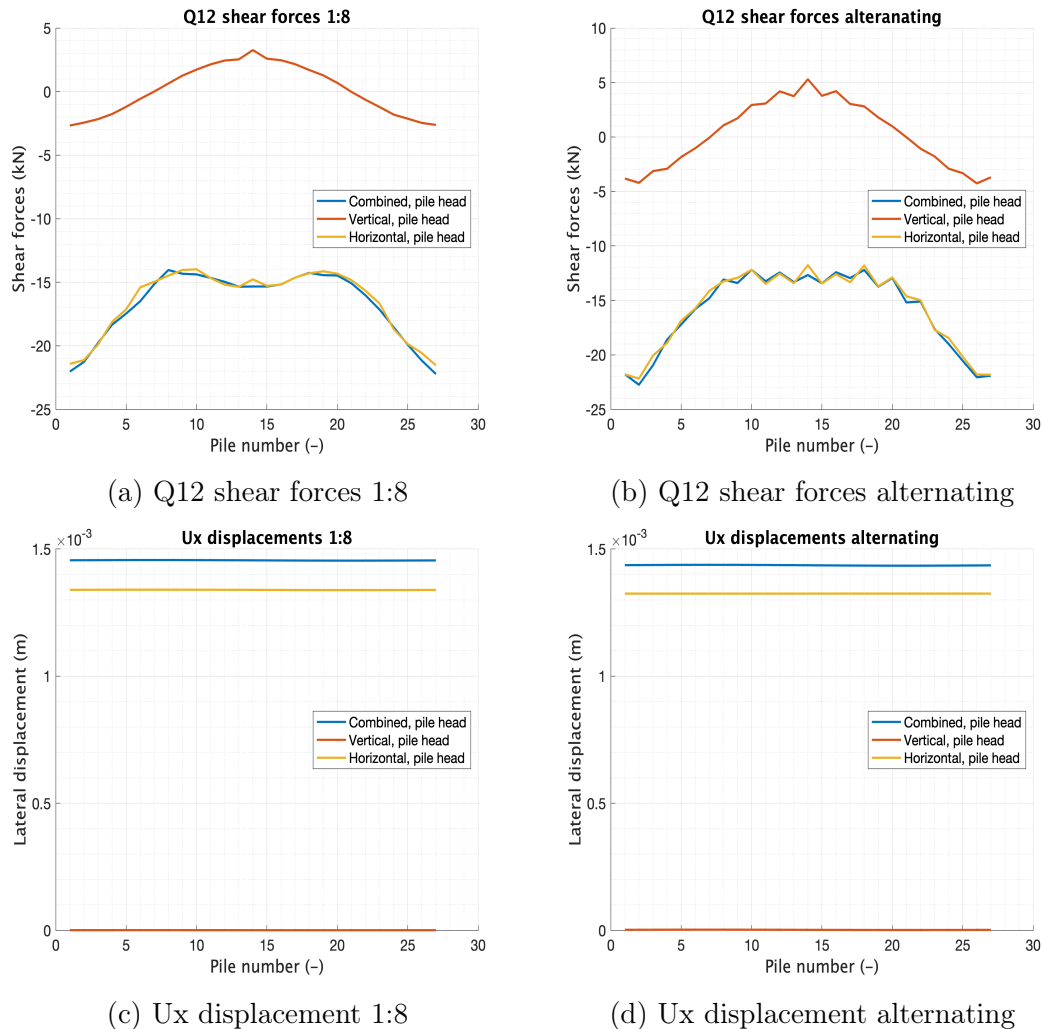


Figure 87: Maximum shear forces per pile for different loading conditions under 1:8 and alternating batter angles

The Q12 shear forces for the 1:8 battered pile group and alternating pile group show roughly the same response. The alternating batter angle shows the influence of the alternating piles, visible as the saw effect. This effect is only visible between piles 9 till 21, which is the dipping part of the structure. As visible, the x displacements are primarily caused by the horizontal loading. There is no difference in displacements over the pile group as the piles have fixed head conditions considering subfigures c and d.

The slight increase in Q12 shear forces for the battered pile group show that the second perpendicular pile group receives a higher efficiency as expected by the perpendicular loading conditions and the lower displacement fields shown in figure 85. The average Q12 shear forces seem to be slightly lower than the average Q12 shear forces of the vertical complex pile group, while the displacements are lower. The increase in axial forces are

therefore not only due to the use of batter angle and redistribution of forces, but also due to the uptake of Q12 shear forces in the axial forces.

Table 18: Q12 shear forces and x displacement for 1:8 and alternating pile groups

Pile	Ux_max (m)		Ux_min (m)		Q12_max (kN)		Q12_min (kN)	
	1:08	Alternating	1:08	Alternating	1:08	Alternating	1:08	Alternating
1	$1.46 * 10^{-3}$	$1.44 * 10^{-3}$	$-4.91 * 10^{-5}$	$-9.72 * 10^{-5}$	16.4	11.68	-23.1	-24.84
4	$1.46 * 10^{-3}$	$1.44 * 10^{-3}$	$-2.57 * 10^{-5}$	$-8.67 * 10^{-5}$	4.3	5.31	-19.8	-20.94
8	$1.46 * 10^{-3}$	$1.44 * 10^{-3}$	$1.08 * 10^{-5}$	$7.20 * 10^{-6}$	4.3	4.40	-15.1	-14.80
12	$1.46 * 10^{-3}$	$1.44 * 10^{-3}$	$-7.26 * 10^{-5}$	$-9.13 * 10^{-5}$	5.2	8.90	-14.7	-13.24
15	$1.46 * 10^{-3}$	$1.44 * 10^{-3}$	$-1.12 * 10^{-4}$	$-1.02 * 10^{-5}$	7.2	8.60	-15.3	-12.66
18	$1.46 * 10^{-3}$	$1.44 * 10^{-3}$	$-7.82 * 10^{-5}$	$-1.01 * 10^{-4}$	5.3	11.42	-14.6	-12.95
22	$1.45 * 10^{-3}$	$1.43 * 10^{-3}$	$1.51 * 10^{-5}$	$2.20 * 10^{-5}$	4.8	3.10	-15.1	-15.19
26	$1.45 * 10^{-3}$	$1.43 * 10^{-3}$	$-2.98 * 10^{-5}$	$-9.29 * 10^{-5}$	3.5	4.29	-19.9	-20.55
AVG	$1.46 * 10^{-3}$	$1.44 * 10^{-3}$	$-4.27 * 10^{-5}$	$-5.63 * 10^{-5}$	6.38	7.21	-17.20	-16.90

The same influence of Q12 and Q13 maxima and minima locations are found for the 1:8 and alternating pile group in comparison with the vertical pile group. The Q12 shear forces have their maxima and minima on pile 1,26 and with pile 15 respectively. The Q13 forces show their maxima and minima at pile 6 till 8 and 22-24 respectively.

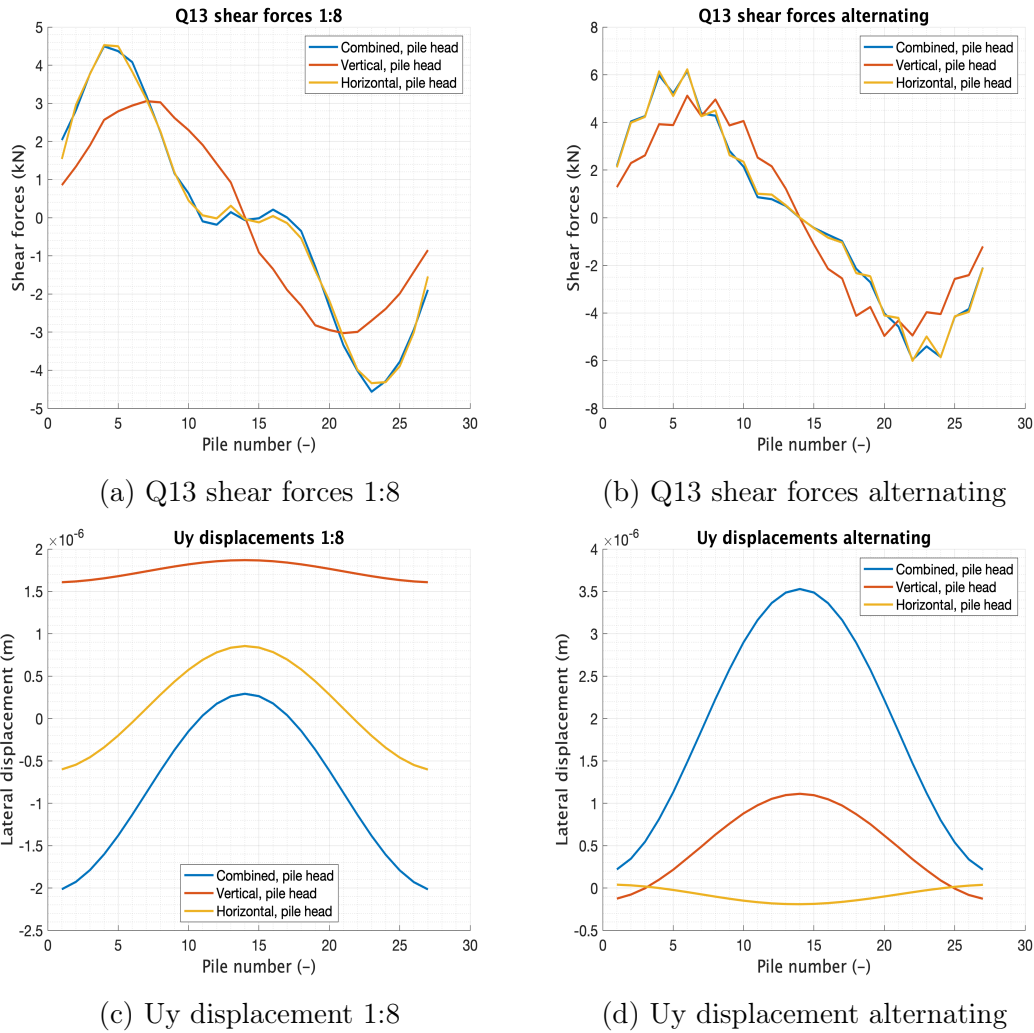


Figure 88: Maximum shear forces per pile for different loading conditions under 1:8 and alternating batter angles

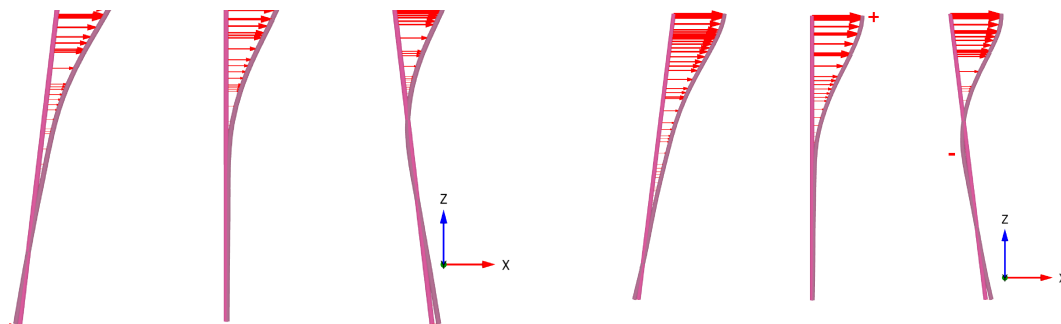
The Q13 shear forces show for the horizontal and combined loading conditions their maxima at pile 5, which should be located at pile 8 locations due to the maximum y displacements. This effect can be described by the y displacements due to vertical loading, as this counters the diagonal orientation of the pile. Further explanation will be given in section 9.3.

Table 19: Q13 shear forces and y displacement for 1:8 and alternating pile groups

Pile	Uy_max (m)		Uy_min (m)		Q13_max (kN)		Q13_min (kN)	
	1:08	Alternating	1:08	Alternating	1:08	Alternating	1:08	Alternating
1	$7.68 * 10^{-6}$	$3.93 * 10^{-6}$	$-4.58 * 10^{-6}$	$-2.37 * 10^{-6}$	2.2	1.23	-1.9	-5.27
4	$9.82 * 10^{-5}$	$1.09 * 10^{-4}$	$-8.82 * 10^{-5}$	$-1.35 * 10^{-4}$	7.4	12.36	-4.1	-4.48
8	$1.54 * 10^{-4}$	$1.56 * 10^{-4}$	$-1.42 * 10^{-4}$	$-2.30 * 10^{-4}$	6.9	17.62	-5.6	-13.61
12	$7.64 * 10^{-5}$	$8.43 * 10^{-6}$	$-7.48 * 10^{-5}$	$-1.33 * 10^{-4}$	4.9	6.78	-3.0	-4.86
15	$1.74 * 10^{-6}$	$3.53 * 10^{-6}$	$-4.85 * 10^{-6}$	$-2.52 * 10^{-6}$	2.3	1.71	-1.8	-1.62
18	$7.33 * 10^{-5}$	$1.41 * 10^{-4}$	$-7.41 * 10^{-5}$	$-8.08 * 10^{-5}$	3.7	8.46	-4.7	-5.33
22	$1.36 * 10^{-4}$	$2.29 * 10^{-4}$	$-1.46 * 10^{-4}$	$-1.45 * 10^{-4}$	5.5	10.20	-6.6	-16.20
26	$9.10 * 10^{-5}$	$1.43 * 10^{-4}$	$-1.01 * 10^{-4}$	$-9.63 * 10^{-5}$	4.9	7.90	-8.4	-9.36
AVG	$7.97 * 10^{-5}$	$1.09 * 10^{-4}$	$-7.94 * 10^{-5}$	$-1.03 * 10^{-4}$	4.73	8.28	-4.51	-7.59

8.3.1 Displacement of piles in x direction

The same conclusion of the vertical pile group are applicable to the 1:8 battered pile group. The leading piles receive the subtraction of vertical and horizontal movement for pile number 1, while the same effect results in addition of the displacements for pile 15. As both loading scenario's result in roughly the same displacements, no difference in pile displacements are visible. Both pile groups are analysed with battered piles on positions 15, 8 and 1 from left to right.

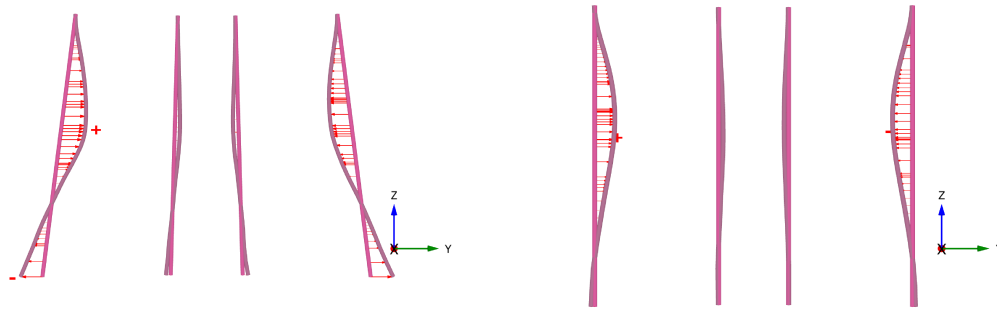


(a) Pile movement Ux (pile number 1 on the right) scaled 2000 for single phase combined loading 1:8 (b) Pile movement Ux (pile number 1 on the right) scaled 2000 for single phase combined loading alternating

Figure 89: Effect of pile location on displacement for 1:8 and alternating battered pile groups. Maximum displacement of $1.45 * 10^{-3}$ and $1.44 * 10^{-3}$ m.

8.3.2 Displacement of piles in y direction

In contrast to the vertical pile group as described before, the 1:8 battered group shows positions with high concentrations of bending moment and lower bending moments. The vertical piles showed a gradual increase and decrease over the total length of the pile. The 1:8 group configuration shows the battered piles, while the alternating pile group shows the vertical piles. The analysed pile numbers are 22, 16, 14, 8 from left to right.



(a) Pile movement U_y (pile number 8 on the right) scaled 5000 for single phase combined loading 1:8 (b) Pile movement U_y (pile number 8 on the right) scaled 5000 for single phase combined loading alternating

Figure 90: Effect of pile location on displacement for 1:8 and alternating battered pile groups. Maximum displacement of $1.5 \cdot 10^{-4}$ and $2.2 \cdot 10^{-4}$ m

Comparing both figures we clearly see the same initial pile head movement. The battered piles have displacements at the lower portion of the pile, where this is almost fixed for the displacement in x direction. For both of the piles the maximum bending displacement is the same, but the the battered piles clearly show a combination of roughly equal positive as negative displacements. This results in almost 1.5 times the total displacement of vertical piles in the y direction in comparison to straight piles.

8.4 Single pile response under batter angles

The efficiencies for the battered piles are calculated by using the same loading conditions and batter angles as used in the complex foundation. The single piles are centered around point 0,0,0 (x,y,z) with their polar coordinates and 28 reference points are created, visualized below.

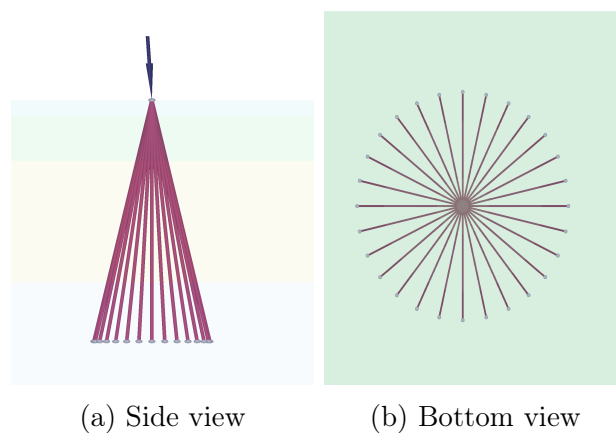


Figure 91: Reference single pile response with true loading direction

Each of the piles is analysed for the applied loading conditions. The 1:8 battered pile group is described by the procedure explained above, the alternating pile group uses the response of vertical piles and the battered piles. The local axis are fixed as explained in section 8.1. For the axial and both the shear forces, the following graphs are created for

the 1:8 battered pile group and alternating pile group.

Plaxis 3D does currently not have a possibility for rotation fixity in order to model single pile fixed head conditions. In order to approximate this behaviour, a long pile plate from -5 till 5 meter in x direction is created above the pile. Again the same negative interface with lower strength parameters is applied to delete any influence of the plate on the horizontal movement. To avoid the rotations, on the edges in positive and negative x direction of the plate a prescribed displacement is set with free x displacement and fixed z and y displacement.

In order to comply to the same loading conditions of the pile groups, the following scenario's are investigated:

- Applying a preset vertical displacement of the average z displacement of the pile group.
- Applying normal combined vertical and horizontal loading conditions.
- Applying combined vertical and horizontal loading conditions with extra set point displacement at the pile head with fixed y and z directions.

The preset vertical displacements resulted in a calculated load of -989 kN which is more than applied in the real model per pile. It was chosen to model the single pile with a point load of 20 kN horizontal and -565 kN vertical, to match the loading conditions of the complex model. As expected by the stiff plate response the -565 kN resulted in only minor z displacements, as the plates are fixed in this direction. In order to take into account the slope that is made surrounding the structure, the top layer should be excavated till a depth of -0.895 meter. It is chosen to delete the complete layer, as this small layer results in large amounts of small elements in the residual 0.105 m. This is less present in the complex model, as this thin layer is only situated directly below the foundation base.

The limitations of the options do result in incorrect axial force readings, as expected by the fixed z displacements. It also influences the stress state of the layers, as almost 14 kN/m² is deleted from the model. This efficiency is therefor calculated with a very approximate response of a reference single pile.

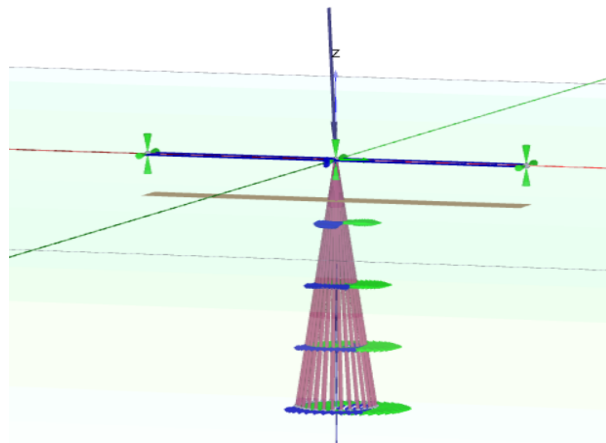
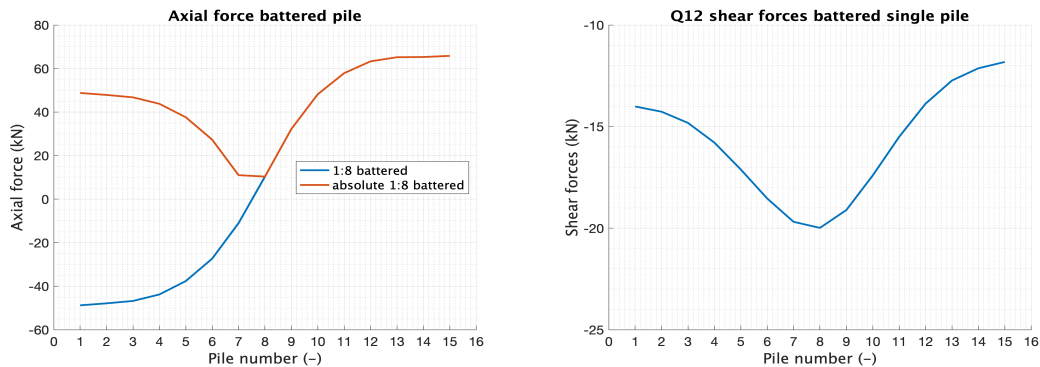
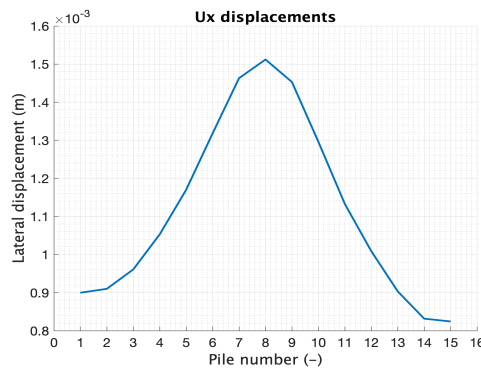


Figure 92: Reference single pile response with true loading direction

Every analysis will activate a single pile, comparable to the loading direction of the 28 piles in the complex battered pile group. As the efficiency of the battered pile group will be assessed to battered piles, the efficiency cannot exceed 1.



(a) Axial force response for battered piles (b) Shear force response for battered piles



(c) Lateral displacement

Figure 93: Single pile response of 1:8 battered piles with approximated rotation fixed pile head conditions. Pile 15 represents the negative batter angle

The single pile response shows that the x displacements are lower for the piles with their batter angle parallel to the loading direction, showing the lowest displacements for negative batter angles. The highest shear forces are found with the piles with the highest displacement and lowest axial forces. Figure 93a shows an axial response which is higher than expected, as the z direction displacements are fixed. It shows that the axial forces are the highest for the piles with their batter angles parallel to the loading direction. It shows that a 1:8 batter angle can result in axial uptake of Q12 shear forces, higher axial uptake resulting in lower x displacement.

The axial capacity of the foundation without failure must give a capacity of at least 1.0. As explained before the batter angle increases this axial response with a factor of $\cos(\tan(1/8))$ where the 1/8 fraction is the angle for each pile with 1:8 batter angle.

$$Axial\ response = \frac{575}{\cos(\arctan(1/8))} = 579.5\ kN \quad (61)$$

$$Axial\ efficiency = 579.5/575 = 1.008 \quad (62)$$

The average axial capacity for the complete 1:8 battered group was 1.011 and 1.007 for the alternating pile group. This shows that not only the batter angle influences the

axial response, but it shows that the extra resulting forces can be the result of axial uptake of the applied horizontal forces. This calculation shows a simplified approach, as stated by Hanna and A.Y.Afram [1987] this should only be used as approximation. This approximation does not take into account the vertical earth coefficient.

8.4.1 Efficiencies of battered pile groups

As explained, the efficiencies for axial and Q13 shear forces cannot be calculated due to the limitations of the single reference pile modelling. Only the Q12 shear force efficiency will be shown, as the x displacements are not fixed for each pile head. For this analysis three different scenario's for the alternating battered group are taken into account, both with the correct single pile reference for the battered piles.

1. A single vertical reference pile
2. Vertical pile in equivalent location pile group
3. Vertical and battered pile in equivalent pile group location

This means that the last two take into account the behaviour of the single reference point already under group efficiencies. This should create a better response, as the round complex layout is already taken into account.

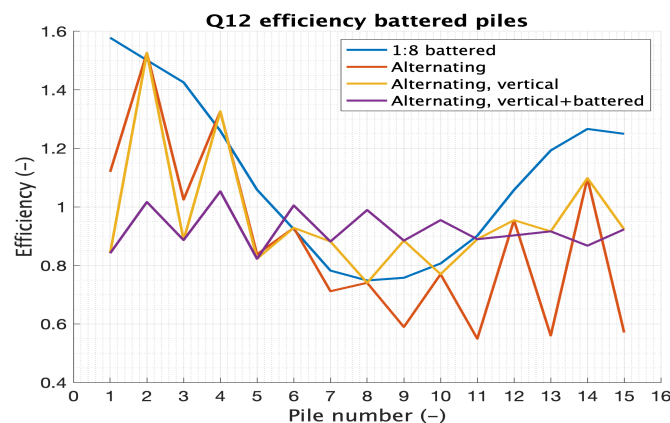


Figure 94: Q12 efficiency for 1:8 and battered pile groups

The Q12 shear forces show with increasing complexity of taking into account the reference pile location a better flat response, showing an average efficiency of 0.89. This is primarily the result of the high vertical complex pile group shear forces, as the battered response show almost an efficiency of 0.97. The application of pile location depended shear forces from groups diminishes the 'single reference pile' point. The flat response is due to comparison of average 'group' shear forces with true group shear forces.

The apparent efficiencies for the 1:8 battered groups are higher due to the single pile reference point, not taking into account any group effect. The average efficiency of this loading scenario shows 1.12. As the x displacements are fixed, the efficiencies do not correctly show the efficiencies intra group but can compare the efficiencies inter group.

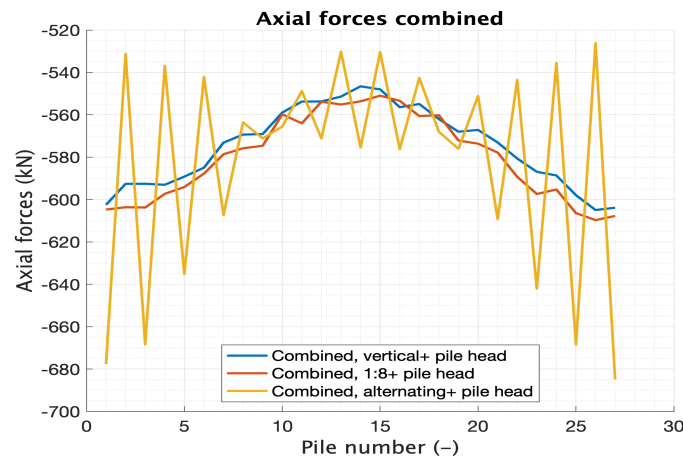
The efficiency calculations show that the single pile response can be of large influence, depending on the efficiency calculations done. In general three calculations can be made for the group efficiency:

- Average single pile response, x displacements and Q12 shear forces, are calculated. The group response can be interpreted from this reference point and generally shows a response lower than 1. This does incorporate the correct modelling of the single reference pile, which was not possible with the battered piles. A possible simplification with D-sheetpiling can be made as single pile for the vertical pile group. A combination with Reese and Impe [2002] can be introduced to take into account the group effect.
- The pile group averages are directly compared with each other, showing a response which gives a better estimation of the influence of batter angles. It does not take into account the single pile-group efficiency, only showing the impact of using batter angles.
- A combined relation of Reese and Impe [2002] and the global group response can be made, to describe the circular group effect. Again a single pile response is needed.

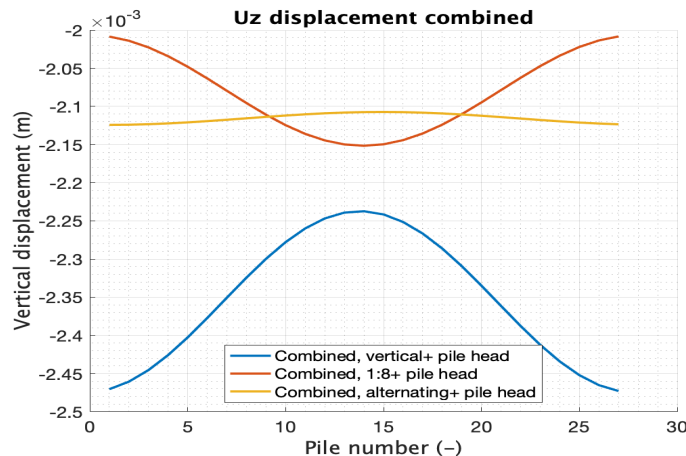
9 Comparison of vertical pile groups with alternating and 1:8 battered pile groups

While the global response of the axial and shear forces for vertical loading are in line with assumptions made before, the response of the 1:8 battered group and the alternating group show differences in locations of maxima and minima and the zero locations of the shear forces. The graphs are combined to show the response curves of the different pile configurations

9.1 Axial forces and displacements



(a) Axial forces per pile for three different pile group configurations



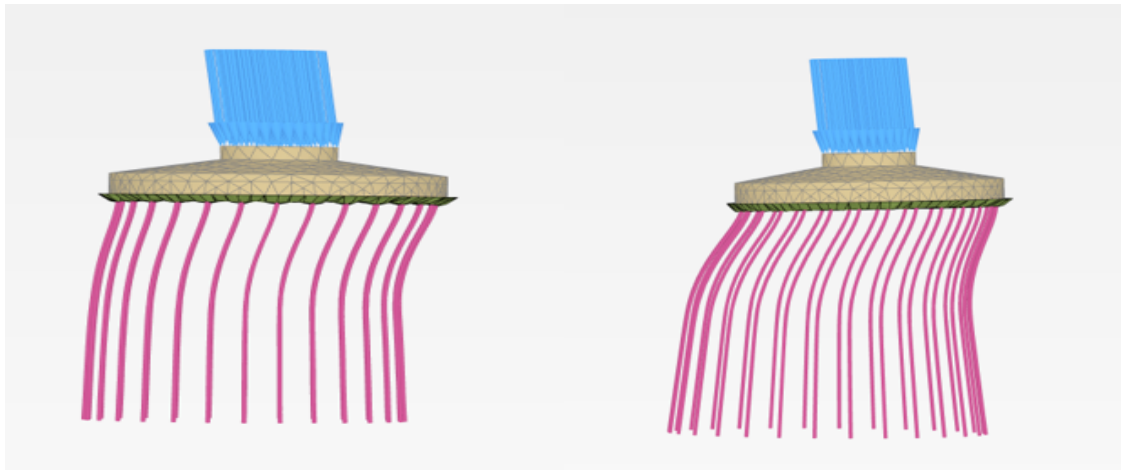
(b) Uz displacement per pile for three different pile group configurations

Figure 95: Comparison of three different pile configurations for axial forces and uz displacement

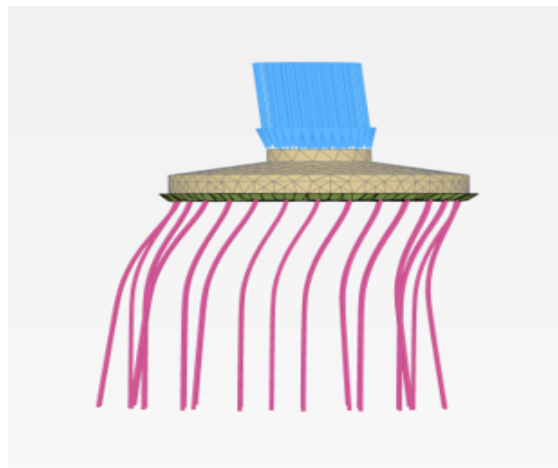
The total axial force show a general increase at the piles at location 1 and a decrease at location 15. The saw effect is clearly visible for the alternating pile group, where the

lower limits are the vertical piles. All the pile groups show the same trend as mentioned above.

The z displacements in figure 95 show the dipping of piles surrounding 1 and uplift at location of pile 15 for vertical piles, while the 1:8 battered piles show the opposite response with the dipping side on the left. The alternating pile group shows a roughly flat response. The movement of the foundation is shown below.



(a) Total displacements vertical pile group, dipping on the right (b) Total displacement 1:8 battered pile group, dipping on the left

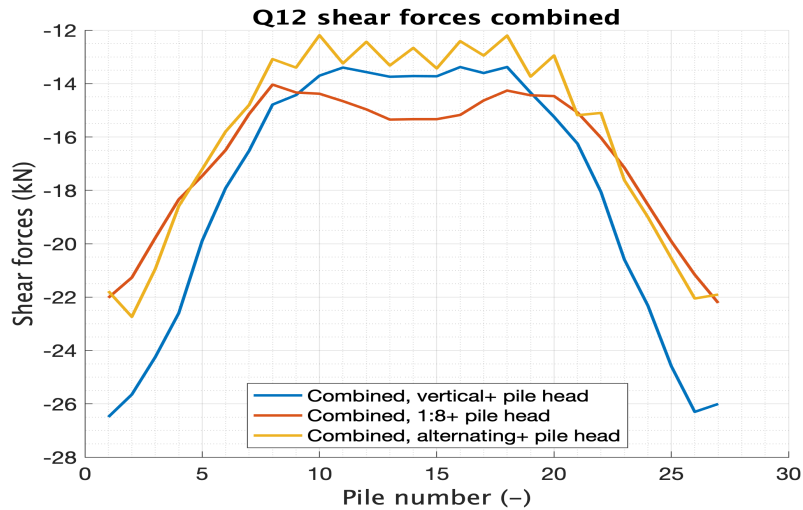


(c) Total displacements alternating pile group, flat response

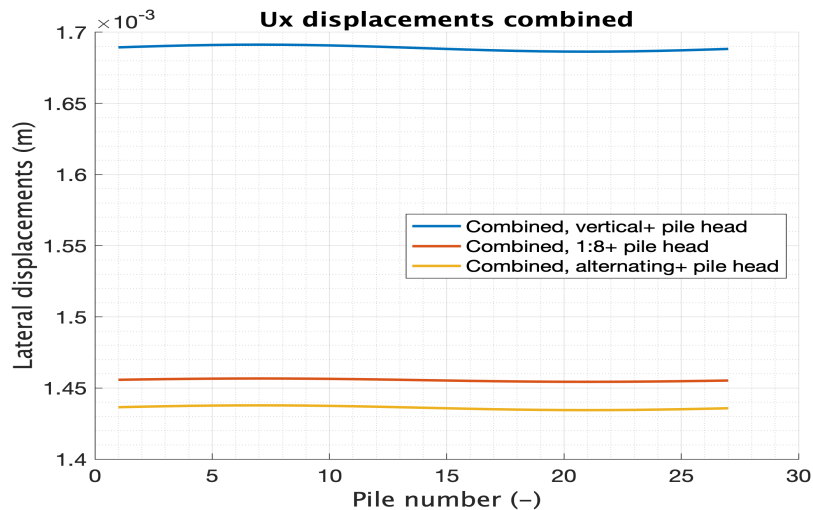
Figure 96: Comparison of three different pile configurations for Q12 shear forces and u_x displacement

The figures of 96 show that the combination of z displacements result in rotation of the foundation pedestal. While rotations are not the limiting factor as mentioned in section 1.5, pedestal rotations are specifications that are also taken into account.

9.2 Q12 shear forces and x displacements



(a) Q12 shear forces per pile for three different pile group configurations



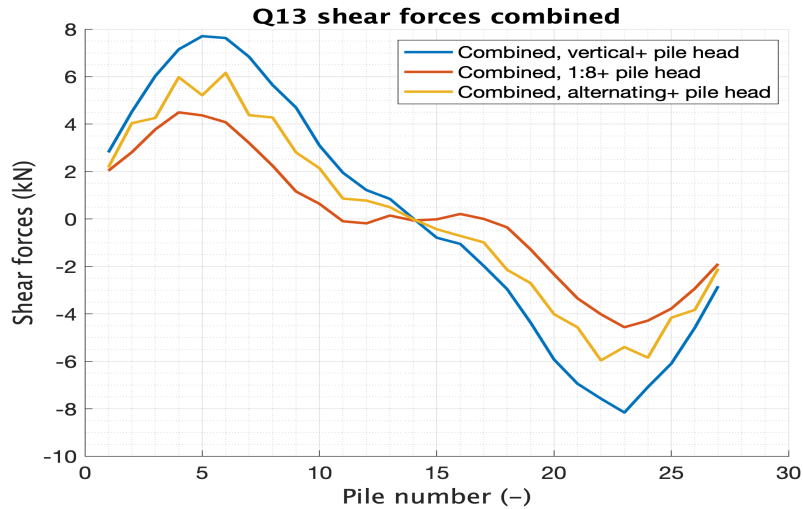
(b) x displacement per pile for three different pile group configurations

Figure 97: Comparison of three different pile configurations for Q12 shear forces and ux displacement

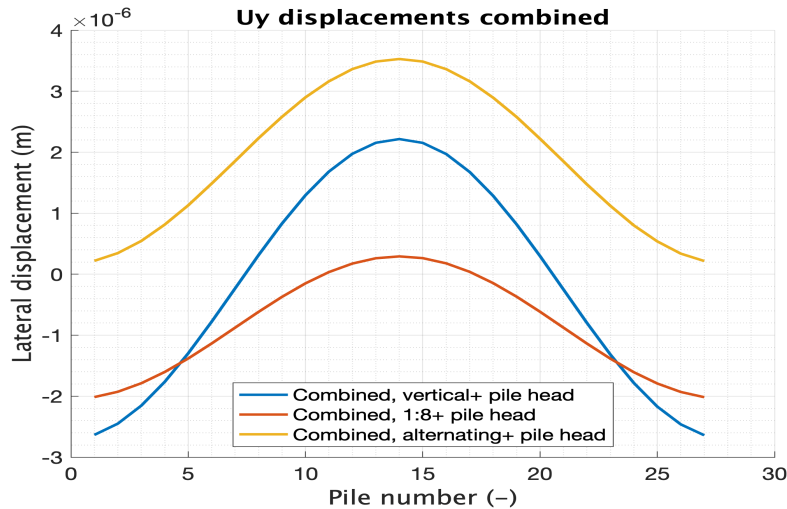
Figure 97a shows the alternations of Q12 shear forces in the middle section between piles 9 and 21. It shows that in general the vertical pile group shows the largest differences between the maxima and minima Q12 shear forces, while the 1:8 battered pile group shows the lowest differences. The largest shear forces are found in the vertical pile group, the lowest with the alternating pile group. Large differences in the maximum shear forces result in larger bending moments for the vertical pile group. The 1:8 battered pile groups shows clearly the increase in shear forces again for the trailing perpendicular pile group, the rest shows their minimum at pile 15.

The x displacements show the highest displacements for vertical pile groups, a similar response for the 1:8 and alternating pile group. As expect all the piles in a group receive the same lateral displacement due to the fixed head conditions.

9.3 Q13 shear forces and y displacements



(a) Q13 shear forces per pile for three different pile group configurations



(b) Uy displacement per pile for three different pile group configurations

Figure 98: Comparison of three different pile configurations for Q13 shear forces and uy displacement

The piles show the highest and lowest Q13 forces around piles 6 and 24. The use of battered piles result in lower Q13 peak shear forces, also showing an increasing horizontal plateau around pile 15. The alternating batter angle only shows the saw effect at the peak shear forces, comparable to the Q12 shear forces.

The maximum displacement locations are not corresponding to the maximum y displacement locations and show very small values as expected by a stiff head response. It is visible that the maximum shear forces are expected at piles 8 and 22, but shows a translation to piles 6 and 24.

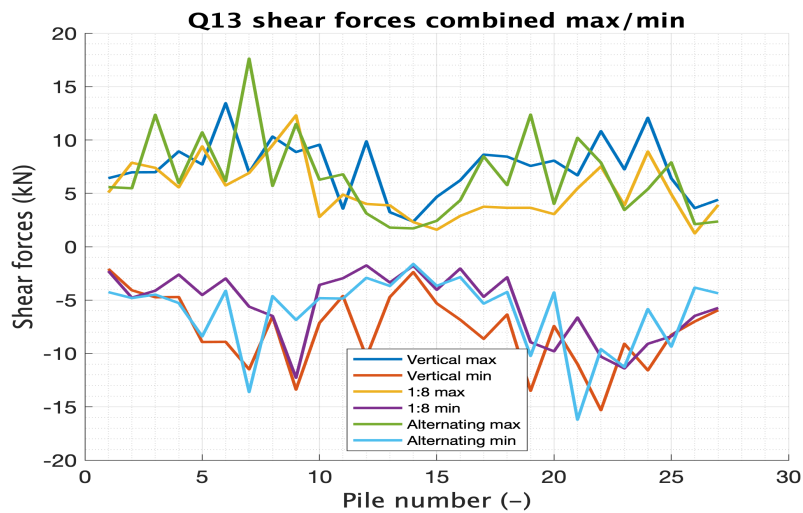
This effect can have several reasons:

1. The local axis definition results in incorrect readings of the Q12 and Q13 shear forces. While this effect should be present due to the slightly battered local axis 2

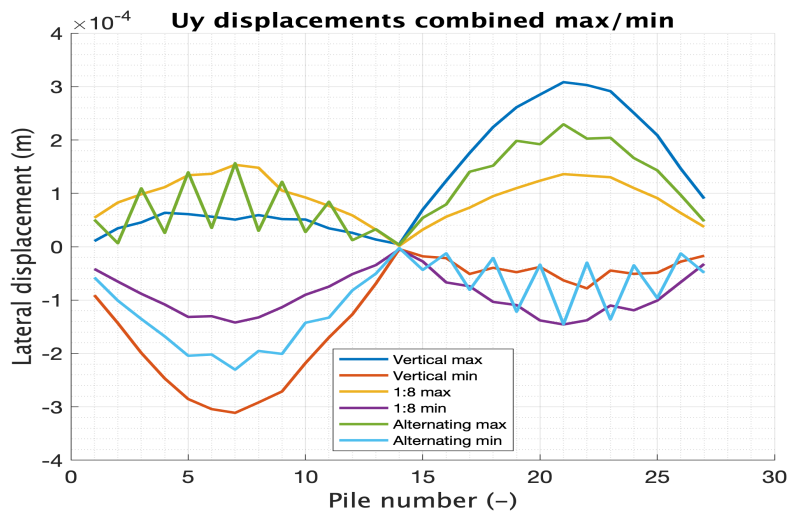
and 3 response for the alternating and 1:8 battered piles, this effect is also visible for the vertical pile group.

- Due to the rotation around the axis of piles 8 and 22 and horizontal translation, a slightly larger portion of the load is applied on the right hand side. This extra load results in slightly larger displacements at these piles as visible in figure 98b for 1:8 horizontal loading. This is only present at pile head level, as greater depths have the normal load distribution over all piles.

To get a better impression of maximum and minimum displacements in y direction, as those are not found at the pile head as with u_x displacement, those are plotted and compared to the maximum Q13 shear force locations.



(a) Q13 shear forces per pile for three different pile group configurations



(b) U_y displacement per pile for three different pile group configurations

Figure 99: Comparison of three different pile configurations for Q13 shear forces and u_y displacement

The maximum and minimum displacements are found at piles 8 and 22 as explained by the presence of the highest Q13 shear forces. The alternating batter angle shows

that the response is in line with the expectations of a combined pile group, resulting in an average displacement between the vertical pile group and 1:8 pile group. For the mirrored response, these displacements alternate exactly between the vertical minimum and maximum of vertical and 1:8 battered pile groups. As explained in the conclusion, the appeared lower displacements when approaching pile 15 are due to the increase in x displacement.

9.4 Conclusion of three different pile group configurations

After consideration of three different pile groups, several trends are visible for the increase or decrease in displacements or stiffness in three different directions. The response of the vertical pile group combined with their location resulted in location dependent response as expected by the literature study in regards to pile efficiency.

1. Axial response

- The axial forces per pile show roughly the same response over the three different complex pile configurations. The use of alternating batter angles result in redistribution of axial forces, showing the 'saw' effect.
- The battered piles receive slightly higher average axial force due to the compensation of the horizontally induced forces by the batter angle. The alternating pile group falls in the middle between the average axial forces of the vertical and 1:8 pile group.
- The movement of pile groups show that the vertical piles and 1:8 battered piles are dipping in different directions. Combination (alternating) results in cancellation of the rotation of the pedestal.

2. Q12 shear force response

- The use of battered piles result in lower lateral displacements.
- Efficiency increase is visible for the 1:8 battered pile group due to the presence of a larger low displacement field within the circular pile group geometry. This increase in efficiency is more in line with what is expected from the ctc distance influence of Reese and Impe [2002].
- Wider range of Q12 shear forces is present for the vertical piles in comparison to the alternating piles. This will result in larger bending moment in the vertical piles.
- The 'saw' effect is only visible for the trailing perpendicular pile group

3. Q13 shear force response

- The maximum displacements in y direction are not found in the pile heads as with x displacements, but in the middle of the pile due to vertical loading. The maximum and minimum displacements show a mirrored response, which show an inward movement of the piles. The displacements are small and roughly 1/5th of the x displacements.
- The response of the y displacements is within the limits of the maxima and minima of the vertical and 1:8 battered pile group. The vertical piles creating the largest inward displacements.
- Apparent decrease in Q13 shear forces at pile 1 and 15 are due to the force readings in fixed directions. The Q13 shear forces are 'translated' to Q12 shear forces.

4. Single pile reference for battered piles

- The modelling circumstances of the single battered pile result in general knowledge of the effect of batter angle on piles, but does not create a good reference point for the group analysis.
 - Parallel orientation of batter angles to the loading direction increases the axial forces and decreases the Q12 shear forces, axial force uptake. The displacements are lower with this parallel batter angles.
 - Single pile efficiency increases by using a batter angle in line with single pile response of Hazzar et al. [2017]
5. Overview of relevant displacements and forces for combined loading conditions. The efficiencies are calculated with the vertical response as reference point.

Table 20: Overview of displacement and axial force distribution for three different pile group configurations

		Vertical	1:8	Alternating	Offset to vertical pile group	
					1:8	Alternating
Average displacement (m)	Uz	$2.36 * 10^{-3}$	$2.08 * 10^{-3}$	$2.12 * 10^{-3}$	1.13	1.11
	Ux	$1.69 * 10^{-3}$	$1.46 * 10^{-3}$	$1.44 * 10^{-3}$	1.16	1.17
	Uy (max)	$3.11 * 10^{-3}$	$1.54 * 10^{-3}$	$2.30 * 10^{-3}$	2.01	1.35
Maximum force difference neighbouring piles (kN)	Axial	11.9	11.9	158.7	1.01	0.08
	Q12	3.0	1.5	3.1	2.0	0.98
	Q13	1.5	1.0	1.8	1.5	0.833
Average force (kN)	Axial	-575.9	-581.2	-578.9	0.99	0.99
	Q12	-18.5	-17.0	-16.3	1.09	1.13
	Q13	0.0	0.0	0.0	20	0.16

The battered pile configurations show large increase in lateral stiffness, but lower than expected by Wang and Orense [2022] and the two pile mirrored pile group considering an extrapolated result. The increases are found to be in line with the findings of Zhang et al. [2002] at higher deflections and under vertical loading conditions near failure.

The displacements in y direction are stated as movement to a single maximum or minimum displacement location. As the vertical pile generally moves to one side, this represents the maximum total movement. The battered piles can result in approximately the same maximum and minimum displacements, which doubles the displacements as stated here in the table.

10 Pile group validation

The second reference for using D-sheetpiling is found for the group effect. When considering a fixed head condition, the displacements are changing as well as the maximum bending moment. In the figure below a calculation with the same setup as for the single pile is performed.

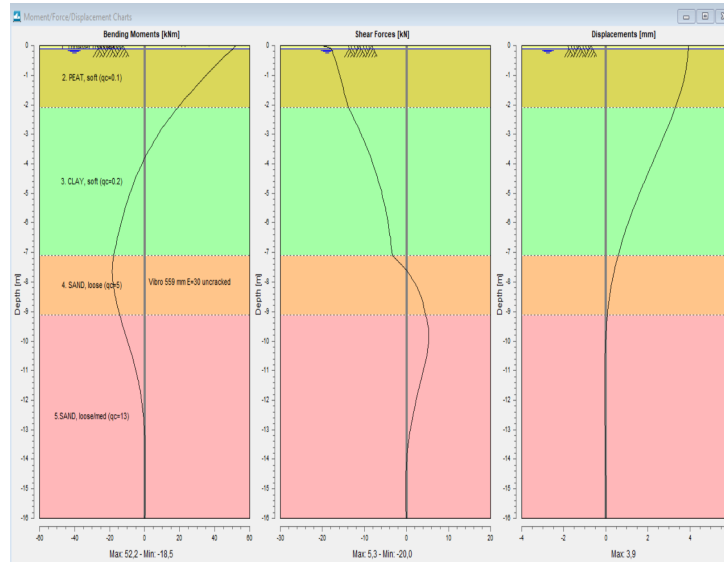


Figure 100: Output of D-sheetpiling for pile with head restrictions and horizontal loading of 20 kN

The lateral displacement of the pile is 3.9 mm with head restrictions. The displacements are much larger than expected and show the limitations of the simplified analytical model. With head restrictions this scenario is tested under the complex foundation and resulted in a maximum total foundation displacement of 1.69 mm. Plaxis 3D also showed that the displacements are very small at a depth of 6 meters for both loading scenario's, where D-sheetpiling showed the displacements till a depth of 10 meters.

The limitations of the analytical model show that under very small loading conditions, the small strain behaviour is not correctly captured. While D-sheetpiling does take into account a limited small strain response shell factor with a limited range, the loading conditions seem to reach the upper limits of this behaviour. The shell factors given by a report of Fugro to CUR, with the title "Door Grond Horizontaal Belaste Palen Bestaande Ontwerpmodellen" showed that the range of applied shell factors are particularly limited with lower density materials. Due to the excavation of the relatively high density loam layer, the limited range shell factors of the peat layer and clay layer result in lower stiffness.

10.0.1 Group efficiency for D-sheetpiling

Application of the relations formulated by Reese and Impe [2002] can be used to approximate the total efficiency of the pile group. The s/b ratio for every section is 3.045, calculated by using the radius and known angle between the piles.

For perpendicular loading:

$$e = 0.64 \left(\frac{s}{b} \right)^{0.34} = 0.93 \quad (63)$$

For parallel loading leading row:

$$e = 0.7 \left(\frac{s}{b} \right)^{0.26} = 0.94 \quad (64)$$

For parallel loading trailing rows:

$$e = 0.48 \left(\frac{s}{b} \right)^{0.38} = 0.74 \quad (65)$$

The total average efficiency of the group is then calculated as $(0.93+0.94+0.74)/3=0.87$. It is assumed now that there are as many leading rows as trailing rows due to the round construction. This same assumption is also applied to the perpendicular pile group. Applying the knowledge as found in the complex vertical geometry we found from the x displacement fields and σ_{xx} stress fields the following relations.

- Perpendicular pile group from pile 25-5 (9 piles)
- Leading parallel pile 6-7-8 and 22, 23, 24 (6 piles)
- Trailing piles for piles from 9 till 21 (13 piles)

This gives the following equation: Perpendicular

$$\frac{9}{28} * 0.64 \left(\frac{1.70}{0.559} \right)^{0.34} = 0.30 \quad (66)$$

Leading pile

$$\frac{6}{28} * 0.7 \left(\frac{1.70}{0.559} \right)^{0.26} = 0.20 \quad (67)$$

Trailing pile

$$\frac{13}{28} * 0.48 \left(\frac{1.70}{0.559} \right)^{0.38} = 0.34 \quad (68)$$

Giving a total efficiency of 0.84. Applying the same procedure for the 1:8 pile group with 10 perpendicular piles to compensate for the higher stress state, and 10 leading piles gives a total efficiency of 0.88. For the alternating group with 9 perpendicular piles and 10 leading piles gives an efficiency of 0.87. The relative increase in efficiency in regards to the vertical pile group with efficiency of 0.84 are found as $0.88/0.84=1.05$ for the 1:8 battered pile group and $0.87/0.84=1.04$ for the alternating pile group. This is in line with the mirrored 2 pile group under stated batter angles as visible in section 5.4.1, giving a increase in efficiency of 1.04 of the battered pile group in regards to straight piles.

To summarize the results, the table below contains the efficiency factors as found by the program's and the efficiency factors approximated by a combination of Plaxis 3D and D-sheetpiling.

Table 21: Overview of efficiency factors for displacements

		Single pile	Complex pile group		
			Vertical	1:8	Alternating
Displacement (m)	D-sheetpiling	$1.60 * 10^{-3}$	-	-	-
	Plaxis	-	$1.69 * 10^{-3}$	$1.46 * 10^{-3}$	$1.44 * 10^{-3}$
Efficiency factor (-)	RHDHV	1	0.8	>0.8	>0.8
	Plaxis 3D	-	0.95	1.10	1.11
	D-sheetpiling/ Plaxis	1	0.84	0.88	0.87

The limitations of the calculation result in an efficiency that cannot be higher than 1, as limited by the empirical relations of Reese and Impe [2002]. When calculating with the efficiency factor of the vertical complex pile foundation, the efficiency multiplier was found to be 1.04. This creates a efficiency of $0.95 * 1.04 = 1.00$ for the 1:8 battered pile group, which shows that no group efficiency of the pile group should be present when considering the displacement factors.

The used efficiency factor of RHDHV of 0.8 is a conservative estimation of the group efficiency factor calculated by combining Plaxis 3D and Reese and Impe [2002] efficiency equations, but also when considering the true Plaxis 3D displacements.

10.1 Structural response

As explained by section 7.2.5, the shear forces and moments are derivatives or integrals of each other, depending on which is the starting point. While sections 8.2 and 8.3 showed increase in axial forces and redistribution of Q12 shear forces, these have effect on the total bending moment each of the piles receives. The bending moments over depth are plotted for the different piles.

The figures show only the response of the first 15 piles. Last chapters showed a mirrored response between pile 1 and 15 and 16 and 28, which would crowd the figures with the same response. An explanation of the direction of the moment is given below.

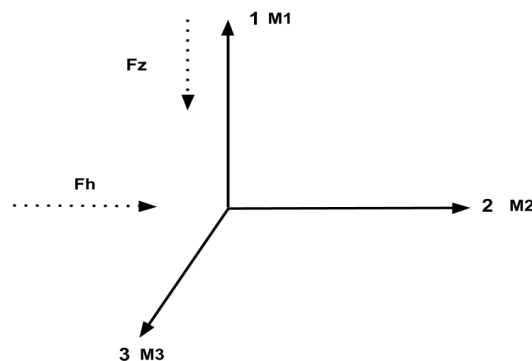


Figure 101: Reading the bending moments in the local coordinate system

Figure 101 shows that we expect to have bending moments larger than zero in the 1-2 plane, the vertical and horizontal loading, and the 1-3 plane, only vertical loading. These correspond with the M3 and M2 bending moments respectively.

The vertical pile group showed the least amount of deviation in the axial pile forces and Q12 shear forces. The orientation of the battered piles do result in Q12 axial force uptake, which should show less bending moment for the battered piles. The M1 bending moment is assumed to be constant and shows very small deviations from the constant response.

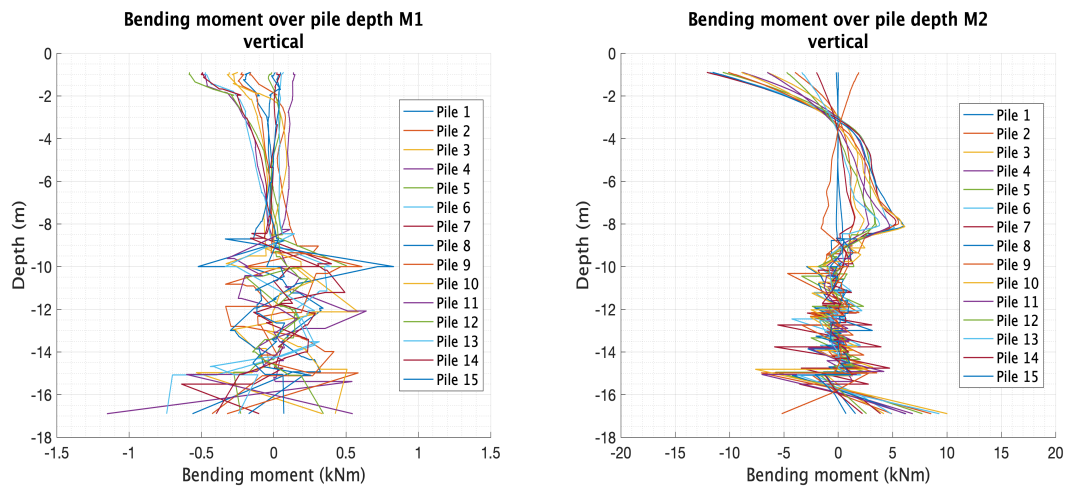
As stated already with the comparison with Reese and Impe [2002], influence of pile properties can only be neglected when the piles receive the same point displacements. As this is only the case in a single pile group due to the fixed head conditions, the comparison

of the bending forces is only relative and only valid at the pile head within a specific pile configuration.

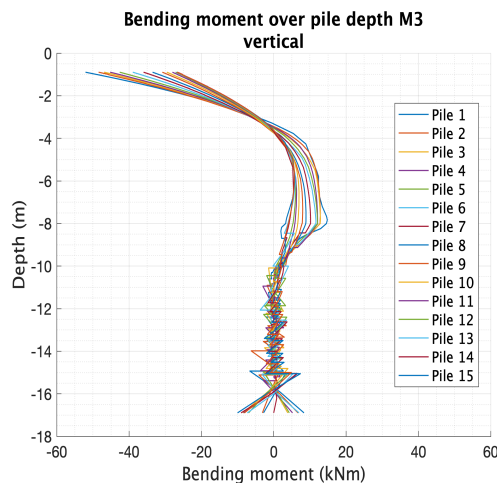
10.1.1 Vertical complex pile group

The M2 and M3 moment show the movement in y and x direction respectively. Figure 102b shows the increase and decrease of the M2 bending moment when increasing the pile numbering. This was explained before as the increase in y displacement till pile 8 and decrease again till pile 15, where the apparent decrease and increase are due to the combined x and y displacements.

The M2 and M3 moment shows almost no bending moment at -10 meters, which is located at -10.895m global depth due to the burial of the foundation. This corresponds with the medium sand layer, while the turning moment happens at -8m, global -8.895 m, or the loose sand layer. As expected by small loading conditions, the piles show an almost fixed response at the deeper medium dense sand layer.



(a) M1 bending moment over pile length (b) M2 bending moment over pile length



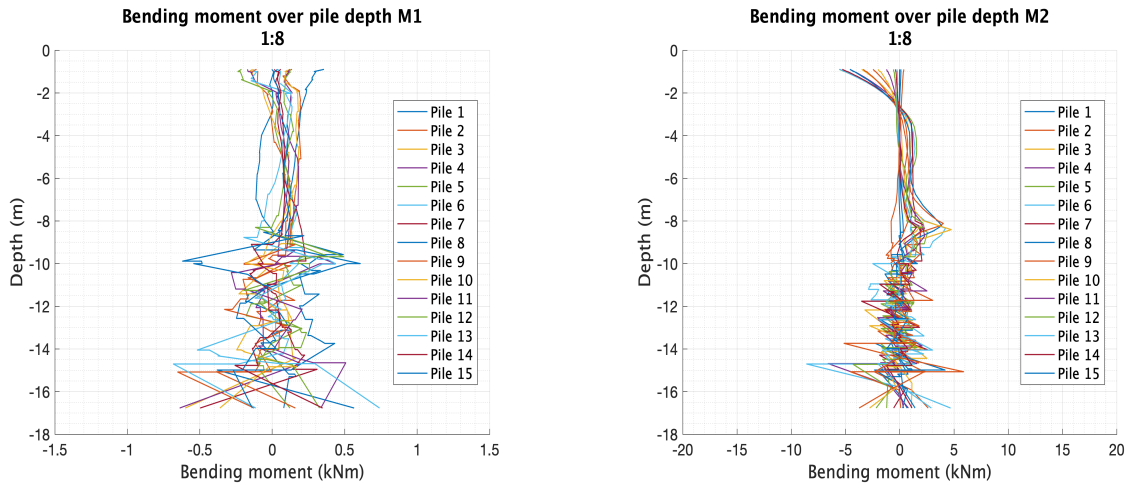
(c) M3 bending moment over pile length

Figure 102: Comparison of vertical pile bending moment over depth for 3 bending moment directions

10.1.2 1:8 Battered piles

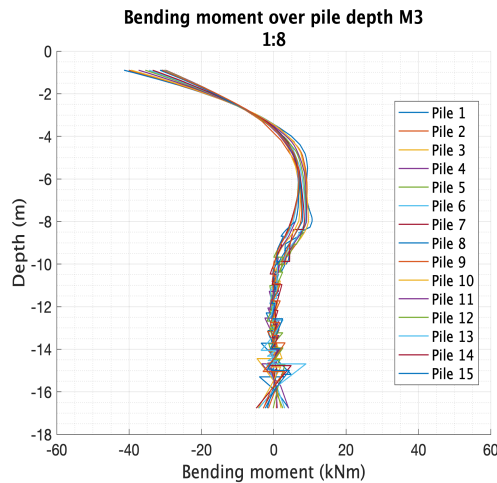
The same conclusions are found with the 1:8 battered group. The M3 bending moments do show a lower bending moment, with a more concentrated and thus less deviated response. This shows that the piles respond roughly the same, independent on their location. The average of the pile head moment decreased from 35.7 kNm to 33.5 kNm. The M2 bending moment almost halved at pile head level and showed a more constant moment over the complete pile length.

Both figure 103b and c show again the fixity at the medium sand layer, the decrease in bending moment starting from the loose sand layer.



(a) M1 bending moment over pile length

(b) M2 bending moment over pile length



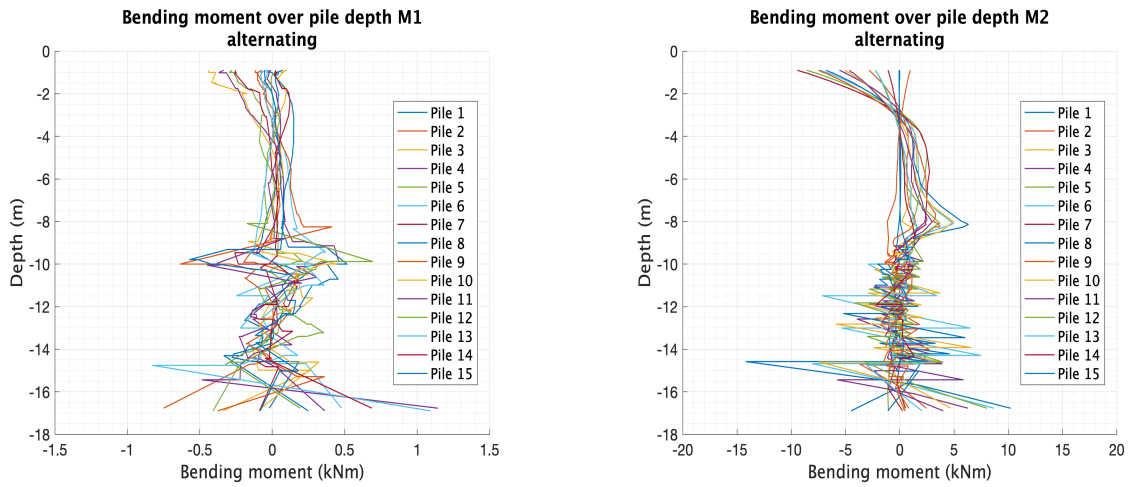
(c) M3 bending moment over pile length

Figure 103: Comparison of 1:8 pile bending moment over depth for 3 bending moment directions

10.1.3 Alternating battered piles

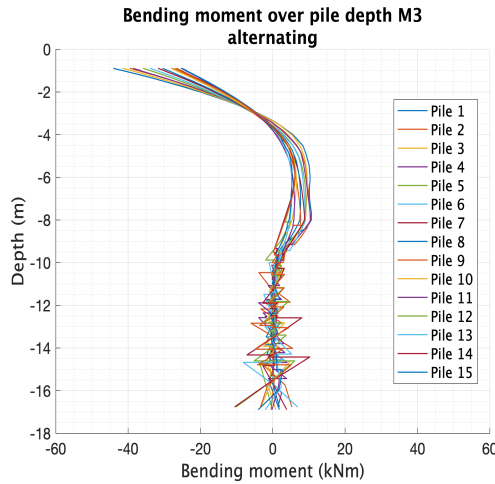
Last sections showed that the alternating battered piles show a response roughly in between both vertical and 1:8 battered piles as suspected by the combination of the complex layouts. The pile head response for both M2 and M3 bending moments is lowered in comparison with vertical piles while the 1:8 battered piles show the lower limits. The average

M3 pile head moment is found to be -31.8 kNm which is lower than the 1:8 battered and vertical pile group. This is due to a lower response for piles 10 till 20 of 26.2 kNm in comparison to 30.5 kNm.



(a) M1 bending moment over pile length

(b) M2 bending moment over pile length



(c) M3 bending moment over pile length

Figure 104: Comparison of alternating pile bending moment over depth for 3 bending moment directions

10.1.4 Single vertical pile moment versus D-sheetpiling

The curvature of M3 bending moment of Plaxis 3D is matched to the curvature of D-sheetpiling. It is chosen to use the bending moments of pile 1 with vertical pile, as this pile should approximate single pile response the best. An average response of the bending moment of 15 piles is also given, to simulate the response of the piles in a group.

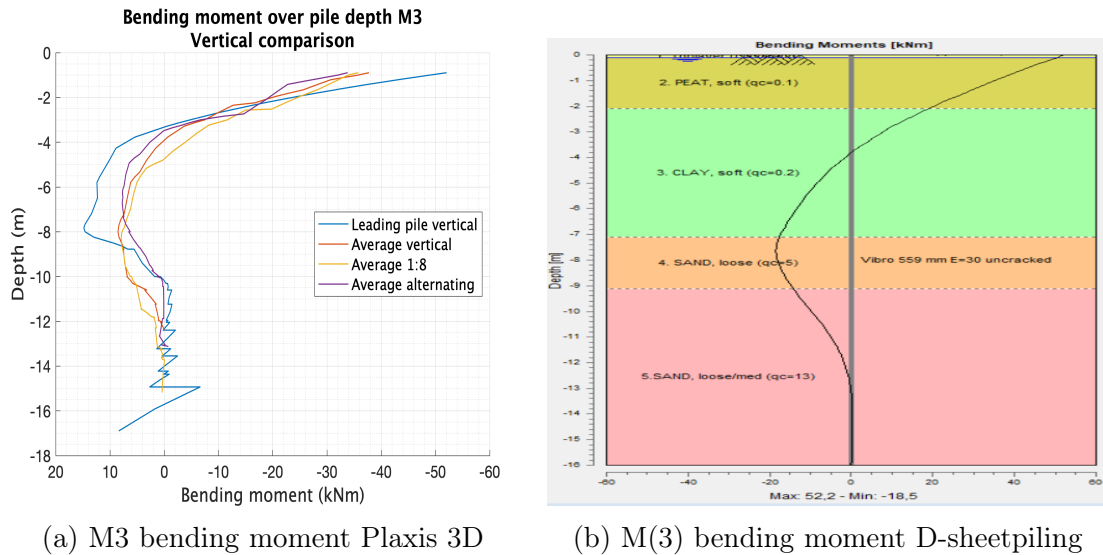


Figure 105: Comparison of Plaxis 3D and d-sheetpiling

The maximum and minimum bending moment of Plaxis 3D and D-sheetpiling are approximately the same at maximum -52.0 versus -52.2 kNm and minimum 14.8 versus 18.5 kNm for leading pile 1. As this pile shows the highest momentum, the average response of the pile groups shows maximum of -35.7 kNm and minimum 8.4 kNm. Where D-sheetpiling shows displacements till lower depths as mentioned before, the moment for the pile also shows the bending moment till roughly -13 meters. When comparing the response with the average response of the total pile group, we see that this lower pile fixity is better approximated by the average M3 bending moment at global depth fixity of -12.895 m. Rollins et al. [2006] already found that Plaxis (2D) can underestimate the moment at greater depths, showing that D-sheetpiling is having a better potential considering the moment over depth modelling.

10.2 Conclusion of pile group validation

Validation of the Plaxis 3D displacements showed that D-sheetpiling is potentially underestimating the small strain stiffness for the peat and clay layer. Due to the difference in 2D and 3D modelling, this result may be taken into account by using shell factors that are not mentioned in the manual. These shell factors are both for the use of 2D to 3D problems and the small strain stiffness of materials.

The small strain stiffness of the material is not well captured, as a single linear E-menard modulus is inserted in the calculations, which translates to a linear relation between displacement and loading conditions. Shell factors may influence this slightly as mentioned by Arend [2010] for the used Brinch-Hansen method.

The behaviour of the piles confirmed the M2 and M3 dependence as expected by the loading conditions. The pile head bending moments showed the concentrated distribution of the piles for the 1:8 battered pile group, the scattered distribution for the vertical piles. All the complex pile groups showed the rough moment fixity in the lower medium sand layer, a decrease in moment for the loose sand layer.

A comparison with Plaxis 3D and D-sheetpiling showed the rough correct implementation of the bending moment distribution over pile length, while having fixity at -10 m,

global -10.895m, for the Plaxis 3D pile and -13 meters for the D-sheetpiling model. The average bending moments over all piles captured the lower fixity better, but underestimated the peak bending moments.

11 Conclusion

The study focused on investigating the influence of pile batter angle on the lateral stiffness of wind turbine foundations. The main research question was formulated as :

"What is the effect of battered piles on the lateral response of wind turbine foundations under horizontal loading conditions using numerical software"

In order to understand the pile behaviour for a schematic Dutch subsurface profile, the use of batter angles was tested on single piles, simplified pile groups and complex pile groups with different battered pile configurations. This ensures that the vertical pile response is understood and can be validated with analytical programs and literature. The use of small lateral loading conditions showed that small strain constitutive models such as Hardening Soil small strain should be used.

A comparative analysis, in which various parameters such as mesh size were varied, showed that the 'new' embedded beam option quickly reaches stable results. The displacements that are calculated with the new embedded beam model are comparable to those that are reached with the in theory better suited for lateral behaviour 'volume pile'. The pile head displacement was compared to analytical software which is generally used and showed again a good fit.

To influence of the use of batter angles was tested on a single free head and a fixed head mirrored two pile group, both the configurations being subjected to several battered angle configurations in the range of $-1/8$ (negative) till $1/8$ (positive). The fixed head conditions with batter angles parallel to the loading conditions resulted in the lowest displacements as found by Wang and Orense [2022] and Hazzar et al. [2017] for negatively battered piles. The fixed head conditions are to a lesser extent present in the simplified and complex pile group, therefor discarding the results of the free head conditions.

The influence of fixed head conditions for 1:8 battered piles is extended to 15 different loading directions, comparable to the orientations of the single piles in the complex wind turbine pile group. The same results are visible as found with the mirrored two pile groups. The piles showed that the axial forces are the largest for piles parallel to the loading directions, showing the axial uptake of shear forces in the piles.

In order to asses the pile reactions in a group, single piles were grouped in different in-line configurations to asses the influence of pile behaviour on the pile position in the groups. The pile behaviour under combined horizontal and vertical loading conditions showed correct responses for use in perpendicular (side-by side) loading groups. The pile behaviour in parallel (in-line) loading conditions showed an increase for the last trailing pile. For the parallel and perpendicular pile group the average efficiency was almost 1, which shows that under the applied loading conditions almost no group behaviour is present for the tested group sizes. The response of the pile groups were compared to empirical relations developed by Reese and Impe [2002] and showed that Plaxis 3D results correctly reflect pile group behaviour. This validation also showed that the increase of efficiency for the last trailing row is also present under the applied testing conditions in the simplified subsurface profile for low etc spacings.

The complex pile group or real case wind turbine foundation was analysed under combined and separate vertical and horizontal loading conditions. The first reference case that was investigated is the configuration with vertical piles. The pile head moment was checked and compared to generally used analytical software, which confirmed the approximate behaviour of the pile rotation clearly visible for vertical pile groups. The shear forces per pile were checked and showed the presence of a leading perpendicular pile group as predicted by Matlock et al. [1980], increasing the shear forces for these piles. The piles behind this leading perpendicular pile group respond as approximately parallel (in-line) piles, visible in gradual decreasing shear forces. A small increment is visible for the trailing perpendicular pile contradictory to Reese and Impe [2002], as the empirical relations showed that this pile group should match the response of the leading perpendicular pile group after large ctc distances.

The piles in the complex foundation were subsequently placed at batter angles 1:8 for the complete group. A model with a complex foundation with alternating batter angles (1:8 and vertical) was also constructed. The 1:8 battered and alternating pile group showed a decrease in lateral and vertical displacements in comparison to the vertical pile group. The 1:8 battered pile group showed an increase in shear forces of the trailing perpendicular pile group, showing a response which is in line with expected perpendicular loading conditions at larger ctc distances. The foundation solution with alternating piles shows alternating axial and shear forces, which is to be expected in view of the alternating batter angle.

Comparison of the three different pile configuration showed three important points:

1. The larger range of shear forces in the vertical pile group shows a large range in bending moments, equivalent to larger horizontal and vertical displacements due to the uplift and dipping behaviour. The 1:8 battered pile group shows an opposite response in regards to vertical displacements, combination of the configurations (alternating) shows cancellation of the displacements (and rotation) in vertical direction.
2. The soil block within the complex pile ring group shows less overlap in higher displacement fields for use of 1:8 battered piles. This effect decreases the pile-soil-pile interaction, increasing the efficiency of the trailing piles.
3. Assessment of the circular pile configuration as a combination of several simplified pile groups showed complications, as described by the behaviour of the trailing perpendicular pile group and example calculations made with Reese and Impe [2002].

The complex foundation was then compared to different possible combinations of group efficiency parameters. A comparison in regards to group displacement and rotation, given as two important design criteria following section 1.5, are shown in the tables 22.

Table 22: Summarizing table for the use of battered piles in complex wind turbine foundations

		Single pile	Complex pile group		
			Vertical	1:8	Alternating
Displacement (m)	D-sheetpiling	$1.60 * 10^{-3}$	-	-	-
	Plaxis 3D	-	$1.69 * 10^{-3}$	$1.46 * 10^{-3}$	$1.44 * 10^{-3}$
Efficiency factor (-)	RHDHV	1	0.8	>0.8	>0.8
	Plaxis 3D	-	0.95	1.10	1.11
	D-sheetpiling-Plaxis	1	0.84	0.88	0.87
Translational stiffness (MN/m)	Plaxis 3D	-	331.4	383.6	388.9
Rotation (m)/(°)	Plaxis 3D	-	$1.15 * 10^{-4} / 8.4 * 10^{-4}$	$-7 * 10^{-5} / -5.1 * 10^{-4}$	$1 * 10^{-7} / 7.3 * 10^{-7}$

12 Recommendations for further research

The results of this thesis research clearly show the positive effect of using batter angle on transverse stiffness of onshore wind turbine pile foundations. There are however many design parameters that will be of influence on the actual gains that can be achieved, such as number and diameter of piles, batter angles and pile axial stiffness. Furthermore, the analysis was performed for a single, average ground profile. The results cannot be transferred directly to other ground conditions. The results also show that batter angle has influence on rotations that develop in the foundation. This can be an important aspect if translation and rotation in operation conditions analyzed integrally, which is not yet normal design practice. Further research into these unknown factor of influence, a sensitivity analysis or otherwise is recommended.

The dynamic aspects of the operational loads on the foundation has not been addressed in this thesis. For the analysis of lateral stiffness that is described in this thesis, it is assumed that analysis with small strain ground parameters is a good approximation in view of the small deformations that occur. Time histories of the governing operation wind loads are nor readily available. Further research into dynamic aspects is deemed worthwhile but would require a joint effort from structural and geo-technical disciplines.

The following points are found to be of influence and not investigated in the research:

Single pile response and the initialisation of the model

1. Single pile response

- Look into the asymptotic behaviour of the embedded beams and their differences with the volume pile in regards to (total) lateral displacement. The analysis also needs to be performed with 20 kN lateral load, to see possible loading depended asymptotic behaviour. A better corresponding asymptotic response should be visible as stated by Smulders et al. [2019].
- Single pile response needs to be analysed with correct rotation fixity to understand the true horizontal behaviour of the piles. The current approach does have influence of extra pile head rotation (non-fixed) or only shows semi-correct x displacement and Q12 shear forces. This will simplify comparing the results with literature as performed in Plaxis 2D.

2. Model initialisation

- An in-depth investigation to create comparable input parameters need to be performed in order to directly compare 2D D-sheetpiling and Plaxis 3D software.
- Perform a sensitivity analysis to check the influence of soil and pile parameters to understand the impact on the lateral displacement and rotation (capacity) of the pile.
- If an actual design in specific ground conditions is analyzed, ground investigation is required. Options for monitoring of field behaviour of the foundation, also during operational phase, should then also be considered.

Simplified group response for layered soils

1. The group response was validated to generally accepted empirical relations developed by Reese and Impe [2002]. Over the years several other P-multipliers are developed such as the AASHTO model for bridge foundations. The models can be compared to establish the higher and lower limits of the group effect.
2. It is unclear if and how existing theories on group efficiency have taken into account pile head fixation. The influence of soil layering on the group effect is also unclear. Additional advances model research and verification in the field is recommended
3. Deformations of the slab (pedestal) foundations and stiffness of the pile-slab connection require in-depth structural analysis and have not been considered within the scope of this thesis. This aspect should however be included in an integral (dynamic) analysis of the behaviour of the tower and foundation.

This approach creates a baseline response, assessment of the FEM input parameters with a sensitivity analysis can result in a more realistic modelling scenario. This also checks if further assumptions made by RHDHV can be applied in regards to structural and soil parameters. This ensures that a range, or margin of error, can be developed and applied to the design in regards to the limiting parameters such as lateral displacement and to lesser extend rotations. After the research is performed, a more efficient way of in-situ testing can be performed to lower the needed total time and costs.

Complex group response

1. Perform a model research with scaled field data
 - Scale model testing in representative dutch soil layering.
 - Use of real (scaled) deformations and forces for every structural element.
2. Create optimized relations for circular wind-turbine foundations in regards to ctc distance and batter angle:
 - Analyse relations between ctc distance and efficiency
 - Increase the range of investigated batter angles
 - Perform analysis not only with vertical and battered piles, but also with a combination of different batter angles.
 - A sensitivity analysis specially for the axial pile stiffness
3. Realistic modelling of structural parameters
 - Use of weak interface surrounding the foundation base in comparison to the use of a slope.
 - The lateral displacements and rotations in every direction needs to be analysed with influence of realistic foundation base parameters (realistic stiffness and strength parameters) to check their impact.
4. In more favorable ground conditions, stiffer overburden, shear resistance of the foundation base plate will also influence group behaviour. Additional research is required to correctly include such effects in a foundation design.

References

- M. Murugan, K. Muthukkumaran, and C. Natarajan. Frp-strengthened rc piles. i: Piles under static lateral loads. *Journal of Performance of Constructed Facilities*, 31: 04017003, 02 2017. 10.1061/(ASCE)CF.1943-5509.0000990.
- K. M. Rollins, K. T. Peterson, and T. J. Weaver. Lateral load behavior of full-scale pile group in clay. *Journal of Geotechnical and Geoenvironmental Engineering*, 124:468–478, 1998.
- A. Swallow and B. Sheil. Group shape effects on the lateral capacity of pile groups in undrained soil. *Géotechnique (Unpublished)*, 01 2021. 10.1680/jgeot.20.P.222.
- K. Rollins, K. Olsen, D. Jensen, B. Garrett, R. Olsen, and J. Egbert. Pile spacing effects on lateral pile group behavior: Analysis. *Journal of Geotechnical and Geoenvironmental Engineering - J GEOTECH GEOENVIRON ENG*, 132:1272–1283, 10 2006. 10.1061/(ASCE)1090-0241(2006)132:10(1272).
- L. Hazzar, M. Hussien, and M. Karray. Numerical investigation of the lateral response of battered pile foundations. *International Journal of Geotechnical Engineering*, 11: 376–392, 06 2017. 10.1080/19386362.2016.1224030.
- L. Zhang, M. McVay, S. Han, P. Lai, and R. Gardner. Effects of dead loads on the lateral response of battered pile group. *Canadian Geotechnical Journal - CAN GEOTECH J*, 39:561–575, 06 2002. 10.1139/t02-008.
- T. Singh and V.K. Arora. Influence of pile inclination on batter pile groups subjected to lateral loading in sand. *International Journal of Geosynthetics and Ground Engineering*, 08 2017. 10.1007/s40891-017-0103-9. URL <https://doi.org/10.1007/s40891-017-0103-9>.
- R. Brinkgreve. Elasticity. <https://brightspace.tudelft.nl/d21/1e/content/289021/viewContent/1770619/View>, 2021a. Accessed: 2022-02-17.
- M. Vuetic and R. Dobry. Effect of soil plasticity on cyclic response. *Journal of Geotechnical Engineering*, 117:89–107, 1991.
- C. Smulders, S. Hosseini, and R. Brinkgreve. Improved embedded beam with interaction surface. *The European Conference on Soil Mechanics and Geotechnical Engineering*, 17, 09 2019. 10.32075/17ECSMGE-2019-0193.
- H.J. Everts. Veerstijfheid paalfunderingen. *Cement*, pages 12–16, 01 1998.
- M. Novak. Dynamic stiffness and damping of piles. *Canadian Geotechnical Journal*, 11: 574–598, 1974.
- J. Zhang, Y. Li, Z. Yan, D. Huang, X. Rong, and Y. Liang. Experimental study of vertical and batter pile groups in saturated sand using a centrifuge shaking table. *Earthquake Engineering and Engineering Vibration*, 05 2021. 10.1139/t94-068.

- L.C Reese and W.F. Impe. Single piles and pile groups under lateral loading. *Applied Mechanics Reviews - APPL MECH REV*, 55, 01 2002. 10.1115/1.1445326.
- Q. Zhang and Z. Zhang. A simplified nonlinear approach for single pile settlement analysis. *Canadian Geotechnical Journal*, 49:1256–1266, 10 2012. 10.1139/t11-110.
- F. Pisanò. Piled foundations axial loading. <https://brightspace.tudelft.nl/d21/le/content/279765/viewContent/2102518/View>, 2020a. Accessed: 2022–01-10.
- F. Pisanò. Piled foundations lateral loading. <https://brightspace.tudelft.nl/d21/le/content/279765/viewContent/2102517/View>, 2020b. Accessed: 2022–01-11.
- M.H. El-Naggar and M. Novak. Nonlinear lateral interaction in pile dynamics. *Soil Dynamics and Earthquake Engineering*, 14(2):141–157, 1995. ISSN 0267-7261. [https://doi.org/10.1016/0267-7261\(94\)00028-F](https://doi.org/10.1016/0267-7261(94)00028-F). URL <https://www.sciencedirect.com/science/article/pii/026772619400028F>.
- D. Datta, A. Varma, J. Seo, and J. Coleman. Investigation of interface non-linearity on non-linear soil structure interaction analyses. *International Conference on Structural Mechanics in Reactor Technology*, 08 2017.
- T. Nogami, K. Konagai, and J. Otani. Nonlinear time domain numerical model for pile group under transient dynamic forces. *International Conferences on Recent Advances in Geotechnical Earthquake Engineering and Soil Dynamics*, 03 1991.
- M. Novak and T. Nogami. Soil-pile interaction in horizontal vibration. *Earthquake Engineering & Structural Dynamics*, 5(3):263–281, 1977. <https://doi.org/10.1002/eqe.4290050305>. URL <https://onlinelibrary.wiley.com/doi/abs/10.1002/eqe.4290050305>.
- K. Georgiadis, S.W. Sloan, and A.V. Lyamin. Ultimate lateral pressure of two side-by-side piles in clay. *Géotechnique*, 63(9):733–745, 2013. 10.1680/geot.12.P.030. URL <https://doi.org/10.1680/geot.12.P.030>.
- A. Lemnitzer, E.R. Ahlberg, P. Khalili-Tehrani, C. Rha, E. Taciroglu, J.P. Stewart, and J.W. Wallace. Experimental testing of a full-scale pile group under lateral loading. *UCLA: Civil and Environmental Engineering*, 2008.
- A. Lemnitzer, E. R. Ahlberg, P. Khalili-Tehrani, C. Rha, E. Taciroglu, J. P. Stewart, and J. W. Wallace. Full scale cyclic large deflection testing of foundation support systems for highway bridges. part i: Drilled shaft foundations. *UCLA: Civil and Environmental Engineering*, 2007.
- M. Ashour and H. Ardalan. Employment of the p-multiplier in pile-group analysis. *Journal of Bridge Engineering*, 16:612–623, 09 2011. 10.1061/(ASCE)BE.1943-5592.0000196.
- M. Ashour, P. Pilling, and G. Norris. Lateral behavior of pile groups in layered soils. *Journal of Geotechnical and Geoenvironmental Engineering - J GEOTECH GEOENVIRON ENG*, 130, 06 2004. 10.1061/(ASCE)1090-0241(2004)130:6(580).
- L. Zhang, M. C McVay, and P. W Lai. Centrifuge modelling of laterally loaded single battered piles in sands. *Canadian Geotechnical Journal*, 36(6):1074–1084, 1999. 10.1139/t99-072. URL <https://doi.org/10.1139/t99-072>.

- A. Hanna and A.Y.Afram. Pull-out capacity of single batter piles in sand. *Canadian Geotechnical Journal*, 23:387–392, 03 1987.
- S. Karthigeyan, V.V.G.S.T. Ramakrishna, and K. Rajagopal. Influence of vertical load on the lateral response of piles in sand. *Computers and Geotechnics*, 33(2):121–131, 2006. ISSN 0266-352X. <https://doi.org/10.1016/j.compgeo.2005.12.002>. URL <https://www.sciencedirect.com/science/article/pii/S0266352X06000103>.
- Y. Wang and R. P. Orense. Consideration of batter angle in pseudo-static analyses of pile foundations. *Computers and Geotechnics*, 147:104767, 2022. ISSN 0266-352X. <https://doi.org/10.1016/j.compgeo.2022.104767>. URL <https://www.sciencedirect.com/science/article/pii/S0266352X22001264>.
- G.G. Meyerhof and Y. Arisoy. Bearing capacity of flexible batter piles under eccentric and inclined, loads in layered soil. *Canadian Geotechnical Journal*, 31:583–590, 01 1994. 10.1139/t94-068.
- P. Bajaj, L. Yadu, and K.C Sandeep. Experimental study of vertical and batter pile groups under lateral loads in sand. *Indian Geotechnical Conference*, 01 2017.
- R. Brinkgreve. Small strains & cyclic loading. <https://brightspace.tudelft.nl/d21/le/content/289021/viewContent/1770617/View>, 2021b. Accessed: 2022–02-17.
- M. Novak and M. Sheta. Dynamic response of piles and pile groups. *2nd Int. Conf. Numer. Method Offshore Piling*, 1982. Accessed: 2021-12-10.
- M. Novak and F. Aboul-ella. Impedance functions of piles in layered media. *Journal of Engineering Mechanics-asce*, 104:643–661, 1978.
- R. L. Kondner and J. S. Zelasko. A hyperbolic stress-strain formulation of sands. *In Proceedings of the 2nd Pan American Conference on Soil Mechanics and Foundation Engineering*, 2:289–324, 1963.
- V. Hardin, B.and Drnevich. Shear modulus and damping in soils: Design equations and curves. *J. Soil Mech. Found. Div.*, 98, 07 1972. 10.1061/JSFEAQ.0001760.
- J. DOS SANTOS and A. GOMES CORREIA. Reference threshold strain of soil. its application to obtain an unique strain-dependent shear modulus curve for soil. *International Conference on soil mechanics and geotechnical engineering*, pages 267–270, 2001.
- T. Benz, R. Schwab, and P. Vermeer. Small-strain stiffness in geotechnical analyses. *Bautechnik*, 86(S1):16–27, 2009. <https://doi.org/10.1002/bate.200910038>. URL <https://onlinelibrary.wiley.com/doi/abs/10.1002/bate.200910038>.
- R. Brinkgreve, E. Engin, and H.K. Engin. Validation of empirical formulas to derive model parameters for sands. pages 137–142, 06 2010. 10.1201/b10551-25.
- V.h Taukoor, C. Rutherford, and S. Olson. A semi-empirical relationship for the small-strain shear modulus of soft clays. *E3S Web of Conferences*, 92:04005, 01 2019. 10.1051/e3sconf/20199204005.
- T. Godlewski. Evaluation of stiffness degradation curves from in situ tests in various soil types. *Archives of Civil Engineering*, 64:285–307, 12 2018. 10.2478/ace-2018-0075.

- J. Santos and A. Correia. Shear modulus of soils under cyclic loading at small and medium strain level. *12th World Conf. on Earthquake Engineering*, 530, 01 2000.
- D.E. Den Arend. Schelpfactoren bij door grond horizontaal belaste palen. 2010.
- H. Matlock, W. B. Ingram, K. Allen, and Dewaine B. Field Tests Of The Lateral-Load Behavior Of Pile Groups In Soft Clay. *All Days*, 05 1980. 10.4043/3871-MS. URL <https://doi.org/10.4043/3871-MS>. OTC-3871-MS.